IMPROVED CHARACTERIZATION OF THE FLEXURAL AND AXIAL COMPRESSIVE RESISTANCE OF WELDED STEEL BOX-SECTION MEMBERS

A Dissertation
Presented to
The Academic Faculty

by

Ajinkya Mahadeo Lokhande

In Partial Fulfillment
of the Requirements for the Degree
Doctor of Philosophy in the
School of Civil Engineering

Georgia Institute of Technology
August 2018

IMPROVED CHARACTERIZATION OF THE FLEXURAL AND AXIAL COMPRESSIVE RESISTANCE OF WELDED STEEL BOX-SECTION MEMBERS

Approved by:

Dr. Donald W. White, Advisor
School of Civil and Environmental Engineering
Georgia Institute of Technology

Dr. Richard W. Neu
School of Mechanical Engineering
Georgia Institute of Technology

Dr. Abdul-Hamid Zureick
School of Civil and Environmental Engineering
Georgia Institute of Technology

Dr. Charles M. King
Senior Steel Specialist
COWI

Dr. Arash Yavari
School of Civil and Environmental Engineering
Georgia Institute of Technology

Date Approved: June 25, 2018

To papa- the ultimate motivation for me in completing my doctoral studies

and

To mummy- my guiding light

ACKNOWLEDGEMENTS

I would like to dedicate this dissertation to my family for their unconditional love and support. I wish to express my deepest gratitude for the guidance provided by my advisor, Dr. Donald White. I am deeply indebted to him for his support and patience, and for the tremendous amount of time and effort he has dedicated to mentoring this thesis work.

I also wish to thank the other members of my committee, Dr. Charles King, Dr. AbdulHamid Zureick, Dr. Arash Yavari and Dr. Richard Neu. Their comments and suggestions have been very helpful. A special thanks to Dr. Charles King. I would also like to thank Mr. Michael Grubb, Mr. Anthony Ream, Dr. Francesco Russo and Mr. John Yadlosky for their guidance.

I wish to thank all my fellow students- Woo Yong, Lakshmi, Thanh, Evan, Oguzhan, Swarnava, Pradeep, Qimen, Amit, Esmaeel, Ryan, Abhiraj, and Ajit for their help and support. I also wish to thank my extended family for their support and encouragement.

Special thanks to my close friends for being there during tough times. I am grateful to have you in my life.

TABLE OF CONTENTS

LIST OF TABLES

LIST OF FIGURES

SUMMARY

The various existing methods for design of welded steel box-section members have major drawbacks with respect to their ability to represent the limit state responses, their generality in terms handling practical dimensions of box-section members, the ease of their application in real world designs, and the correlation between the resistance predicted by these methods and results from experimental tests and finite element test simulations. The objective of this research is the conceptual and theoretical development and improvement of methods for characterization of the flexural and axial compressive resistance of non-composite welded steel box-section members, and the evaluation of the performance of these methods using data compiled from existing experimental tests and generated from parametric studies performed using finite element test simulations.

An important aspect of the calculation of flexural and axial compressive resistance of box-section members is obtaining a good quantification of the ultimate compressive resistance of longitudinally stiffened and non-longitudinally stiffened component plates. The proposed method for calculating the axial compressive resistance of longitudinally stiffened plates is derived using an orthotropic plate idealization, but is expressed as an intuitive and easy-to-use column on elastic foundation model. This model considers the contributions from the longitudinal bending stiffness, transverse bending stiffness, and torsional stiffness of the plate. The proposed methods for characterization of the flexural and axial compressive resistance of non-composite welded box-section members are comprehensive in terms of their handling of limit state responses of practical box-section members, and have a strong theoretical background, yet are simple and design-friendly.

The strength predictions using the proposed methods show a good correlation with the results from experimental tests and from parametric studies performed using finite element test simulations.

CHAPTER 1. INTRODUCTION

Steel box-section members are highly efficient in resisting loads and are used in various important areas of highway bridge construction as well in building construction. The applications include but are not necessarily limited to truss members, arch ribs and ties, rigid-frame members, columns, edge girders, floor beams and steel tower legs. Some of these applications are highlighted in Figure 1-1 through Figure 1-3. Welded steel box sections can range from relatively small sections with nonslender or slender plates not containing any stiffeners, to relatively large sections composed of thin plates with multiple transverse and longitudinal stiffeners.

Figure 1-1 Akashi Kaikyo Bridge (Chou, 2011)

Figure 1-2 Lupu Bridge (GSG, 2013)

Figure 1-3 Inside view of the 14' tall x 4' wide - transversely and longitudinally stiffened tie girder of Hoan Bridge, courtesy of Dr. Francesco Russo (Michael Baker International).

There is great potential for improvement of existing methods for a better representation of the limit states responses, greater generality and ease of design application, and a better correlation with results from experimental tests and finite element

test simulations. Additionally, the fundamental consistency between many of the existing methods for design of these members, where the underlying mechanics and design behavior are essentially the same, needs to be improved.

Especially in the design-build arena, there is tremendous pressure for designers to optimize initial construction cost. For steel compression elements, this can lead to a preference for the use of thinner stiffened plates (i.e., plates containing longitudinal stiffeners) in larger structural components. At present, the AASHTO (2017) Specifications provide limited guidance regarding the design of bridge components containing stiffened plate elements. This lack of guidance can easily lead design engineers to misinterpret or inadvertently misapply important considerations. This can lead to either unsafe or overly conservative inefficient designs.

Thus, the objectives of this research are:

(1) The conceptual and theoretical development and improvement of methods for characterization of the flexural and axial compressive resistance of non-composite welded steel box-section members, and

(2) The evaluation of the performance of these methods using data compiled from existing experimental tests and generated from parametric studies performed using finite element test simulations.

The primary and supporting contributions to the body of knowledge from this research are as follows:

Primary contributions:

(1) Development of new methods and improvement of existing methods for a conceptually unified characterization of the flexural and axial compressive resistance of non-longitudinally stiffened welded box-section members, and ensuring a good correlation with results from experimental tests and finite element test simulations.

(2) Development of new methods and improvement of existing methods for a conceptually unified characterization of the flexural and axial compressive resistance of longitudinally stiffened welded box-section members, and ensuring a good correlation with results from experimental tests and finite element test simulations.

Supporting contributions:

(1) Improved quantification of the postbuckling resistance of non-longitudinally stiffened plates subjected to uniform axial compression in welded box-section members.

(2) Improved characterization of the ultimate compressive resistance of longitudinally stiffened plates.

At the present time (2018), there is no experimental or finite element simulation data in the literature investigating the interaction between flexural and local buckling in longitudinally stiffened welded steel box columns. Hence an important new development, as a part of the second primary contribution, is the development of finite element test simulation data for these types of components considering the interaction between global (flexural) and local buckling.

The organization of this document is as follows:

- Chapter 2 discusses an improved quantification of the ultimate compressive resistance of non-longitudinally stiffened plates.
- Chapter 3 provides a detailed explanation of a method for improved characterization of the flexural resistance of non-longitudinally stiffened box-section members.
- Chapter 4 provides a detailed explanation of a method for improved characterization of the ultimate compressive resistance of longitudinally stiffened plates.
- Chapter 5 discusses an improved quantification of the axial compressive resistance of non-longitudinally stiffened as well as longitudinally stiffened welded box-section members.
- Chapter 6 provides a detailed explanation of a method for improved characterization of the flexural resistance of longitudinally stiffened box-section members.
- Chapter 7 provides a summary of the key contributions from this research, and gives recommendations for future work.

CHAPTER 2. ULTIMATE COMPRESSIVE RESISTANCE OF NON-LONGITUDINALLY STIFFENED PLATES

A good prediction of the postbuckling resistance of non-longitudinally stiffened plates is essential for a good quantification of the axial compressive resistance and flexural resistance of non-longitudinally stiffened box-section members. This chapter discusses an improved quantification of the postbuckling resistance of non-longitudinally stiffened plates subjected to uniform axial compression in welded box-section members.

2.1 Need for improvement

It is widely known that slender unstiffened plates, in welded box sections subjected to axial compression, have significant postbuckling resistance. Schillo (2017a), and White and Lokhande (2017) provide a historical background of the calculation of local buckling and postbuckling resistance. A common way of considering the postbuckling resistance is via the use of effective widths as shown in Figure 2-1.

Research ranging back to the early work by Dowling and others in the 1970s and reflected in BS 5400-3:2000 (BSI 2000) indicates that for members composed of general welded plate assemblies, the plate local buckling and postbuckling resistances are lower than that indicated by Winter's classical effective width equation (Winter, 1970). Johansson and Veljkovic (2009), and Schillo (2017a) have also found Winter's effective width equation to be unconservative for unstiffened plates in welded box-section members.

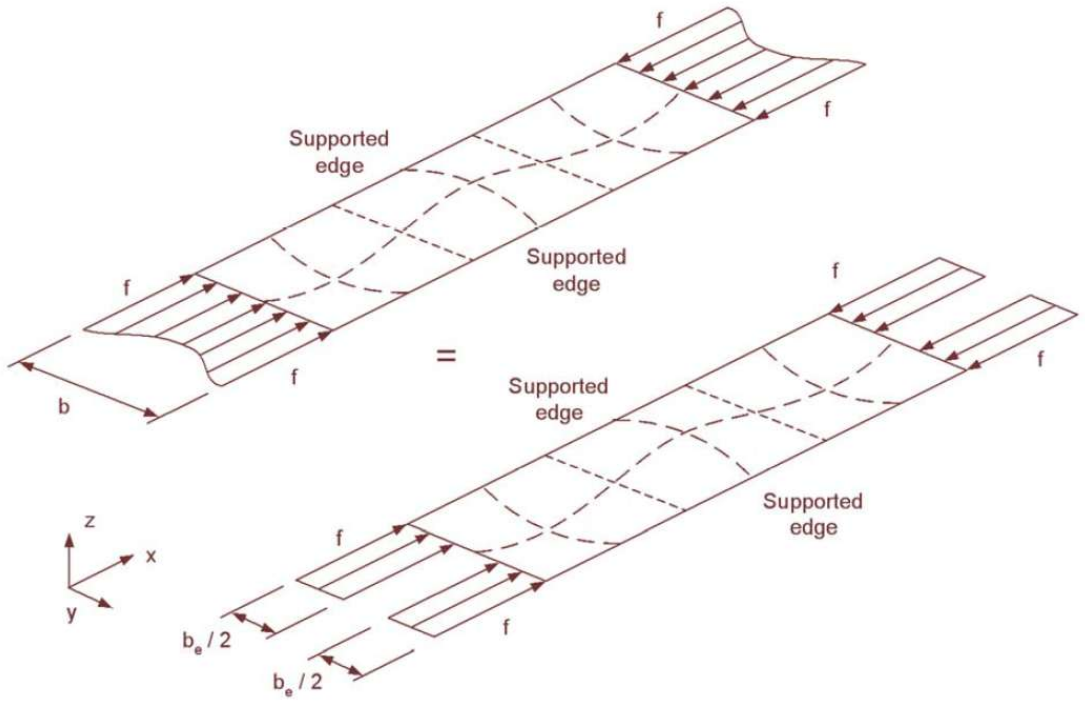

Figure 2-1 Representative physical longitudinal stress distribution across the width of a post-buckled simply supported plate versus idealized equivalent stress distribution acting on the plate effective width.

Figure 2-2 from Lindner et al. (1994), shows the results of local buckling tests compared with Winter's resistance curve. $\bar{\lambda}_p = \sqrt{\frac{F_y}{\sigma_{cr}}}$ where σ_{cr} is the elastic critical plate buckling stress. Figure 2-3 from Schillo (2017a) shows a comparison of test data to the strength prediction using Winter's classical effective width equation. In Figure 2-3, the partial safety factor, γ_M^*, for Winter's equation is 1.3, and the partial safety factor, γ_M^*, for Schillo's equation is 1.06 (Schillo and Taras 2018). This safety factor is used with resistance curves (representing mean reduction values) to ensure a defined level of failure probability and fully comply with the safety standard EN 1990. The safety factor is for material and geometric properties.

It can be observed that the predictions using Winter's effective width equation are slightly unconservative for higher plate slenderness values, and reasonably good for plate slenderness values closer to the nonslender plate limit. However, the predictions are unconservative in the range of intermediate plate slenderness values. As pointed out by Schillo (2017a), "…….*the so-called Winter-curve, which was derived by George Winter using a semi-empirical approach in 1947. This design curve reproduces the mean reduction values achieved in the experiments conducted by Winter and other researchers at that time. More recent tests on welded, squared box sections from steel grades S275 up to S960, and also the 34 experiments conducted within this study, showed the un-conservativeness of the Winter-curve with increasing local slenderness, independently of steel grade*."

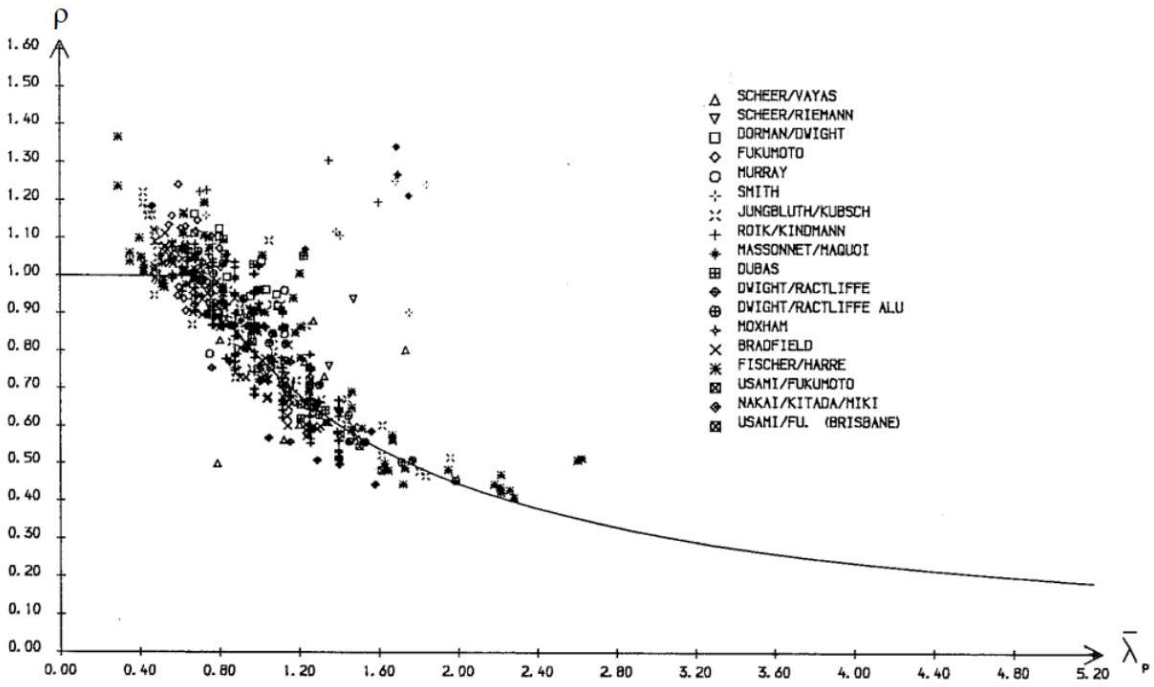

Figure 2-2 Results of local buckling tests, compared with the Winter resistance curve; from Lindner et al. (1994)

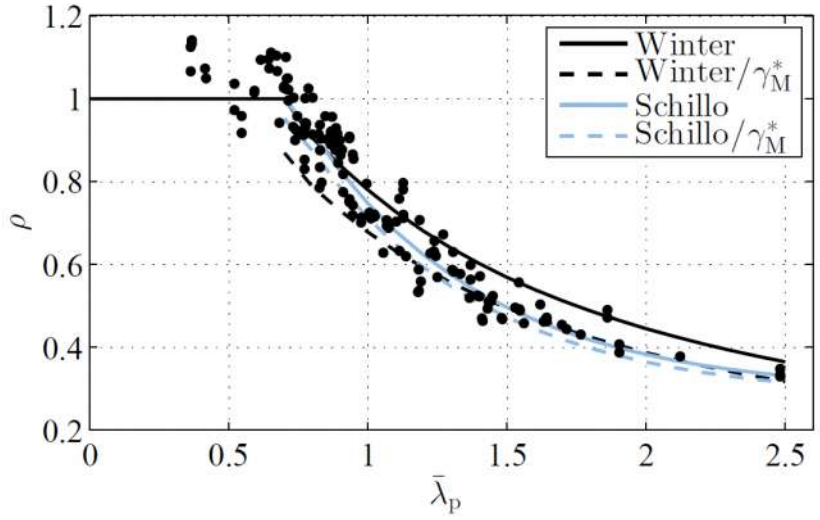

Figure 2-3 Comparison of test data to the strength predictions using Winter's effective width equation, and predictions using the local buckling resistance curve proposed by Schillo (2017a) using an improved best-fit exponential function using least square method (Schillo 2017a)

Schillo (2017b) points out a reason for the un-conservativeness of Winter's effective width equation when applied to non-longitudinally stiffened plates in welded box-section members- The design formulae do not take into account the fact that the tests used by Winter for the derivation of the resistance curve used cold-formed sections, where the strengthening effect of the cold forming process in the corners leads to higher capacity. This strengthening effect is absent in welded box-section members, resulting in unconservative predictions using Winter's effective width equation.

Johansson and Veljkovic (2009) discuss the optimism of the Winter's effective width equation for plates with large residual stresses, i.e., for plates in welded boxes with large welds, by pointing to the work by Clarin (2007). Taras et al. (2013) found that the strengths from FE test simulations of unstiffened plates correlate with the strength predictions using the Winter's curve when the amplitude of the local imperfection is taken

as plate width/400 in the simulations. This imperfection amplitude is much smaller than the EN 1090 tolerance which is equal to plate width/200. Thus, they found that even for simply supported plates subjected to uniform axial compression (plate buckling coefficient equal to four) Winter's curve can be approximated only if the amplitude of plate imperfections in the FE simulations is taken to be much lower than the tolerance; Winter's equation would be optimistic for imperfection amplitudes closer to the tolerance (Taras 2016). Therefore, Winter's effective width equation is not correct for all levels of plate slenderness, residual stresses and geometrical imperfections that are encountered in modern steel construction (King 2017b).

Additionally, a small parametric study was performed by Lokhande and White (2017), using FE test simulations, on non-longitudinally stiffened welded box stub columns with different combinations of component plate slenderness. The amplitude of plate imperfection used in these tests was plate width/200. Table 2-1 gives the cross-section dimensions of the stub columns considered in this parametric study. Figure 2-4 illustrates the variables used in Table 2-1. The lengths of the stub-columns were taken between 1.5 to 2.5 times the widths of the box-section component plates. The results of the parametric study are shown in Table 2-2, and are consistent with the observations from Figure 2-3 expect the predictions using Winter's effective width equation are conservative for very high plate slenderness values, i.e., the predictions using Winter's effective width equation are:

- Unconservative in the range of intermediate plate slenderness values
- Reasonably good for plate slenderness values closer to the nonslender plate limit
- Conservative for very high plate slenderness values

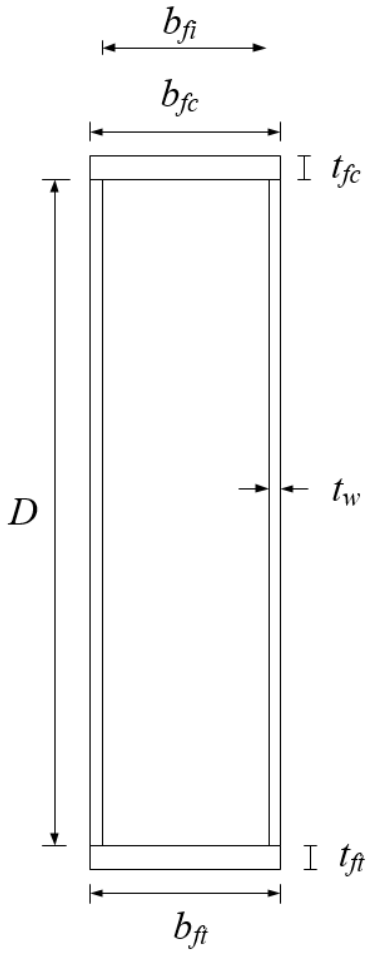

Figure 2-4 Non-longitudinally stiffened box cross-section

Table 2-1 Cross-section dimensions of the stub columns considered in the parametric study

Member number	b_{fc} (in.)	t_{fc} (in.)	b_{ft} (in.)	t_{ft} (in.)	D (in.)	t_w (in.)	Length (ft.)
1	23.0	1.2	23.0	1.2	23.0	0.5	3.1
2	25.0	1.5	25.0	1.5	50.0	0.5	4.8
3	22.0	0.5	22.0	0.5	22.0	0.5	2.9
4	50.0	1.5	50.0	1.5	50.0	0.5	6.6
5	50.0	0.5	50.0	0.5	50.0	0.5	6.8

Table 2-2 Summary of box stub columns considered in the parametric study and the performance of the Winter's effective width equation as given in AISC (2016)

Member number	Flange slenderness	Web slenderness	Strength from test simulation / Strength predicted using classical Winter's effective width equation as given in AISC (2016)
1	18	46	0.95
2	16	100	1.03
3	42	44	0.88
4	33	100	0.83
5	98	100	1.11

The plate buckling curves used in AASHTO (2017) and Eurocode [CEN (2006)] are based on the classical Winter's curve and are almost identical. For unstiffened plates in welded boxes, BS 5400-3:2000 (BSI 2000) recommends the use of BS5400 Curve 2 which is below the curves in AASHTO and Eurocode. However, a drawback of the curves in BS5400-3:2000 (BSI 2000) is that they have many change points (King 2017b), as can be seen from the equations given in Annex G.5 of BS 5400-3:2000 (BSI 2000). This is inconvenient for design. Schillo (2017a) has proposed a local buckling resistance curve using an improved best-fit exponential function using least square method, as shown in Figure 2-3. However, due to the familiarity of design engineers with Winter's curve, a simple modification to the Winter's classical effective width equation is considered a better choice to capture the observed lower strengths, instead of using a new plate buckling curve. Different aspects related to the various incarnations of the effective width equations are discussed in detail in White and Lokhande (2017).

2.2 Improved estimate of the postbuckling resistance

A simple downward shift of the Winter's curve along with a corresponding reduction in the width-to-thickness limit at which plates are fully effective up to the yield strength of the material is proposed. In comparison to Winter's curve and Schillo's (2017a) curve, this shifted curve is as shown in Figure 2-5.

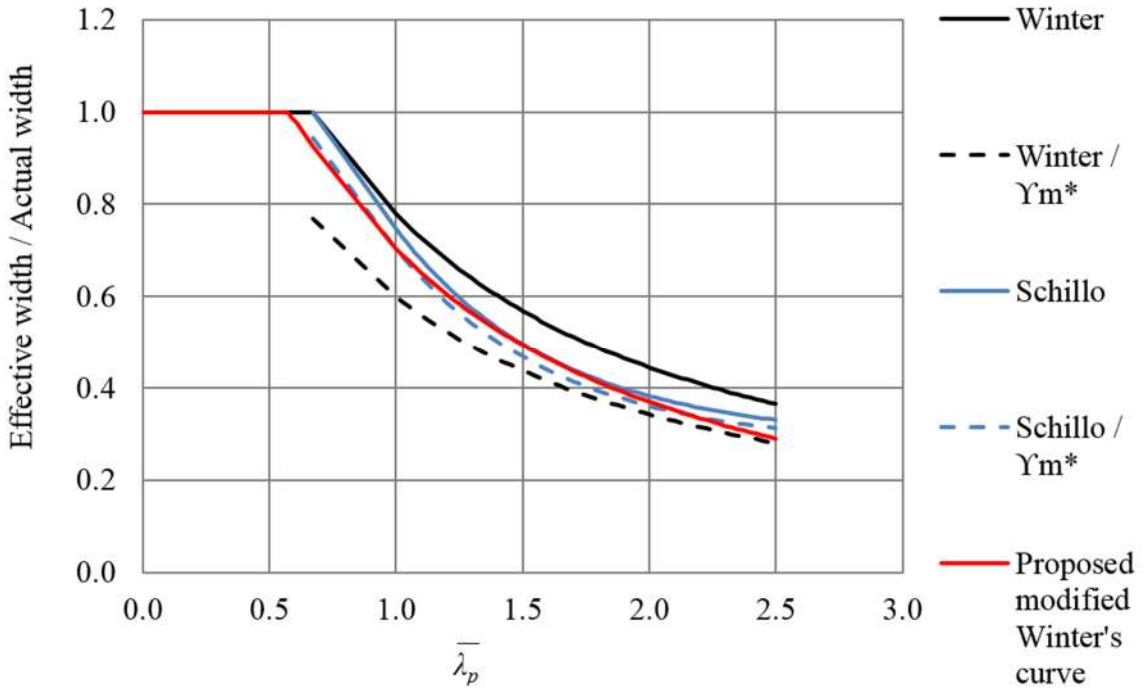

Figure 2-5 Proposed modified form of Winter's curve

The proposed modified form of Winter's classical effective width equation is explained below:

If $\frac{b}{t_{fc}} \leq \lambda_r \sqrt{\frac{F_y}{F_{cr}}}$ then,

$$b_e = b \tag{1}$$

and if $\frac{b}{t_{fc}} > \lambda_r \sqrt{\frac{F_y}{F_{cr}}}$ then,

$$b_e = b\left[\left(1 - c_1\sqrt{\frac{F_{el}}{F_{cr}}}\right)\sqrt{\frac{F_{el}}{F_{cr}}} - c_3\right] \tag{2}$$

in which:

- c_1 = effective width imperfection adjustment factor = 0.22
- c_3 = effective width imperfection adjustment factor = 0.075
- $c_2 = \left(1 - \sqrt{1 - 4c_1(1 + c_3)}\right) \Big/ (2c_1)$ (3)

  = effective width imperfection adjustment factor = 1.74
- $F_{el} = \left(c_2 \frac{\lambda_r}{(b/t)} \right)^2 F_y$ (4)

  = elastic local buckling stress (ksi)
- b = gross width of the plate
- b_e = effective width of the plate
- $\lambda_r = 1.09\sqrt{\frac{E}{F_{yc}}}$ (5)

  = width-to-thickness ratio limit
- F_{cr} = Uniform compressive stress on the plate. For axial compressive resistance of box-section members, this is equal to the flexural buckling stress calculated using gross cross-section properties. For flexural resistance of box-section members, F_{cr} is conservatively taken equal to the yield strength of the compression flange.

Table 2-3 compares the modified Winter's equation to the test simulation results generated in this research. It can be observed that, although in general the proposed effective width equation gives a good prediction of the ultimate compressive strength, the prediction becomes substantially conservative for the extreme case of member number 5, where all the component plates of the box-section have very high slenderness. As seen

from Table 2-2 and Table 2-3, the shift in Winter's equation has a significant impact on the axial compressive resistance of a welded box-section member.

Table 2-3 Summary of box stub columns considered in the parametric study and the performance of the proposed modified Winter's equation

Member number	Flange slenderness	Web slenderness	Strength from test simulation / Strength predicted using the modified Winter's equation
1	18	46	0.99
2	16	100	1.08
3	42	44	1.05
4	33	100	0.94
5	98	100	1.41

CHAPTER 3. FLEXURAL RESISTANCE OF RECTANGULAR WELDED NON-LONGITUDINALLY STIFFENED BOX SECTION MEMBERS

This chapter provides a detailed explanation of a new method for an improved characterization of the flexural resistance of welded non-longitudinally stiffened box-section members. A review of the current codified methods and prior research related to the calculation of flexural resistance of welded non-longitudinally stiffened box-section members is provided in Section 3.1. The proposed method is explained in Section 3.2. Section 3.3 discusses the evaluation of the performance of the proposed method. The salient features of the proposed method are discussed in Section 3.4.

3.1 Literature review

Sections 3.1.1 and 3.1.2 highlight the motivation for this thrust of the research.

3.1.1 Codified methods

Sections 3.1.1.1, 3.1.1.2 and 3.1.1.3 discuss the shortcomings of the AASHTO (2017), Eurocode (CEN 2005; CEN 2006) and AISC (2016) methods for calculating the flexural resistance of non-longitudinally stiffened welded box-section members.

3.1.1.1 AASHTO

The AASHTO (2017) method for calculating the flexural resistance has the following shortcomings:

1) AASHTO (2017) Article 6.12.2.2.2 does not address general singly-symmetric welded box-section beams.

2) This article does not address flange local buckling and web bend buckling in welded box-section beams.

3) This article also does not address welded box-section beams with hybrid webs.

4) For lateral torsional buckling (LTB), Article 6.12.2.2.2 assumes that the resistance is governed by inelastic LTB. This is a good assumption because the unbraced lengths have to be very long for elastic LTB to govern. For practical box-section beams, inelastic LTB will always govern instead of elastic LTB. Based on this assumption, AASHTO (2017) gives an equation for predicting the inelastic LTB resistance based on the traditional CRC (Column Research Council) column equation. The maximum flexural resistance predicted by this inelastic LTB equation is the yield moment of the gross cross section. However, in the studies discussed in Section 3.3, it is found that for shorter box-section members with compact flanges and compact or non-compact webs, the flexural resistance is largely governed by the cross-section capacity which is higher than the yield moment and up to the plastic moment of the gross cross-section. It is also found that for members with a noncompact or slender compression flange and non-compact webs, the cross-section resistance is larger than the yield moment of the effective cross-section, and for members

with a noncompact or slender compression flange and compact webs, the cross-section resistance is only slightly smaller than the plastic moment capacity of the effective cross-section based on the effective width of the compression flange taking into account its postbuckling resistance. Box sections with these characteristics are encountered in applications where the member is subjected to biaxial bending. The relatively slender webs become flanges when the box is subjected to bending about the other principal axis. Thus, there is large reserve strength that is not taken into account by the AASHTO (2017) equations. The definitions of compact, non-compact, slender webs; and compact, noncompact and slender flanges are discussed in Section 3.2.1.

3.1.1.2 Eurocode

The Eurocode (CEN 2005; CEN 2006) method for calculating the flexural resistance has the following shortcomings:

1) The Eurocode method requires an iterative or at least a two-step calculation to determine the effective cross-section for Class 4 sections. As per Eurocode (CEN 2005; CEN 2006), " *Class 1 cross-sections are those which can form a plastic hinge with the rotation capacity required from plastic analysis without reduction of the resistance; Class 2 cross-sections are those which can develop their plastic moment resistance, but have limited rotation capacity because of local buckling; Class 3 cross-sections are those in which the stress in the extreme compression fiber of the steel member assuming an elastic distribution of stresses can reach the yield strength, but local buckling is liable to prevent development of the plastic moment resistance; Class 4 cross-sections are those in which local buckling will occur before the attainment of yield stress in one or more parts of the cross-section*."

2) Another limitation of the Eurocode is that it classifies a cross-section based on the most unfavorable class of its compression parts. This can lead to overly conservative predictions in some cases, where the cross-section is classified as Class 3 or Class 4, but the actual resistance is larger than the yield moment of the effective cross-section and in some cases just slightly smaller than the plastic moment capacity of the effective cross-section. An example of such a case is a box-section member with a noncompact or slender compression flange and compact or non-compact webs. The practicality of this type of member is explained above. Thus, there is large reserve strength that is not taken into account by the equations in the Eurocode (CEN 2005; CEN 2006).

3) For cross-section resistance, the Eurocode accounts for the limit state of tension flange yielding in Class 4 sections by calculating the section modulus of the effective cross section corresponding to the flange having the maximum elastic stress. It has been found in the parametric studies discussed in Section 3.3 that for Class 4 (e.g., slender web) singly-symmetric cross-sections with a larger effective compression flange than the tension flange, the cross-section resistance is larger than that corresponding to the limit state of tension flange yielding. That is, these types of sections have significant reserve strength beyond the first yielding of the tension flange. The Eurocode equations under-predict the resistance of such cross sections.

3.1.1.3 AISC

The AISC (2016) method for calculating the flexural resistance has the following shortcomings:

1) For box sections with compact webs and a slender compression flange, the cross-section resistance predicted by AISC (2016) is the yield moment of the effective cross-section. However as mentioned earlier, for these box sections the cross-section resistance is larger than the yield moment and just slightly smaller than the plastic moment capacity of the effective cross-section. Thus, there is large reserve strength which is not taken into account by the equations in AISC (2016).

2) For box sections with slender webs and a slender compression flange, the cross-section resistance predicted by AISC (2016) is $R_{pg}F_{cr}S_{xc}$, where F_{cr} is the local buckling stress of the compression flange. This representation does not account for the post-buckling resistance of the compression flange.

3) According to AISC (2016), the flexural resistance is the minimum of the strengths corresponding to the limit states of yielding (plastic moment), flange local buckling, web local buckling and lateral torsional buckling. This approach does not account for the interaction between local buckling and global buckling (lateral torsional buckling).

4) In AISC (2016), the compression flange stress at the onset of nominal yielding within the cross-section, including residual stress effects, is taken as 0.7 times the yield strength of the compression flange, F_{yc}. Additionally, the equation for the length L_r is calculated by solving for the unbraced length by equating the elastic lateral torsional buckling moment

equal to $0.7F_{yc}S_{xc}$. In the proposed method, the length L_r is calculated as only 30% of the length obtained by solving for the unbraced length by equating the elastic lateral torsional buckling moment to $0.5F_{yc}S_{xce}$. As discussed in Section 3.3, the strengths predicted using the proposed method correlate well with the inelastic LTB resistances obtained from test simulations. Thus, this research indicates that the inelastic LTB resistance calculated in AISC (2016) by considering a linear interpolation between L_p and the AISC L_r expression over-predicts the inelastic LTB resistance of welded box-section members.

5) There is a significant discontinuity in the resistances predicted by AISC (2016) equations F7-6 and F7-9 for cases with a slender flange when the webs transition from non-compact to slender.

It should be noted that the 2022 draft AISC provisions avoid the drawbacks in point #2 and point #5, by not allowing box-section members with a slender compression flange and slender webs.

3.1.2 Prior research

Kim and Yoo (2008) built on the work by Nakai et al. (1990) to propose improved predictor equations for the flexural resistance of rectangular box-section members. These equations have been developed using regression analysis considering the following parameters:

- Aspect ratio of the box cross-section
- Yield stress
- Width-to-thickness of the compression flange

- Width-to-thickness of the web plate
- Interaction between flange and web plates

These equations have the following shortcomings:

- These equations predict only the cross-section resistance. There is no dependence of the resistance on the length of the box-section member. Hence, there is no consideration of any reduction in the resistance due to inelastic lateral torsional buckling of the box-section member. In the parametric studies discussed in Section 3.3, it is found that for longest practical box-section beams the inelastic lateral torsional buckling resistance can be as small as 76.3% of the cross-section resistance.

  Also, the 64 hypothetical box-section members studied by Kim and Yoo (2008) had aspect ratios between 1 and 1.8. However, practical box-section members can be much narrower and deeper than the one's studied by Kim and Yoo (2008).
- These equations do not address any interaction between local buckling (i.e., flange local buckling or web bend buckling) and global buckling (lateral torsional buckling).
- These equations are not applicable to hybrid box-section members.
- There is no consideration of the postbuckling resistance of the compression flange.

Therefore, based on the discussion in Sections 3.1.1 and 3.1.2, clearly there is a need to gain a better understanding of the behavior of non-longitudinally stiffened welded steel box-section beams, and to develop a method for an improved characterization of the flexural resistance of these types of members.

3.2 Proposed method

This section explains the proposed method. Section 3.2.1 explains the classification of web and flange plates, and provides equations for various strength factors. The calculation of cross-section flexural resistance and the member inelastic lateral torsional buckling resistance using the proposed method are explained in Sections 3.2.2 and 3.2.3 respectively. Section 3.2.4 discusses the limits on the box cross-section dimensions for which the proposed method is applicable.

The equations of the proposed method are expressed in terms of an effective cross-section (denoted by the subscript *e*) based on the effective width of the compression flange, b_e, taking into account the post-buckling response of a noncompact or slender compression flange (or the full width of a compact compression flange). The calculation of the effective width of the compression flange, b_e, was explained in CHAPTER 2.

3.2.1 Section classification: Flanges and Webs

The following sub-sections explain the classification of web and flange plates, and provide equations for various strength factors in the proposed method.

3.2.1.1 Webs

In the proposed method, the web slenderness is given by $\lambda_w = \frac{2D_{ce}}{t_w}$ and the webs are classified as:

- Compact if $\lambda_w \leq \lambda_{pw}$, where

$$\lambda_{pw} = 3.1\left(\frac{D_{ce}}{D_{cpe}}\right)\sqrt{\frac{E}{F_{yc}}} \tag{6}$$

- Noncompact if $\lambda_{pw} < \lambda_w \leq \lambda_{rw}$, where

$$\lambda_{rw} = 4.6\sqrt{\frac{E}{F_{yc}}} \tag{7}$$

- Slender if $\lambda_w > \lambda_{rw}$

where D_{ce} and D_{cpe} are the distances of the elastic and plastic neutral axis from the inside surface of the compression flange in the effective cross-section respectively.

The limiting web slenderness ratio, λ_{pw}, is somewhat larger than the value specified for doubly symmetric noncomposite box sections in AISC (2016), and is slightly larger than the Class 2 limit for noncomposite box sections specified in CEN (2005). Compact web sections can develop the plastic moment resistance of the cross-section, M_p, contingent on the satisfaction of other plate slenderness and member unbraced length requirements necessary to develop the plastic moment. The slenderness limit for a noncompact web, λ_{rw}, is slightly larger than the Eurocode Class 3 limit for non-composite box sections and is intended to ensure that the yield moment of the cross-section can be developed, contingent on the satisfaction of other plate slenderness and unbraced length requirements necessary to develop the yield moment.

The parameters R_{pc}, R_b and R_h are defined as the web plastification factor, web load-shedding factor and hybrid factor respectively. The web load-shedding factor, R_b, is calculated using the provisions in AASHTO (2017) Article 6.10.1.10.2, with

$\lambda_{rw} = 4.6\sqrt{\frac{E}{F_{yc}}}$, and with a_{wc} determined with $b_{fc}t_{fc}$ taken as one-half of the total effective compression flange area $\frac{b_e t_{fc}}{2}$. This factor accounts for the reduction in the section flexural resistance caused by the shedding of compressive stresses due to bend buckling of the slender web, and the corresponding increase in the flexural stress within the compression flange. The hybrid factor, R_h, is calculated using AASHTO (2017) Eq. 6.10.1.10.1-1 with A_{fn} taken as one-half of the total effective compression flange area $\frac{b_e t_{fc}}{2}$ if $D_n = D_{ce}$, and A_{fn} taken as $\frac{b_{ft} t_{ft}}{2}$ if $D_n = D - D_{ce}$. This factor accounts for the early yielding of the webs in a hybrid box-section. The values of R_{pc} and R_b for different web slenderness are given in Table 3-1. In Table 3-1:

- S_{xce} is the elastic section modulus of the effective cross-section about the axis of bending to the compression flange.
- M_{pe} = Plastic moment capacity of the effective cross-section.
- $M_{yce} = F_{yc} S_{xce}$ (8)

  where F_{yc} is the yield strength of the compression flange.

Table 3-1 Values of R_{pc} and R_b

Web classification	R_{pc}	R_b
Compact web	$R_{pc} = \frac{M_{pe}}{M_{yce}}$ (9)	$R_b = 1$
Noncompact web	$R_{pc} = \left[1 - \left(1 - \frac{R_h M_{yce}}{M_{pe}}\right)\left(\frac{\lambda_w - \lambda_{pw}}{\lambda_{rw} - \lambda_{pw}}\right)\right]\frac{M_{pe}}{M_{yce}} \leq \frac{M_{pe}}{M_{yce}}$ (10)	$R_b = 1$
Slender web	$R_{pc} = R_h$ (11)	R_b calculated using AASHTO (2017) Eq. 6.10.1.10.2-3, with $\lambda_{rw} = 4.6\sqrt{E/F_{yc}}$ and a_{wc} determined with $b_{fc}t_{fc}$ taken as $\frac{b_e t_{fc}}{2}$, D_c taken as D_{ce}.

3.2.1.2 Flanges

The compression flange slenderness is given by $\lambda_f = \frac{b_{fi}}{t_{fc}}$, where $b_{fi} = b_{fc} - 2t_w$ as shown in Figure 2-4. The flange is classified in the proposed method as:

- Compact if $\lambda_f \leq \lambda_{pf}$ where,

$$\lambda_{pf} = 1.09\sqrt{\frac{E}{F_{yc}}} \quad (12)$$

- Noncompact if $\lambda_{pf} < \lambda_f \leq \lambda_{rf}$ where,

$$\lambda_{rf} = 1.7\sqrt{\frac{E}{F_{yc}}} \tag{13}$$

- Slender if $\lambda_f > \lambda_{rf}$

λ_{pf} is the same as the nonslender limit for a plate subjected to uniform axial compression (see Eq. 5). λ_{pf} specified in Eq. 12 is comparable to the compact flange limit in AISC (2016), and to the Class 1 flange limit in CEN (2005), which is intended to ensure that the section can form a plastic hinge with a rotation capacity sufficient for plastic analysis, contingent on the satisfaction of other necessary plate slenderness and unbraced length requirements. This more restrictive limit is also related to the shift in Winter's classical plate effective width curve discussed earlier in Section 2.2. Unlike noncompact and slender flanges, there is no reduction in the compressive resistance of compact flanges due to local buckling. R_f is a compression flange slenderness factor that accounts for the inability of a noncompact or slender compression flange to:

- Develop large inelastic strains without a reduction in the flange force contribution, when the webs are nonslender,
- Accept stress shed due to the bend buckling of slender webs.

The significance of R_f is explained in Section 3.4. It is defined as follows:

- $R_f = 1.0$ for a compact flange
- $R_f = \left[1 - 0.15\left(\frac{\lambda_f - \lambda_{pf}}{\lambda_{rf} - \lambda_{pf}}\right)\right] \le 1.0$ for a noncompact flange (14)

- $R_f = 0.85$ for a slender flange.

3.2.2 Cross-section resistance

Tables 3-2 and 3-3 explain the calculation of cross-section flexural resistance, M_{cs}. In these tables, S_{xte} is the elastic section modulus of the effective cross-section about the axis of bending to the tension flange.

Table 3-2 Cross-section flexural resistance when $S_{xce} \le S_{xte}$ (elastic stress in the flange in flexural compression is greater than or equal to the stress in the flange in flexural tension)

Web slenderness	Flexural resistance	Simplified flexural resistance equation
Compact web	$M_{cs} = R_f M_{pe}$ (15)	$M_{cs} = R_f R_b R_{pc} M_{yce}$ (16)
Noncompact web	$M_{cs} = R_f \left[M_{pe} - \left(\frac{\lambda_w - \lambda_{pw}}{\lambda_{rw} - \lambda_{pw}} \right) \left(M_{pe} - R_h M_{yce} \right) \right]$ (17)	
Slender web	$M_{cs} = R_f R_b R_h M_{yce}$ (18)	

Table 3-3 Cross-section flexural resistance when $S_{xce} > S_{xte}$ (elastic stress in the flange in flexural compression is smaller than the stress in the flange in flexural tension)

Web slenderness	Flexural resistance
Compact web	$M_{cs} = R_f M_{pe}$ (19)
Noncompact web	$M_{cs} = R_f \left[M_{pe} - \left(\frac{\lambda_w - \lambda_{pw}}{\lambda_{rw} - \lambda_{pw}} \right) \left(M_{pe} - M_{yct} \right) \right]$ (20) where M_{yct} is the flexural resistance corresponding to the stress distribution shown in Figure 3-1
Slender web	The flexural resistance is calculated as R_f times the moment corresponding to the stress distribution shown in Figure 3-2

In Figure 3-1 and Figure 3-2, $F_{yf} = F_{yc}$ as both flanges are assumed to have the same yield strength.

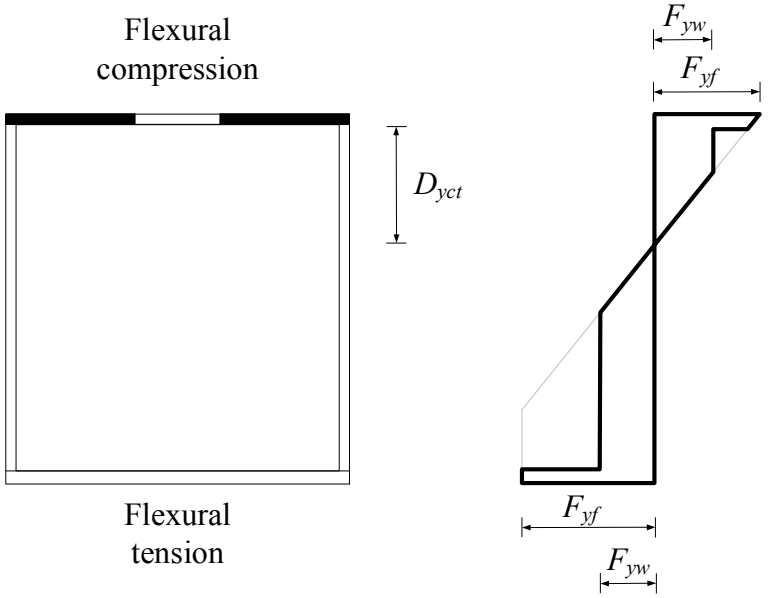

Figure 3-1 Stress distribution for calculation of M_{yct}

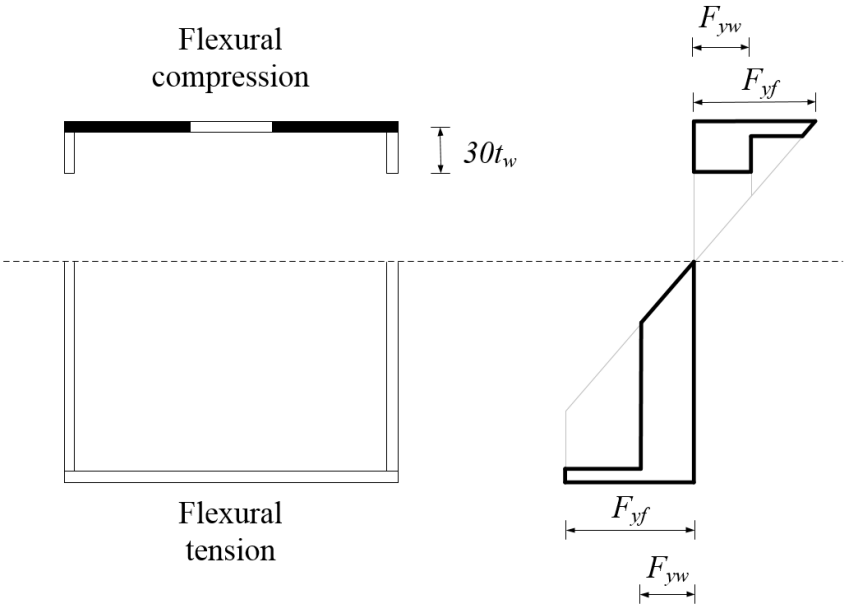

Figure 3-2 Stress distribution employed for calculation of M_{cs} for a slender-web cross-section ($\lambda_w > \lambda_{rw}$)

Unlike the case with $S_{xce} \le S_{xte}$, it is recommended that the AASHTO R_h expression should not be used to address hybrid box sections for cases shown in Figure 3-1 and Figure 3-2. This is because R_h is derived considering the first yield of the flange; it does not account for the spread of yielding in the tension zone of the cross-section due to early yielding of the tension flange. A strain-compatibility analysis is recommended to account for web bend buckling, hybrid web effects and inelastic strength reserve corresponding to the spread of yielding in the tension zone. The closed form equation for M_{yct} corresponding to the stress distribution in Figure 3-1 is

$$M_{yct} = \frac{F_{yw} d^2 t_w}{2} + \frac{F_{yf} d \left(b_{fc.eff} t_{fc} + b_{ft} t_{ft} \right)}{2} - \frac{F_{yw}{}^3 d^2 t_w}{6 F_{yf}{}^2} - \frac{F_{yw} \left(b_{fc.eff} t_{fc} - b_{ft} t_{ft} \right)^2}{24 t_w}$$
$$- \frac{F_{yf}{}^2 \left(b_{fc.eff} t_{fc} - b_{ft} t_{ft} \right)^2}{8 F_{yw} t_w} + \frac{F_{yw}{}^2 d \left(b_{fc.eff} t_{fc} - b_{ft} t_{ft} \right)}{6 F_{yf}} \qquad (21)$$

where:

- In the above equation the variation of stresses between the upper face and lower face of the flanges is neglected, and the top and bottom flange are assumed to be separated by a distance

$$d = D + \frac{t_{fc}}{2} + \frac{t_{ft}}{2} \tag{22}$$

- $b_{fc.eff} = b_{fi.eff} + 2t_w$ (23)
- $b_{fi.eff}$ is calculated using the modified Winter's effective width equation explained in Section 2.2, with $b = b_{fi}$ and $b_e = b_{fi.eff}$

Equation 21 is only applicable when $D_{yct} > 0$, where

$$D_{yct} = \frac{F_{yf} b_{ft} t_{ft} - F_{yf} b_{fc.eff} t_{fc} + 2F_{yw} d t_w}{4F_{yw} t_w} \tag{24}$$

If $D_{yct} \leq 0$, then $M_{yct} = M_{pe}$.

3.2.3 Inelastic lateral torsional buckling resistance

When the unbraced length, L_b, is less than L_p, the flexural resistance is the cross-section resistance, calculated as explained in Table 3-2 and 3-2; where L_p is the limiting unbraced length to achieve the cross-section flexural resistance under uniform moment.

$$L_p = \frac{0.16}{M_{yce}} \sqrt{EI_y \left(20\beta_x M_{yce} + GJ\right)} \tag{25}$$

This length is calculated by solving for L_b after equating the theoretical elastic lateral torsional buckling moment of a singly-symmetric box-section member (Peköz, 1969), M_{cr}, to $15M_{pe}$, taking C_b equal to 1.0 and approximating M_{pe} as $1.3M_{yce}$. The coefficient 15 is based on the ratio of the elastic lateral torsional buckling moment, M_{cr}, to the plastic moment, M_p, for doubly-symmetric box-section members corresponding to $L_b = L_p$ in AISC (2016). The theoretical elastic lateral torsional buckling moment of a singly-symmetric box-section member is,

$$M_{cr} = \frac{C_b \pi^2 E I_y}{L_b^2}\left[\frac{\beta_x}{2} + \sqrt{\left(\frac{\beta_x}{2}\right)^2 + \frac{GJL_b^2}{EI_y\pi^2}}\right] \tag{26}$$

When L_b is greater than L_p, the inelastic lateral torsional buckling resistance is expressed as follows:

$$M_n = C_b\left[M_{CS} - \left(M_{CS} - F_{yr}S_{xce}\right)\left(\frac{L_b - L_p}{L_r - L_p}\right)\right] \le M_{CS} \tag{27}$$

where:

- M_{CS} is the cross-section resistance. It is calculated as explained in Tables 3-2 and 3-3.
- $F_{yr} = 0.5F_{yc}$ (28)

  F_{yr} is the compression flange stress at the onset of nominal yielding within the cross-section, including residual stress effects, for moment applied about the axis of bending. This value is determined based on test simulation studies discussed in

Section 3.3. Since $F_{yc} = F_{yt}$, for practical box cross-sections, the moment $F_{yr}S_{xce}$ corresponds to a stress state when the tension flange has not yielded.

- L_b denotes the unbraced length. The maximum practical unbraced length is taken as the smaller of 30D and 200r_y, for all box-section members satisfying the cross-section proportion limits given in Section 3.2.4. The limit of 30 times D is slightly larger than the L/D limit of 24 considered in the Commentary for Section F7 in AISC (2016), which is an extreme deflection limit. The limit of L/r_y=200 is set based on a practical upper limit on the slenderness of a column undergoing flexural buckling. This maximum practical unbraced length is much smaller than the unbraced length corresponding to the transition between inelastic LTB and elastic LTB. Therefore, elastic lateral torsional buckling need not be considered for box-section members satisfying the cross-section proportion limits in Section 3.2.4.

- $$L_r = \frac{0.94}{F_{yr}S_{xce}}\sqrt{EI_y\left(\beta_x F_{yr}S_{xce} + GJ\right)} \tag{29}$$

  L_r is the limiting unbraced length for calculation of the lateral torsional buckling resistance. It is calculated by solving for L_b with M_{cr} taken equal to $F_{yr}S_{xce}$, C_b taken equal to 1.0 and taking 30 percent of that value. This value is determined based on test simulation studies discussed in Section 3.3.

- C_b is the moment gradient modifier determined as specified in AASHTO (2017) Article A6.3.3.

- $$J = \frac{4A_m^2}{\left(\frac{b_m}{t_{fc}} + \frac{b_m}{t_{ft}} + \frac{2h_m}{t_w}\right)} \tag{30}$$

  It is the St. Venant torsional constant.

- β_x is the mono-symmetry parameter of the gross cross-section. It is equal to zero for a doubly symmetric cross-section and is a positive value when the larger flange is in compression. It is calculated fundamentally (Peköz, 1969) as,

$$\beta_x = \frac{1}{I_x}\int_A y\left(x^2 + y^2\right)dA - 2y_o \tag{31}$$

Figure 3-3 shows a singly-symmetric non-longitudinally stiffened box cross-section. For a rectangular box-section, β_x may be expressed as

$$\beta_x = \frac{1}{I_x}\left(\frac{h_{mt}t_{ft}b_m^3}{12} + h_{mt}^3 b_m t_{ft} + \frac{b_m^2 t_w}{4}\left(h_{mt}^2 - h_{mc}^2\right) + \frac{t_w}{2}\left(h_{mt}^4 - h_{mc}^4\right) - \frac{h_{mc}t_{fc}b_m^3}{12} - h_{mc}^3 b_m t_{fc}\right) - 2y_o \tag{32}$$

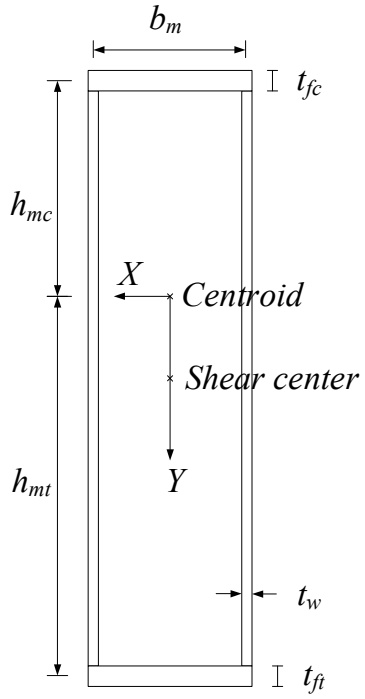

Figure 3-3 Singly-symmetric non-longitudinally stiffened box cross-section

Neglecting terms involving b_m^2 and b_m^3 since they are relatively small for box sections with large $\frac{D}{b_{fc}}$ (King 2016); β_x may be expressed as

$$\beta_x = \frac{1}{I_x}\left(h_{mt}^3 b_m t_{ft} + \frac{t_w}{2}\left(h_{mt}^4 - h_{mc}^4\right) - h_{mc}^3 b_m t_{fc} \right) - 2y_o \tag{33}$$

- y_o is the distance between the shear center (Young 2002) and the centroid of the gross cross-section. The term y_o is a negative value when the larger flange is in compression.

$$y_o = \left[\frac{{h_m}^2 b_m^2}{12 I_{ym}} \left(9t_w + \frac{t_{ft} b_m}{h_m} - \frac{12\left(h_m + t_w b_m / t_{ft}\right)}{2h_m / t_w + b_m / t_{ft} + b_m / t_{fc}} \right) \right] - \left[D_c + \frac{t_{fc}}{2} \right] \tag{34}$$

where:

- $b_m = b_{fc} - t_w$ (35)
- $h_m = D + \frac{t_{fc}}{2} + \frac{t_{ft}}{2}$ (36)
- $h_{mc} = D_c + \frac{t_{fc}}{2}$ (37)
- $h_{mt} = D - D_c + \frac{t_{ft}}{2}$ (38)
- $A_m = b_m h_m$ (39)

- $I_{ym} = \frac{{b_m}^3\left(t_{fc} + t_{ft}\right)}{12} + \frac{t_w h_m {b_m}^2}{2}$ (40)

is the moment of inertia about the minor principal axis of the gross cross-section, calculated neglecting the contribution of the moment of inertia of the webs about their centroidal axis parallel to the minor principal axis of the gross cross-section. .

- A is the gross cross-sectional area of the box-section.
- D_c is the depth of the web in compression in the elastic range for the gross box cross-section taken from the inside of the compression flange.
- G is the shear modulus of elasticity for steel = $0.385E$.
- I_x is the moment of inertia about the major principal axis of the gross cross-section.
- r_y is the radius of gyration about the minor axis.

In lieu of calculating L_p and L_r using Eq. 33 for β_x, as a simplification L_p and L_r can be calculated using $\beta_x = 0$, i.e.,

$$L_p = \frac{0.1Er_y\sqrt{JA}}{M_{yce}} \tag{41}$$

and

$$L_r = \frac{0.6Er_y\sqrt{JA}}{F_{yr}S_{xce}} \tag{42}$$

The maximum difference in M_n calculated using Eqs. 41 and 42 for L_p and L_r, and M_n calculated using Eqs. 25 and 29 for L_p and L_r is only 0.54% (0.54% lower and 0.24% higher than that obtained using Eqs. 25 and 29), for the box-section members considered in the parametric study discussed later in Section 3.3. The parametric study in Section 3.3 considers large D/b_{fc} ratios (within the box-section proportion limits discussed in Section 3.2.4) and longest practical lengths for inelastic lateral torsional buckling. Thus, for practical box-section members the parametric study considers all the extreme cases for

lateral torsional buckling, and therefore it is safe to use the above discussed simplification, i.e., using Eqs. 41 and 42 for L_p and L_r. If the limit of the ratio of thickness of thickest plate to thinnest plate being welded should be less than or equal to 3.0, is removed (This limit is applied for the parametric study design discussed in Section 3.3.1), then the following three extreme singly-symmetric box-section members (with shear center below the centroid) and with $L = L_{\max} = 30D$ are possible:

- Member 1: $b_{fc} = b_{ft} = 64$ in., $t_{fc} = 0.64$ in., $t_{ft} = 4$ in., $D = 180$ in., $t_w = 4$ in, $L = 30D = 5400$ in.
- Member 2: $b_{fc} = b_{ft} = 64$ in., $t_{fc} = 0.64$ in., $t_{ft} = 4$ in., $D = 360$ in., $t_w = 4$ in, $L = 30D = 10800$ in.
- Member 3: $b_{fc} = b_{ft} = 64$ in., $t_{fc} = 0.64$ in., $t_{ft} = 4$ in., $D = 384$ in., $t_w = 2.56$ in, $L = 30D = 11520$ in.

The largest difference between the flexural resistance calculated using Eqs. 41 and 42 for L_p and L_r, and using Eqs. 25 and 29 for L_p and L_r, is only 0.98% (corresponding to member 2). Thus it is safe to use Eqs. 41 and 42 for L_p and L_r based on $\beta_x = 0$. Therefore, the proposed method recommends the use of Eqs. 41 and 42 for calculating L_p and L_r respectively.

3.2.4 Box section proportion limits

The proposed method is applicable to box-section members whose cross-section dimensions are within the following limits:

- $\frac{D}{t_w} \leq 150$ (43)

  This is a practical upper limit on the slenderness of webs without longitudinal stiffeners, and is the same as that for I-sections in AASHTO (2017)

- $b_{fc} \geq D/6$ (44)

  This is a practical minimum limit for the outside width of box sections.

- $b_{fi}/t_{fc} \leq 90$ (45)

  This limit is set to avoid the following issues that could be encountered when using a very thin flange plate, pending further research:

  - Vibration of excessively thin plates during transportation.
  - Localized plate bending stresses induced by handling and erection operations.
  - Vibration of excessively thin plates due to in-service loadings on the completed bridge.
  - Localized plate bending stresses due to box-section distortion (i.e., distortion transverse bending stresses) as well as secondary stresses due to out-of-plane deformation of the box-section bottom flange.
  - "Bending reluctance" of excessively thin flanges, that is, the tendency for excessively thin flanges to not bend fully along with the overall curvature of the box-section member.

- Localized out-of-plane deflection due to a concentrated transverse load applied to the bottom flange, or to a plate panel within the bottom flange.
- Buckling of thin bottom flange plates intended to serve predominantly in tension, due to unanticipated or accidental axial compression in the plates during handling and transportation, erection, and in the final service condition, particularly in the vicinity of inflection points in continuous-span girders or near locations where longitudinal stiffeners are terminated.
- Perception of vertical vibrations, or general "sponginess" in bottom flanges of box girders, by bridge inspection personnel. These vibrations may be due to transient live loads on the bridge or due to the individual's movements when walking the inside of the box girder.
- Potential "oil canning" of thin plates in bottom flanges, i.e., snapping in or out of the plates between edge supporting elements when pushed on by a light force.

- Slenderness of flange extensions on welded box sections, less than or equal to $0.38\sqrt{\frac{E}{F_y}}$. This ensures that the flange extensions are not subject to any strength reduction associated with local buckling under flexural compression.

3.3 Evaluation of the performance of the proposed method

The performance of the proposed method is evaluated via a parametric study performed using finite element (FE) test simulations. Section 3.3.1 explains the parametric study design. The results of the parametric study are discussed in Section 3.3.2. The finite element modelling of these box-section members is explained in Appendix A. At the

present time (2018), in the literature there is no experimental data for non-longitudinally stiffened welded box-section members subjected to pure bending.

3.3.1 Parametric study design

The parametric study is divided into two parts, the first part focusing on homogeneous beams and the second part on hybrid beams. The beams are selected such that they address all practically possible combinations of flange and web plate slenderness, and allow the consideration of cross-section resistance as well as inelastic LTB resistance. Box-section members satisfying the section proportion limits of Section 3.2.4 are not governed by elastic LTB for any practical unbraced length, as explained in Section 3.2.3.

Table 3-4 provides a summary of the box-section beams considered in the parametric study. Column 2 in Table 3-4 provides a notation that summarizes the slenderness of the different plates in the cross-section. In Column 2, the first letter corresponds to the slenderness of the flange in flexural compression, the second letter corresponds to the slenderness of the flange in flexural tension and the third letter corresponds to the slenderness of the webs. The nomenclature used in Column 2 of Table 3-4 is summarized in Table 3-5. The compact and noncompact flange limits in Table 3-5 are slightly different from those specified in Section 3.2.1.2 because the limits in Section 3.2.1.2 have been finalized after taking into consideration the results of the parametric study. The third through the fifth columns of Table 3-4 show the different member lengths considered in the study. The cross-section dimensions and lengths of the various cases listed in Table 3-4 are provided in Appendix B. In Table 3-4 the gray cells indicate the

lengths considered for each cross-section. The following practical limits were considered while finalizing the cross-section dimensions:

- Minimum and maximum plate thickness equal 0.5 in. and 4 in. respectively.
- Ratio of thickness of thickest plate to thinnest plate being welded, less than or equal to 3.0.
- Ratio of the total area of the two webs to the area of compression flange, less than or equal to 12.
- Ratio of area of the two webs to the total area of the flanges, less than or equal to 6.

In addition to the cases in Table 3-4, the flexural resistance of a box-section member with cross-section 6 (C-N-S) having an aspect ratio of 6 is studied for a larger number of member lengths to obtain a detailed evaluation of the performance of the proposed equations in capturing the variation of the flexural resistance with changes in length of the box-section member.

Table 3-4 Summary of box-section members considered in the parametric study (gray cells indicate the lengths considered for each cross-section)

Cross-Section Number	Flange and web slenderness	Length $\approx 0.5L_p$ (Cross-Section resistance)	Length $\approx \frac{0.5L_p + L_{\max}}{2}$ (Inelastic LTB)	Length = L_{max} = min($200r_y$, $30D$) (Inelastic LTB)
1	C-C-CW			
2	C-C-NW			
3	C-C-SW			
4	C-N-CW			
5	C-N-NW			
6	C-N-SW			
7	C-S-CW			
8	C-S-NW			
9	C-S-SW			
10	N-C-CW			
11	N-C-NW			
12	N-C-SW			
13	N-N-CW			
14	N-N-NW			
15	N-N-SW			
16	N-S-CW			
17	N-S-NW			
18	N-S-SW			
19	S60-C-CW			

Table 3-4 (continued) Summary of box-section members considered in the parametric study (gray cells indicate the lengths considered for each cross-section)

Cross-Section Number	Flange and web slenderness	Length $\approx 0.5L_p$ (Cross-Section resistance)	Length $\approx \frac{0.5L_p + L_{\max}}{2}$ (Inelastic LTB)	Length = L_{max} = min($200r_y$, $30D$) (Inelastic LTB)
20	S60-C-NW			
21	S60-C-SW			
22	S60-N-CW			
23	S60-N-NW			
24	S60-N-SW			
25	S60-S60-CW			
26	S60-S60-NW			
27	S60-S60-SW			
28	S100-C-CW			
29	S100-C-NW			
30	S100-C-SW			
31	S100-N-CW			
32	S100-N-NW			
33	S100-N-SW			
34	S100-S100-CW			
35	S100-S100-NW			
36	S100-S100-SW			
37	C-S150-CW			
38	C-C-HCW			

Table 3-4 (continued) Summary of box-section members considered in the parametric study (gray cells indicate the lengths considered for each cross-section)

Cross-Section Number	Flange and web slenderness	Length $\approx 0.5L_p$ (Cross-Section resistance)	Length $\approx \frac{0.5L_p + L_{\max}}{2}$ (Inelastic LTB)	Length = L_{max} = min($200r_y$, $30D$) (Inelastic LTB)
39	C-C-HNW			
40	C-C-HSW			
41	N-N-HCW			
42	N-N-HNW			
43	N-N-HSW			
44	S100-S100-HCW			
45	S100-S100-HNW			
46	S100-S100-HSW			

Table 3-5 Nomenclature used in Column 2 of Table 3-4

Notation	Explanation
C	Compact flange $\lambda_f \le 1.1\sqrt{\frac{E}{F_{yc}}}$
N	Noncompact flange $1.1\sqrt{\frac{E}{F_{yc}}} < \lambda_f \le 1.4\sqrt{\frac{E}{F_{yc}}}$
S60, S100, S150	Slender flange with b_{fi}/t_f = 60, 100 and 150 respectively, where t_f is the thickness of the flange
CW and HCW	Homogeneous and hybrid compact webs respectively, $\lambda_w \le \lambda_{pw}$
NW and HNW	Homogeneous and hybrid noncompact webs respectively, $\lambda_{pw} < \lambda_w \le \lambda_{rw}$
SW and HSW	Homogeneous and hybrid slender webs respectively, $\lambda_w > \lambda_{rw}$

3.3.2 Results and discussion

The predictions using the proposed method (using Eqs. 41 and 42 for L_p and L_r, and using strain-compatibility analysis for cases with $S_{xce} > S_{xte}$) show a good correlation with the results of the parametric study performed using finite element simulations. The mean, median and coefficient of variation of the ratio of the flexural resistance from test simulation to the strength predicted using the proposed method are equal to 1.06, 1.05 and 0.06 respectively. Figure 3-4, Figure 3-5 and Figure 3-6 show a comparison of the member strengths from test simulation with the strengths predicted using the proposed method, the method in the Eurocode (CEN 2005; ;CEN 2006), the method in AASHTO (2017) Article 6.12.2.2.2 and the method in AISC (2016), for homogeneous box-section members with lengths approximately equal to $0.5L_p$, $\frac{0.5L_p + L_{\max}}{2}$ and $L_{\max}$ respectively. Figure 3-7 shows a comparison of the member strength from test simulation with the strength predicted using the proposed method for hybrid box-section members with lengths approximately equal to $0.5L_p$ and $L_{\max}$.

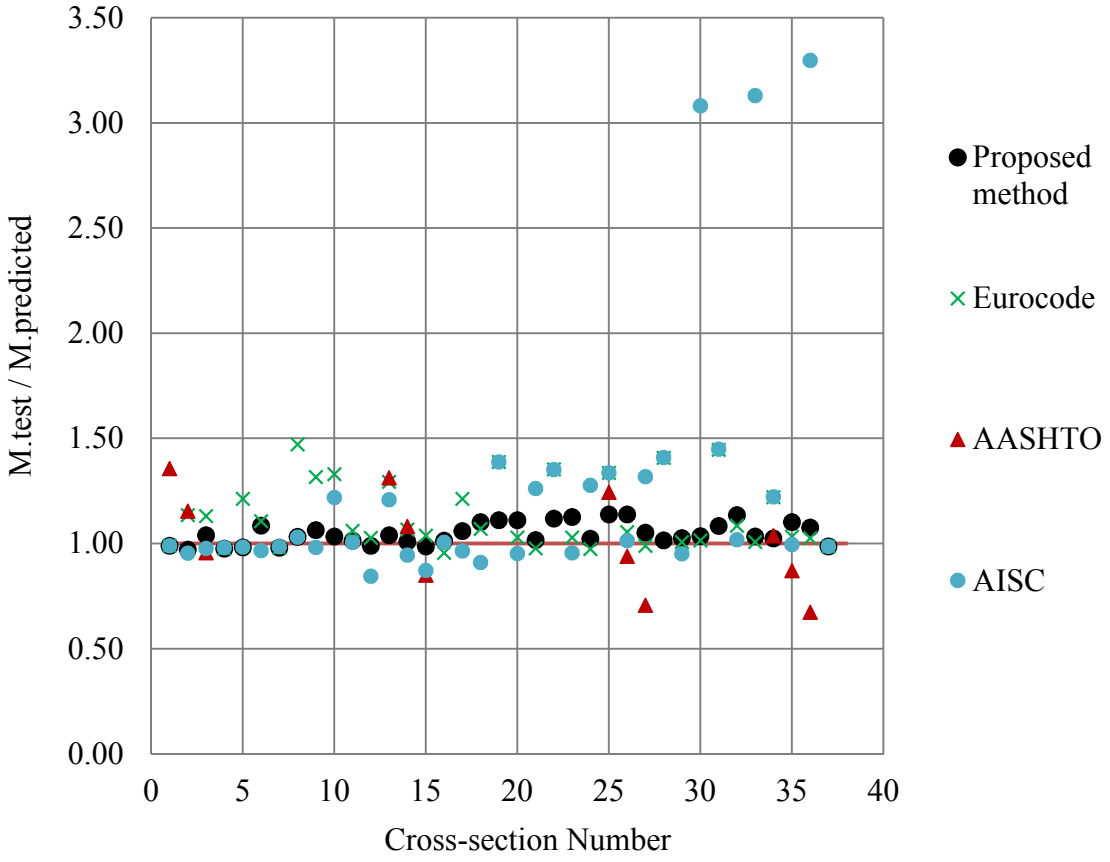

Figure 3-4 Comparison of the member strength from test simulation with the strength predicted using the proposed method, the method in Eurocode, the method in AASHTO (2017) Article 6.12.2.2.2 and the method in AISC (2016), for homogeneous box-section members with length $\approx 0.5L_p$

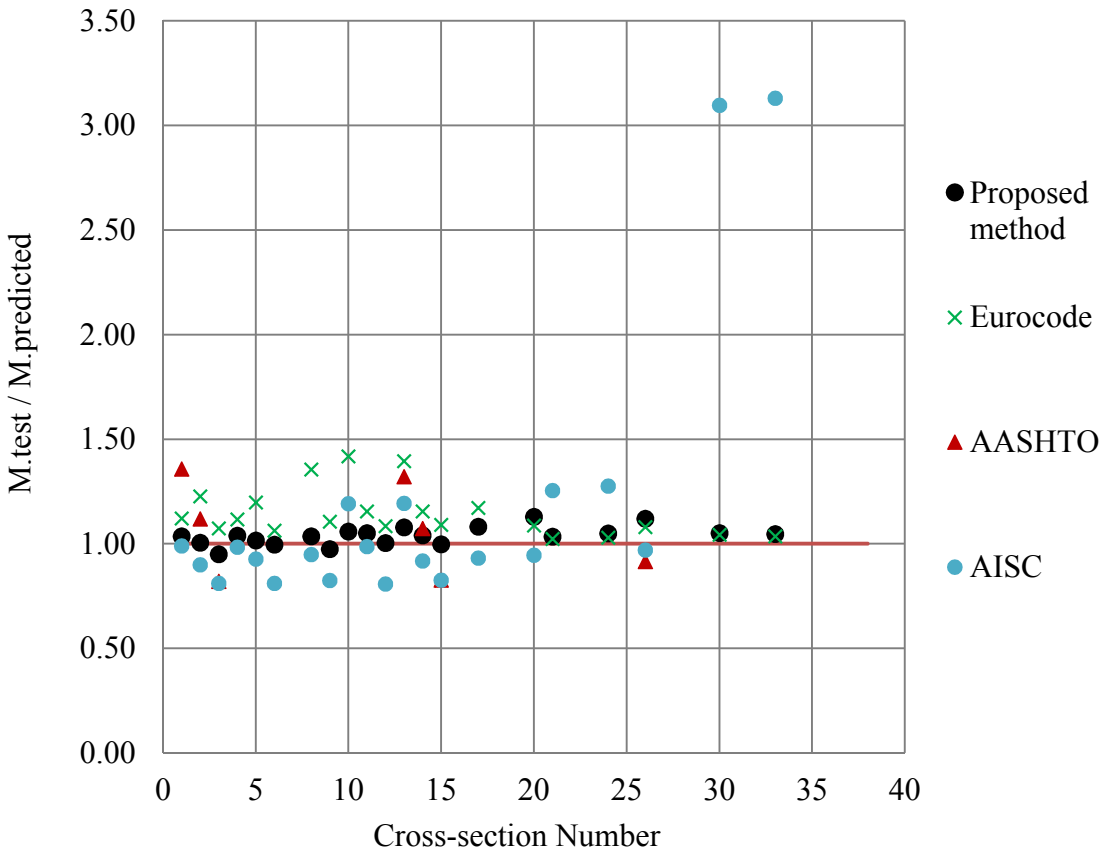

Figure 3-5 Comparison of the member strength from test simulation with the strength predicted using the proposed method, the method in Eurocode, the method in AASHTO (2017) Article 6.12.2.2.2 and the method in AISC (2016), for homogeneous box-section members with length $\approx \frac{0.5L_p + L_{\max}}{2}$

The good performance of the proposed equations for cross-sections 19 to 36 in Figure 3-4, clearly shows that for cases with a noncompact or slender compression flange and non-compact webs, the cross-section resistance is larger than the yield moment and up to R_f times the plastic moment capacity of the effective cross-section for box sections with compact webs. This point is reinforced by observing that for cases with noncompact or slender compression flanges and compact webs (cross sections 19, 22, 25, 28, 31 and 34)

in Figure 3-4, the predictions using the Eurocode method are overly conservative. As discussed in Section 3.1.1.2, the predictions using the Eurocode method are overly conservative for these cases because they classify a cross-section based on the most unfavorable class of its compression parts and hence end up limiting the predicted cross section resistance of box sections with a noncompact or slender compression flange and compact webs to yield moment of the effective cross-section. Although box sections with a noncompact or slender compression flange and compact or non-compact webs are more unusual, they may be encountered when considering biaxial bending as discussed earlier in Section 3.1.1.2.

A good prediction of cross-section resistance using the proposed method for extreme singly-symmetric sections ($\frac{b_{fc}}{t_{fc}}$ between 17.7 to 19.5, and $\frac{b_{ft}}{t_{ft}}$ between 106 to 156) with a larger compression flange (cross-sections 7, 8, 9 and 37) in Figure 3-4, clearly shows that for box-section members the limit state of tension flange yielding is not required. Also as discussed in Section 3.1.1.2, the Eurocode method gives conservative cross-section resistance predictions for singly-symmetric Class 4 box-section members with larger compression flange, as it considers tension flange yielding by calculating the section modulus corresponding to the flange with the maximum elastic stress. This can be seen by the conservative prediction using Eurocode for cross-section 9.

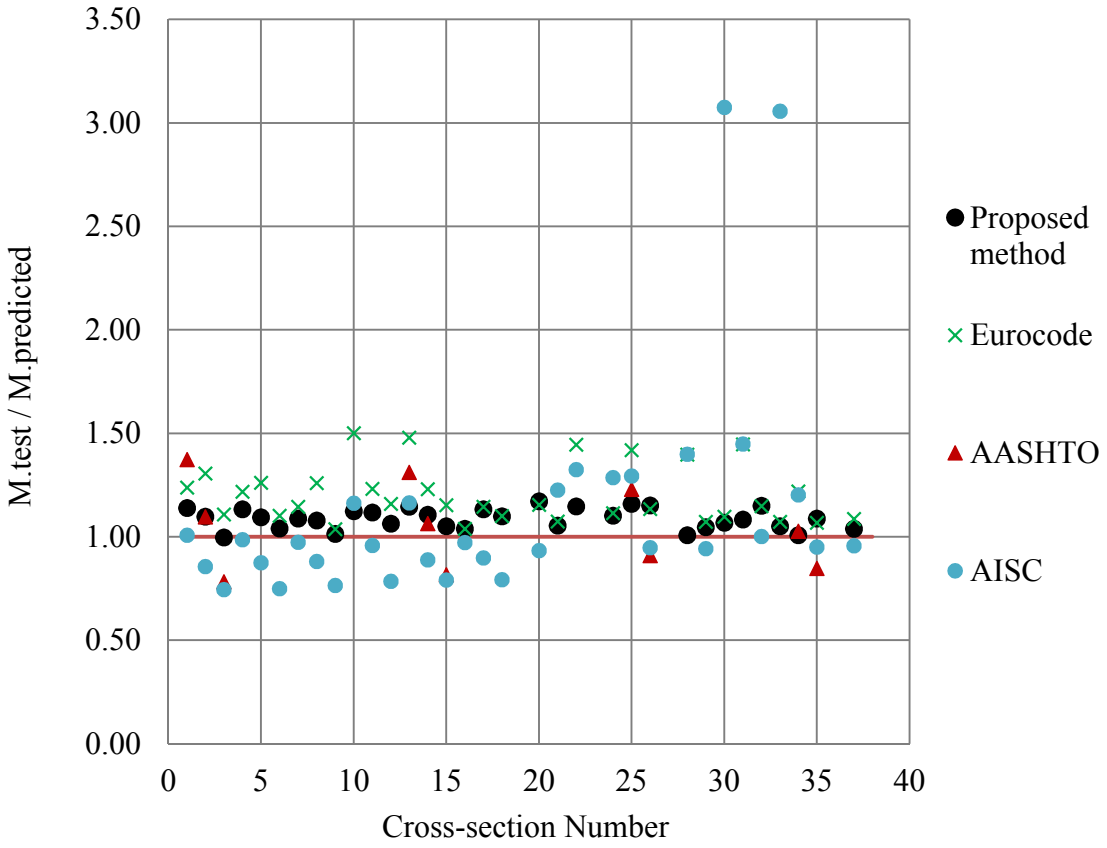

Figure 3-6 Comparison of the member strength from test simulation with the strength predicted using the proposed method, the method in Eurocode, the method in AASHTO (2017) Article 6.12.2.2.2 and the method in AISC (2016), for homogeneous box-section members with length = L_{max} = min(200r_y,30D)

It can be observed from Figure 3-4 that for members with a compact compression flange and compact or non-compact webs, the cross-section resistance is higher than the yield moment and up to the plastic moment of the gross cross-section. Thus for cross-sections 1, 2, 13 and 14, the strength predicted using the AASHTO (2017) method is conservative since the maximum flexural resistance predicted by the inelastic LTB equation in AASHTO (2017) is limited to the yield moment of the gross cross-section. The

inelastic LTB equation in AASHTO (2017) over-predicts the strength of box-section members with slender webs because it does not account for web bend buckling.

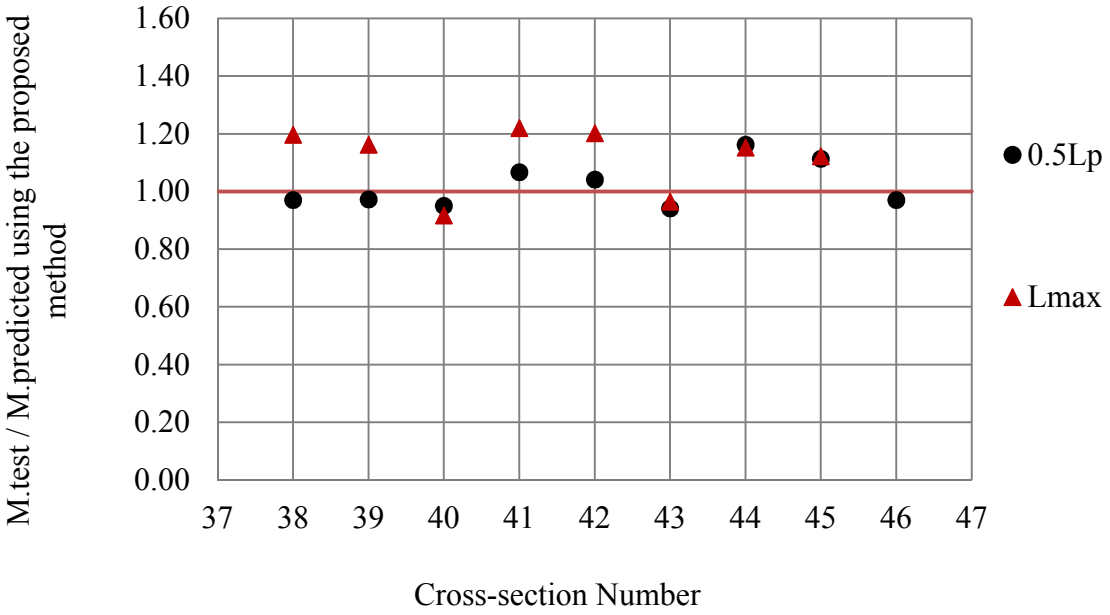

Figure 3-7 Comparison of the member strength from test simulation with the strength predicted using the proposed method for hybrid box-section members with lengths $0.5L_p$ and L_{max}

As mentioned earlier in Section 3.1.1.3, for box sections with slender webs and a slender compression flange, the cross-section resistance predicted by AISC (2016) is $R_{pg}F_{cr}S_{xc}$, where F_{cr} is the local buckling stress of the compression flange. This representation does not account for the post-buckling resistance of the compression flange. This is the reason for the conservatism in strength predictions for cross-sections 30, 33, 36 in Figure 3-4, and cross-sections 30, 33 in Figure 3-5 and Figure 3-6.

It can be observed from Figure 3-5 and Figure 3-6 that the inelastic LTB resistance calculated by considering a linear interpolation between L_p given by Eq. 41 and L_r given

by Eq. 42 gives good correlation with the strengths from the test simulations and performs much better than the methods in AASHTO, Eurocode and AISC. Figure 3-7 clearly shows that the proposed method performs well in predicting the cross-section resistance and inelastic LTB resistance of hybrid box-section members.

Figure 3-8 shows the variation of flexural resistance with change in length of a box-section member with cross-section # 6 (C-N-S) having an aspect ratio of six. For this member, the reduction in flexural resistance at L_{max} is 22.4% compared to the plateau resistance. It can be seen that the inelastic LTB resistance calculated by considering a linear interpolation between L_p and L_r (using Eqs. 41 and 42 for L_p and L_r respectively) gives reasonably good predictions. In the parametric study, the maximum reduction in flexural resistance at L_{max} compared to the plateau resistance is obtained for a box-section member with cross-section 3 (C-C-S). The reduction for that case is equal to 23.7%.

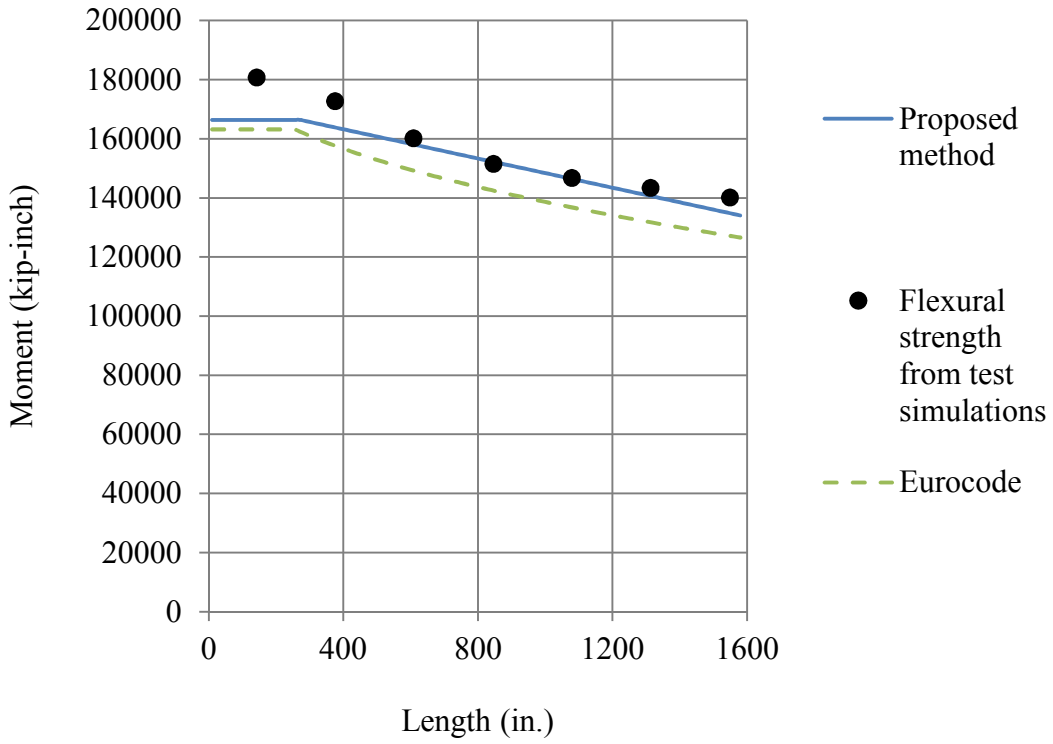

Figure 3-8 Variation of flexural resistance with change in length of a box-section member with cross-section # 6 (C-N-S) having an aspect ratio of six

3.4 Salient features of the proposed method

The proposed method encapsulates a significant advancement in the understanding of the behavior of rectangular non-longitudinally stiffened welded box-section beams, and provides a conceptually unified characterization of their resistance which correlates well with the results of the parametric study. The salient features of this method are as follows:

1) The proposed method better handles the following:

- It accounts for:

- Flange local buckling and the corresponding postbuckling resistance via the use of an effective cross-section based on the effective width of the compression flange. An improved calculation of the postbuckling resistance of non-longitudinally stiffened plates subjected to uniform axial compression in welded box-section members is proposed, as discussed in CHAPTER 2.
- Web-bend buckling and the corresponding postbuckling resistance via the web-bend buckling factor or an effective web section. This avoids the need to perform iterative or two-step calculations when obtaining an effective cross-section.
- Lateral torsional buckling: The method recognizes that for the longest and narrowest practical non-longitudinally stiffened box-section beams the reduction in the flexural resistance relative to the cross-section resistance can be measurable. In the parametric studies discussed in Section 3.3, it is found that for the longest practical box-section beams the inelastic lateral torsional buckling resistance can be as small as 76.3% of the cross-section resistance.
- The proposed method addresses the interaction between local postbuckling (i.e., flange local buckling or web bend buckling) and global buckling (lateral torsional buckling). This interaction is considered via the use of effective section properties and/or the AASHTO web bend buckling factor, in the proposed inelastic lateral torsional buckling equation.

- The method addresses all practical ranges of web and flange plate slenderness, i.e.:
  - Compact, noncompact and slender compression flanges.
  - Compact, noncompact and slender webs.
- In bridges it is common that fabricated boxes may be singly symmetric. The proposed method can handle singly as well as doubly symmetric box-section members. For lateral torsional buckling, this is accomplished via the mono-symmetry parameter, which accounts for the fact that in singly-symmetric sections the shear center and centroid do not coincide and the effect of this attribute on the LTB resistance. The proposed method also provides an improved characterization of the cross-section resistance of singly-symmetric box-section members as discussed in point #2 and point #4 of this section.
- It is possible for steel box-section members subjected to flexure to have webs with lower yield strengths than that of the flanges. The proposed method addresses hybrid as well as homogenous box-section members. To accomplish this, the proposed method uses the R_h factor when calculating the flexural resistance for cases with $S_{xce} \le S_{xte}$. However, the method uses the stress distribution corresponding to the limit state of yielding of the compression flange of the effective cross-section when calculating the flexural resistance for cases with $S_{xce} > S_{xte}$. This is because R_h has been derived considering the first yield of a flange. However, the proposed method recognizes the inelastic reserve strength corresponding to the spread of yielding in the tension zone (including the hybrid web effects) for cases with $S_{xce} > S_{xte}$.

Thus the proposed method better characterizes the flexural resistance of all practical non-longitudinally stiffened welded box-section members.

2) The proposed method eliminates the need to consider a separate tension flange yielding (TFY) limit state. For sections with $S_{xce} > S_{xte}$, the member response is addressed rigorously via the direct calculation of the yield moment of the compression flange, considering early yielding of the section on the tension side of the neutral axis, and considering hybrid web, slender web and noncompact or slender compression flange effects as applicable. This allows the consideration of large reserve strengths up to 43% higher than those predicted by the Eurocode equations, and correlates well with the observations from the parametric study discussed in Section 3.3.

3) A study of the axial load versus axial shortening characteristics of a non-longitudinally stiffened plate for different values of plate slenderness shows that except for plates with width-to-thickness ratios less than or equal to approximately 20, the ability of a plate to sustain load decreases with increase in inelastic axial compressive strains beyond the peak load. The ultimate load carrying capacity of these plates is considered via the use of an effective width. If such slender plates are used as a compression flange in a box-section beam; then the flange plate should be able to sustain large inelastic axial compressive strains so that the nonslender webs can plasticize. However, it is known that the flange force contribution decreases with increase in the inelastic axial compressive strain. To account for this behavior, a compression flange slenderness factor, R_f, is used in the proposed method. This factor accounts for:

- The inability of a noncompact or slender compression to develop large inelastic strains without a reduction in the flange force contribution when the webs are nonslender.
- The inability of a noncompact or slender compression flange to accept stresses shed due to the bend buckling of a slender web.

4) Development of a cross-section model based on an effective width of the compression flange taking into account its postbuckling resistance. For box-section members with compact or noncompact webs, the proposed method allows the consideration of cross-section resistance larger than the yield moment and up to R_f times the plastic moment capacity of the effective cross-section. Box sections with compact or noncompact webs and a noncompact or slender compression flange can be encountered when considering biaxial bending. A box-section member with slender webs and compact flanges becomes a box-section member with compact webs and a noncompact or slender compression flange when considering bending about its other principal axis. The proposed method results in a significant improvement in the characterization of the cross-section capacity, allowing the consideration of large reserve strengths up to 37 % higher than those predicted by the AASHTO (2017) method and 39 % higher than those predicted by the Eurocode [CEN (2005); CEN (2006)] method.

5) The AISC plate slenderness limits for compact webs and compact flanges in box-section box sections are based on ensuring that the cross-section flexural resistance is M_p (plastic moment capacity) and that the section has sufficient rotation capacity. For plastic design these limits correspond to the Class 1 limits in Eurocode. However, if the only aim is to

be able to achieve a resistance equal to M_p, these plate slenderness limits can be relaxed. The proposed method utilizes relaxed plate slenderness limits for compact webs as can be seen from Table 3-6, where D_{ce} and D_{cpe} are depths of the webs in compression in the elastic range and at the plastic moment respectively, measured from the inside of the compression flange of the effective box cross-section. These limits are intended to be Class 2 limits. Although the aim is to relax the plate slenderness limit for compact flanges, this limit is made stricter in order to address the unconservatism observed in the classical Winter's effective width equation for characterizing the compressive resistance of non-longitudinally stiffened plates in welded box-section members, as discussed CHAPTER 2.

Table 3-6 Comparison of plate slenderness limits in AISC (2016) and the proposed method

	AISC (2016)	Proposed method
Compact web limit	$2.42\sqrt{\frac{E}{F_y}}$	$3.1\left(\frac{D_{ce}}{D_{cpe}}\right)\sqrt{\frac{E}{F_y}}$
Compact flange limit	$1.12\sqrt{\frac{E}{F_y}}$	$1.09\sqrt{\frac{E}{F_y}}$

CHAPTER 4. ULTIMATE COMPRESSIVE RESISTANCE OF LONGITUDINALLY STIFFENED PLATES

A good quantification of the ultimate compressive resistance of longitudinally stiffened plates is crucial for a good prediction of the axial compressive or flexural resistance of longitudinally stiffened welded box-section members. Section 4.1 reviews the current codified methods and prior research related to the calculation of the ultimate compressive resistance of longitudinally stiffened plates. The proposed method is explained in Section 4.2. Section 4.3 discusses the evaluation of the performance of the proposed method. The salient features of the proposed method are discussed in Section 4.4.

4.1 Literature review

This section reviews the current codified methods and prior research related to the calculation of the ultimate compressive resistance of longitudinally stiffened plates. This highlights the motivation for this thrust of the research.

4.1.1 General

Any method for calculating the ultimate compressive resistance of longitudinally stiffened plates should address the following potential failure modes of a longitudinally stiffened plate subjected to uniform axial compression:

- Overall buckling of a longitudinally stiffened plate with the plate subjected to flexural compression (as shown in Figure 4-1a).

- Overall buckling of a longitudinally stiffened plate with the longitudinal stiffener tip subjected to flexural compression (as shown in Figure 4-1b).
- Local buckling of the plate subpanels between the longitudinal stiffeners (as shown in Figure 4-1c).
- Tripping of the longitudinal stiffeners, i.e., torsional buckling of the stiffener about the stiffener-plate boundary (as shown in Figure 4-1d).
- Local buckling of the stiffener component plates.

In addition, generally there will be some interaction between these distinct failure modes. Figure 4-2 shows a failure involving the interaction between local buckling and overall buckling of a longitudinally stiffened plate.

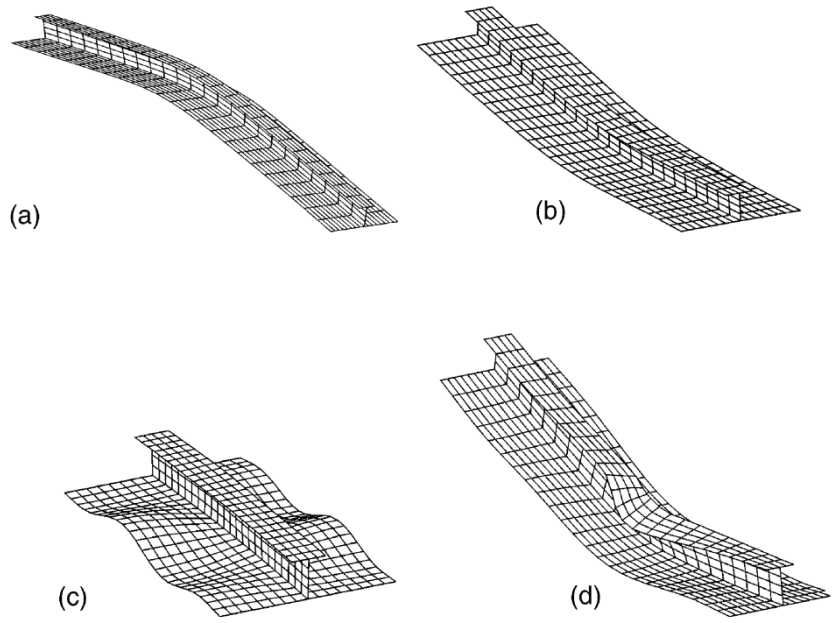

Figure 4-1 Typical buckling modes. (a) Overall buckling (plate in flexural compression); (b) overall buckling (stiffener tip in flexural compression); (c) plate buckling; and (d) stiffener tripping. (Sheikh et al. 2002).

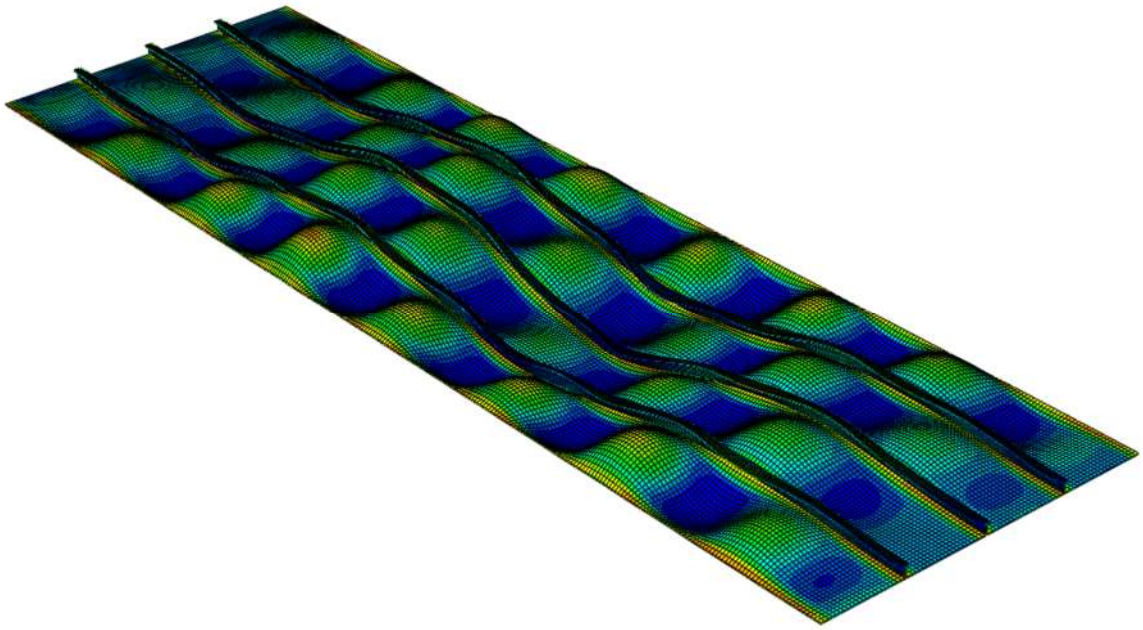

Figure 4-2 Representative failure mode involving interaction between local and overall buckling of a longitudinally stiffened plate

The prediction of the compressive resistance of longitudinally stiffened plates typically involves two steps:

1) Calculating the buckling strength,

2) Calculating the ultimate compressive strength.

Table 4-1 provides a broad summary of the existing methods for calculating the buckling resistance, and the ultimate compressive resistance of longitudinally stiffened plates. The various codified procedures use different combinations and forms of the methods listed in Table 4-1.

Table 4-1 Summary of existing methods for calculating the buckling resistance, and the ultimate compressive resistances of longitudinally stiffened plates

Buckling resistance	Ultimate compressive resistance
1) Strut idealization: The strut model is based on treating a longitudinally stiffened plate as a series of separate columns comprised of the longitudinal stiffener and an associated width of the plate, as shown in Figure 4-3. **2) Column on elastic foundation (CEF) idealization:** The CEF model considers a longitudinal stiffener strut (i.e., the longitudinal stiffener and an associated width of the plate) resting on an elastic foundation representing the transverse bending stiffness of the plate. Thus it avoids the limitation of the strut idealization of neglecting the transverse bending stiffness of the plate. This transverse bending stiffness can be significant especially in relatively narrow plates with one or two longitudinal stiffeners, which are commonly used in North America. **3) Orthotropic plate idealization:** The orthotropic plate idealization smears the stiffness characteristics of the longitudinal stiffeners over the entire plate. Thus, it takes into account the longitudinal bending, transverse bending, and torsional stiffness of the stiffened plate.	**1) Column strength curve:** Mapping to a column strength curve results in no consideration of the plate postbuckling resistance. Column strength curves have a short plateau (see Figure 4-4). **2) Plate strength curve:** Mapping to a plate strength curve, e.g., Winter's curve or von Karman's curve, results in a consideration of the postbuckling resistance. Plate strength curves have a longer plateau (see Figure 4-4). von Karman's equation is based on the assumption of an ideal concentrically-loaded, perfectly flat plate. However, in reality all plates have some initial out-of-flatness because of which it is a load-deflection problem rather than sudden buckling at the theoretical bifurcation point. This is taken into account in Winter's curve. **3) Interpolation between column and plate strength curves:** Because of the lack of an explicit compressive strength curve for longitudinally stiffened plates, the Eurocode (CEN 2006) requires an interpolation between column and plate ultimate strength curves. Figure 4-4 clearly shows the higher compressive resistance for plates, due to postbuckling, and also the longer plateau for plate ultimate strengths compared to column strengths.

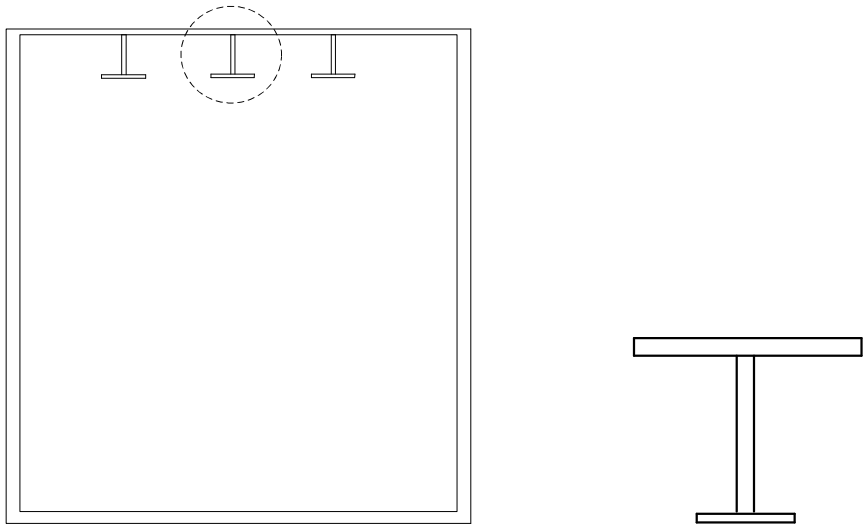

Figure 4-3 Longitudinally stiffened box and a stiffener strut

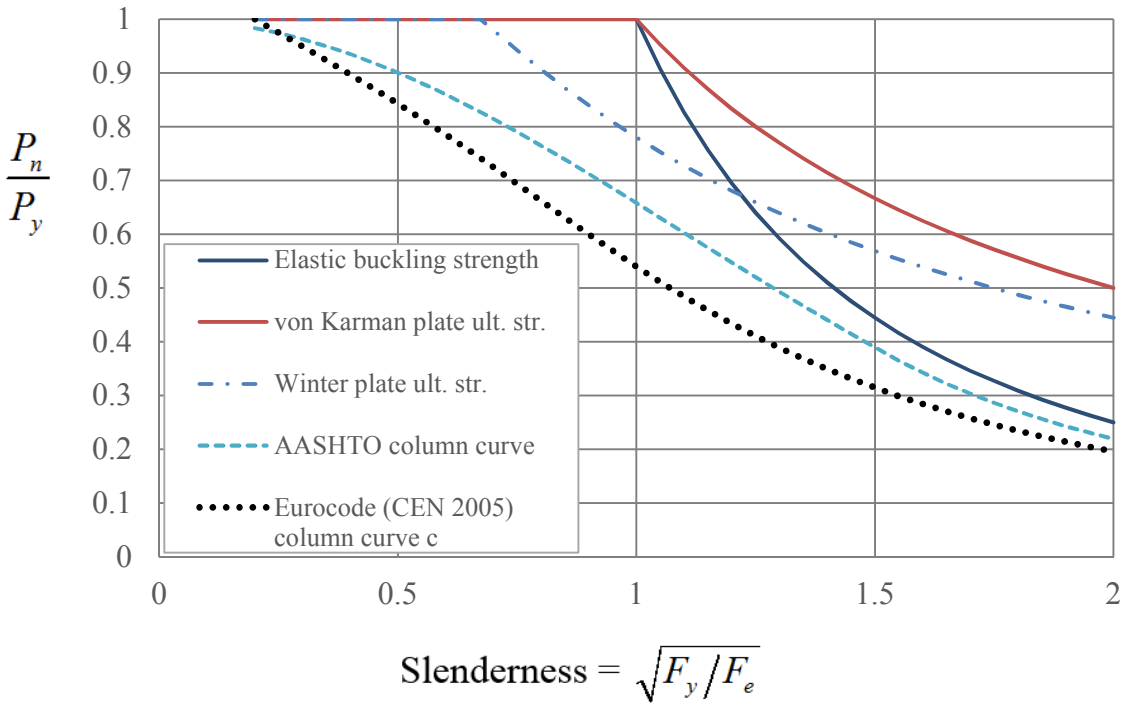

Figure 4-4 Axial compressive strength curves

4.1.2 Codified methods

This section provides a review of the various codified methods.

4.1.2.1 AASHTO (2017) Article 6.11.8.2

Provisions for calculating the ultimate compressive strength of longitudinally stiffened plates are given in Section 6.11.8.2 of AASHTO (2017). AASHTO (2017) calculates the axial compressive strength of a stiffened plate as the axial compressive buckling resistance of the subpanel between longitudinal stiffeners. It does not take into account the post-buckling resistance of the subpanels. For plates with one or two longitudinal stiffeners, the buckling coefficient is dependent on the moment of inertia of the longitudinal stiffeners. The formulae for plates with one or two longitudinal stiffeners assume infinitely long plates, i.e., no transverse stiffeners. White (2012) points out that these equations "*...which originate from Vincent (1969), are approximate equations that give values close to theoretical elastic buckling solutions for infinitely long, longitudinally stiffened plates from Goldberg and Levy (1957)*". The required moment of inertia of the longitudinal stiffeners to achieve a desired value of the plate buckling coefficient begins to increase dramatically as the number of stiffeners is increased beyond one. Hence, AASHTO (2017) recommends not exceeding one longitudinal stiffener.

For plates with more than two longitudinal stiffeners, AASHTO (2017) suggests adding transverse stiffeners to reduce the size of the longitudinal stiffeners. Article C6.11.11.2 gives requirements for the rigidity and spacing of the transverse stiffeners. However as pointed out by King (2017a), for plates with transverse stiffeners and more

than two longitudinal stiffeners, the value of the plate buckling coefficient in AASHTO (2017) is independent of the moment of inertia of the longitudinal stiffener.

The AASHTO (2017) method for calculating the ultimate compressive strength of longitudinally stiffened plates has the following shortcomings:

1) For slender plate subpanels susceptible to local buckling, the strength is limited to elastic buckling of the subpanel between the longitudinal stiffeners. This neglects the significant postbuckling resistance of the longitudinally stiffened plate subpanels.

2) The longitudinal stiffeners in wide plates with more than two longitudinal stiffeners tend to behave as unconnected struts. The key property influencing the compressive resistance of these types of plates is the moment of inertia of their longitudinal stiffeners. However, as pointed out by King (2017a), for these types of plates, the plate buckling coefficient in AASHTO, and hence the stiffened plate resistance, is independent of this key property.

3) For plates with more than two longitudinal stiffeners, AASHTO suggests the use of transverse stiffeners and requires the longitudinal stiffeners to satisfy a minimum moment of inertia requirement. This limits the designer's options in seeking the greatest design economy.

4) AASHTO (2017) requires a spacing of transverse stiffeners less than three times the width of the stiffened plate for the stiffeners to be considered effective. It would be better to provide design engineers more flexibility in choosing the transverse stiffener spacing.

5) AASHTO (2017) does not recognize the larger resistance of subpanels adjacent to the plate longitudinal edges. This aspect of the response is discussed in detail in Section 4.2.

6) AASHTO (2017) does not provide any guidance to prevent tee and angle section stiffener torsional buckling about the edge attached to the plate, i.e., "tripping" of the stiffeners (shown in Figure 4-1d and Figure 4-5). A tripping failure involves a drastic reduction in strength beyond the peak load; and hence such a failure must be avoided.

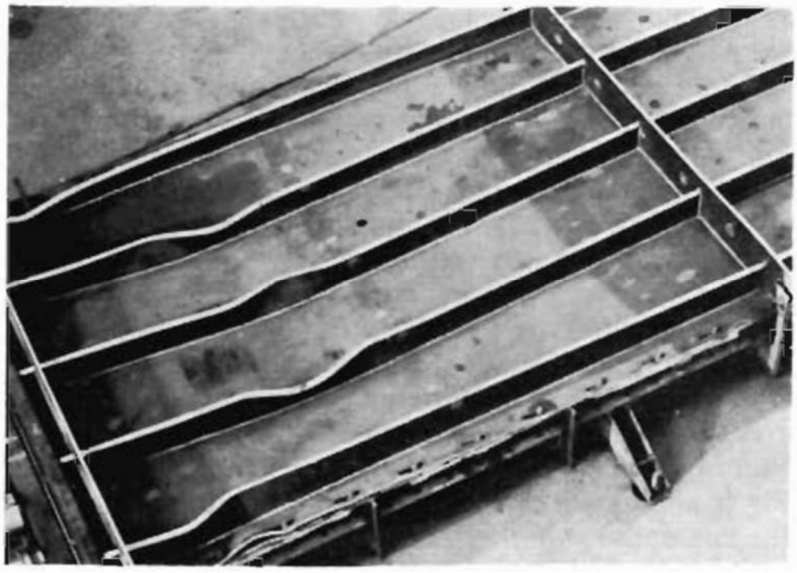

Figure 4-5 Tripping failure (Murray 1973)

4.1.2.2 AISI (2016)

The AISI (2016) method for calculating the ultimate compressive strength of longitudinally stiffened plates has the following drawbacks:

1) The method is intended for plates containing formed stiffeners. It does not have any provisions addressing stiffener local buckling, i.e., tripping of the stiffener or local buckling of the stiffener component plates.

2) The buckling coefficient is calculated as the minimum of the coefficients for buckling of the plate between longitudinal stiffeners (as shown in Figure 4-6) and overall buckling of the plate along with the longitudinal stiffeners (as shown in Figure 4-7). Thus it does not account directly for any interaction between local buckling of subpanels and overall buckling of the plate involving transverse displacement of the stiffeners.

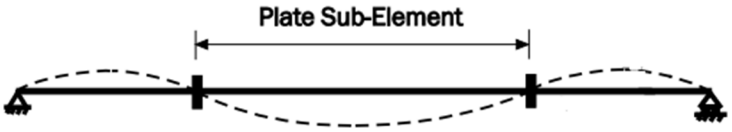

Figure 4-6 Local buckling (AISI 2016)

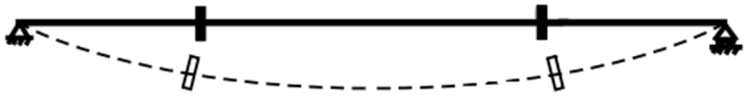

Figure 4-7 Overall buckling of the plate along with the stiffeners (AISI 2016)

3) The ultimate compressive strength of the stiffened plate is calculated by considering its postbuckling resistance using the Winter's effective width equation for unstiffened plates. It is inappropriate to count on this postbuckling resistance in all cases. For example, a wide thin plate with a large number of longitudinal stiffeners, where the longitudinal stiffeners and the tributary widths of the plate tend to behave as unconnected stiffener struts, will tend to have limited postbuckling resistance.

4.1.2.3 BS 5400 (BSI 2000)

BS 5400:3 (BSI 2000) uses a strut approach for calculating the ultimate compressive resistance of longitudinally stiffened plates. As explained in Table 4-1, the strut model is based on treating a longitudinally stiffened plate as a series of separate columns comprised of the longitudinal stiffener and an associated effective width of the plate. The effective width accounts for the postbuckling resistance of the subpanels between longitudinal stiffeners. BS 5400:3 has charts for calculating the effective width of the sub-panels.

The strength of the strut is calculated using a Perry-Robertson formula for a simply supported, imperfect column. BS 5400: 3 (BSI 2000) requires the design engineer to calculate an equivalent imperfection for the longitudinal stiffener strut which is related to the slenderness of the strut, residual stresses, and to the load eccentricity that may be present when evaluating the strength of stiffened flanges in box beams.

BS 5400:3 (BSI 2000) checks the following limits states:

- Yielding of stiffener tip in compression and
- Postbuckling or yielding of the plate.

Checking for the first yield of the stiffener is consistent with the observations by previous researchers (Murray 1973, Horne and Narayanan 1977) that there is little margin of strength above the load at which yielding first occurs in a stiffener. King (2017b) gives a possible reason for these observations, that many of the tests in the 1960's and 70's used bulb-flat stiffeners which were very slender, thus being more susceptible to tripping once

the bulb portion of the stiffener yields. In BS 5400:3 (BSI 2000), instability of the longitudinal stiffener is prevented by imposing restrictions on its dimensions.

A major limitation of the BS 5400: 3 (BSI 2000) method is that it does not account for the resistance offered by the transverse bending stiffness of the plate when the plate is transversely stiffened. It also does not account for the contribution from the torsional stiffness of the plate.

4.1.2.4 Eurocode (CEN 2006)

Eurocode aims to avoid the limitation of the strut approach of not accounting for the resistance offered by the plate, by using a column on elastic foundation model for plates with one or two longitudinal stiffeners. It recommends an orthotropic plate approach for plates with three or more longitudinal stiffeners subjected to compression.

The Eurocode (CEN 2006) method for calculating the ultimate compressive strength of longitudinally stiffened plates has the following limitations:

1) Because of the lack of availability of an ultimate compressive strength curve for stiffened plates, the Eurocode provisions interpolate between a column strength curve (no postbuckling resistance and a short plateau length) and a non-longitudinally stiffened plate strength curve (consideration of postbuckling resistance and a longer plateau length). The calculations associated with this interpolation approach are relatively long and cumbersome. As a result the design engineer can easily lose track of the parameters influencing the compressive resistance of the plate; hindering the ability to produce optimum designs.

2) The Eurocode method accounts for larger resistance of the half-width of the edge subpanels closest to the edge supports by considering that they reach the yield stress. However, as discussed later in this Section 4.2, the maximum resistance of the stiffened plate typically occurs before the half-width of the subpanel closest to the edge support reaches the yield stress.

3) For plates with one or two longitudinal stiffeners, the Eurocode calculations do not account for the contribution from the torsional stiffness of the plate.

4) The Eurocode provisions use different approaches for plates with one or two longitudinal stiffeners, and for plates with three or more longitudinal stiffeners. From the point of view of conceptually consistency, it would be preferable to use the same approach for plates with any number of longitudinal stiffeners. Section 4.2 and Appendix C provide justification for the use of orthotropic plate approach for any number of longitudinal stiffeners.

4.1.3 Prior research

There has been a large amount of research activity focussed on understanding the behaviour and quantifying the resistance of longitudinally stiffened plates subjected to uniform axial compression. Ziemian (2010) provides a summary of the prior research. The recommendations from prior research have been adopted in the various codified methods discussed in Section 4.1.2.

Timoshenko (1921) calculates the buckling stress of plates with one to three equally spaced longitudinal or transverse stiffeners. He considers hinged plate edges, and uses the

energy method for the solution. Chwalla (1936a and 1936b) considers a plate with one longitudinal stiffener in the middle of the plate stressed by pure bending, compression, or shear, and solves the problem using the energy method. Barbre (1939) develops complete buckling conditions for stiffened plates subjected to uniform compression. Wittrick (1968) performs a theoretical study to provide an approach for calculating the buckling stress of stiffened panels subjected to uniform longitudinal compression. Timoshenko (1921), Chwalla (1936a and 1936b), Barbre (1939), and Wittrick's (1968) work focusses on calculating the buckling stress of stiffened plates. As discussed in Section 4.1.1, the prediction of the compressive resistance of longitudinally stiffened plates involves two steps: 1) Calculating the buckling strength, and 2) Calculating the ultimate compressive strength.

Wolchuk and Mayrbaurl (1980) provide a method to quickly calculate the ultimate compressive strength of stiffened plates as a function of geometric parameters using an interaction diagram. This method uses an easy to understand strut model and is based largely on the theoretical work by Little (1976). The strut is comprised of the longitudinal stiffener and full tributary width of the associated plate. Wolchuk and Mayrbaurl (1980) account for the restraint provided by the transverse bending stiffness of the plate by considering a reduced effective length while calculating the strength of the stiffener strut. However, they do not account for the contribution from the torsional stiffness of the plate. They also do not recognize the larger resistance of subpanels adjacent to the plate longitudinal edges.

Yoo et al. (2001) and Choi et al. (2009) provide an equation for the minimum moment of inertia of longitudinal stiffeners to ensure the failure mode shown in Figure 4-6,

which they refer to as the "anti-symmetric buckling mode". This equation was derived using regression analysis of a large quantity of data obtained from finite element analyses. They also propose a plate strength curve that uses an inverse parabolic curve based on the CRC (1960) column curve, for the transition region between the yield plateau and elastic buckling. Their approach has many of the same shortcomings as the AASHTO (2017) method. Their approach neglects the significant postbuckling resistance of the longitudinally stiffened subpanels. It also does not recognize the larger resistance of subpanels adjacent to the plate longitudinal edges.

Herman (2001) tested the validity of the AASHTO design equations using finite element analyses and experimental tests. She recommends the use of approaches that allow the consideration of initial imperfections, residual stresses and longitudinal stiffener displacement, which better represents the observed behavior that longitudinal stiffeners do not form straight nodal lines. Strut-based models allow the consideration of these effects.

Schafer (1997) proposes a method for calculating the buckling and postbuckling resistance of longitudinally stiffened plates considering overall buckling of the plate along with the longitudinal stiffeners (see Figure 4-7) and local buckling of the subpanels (see Figure 4-6). The overall buckling of the plate along with the longitudinal stiffeners is based on an orthotropic plate idealization of the longitudinally stiffened plate. The recommendations by Schafer (1997) have been adopted in AISI (2016). The shortcomings of the AISI (2016) method for calculating the compressive resistance of longitudinally stiffened plates were discussed in Section 4.1.2.2.

Therefore, based on the discussions in Sections 4.1.1, 4.1.2, and 4.1.3, there is a need for a comprehensive yet designer-friendly (simple and intuitive) method for characterizing the ultimate compressive resistance of longitudinally stiffened plates.

4.2 Proposed Method

The proposed method is based on the developments by King (2017a). Sections 4.2.1 and 4.2.2 explain the calculation of the buckling and ultimate compressive resistance of longitudinally stiffened plates. Section 4.2.3 explains the restrictions on the longitudinal stiffener cross-section dimensions to prevent local buckling and tripping of the stiffeners. Section 4.2.4 explains the identification of five non-dimensional parameters that influence the compressive resistance of longitudinally stiffened plates.

4.2.1 Elastic Buckling resistance

The proposed method is based on an orthotropic plate idealization. Thus it considers all three contributions to the buckling resistance – longitudinal bending stiffness, transverse bending stiffness, and torsional stiffness. The differential equation of equilibrium for the orthotropic plate idealization of a longitudinally stiffened plate, simply supported on all four edges and subjected to uniformly distributed compressive load in its longitudinal direction, is

$$D_x \frac{\partial^4 \delta}{\partial x^4} + 2H \frac{\partial^4 \delta}{\partial x^2 \partial y^2} + D_y \frac{\partial^4 \delta}{\partial y^4} = -\frac{P_x}{b_{sp}} \frac{\partial^2 \delta}{\partial x^2} \tag{46}$$

where:

- x is the longitudinal direction of the plate;

- y is the lateral direction of the plate;
- δ is the transverse displacement of the plate;
- $D_x = \frac{EI_s}{w}$ (47)

  = flexural stiffness for bending about the y axis

- $I_s = I_x + \frac{wt_{sp}^{\ 3}}{12(1-\nu^2)} + wt_{sp}c_1^2$ (48)

  As a conservative simplification one may instead calculate I_s as

  $$I_s = I_x + \frac{wt_{sp}^{\ 3}}{12} + wt_{sp}c_1^2 \quad (49)$$

- I_x is taken as the moment of inertia of an individual longitudinal stiffener about an axis parallel to the face of the longitudinally stiffened plate element and passing through the centroid of the stiffener strut (the stiffener strut is composed of the longitudinal stiffener plus the tributary width of the longitudinally stiffened plate element under consideration).
- c_1 is the distance between the centroid of the longitudinally stiffened plate element and the centroid of the stiffener strut.
- $D_y = \frac{Et_{sp}^{\ 3}}{12\left(1-\nu^2\right)} = EI_p$ (50)

  = flexural stiffness for bending about the x axis;

  Equation 50 does not include any contribution from the transverse stiffeners because it is assumed that the transverse stiffeners (if present) are designed to hold a node line, i.e., buckling occurs between the transverse stiffeners and the transverse displacement of the transverse stiffeners is zero.

- $I_p = \dfrac{t_{sp}^{\ 3}}{12(1-\nu^2)}$ (51)

- $H = \dfrac{Et_{sp}^{\ 3}}{12(1-\nu^2)} = EI_p = D_y$ (52)

  = torsional stiffness;

  The torsional rigidity of the longitudinal stiffeners is neglected.

- E is the modulus of elasticity;

- P_x is the buckling load of the longitudinally stiffened plate.

Figure 4-8 illustrates the dimensional and area variables employed above and in the subsequent discussions for a representative longitudinally stiffened plate.

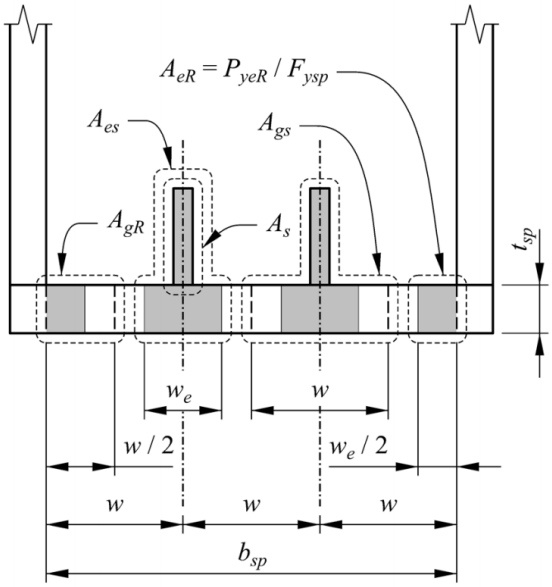

Figure 4-8 Illustration of variables for a longitudinally stiffened plate

The derivation of the differential equation of equilibrium for the orthotropic plate idealization of a longitudinally stiffened plate simply supported on all four edges and

subjected to uniformly distributed compressive load in its longitudinal direction can be found in Brush and Almroth (1975) and Allen and Bulson (1980). The kinematic and equilibrium relationships for the orthotropic plate are the same as that for an isotropic plate; only the constitutive relations are different. Knowing this and taking into account the two assumptions mentioned above, i) Transverse stiffeners (if present) are designed to hold a node line, ii) Torsional rigidity of the longitudinal stiffeners is neglected; it can be shown that the only difference between the differential equation of equilibrium for the orthotropic plate and for an isotropic plate is that the orthotropic plate has a larger flexural stiffness for bending about the y axis, D_x, because of the presence of longitudinal stiffeners. In other words, for an isotropic plate $D_x = D_y = H = EI_p$, whereas for an orthotropic plate (assuming transverse stiffeners are designed to hold a node line, and torsional rigidity of the longitudinal stiffeners is neglected) $D_y = H = EI_p$ but D_x is larger because of the presence of longitudinal stiffeners.

The buckling mode of the stiffened plate is given by,

$$\delta = \delta_{\max} \sin\frac{\pi x}{\ell} \sin\frac{\pi y}{b_{sp}} \tag{53}$$

where ℓ is the buckling length, taken as the smaller of the transverse stiffener spacing, *a*, and the characteristic buckling length, ℓ_c, explained later in this section. This can be justified as follows.

The buckling mode may be considered generally to be represented by a complete Fourier series Eq. 54 for a plate without intermediate transverse stiffeners, and Eq. 55 for a plate with intermediate transverse stiffeners; where L is the total length of the plate.

$$\delta = \sum_{m}^{\infty}\sum_{n}^{\infty}\delta_{mn}\sin\frac{m\pi x}{L}\sin\frac{n\pi y}{b_{sp}} \tag{54}$$

$$\delta = \sum_{m}^{\infty}\sum_{n}^{\infty}\delta_{mn}\sin\frac{m\pi x}{a}\sin\frac{n\pi y}{b_{sp}} \tag{55}$$

Assuming an infinitely long plate for plates without intermediate transverse stiffeners, the buckled mode for plates with or without intermediate transverse stiffeners can be written as

$$\delta = \sum_{m}^{\infty}\sum_{n}^{\infty}\delta_{mn}\sin\frac{m\pi x}{\ell}\sin\frac{n\pi y}{b_{sp}} \tag{56}$$

However, since we are only concerned with calculating a buckling load corresponding to an overall buckling mode as shown in Figure 4-7 (the proposed method accounts for local buckling, and the interaction between local buckling of subpanels and overall buckling of the plate, by using effective section properties when calculating the ultimate compressive resistance of the longitudinally stiffened plate), n should be equal to one and therefore we have

$$\delta = \sum_{m}^{\infty}\delta_{\max}\sin\frac{m\pi x}{\ell}\sin\frac{\pi y}{b_{sp}} \tag{57}$$

It is known that the buckled shape of a simply supported isotropic plate subjected to uniform compression in the longitudinal direction is a double sine curve (Allen and Bulson 1980). Because the buckled shape of an orthotropic plate should also be a sine curve in the longitudinal direction, m should be equal to one. Therefore the buckling mode of the stiffened plate is as given in Eq. 53.

Next, let us consider the implications of the following two approximations:

1) Assuming an infinitely long plate for plates without intermediate transverses stiffeners.

This will result in slightly conservative strength predictions when $L > \ell_c$ and L is not an integer multiple of ℓ_c. For a plate without intermediate transverse stiffeners the minimum buckling load corresponds to a buckling length equal to ℓ_c when $L > \ell_c$ (i.e., when $L > \ell_c$ for minimum buckling load the total length of the plate should be an integer multiple of ℓ_c). If L is not an integer multiple of ℓ_c, when $L > \ell_c$, then the actual buckling load will higher than the buckling load predicted by the proposed method corresponding to a buckling length equal to ℓ_c. This conservatism reduces for larger values of $\frac{L}{\ell_c}$.

2) Taking ℓ as the smaller of the transverse stiffener spacing, *a*, and the characteristic buckling length, ℓ_c.

For plates with intermediate transverse stiffeners, this will result in slightly conservative strength predictions when $a > \ell_c$ and a is not an integer multiple of ℓ_c. For a plate with intermediate transverse stiffeners the minimum buckling load corresponds to

a buckling length equal to ℓ_c when $a > \ell_c$ (i.e., when $a > \ell_c$, for minimum buckling load a should be an integer multiple of ℓ_c). If a is not an integer multiple of ℓ_c, when $a > \ell_c$, then the actual buckling load will higher than the buckling load predicted by the proposed method corresponding to a buckling length equal to ℓ_c. However, this is not considered to be a drawback because a salient feature of the proposed method is that since designers know ℓ_c they should be able to decide an optimum spacing of the transverse stiffeners.

Substituting the displacement solution given in Eq. 53, which satisfies the differential equation of equilibrium and the specified boundary conditions, one can write the solution to the governing equation as:

$$\frac{P_x}{b_{sp}}\left(\frac{\pi}{\ell}\right)^2 = \frac{EI_s}{w}\left(\frac{\pi}{\ell}\right)^4 + 2EI_p\left(\frac{\pi}{\ell}\right)^2\left(\frac{\pi}{b_{sp}}\right)^2 + EI_p\left(\frac{\pi}{b_{sp}}\right)^4 \tag{58}$$

$$P_x = \frac{b_{sp}EI_s}{w}\left(\frac{\pi}{\ell}\right)^2 + 2b_{sp}EI_p\left(\frac{\pi}{b_{sp}}\right)^2 + b_{sp}EI_p\left(\frac{\pi}{b_{sp}}\right)^4\left(\frac{\ell}{\pi}\right)^2 \tag{59}$$

Since $b_{sp} = (n+1)w$, where n is the number of longitudinal stiffeners

$$P_x = (n+1)EI_s\left(\frac{\pi}{\ell}\right)^2 + 2b_{sp}EI_p\left(\frac{\pi}{b_{sp}}\right)^2 + b_{sp}EI_p\left(\frac{\pi}{b_{sp}}\right)^4\left(\frac{\ell}{\pi}\right)^2 \tag{60}$$

Thus, we have calculated the elastic buckling load of a longitudinally stiffened plate using the orthotropic plate idealization. Equation 60 when expressed as stress, is equivalent to the distortional buckling stress calculated as $k_d \frac{\pi^2 E}{12(1-\nu^2)}\left(\frac{t}{b_o}\right)^2$ in Appendix 1 of AISI

(2016). This elastic buckling load calculated using an orthotropic plate idealization can also be expressed in a convenient and intuitive form using the column on elastic foundation model along with the torsional stiffness of the plate, as explained below.

The buckling load per individual stiffener strut width, *w*, may be expressed as,

$$\frac{P_x}{(n+1)} = EI_s\left(\frac{\pi}{\ell}\right)^2 + 2\frac{1}{(n+1)}b_{sp}EI_p\left(\frac{\pi}{b_{sp}}\right)^2 + b_{sp}\frac{1}{(n+1)}EI_p\left(\frac{\pi}{b_{sp}}\right)^4\left(\frac{\ell}{\pi}\right)^2 \tag{61}$$

Rearranging terms,

$$\frac{P_x}{(n+1)} = EI_s\left(\frac{\pi}{\ell}\right)^2 + b_{sp}\frac{1}{(n+1)}EI_p\left(\frac{\pi}{b_{sp}}\right)^4\left(\frac{\ell}{\pi}\right)^2 + 2\frac{1}{(n+1)}b_{sp}EI_p\left(\frac{\pi}{b_{sp}}\right)^2 \tag{62}$$

Simplifying,

$$\frac{P_x}{(n+1)} = EI_s\left(\frac{\pi}{\ell}\right)^2 + \frac{\pi^4}{(n+1)}\frac{EI_p}{b_{sp}^3}\frac{\ell^2}{\pi^2} + 2\frac{1}{(n+1)}b_{sp}E\frac{t_{sp}^{\ 3}}{12(1+\nu)(1-\nu)}\left(\frac{\pi}{b_{sp}}\right)^2 \tag{63}$$

$$\frac{P_x}{(n+1)} = \left[EI_s\frac{\pi^2}{\ell^2} + \frac{\pi^4}{(n+1)}\frac{EI_p}{b_{sp}^3}\frac{\ell^2}{\pi^2}\right] + \frac{\pi^2}{3(n+1)(1-\nu)}\frac{Gt_{sp}^{\ 3}}{b_{sp}} \tag{64}$$

$$\frac{P_x}{(n+1)} = \left[EI_s\frac{\pi^2}{\ell^2} + \pi^4 w\frac{EI_p}{b_{sp}^4}\frac{\ell^2}{\pi^2}\right] + \frac{\pi^2}{(1-\nu)b_{sp}^2}\frac{Gwt_{sp}^3}{3} \tag{65}$$

This can be written as,

$$P_{es} = P_{esF} + P_{esT} \tag{66}$$

where:

- $P_{es} = \dfrac{P_x}{(n+1)}$ (67)

  = Buckling load of a stiffener strut (kip)

- $P_{esF} = \left[\dfrac{\pi^2 EI_s}{\ell^2} + k_p \dfrac{\ell^2}{\pi^2} \right]$ (68)

  = elastic flexural buckling resistance of an individual stiffener strut (kip)

- $P_{esT} = \dfrac{\pi^2}{(1-\nu) b_{sp}^2} \dfrac{Gwt_{sp}^3}{3}$ (69)

  = plate torsional stiffness contribution to the elastic buckling resistance of an individual stiffener strut (kip)

- $k_p = \pi^4 w \dfrac{EI_p}{b_{sp}^4}$ (70)

  = plate transverse stiffness coefficient (kip/inch^2)

For an infinitely long plate the characteristic buckling length, ℓ_c, is the length that results in the minimum value of P_{es}. Therefore,

$$\frac{dP_{es}}{d\ell_c} = \frac{d\left(\dfrac{\pi^2 EI_s}{\ell_c^{\,2}} + k_p \dfrac{\ell_c^{\,2}}{\pi^2} \right)}{d\ell_c} = 0 \tag{71}$$

gives

$$\ell_c = \left(\frac{EI_s \pi^4}{k_p} \right)^{1/4} \tag{72}$$

It is commonly believed that the orthotropic plate idealization provides a good representation of a longitudinally stiffened plate only for plates with three or more longitudinal stiffeners. However, it can be shown that the orthotropic plate idealization presented here works well even for plates with one or two longitudinal stiffeners. It is shown in Appendix C that, for plates with one or two longitudinal stiffeners the buckling load calculated by considering a column on elastic foundation model (where the column represents the stiffener strut and the elastic foundation stiffness represents the transverse bending stiffness of the plate) along with the consideration of torsional stiffness of the plate, gives a buckling load approximately equal to that obtained using the orthotropic plate idealization discussed above. This justifies the use of the orthotropic plate approach by the proposed method for any number of longitudinal stiffeners.

4.2.2 Ultimate compressive resistance

Knowing the elastic buckling load $P_{es} = P_{esF} + P_{esT}$, the ultimate compressive strength of a longitudinally stiffened plate can be calculated as

$$P_{nsp} = \sum P_{ns} + 2P_{nR} \tag{73}$$

where:

- $P_{ns} = P_{nsF} + 0.15P_{esT} \le P_{yes}$

  = nominal compressive resistance of an individual stiffener strut composed of the stiffener plus the tributary width of the longitudinally stiffened plate (kip);

- P_{nsF} = nominal flexural buckling resistance of an individual stiffener strut determined by mapping the elastic flexural buckling load P_{esF} via the AISC/AASHTO column curve as shown below:

  If $\frac{P_{ys}}{P_{esF}} \leq 2.25$, then

  $$P_{nsF} = 0.658^{\frac{P_{ys}}{P_{esF}}} P_{yes} \tag{74}$$

  Otherwise,

  $$P_{nsF} = 0.877 \frac{P_{esF}}{A_{gs}} A_{es} \tag{75}$$

- $P_{yes} = F_{ysp} A_{es}$ (76)

  = effective yield load of an individual stiffener strut (kip);

- $$P_{nR} = \left(1 - \frac{P_{ns}}{P_{yes}}\right)\left(F_{ysp} + \frac{P_{ns}}{A_{es}}\right)0.45 A_{gR} + \left(\frac{P_{ns}}{P_{yes}}\right) P_{yeR} \leq P_{yeR} \tag{77}$$

  = compressive resistance provided by the half-width of a subpanel adjacent to a transversely-restrained longitudinal edge of the longitudinally stiffened plate (kip). This equation recognizes that the edge stress is larger than the ultimate stress of the stiffener strut and it also takes into account the observations from the parametric study discussed in Section 4.3.1, and the observations made by King (2017a) that the edge stress is typically less than yield stress under the ultimate strength condition.

  This equation specifies a simple linear interpolation between (1) the yield load of the edge, P_{yeR}, based on the plate effective width tributary to the edge, in the limit

that P_{ns} is equal to P_{yes}, and (2) the compression force given by $0.45\left(F_{ysp} + P_{ns}/A_{es}\right)$ acting on A_{gR}, in the limit that P_{ns} becomes small.

Figure 4-9 shows the stress distribution and the corresponding effective width when P_{ns} is equal to P_{yes}, which corresponds to a local buckling mode. Figure 4-10 shows the stress distribution and the corresponding effective width when P_{ns} becomes small, which corresponds to an overall buckling mode.

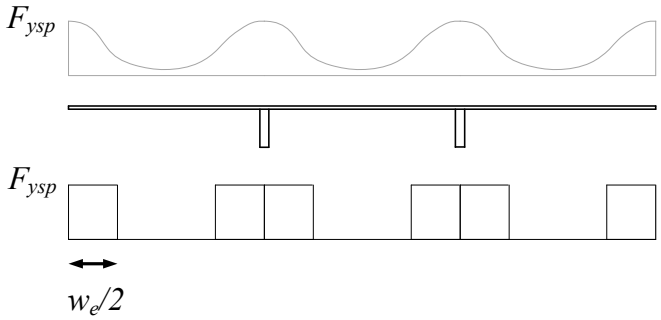

Figure 4-9 Stress distribution and the corresponding effective width when P_{ns} is equal to P_{yes}

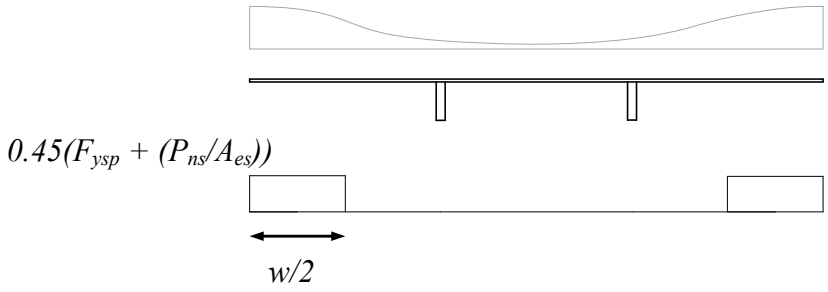

Figure 4-10 Stress distribution and the corresponding effective width when P_{ns} becomes small

- $P_{yeR} = F_{ysp}\dfrac{w_e}{2}t_{sp}$ (78)

  = effective yield load of the half-width of a subpanel adjacent to a transversely-restrained longitudinal edge of the longitudinally stiffened plate (kip);

- $P_{yR} = F_{ysp} \frac{w}{2} t_{sp}$ (79)

  = yield load of the half-width of a subpanel adjacent to a transversely-restrained longitudinal edge of the longitudinally stiffened plate (kip);

- $P_{ys} = F_{ysp} A_{gs}$ (80)

  = yield load of an individual stiffener strut (kip);

- $A_{es} = A_s + w_e t_{sp}$ (81)

  = effective area of an individual stiffener strut (in.^{2});

- $A_{gR} = \frac{w}{2} t_{sp}$ (82)

  = gross area of the half-width of a subpanel adjacent to a transversely-restrained longitudinal edge of the longitudinally stiffened plate (in.^{2});

- $A_{gs} = A_s + w t_{sp}$ (83)

  = gross area of an individual stiffener strut (in.^{2});

- A_s = gross area of an individual longitudinal stiffener, excluding the tributary width of the longitudinally stiffened plate element under consideration (in.^{2});
- F_{ysp} = specified minimum specified yield strength of the longitudinally stiffened plate (ksi);
- w_e = effective width of the plate between the longitudinal stiffeners or between a longitudinal stiffener and the transversely-restrained longitudinal edge of the longitudinally stiffened plate, as applicable. This width is calculated as follows:

- For plates with one longitudinal stiffener, it is calculated using the modified Winter's effective width equation discussed in Section 2.2, with F_{cr} taken as F_{ysp} and with λ_r taken as $1.09\sqrt{E/F_{ysp}}$,
- For plates with two or more longitudinal stiffeners, it is calculated using the Winter's effective width equation as given in AISC (2016), with F_{cr} taken as F_{ysp} and with λ_r taken as $1.49\sqrt{E/F_{ysp}}$. This is a simple, approximate way of accounting for the larger available buckling and postbuckling resistance due to the restraint from the adjacent subpanels.

The postbuckling resistance of non-longitudinally stiffened plates is directly proportional to the middle surface strains present during bending, i.e., stretching of the middle plane of the plate during bending. This is influenced by the constraints along the unloaded edges of the plate. Allen and Bulson (1980) provide a good discussion of the influence of the constraints along the unloaded edges of the plate. Tensile lateral middle surface stresses stiffen the plate and provide larger resistance to the transverse displacement of the plate. Figure 4-11 shows the alternative tensile and compressive lateral middle surface stress distribution when the unloaded edges are constrained to remain straight.

If the unloaded edges are not constrained to remain straight (free to move laterally inwards or outwards), then there are no lateral middle surface stresses, as shown in Figure 4-12. In the proposed method, the postbuckling resistance of the subpanels between longitudinal stiffeners is calculated by treating them as non-longitudinally stiffened plates. The adjacent subpanels provide lateral restraint,

resulting in a larger postbuckling resistance. The proposed method accounts for this larger postbuckling resistance in a simple, approximate way by using Winter's effective width equation instead of the modified Winter's effective width equation for plates with two or more longitudinal stiffeners.

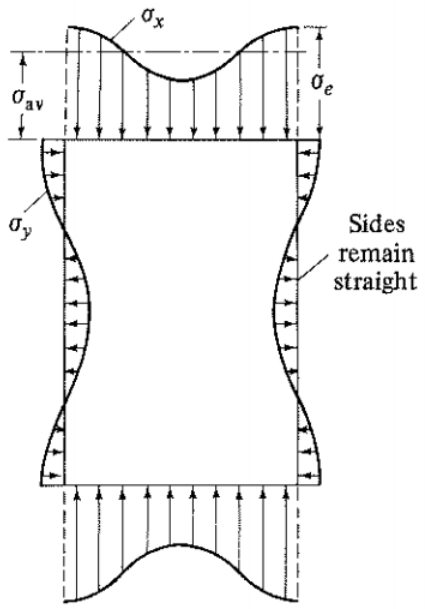

Figure 4-11 Postbuckled stress distribution when unloaded edges are constrained to remain straight (Credit: Allen and Bulson 1980)

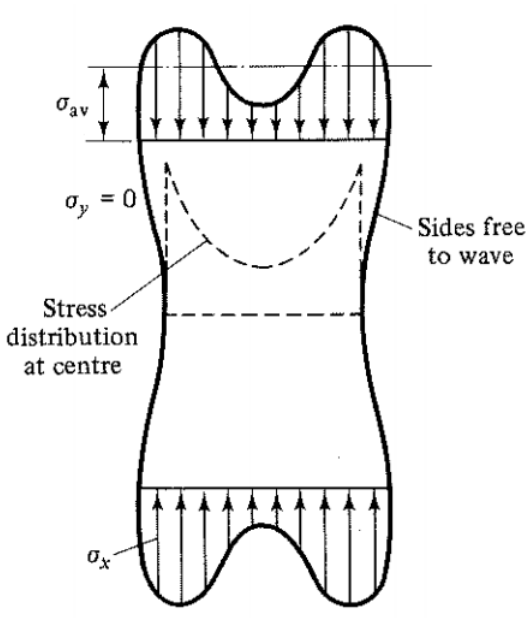

Figure 4-12 Postbuckled stress distribution when sides are free to move laterally inwards or outwards (Credit: Allen and Bulson 1980)

P_{esT} is multiplied by the calibration factor 0.15 to capture the plate torsional stiffness contribution to the resistance of the stiffener struts. King (2017a) shows that as the buckling resistance of a plate approaches yield stress, the torsional stiffness provides much of the stability to the plate;

Unlike AISI (2016), the proposed method accounts for the interaction between local buckling of subpanels and overall buckling of the plate involving transverse displacement of the stiffeners, by using effective section properties (using effective widths of the subpanels between longitudinal stiffeners, taking into account their postbuckling resistance) while calculating the flexural buckling resistance of the individual stiffener struts, P_{nsF}. Also, the calculation of P_{nR} considers the possibility of a failure mode involving the combination of local buckling of the subpanels and overall buckling of the plate involving transverse displacement of the stiffeners.

4.2.3 Restrictions on longitudinal stiffener cross-section dimensions

The proposed method is applicable to plates with longitudinal stiffeners that satisfy the following requirements:

- The specified minimum yield strength of the stiffeners shall not be less than the specified minimum yield strength of the plate to which they are attached. This ensures that the longitudinal stiffener does yield before the plate, avoiding a situation where the early yielding of the longitudinal stiffener nullifies the stiffening of the plate.
- The slenderness of the longitudinal stiffener cross-section elements shall be such that local buckling does not impact the resistance of the longitudinal stiffeners.
- Additionally, tee and angle section stiffeners shall satisfy the following requirement which ensures that torsional buckling of these stiffeners about the edge of the stiffener attached to the plate is prevented:

$$\frac{J_s}{I_{ps}} \geq 5.0 \frac{F_{ysp}}{E} \tag{84}$$

In this equation, J_s is the St. Venant torsional constant of the longitudinal stiffener alone, not including the contribution from the stiffened plate and I_{ps} is the polar moment of inertia of the longitudinal stiffener alone about the attached edge. For flat plate stiffeners, this corresponds to a plate slenderness limit of $0.45\sqrt{E/F_y}$, which is the nonslender plate limit specified in AASHTO (2017) Article 6.9.4.2.1. Equation 84 is derived by imposing the limit

$$F_{cr.tor} \geq 1.923 F_y \tag{85}$$

where

$$F_{cr.tor} = \frac{GJ_s}{I_{ps}} \tag{86}$$

= elastic torsional buckling stress of the stiffener for buckling about the edge attached to the plate. This is similar to the approach used in Eurocode (CEN 2006), and is discussed in Johansson et al. (2007).

Bleich (1952) gives an equation for buckling stress for torsional buckling with enforced axis of rotation (constrained axis torsional buckling). In many practical cases the warping contribution to the torsional resistance tends to be small because of the large distance between the locations of torsional restraint at transverse stiffeners and/or diaphragms. Therefore, conservatively neglecting the warping contribution to the torsional resistance we obtain the result in Eq. 86.

4.2.4 Identification of five non-dimensional parameters that influence the elastic buckling resistance of longitudinally stiffened plates

The elastic buckling load is derived in Section 4.2.1 and is given by

$$P_{es} = \frac{P_x}{(n+1)} = P_{esF} + P_{esT} = \left[EI_s \frac{\pi^2}{\ell^2} + \pi^4 w \frac{EI_p}{b_{sp}^4} \frac{\ell^2}{\pi^2} \right] + \frac{\pi^2}{(1-\nu) b_{sp}^2} \frac{Gwt_{sp}^3}{3} \tag{87}$$

Replacing ℓ by $\left(\frac{\ell}{\ell_c} \right) \ell_c$ gives

$$P_{es} = P_{esF} + P_{esT} = \left[EI_s \frac{\pi^2}{\left(\frac{\ell}{\ell_c}\right)^2 \left(\frac{EI_s\pi^4}{k_p}\right)^{1/2}} + k_p \frac{\left(\frac{\ell}{\ell_c}\right)^2 \left(\frac{EI_s\pi^4}{k_p}\right)^{1/2}}{\pi^2} \right] + \left[\frac{\pi^2}{3(n+1)(1-\nu)} \frac{Gt_{sp}{}^3}{b_{sp}} \right] \tag{88}$$

which simplifies to

$$P_{es} = P_{esF} + P_{esT} = \left[\sqrt{\frac{k_p EI_s}{\left(\frac{\ell}{\ell_c}\right)^4}} + \sqrt{\left(\frac{\ell}{\ell_c}\right)^4 k_p EI_s} \right] + \left[\frac{\pi^2}{3(n+1)(1-\nu)} \frac{Gt_{sp}{}^3}{b_{sp}} \right] \tag{89}$$

The corresponding buckling stress is obtained by dividing by A_{gs}.

$$\frac{P_{es}}{A_{gs}} = F_{esF} + F_{esT} = \frac{1}{A_{gs}} \left[\sqrt{\frac{k_p EI_s}{\left(\frac{\ell}{\ell_c}\right)^4}} + \sqrt{\left(\frac{\ell}{\ell_c}\right)^4 k_p EI_s} \right] + \frac{1}{A_{gs}} \left[\frac{\pi^2}{3(n+1)(1-\nu)} \frac{Gt_{sp}{}^3}{b_{sp}} \right] \tag{90}$$

a) Focusing first on the flexural buckling component, F_{esF}:

$$F_{esF} = \frac{1}{A_{gs}} \left[\sqrt{\frac{k_p EI_s}{\left(\frac{\ell}{\ell_c}\right)^4}} + \sqrt{\left(\frac{\ell}{\ell_c}\right)^4 k_p EI_s} \right] \tag{91}$$

$$F_{esF} = \frac{1}{A_{gs}}\left[\sqrt{\frac{1}{\left(\frac{\ell}{\ell_c}\right)^4}\pi^4 w\frac{EI_p}{b_{sp}^4}EI_s} + \sqrt{\left(\frac{\ell}{\ell_c}\right)^4\pi^4 w\frac{EI_p}{b_{sp}^4}EI_s}\right] \tag{92}$$

$$F_{esF} = \frac{1}{A_{gs}}\left[\sqrt{\frac{1}{\left(\frac{\ell}{\ell_c}\right)^4}\pi^4\frac{b_{sp}}{(n+1)}\frac{EI_p}{b_{sp}^4}EI_s} + \sqrt{\left(\frac{\ell}{\ell_c}\right)^4\pi^4\frac{b_{sp}}{(n+1)}\frac{EI_p}{b_{sp}^4}EI_s}\right] \tag{93}$$

$$F_{esF} = \frac{1}{A_{gs}}\left[\frac{1}{\left(\frac{\ell}{\ell_c}\right)^2}\pi^2\frac{E}{b_{sp}^2}\sqrt{\frac{1}{12(1-\nu^2)}\frac{b_{sp}t_{sp}^3}{(n+1)}I_s} + \left(\frac{\ell}{\ell_c}\right)^2\pi^2\frac{E}{b_{sp}^2}\sqrt{\frac{1}{12(1-\nu^2)}\frac{b_{sp}t_{sp}^3}{(n+1)}I_s}\right] \tag{94}$$

Multiplying and dividing by $\frac{wt_{sp}^3}{12(1-\nu^2)}$

$$F_{esF} = \frac{1}{A_{gs}}\left[\begin{array}{l}\frac{1}{\left(\frac{\ell}{\ell_c}\right)^2}\frac{\pi^2}{b_{sp}^2}\frac{Et_{sp}^3}{12(1-\nu^2)}w\frac{12(1-\nu^2)}{t_{sp}^3}\frac{1}{w}\sqrt{\frac{wt_{sp}^3}{12(1-\nu^2)}I_s} \\ +\left(\frac{\ell}{\ell_c}\right)^2\frac{\pi^2}{b_{sp}^2}\frac{Et_{sp}^3}{12(1-\nu^2)}w\frac{12(1-\nu^2)}{t_{sp}^3}\frac{1}{w}\sqrt{\frac{wt_{sp}^3}{12(1-\nu^2)}I_s}\end{array}\right] \tag{95}$$

$$F_{esF} = \frac{1}{A_{gs}}\left[\left(\frac{1}{\left(\frac{\ell}{\ell_c}\right)^2}+\left(\frac{\ell}{\ell_c}\right)^2\right)\frac{\pi^2}{b_{sp}^2}\frac{Et_{sp}^3}{12(1-\nu^2)}w\frac{12(1-\nu^2)}{t_{sp}^3}\frac{1}{w}\sqrt{\frac{wt_{sp}^3}{12(1-\nu^2)}I_s}\right] \tag{96}$$

$$F_{esF} = \frac{1}{A_{gs}}\left[\left(\frac{1}{\left(\frac{\ell}{\ell_c}\right)^2} + \left(\frac{\ell}{\ell_c}\right)^2\right)\frac{\pi^2}{b_{sp}^2}\frac{Et_{sp}^3}{12(1-\nu^2)}w\sqrt{\frac{12(1-\nu^2)}{wt_{sp}^3}I_s}\right] \tag{97}$$

Since $b_{sp} = (n+1)w$, F_{esF} can be written as

$$F_{esF} = \left(\frac{1}{\left(\frac{\ell}{\ell_c}\right)^2} + \left(\frac{\ell}{\ell_c}\right)^2\right)\frac{\pi^2 E}{12(1-\nu^2)w^2}\frac{t_{sp}^3}{(n+1)^2}\frac{w}{A_{gs}}\left(\sqrt{\frac{I_s}{wI_p}}\right) \tag{98}$$

$$F_{esF} = \frac{\pi^2 E}{12(1-\nu^2)}\frac{1}{(n+1)^2}\frac{1}{\left(\frac{w}{t_{sp}}\right)^2}\frac{1}{\left(\frac{A_{gs}}{wt_{sp}}\right)}\left(\sqrt{\frac{I_s}{wI_p}}\right)\left[\frac{1}{\left(\frac{\ell}{\ell_c}\right)^2} + \left(\frac{\ell}{\ell_c}\right)^2\right] \tag{99}$$

b) Second, focusing on the torsional stiffness component, F_{esT}

$$F_{esT} = \frac{1}{A_{gs}}\left[\frac{\pi^2}{3(n+1)(1-\nu)}\frac{Gt_{sp}{}^3}{b_{sp}}\right] \tag{100}$$

$$F_{esT} = \frac{1}{A_{gs}}\left[\frac{1}{12(1-\nu^2)}\frac{b_{sp}t_{sp}^3}{(n+1)}2\pi^2\frac{E}{b_{sp}^2}\right] \tag{101}$$

$$F_{esT} = \frac{1}{A_{gs}}\left[\frac{2\pi^2}{b_{sp}^2}\frac{Et_{sp}^3}{12(1-\nu^2)}\frac{b_{sp}}{(n+1)}\right] \tag{102}$$

$$F_{esT} = \frac{1}{A_{gs}}\left[\frac{2\pi^2}{b_{sp}^2}\frac{Et_{sp}^3}{12(1-\nu^2)}w\right] \tag{103}$$

Since $b_{sp} = (n+1)w$, F_{esT} can be written as

$$F_{esT} = \frac{\pi^2 E}{6(1-\nu^2)w^2}\frac{t_{sp}^3}{(n+1)^2}\frac{w}{A_{gs}} \tag{104}$$

$$F_{esT} = \frac{\pi^2 E}{6(1-\nu^2)}\frac{1}{(n+1)^2}\frac{1}{\left(\frac{w}{t_{sp}}\right)^2}\frac{1}{\left(\frac{A_{gs}}{wt_{sp}}\right)} \tag{105}$$

Thus, the buckling stress can be written as,

$$\frac{P_{es}}{A_{gs}} = F_{esF} + F_{esT}$$

$$= \frac{\pi^2 E}{12(1-\nu^2)}\frac{1}{(n+1)^2}\frac{1}{\left(\frac{w}{t_{sp}}\right)^2}\frac{1}{\left(\frac{A_{gs}}{wt_{sp}}\right)}\left(\sqrt{\frac{I_s}{wI_p}}\right)\left[\frac{1}{\left(\frac{\ell}{\ell_c}\right)^2} + \left(\frac{\ell}{\ell_c}\right)^2\right] \tag{106}$$

$$+ \frac{\pi^2 E}{6(1-\nu^2)}\frac{1}{(n+1)^2}\frac{1}{\left(\frac{w}{t_{sp}}\right)^2}\frac{1}{\left(\frac{A_{gs}}{wt_{sp}}\right)}$$

$$\frac{P_{es}}{A_{gs}} = \frac{\pi^2 E}{12(1-\nu^2)}\frac{1}{(n+1)^2}\frac{1}{\left(\frac{w}{t_{sp}}\right)^2}\frac{1}{\left(\frac{A_{gs}}{wt_{sp}}\right)}\left[\sqrt{\frac{I_s}{wI_p}}\left(\frac{1}{\left(\frac{\ell}{\ell_c}\right)^2} + \left(\frac{\ell}{\ell_c}\right)^2\right) + 2\right] \tag{107}$$

Based on the above development, the following five non-dimensional parameters can be identified which influence the elastic buckling resistance of longitudinally stiffened plates:

- n

- $\frac{w}{t_{sp}}$
- $\frac{A_{gs}}{wt_{sp}}$
- $\frac{I_s}{wI_p}$
- $\frac{\ell}{\ell_c}$

It can be noted that both $\frac{A_{gs}}{wt_{sp}}$ and $\frac{I_s}{wI_p}$ provide a measure of the contribution of the stiffener strut compared to the contribution from the associated plate width. The subsequent studies show that the influence of $\frac{I_s}{wI_p}$ is relatively minor, however. This might be anticipated, since this term $\frac{I_s}{wI_p}$ appears under the radical.

4.3 Evaluation of the performance of the proposed method

The performance of the proposed method is evaluated using data from a parametric study performed using finite element test simulations, as well as using available experimental data. It is found that the predictions using the proposed method correlate well with benchmark results, and are significantly better than the predictions using the methods in AASHTO (2017), AISI (2016), and Eurocode (CEN 2006).

4.3.1 Parametric study performed using finite element test simulations

Section 4.3.1.1 explains the parametric study design. Section 4.3.1.2 provides a discussion of the parametric study results. The finite element modelling of the plates is explained in Appendix A.

4.3.1.1 Parametric study design

A total of 118 cases are studied, considering various practical combinations of the non-dimensional parameters affecting the compressive resistance of a longitudinally stiffened plate, discussed in Section 4.2.4. The parametric study is divided into four groups:

Group 1: Long and narrow plates with one or two flat longitudinal stiffeners, and no intermediate transverse stiffeners. These types of plates have significant transverse bending stiffness, and are commonly used in North America.

Group 2: Same as Group 1, except Tee stiffeners are used in place of the flat longitudinal stiffeners. The objective here is to compare the results with the corresponding Group 1 cases to determine the significance of the stiffener type, i.e., the influence of the parameter $\frac{I_s}{wI_p}$ on the compressive resistance.

Group 3: Short and wide plates with three or five flat longitudinal stiffeners, and three intermediate transverse stiffeners. These plates have relatively small transverse bending stiffness, and can be idealized as a series of disconnected stiffener struts.

Group 4: Same as Group 3, except Tee stiffeners are used in place of the flat longitudinal stiffeners. The objective here is to compare with the corresponding Group 3 cases to determine the significance of the stiffener type.

A summary of various cases in Groups 1 and 2 is provided in Table 4-2 in terms of the non-dimensional parameters that influence the strength. Similarly, a summary of various cases in Groups 3 and 4 is provided in Table 4-3 in terms of these parameters. The buckling length and the total length of the plate for Group 1 and 2 cases are taken as ℓ_c and $5\ell_c$ respectively. The total length of the plate for Group 3 and 4 cases is taken as four times the transverse stiffener spacing. For Group 3 and 4 cases the transverse stiffener spacing is less than ℓ_c. The cross-section dimensions and lengths of the various Group 1 through Group 4 cases are provided in Appendix D. For the non-dimensional parameters in Table 4-2 and Table 4-3, the longitudinal stiffeners are sized to just satisfy the minimum requirements discussed in Section 4.2.3, to prevent local buckling of the stiffener component plates and tripping of the stiffener.

Table 4-2 Summary of Group 1 and Group 2 cases in terms of the non-dimensional parameters; buckling length and the total length of the plate are ℓ_c and $5\ell_c$ respectively

Case #	n	$\frac{w}{t_{sp}}$	$\frac{A_{gs}}{wt_{sp}}$		Case #	n	$\frac{w}{t_{sp}}$	$\frac{A_{gs}}{wt_{sp}}$
1	1	20	1.05		16	2	40	1.15
2	1	20	1.10		17	2	40	1.20
3	1	20	1.20		18	2	40	1.30
4	1	20	1.40		19	2	40	1.40
5	2	20	1.07		20	2	40	1.60
6	2	20	1.10		21	1	60	1.20
7	2	20	1.16		22	1	60	1.30
8	2	20	1.25		23	1	60	1.40
9	2	20	1.40		24	1	60	1.50
10	2	20	1.60		25	1	60	1.60
11	1	40	1.15		26	2	60	1.20
12	1	40	1.20		27	2	60	1.32
13	1	40	1.30		28	2	60	1.48
14	1	40	1.40		29	2	60	1.60
15	1	40	1.60					

Table 4-3 Summary of Group 3 and Group 4 cases in terms of the non-dimensional parameters; total length of the plate is four times the transverse stiffener spacing

Case #	n	$\frac{w}{t_{sp}}$	$\frac{A_{gs}}{wt_{sp}}$	Buckling length, ℓ
1	5	20	1.10	$\ell = a \le \ell_c$ such that $\frac{P_{ns}}{P_{yes}} \approx 0.93F_{ysp}$
2	5	20	1.20	$\ell = a \le \ell_c$ such that $\frac{P_{ns}}{P_{yes}} \approx 0.93F_{ysp}$
3	5	20	1.30	$\ell = a \le \ell_c$ such that $\frac{P_{ns}}{P_{yes}} \approx 0.93F_{ysp}$
4	5	20	1.40	$\ell = a \le \ell_c$ such that $\frac{P_{ns}}{P_{yes}} \approx 0.93F_{ysp}$
5	5	20	1.50	$\ell = a \le \ell_c$ such that $\frac{P_{ns}}{P_{yes}} \approx 0.93F_{ysp}$
6	5	20	1.10	$\ell = a \le \ell_c$ such that $\frac{P_{ns}}{P_{yes}} \approx 0.75F_{ysp}$
7	5	20	1.20	$\ell = a \le \ell_c$ such that $\frac{P_{ns}}{P_{yes}} \approx 0.75F_{ysp}$
8	5	20	1.30	$\ell = a \le \ell_c$ such that $\frac{P_{ns}}{P_{yes}} \approx 0.75F_{ysp}$
9	5	20	1.40	$\ell = a \le \ell_c$ such that $\frac{P_{ns}}{P_{yes}} \approx 0.75F_{ysp}$
10	5	20	1.50	$\ell = a \le \ell_c$ such that $\frac{P_{ns}}{P_{yes}} \approx 0.75F_{ysp}$
11	5	20	1.10	$\ell = a \le \ell_c$ such that $\frac{P_{ns}}{P_{yes}} \approx 0.55F_{ysp}$

12	5	20	1.20	$\ell = a \le \ell_c$ such that $\frac{P_{ns}}{P_{yes}} \approx 0.55F_{ysp}$
13	5	20	1.30	$\ell = a \le \ell_c$ such that $\frac{P_{ns}}{P_{yes}} \approx 0.55F_{ysp}$
14	5	20	1.40	$\ell = a \le \ell_c$ such that $\frac{P_{ns}}{P_{yes}} \approx 0.55F_{ysp}$
15	5	20	1.50	$\ell = a \le \ell_c$ such that $\frac{P_{ns}}{P_{yes}} \approx 0.55F_{ysp}$
16	3	60	1.20	$\ell = a \le \ell_c$ such that $\frac{P_{ns}}{P_{yes}} \approx 0.93F_{ysp}$
17	3	60	1.30	$\ell = a \le \ell_c$ such that $\frac{P_{ns}}{P_{yes}} \approx 0.93F_{ysp}$
18	3	60	1.40	$\ell = a \le \ell_c$ such that $\frac{P_{ns}}{P_{yes}} \approx 0.93F_{ysp}$
19	3	60	1.50	$\ell = a \le \ell_c$ such that $\frac{P_{ns}}{P_{yes}} \approx 0.93F_{ysp}$
20	3	60	1.60	$\ell = a \le \ell_c$ such that $\frac{P_{ns}}{P_{yes}} \approx 0.93F_{ysp}$
21	3	60	1.20	$\ell = a \le \ell_c$ such that $\frac{P_{ns}}{P_{yes}} \approx 0.75F_{ysp}$
22	3	60	1.30	$\ell = a \le \ell_c$ such that $\frac{P_{ns}}{P_{yes}} \approx 0.75F_{ysp}$
23	3	60	1.40	$\ell = a \le \ell_c$ such that $\frac{P_{ns}}{P_{yes}} \approx 0.75F_{ysp}$
24	3	60	1.50	$\ell = a \le \ell_c$ such that $\frac{P_{ns}}{P_{yes}} \approx 0.75F_{ysp}$

25	3	60	1.60	$\ell = a \le \ell_c$ such that $\frac{P_{ns}}{P_{yes}} \approx 0.75F_{ysp}$
26	3	60	1.20	$\ell = a \le \ell_c$ such that $\frac{P_{ns}}{P_{yes}} \approx 0.55F_{ysp}$
27	3	60	1.30	$\ell = a \le \ell_c$ such that $\frac{P_{ns}}{P_{yes}} \approx 0.55F_{ysp}$
28	3	60	1.40	$\ell = a \le \ell_c$ such that $\frac{P_{ns}}{P_{yes}} \approx 0.55F_{ysp}$
29	3	60	1.50	$\ell = a \le \ell_c$ such that $\frac{P_{ns}}{P_{yes}} \approx 0.55F_{ysp}$
30	3	60	1.60	$\ell = a \le \ell_c$ such that $\frac{P_{ns}}{P_{yes}} \approx 0.55F_{ysp}$

4.3.1.2 Results and Discussion

Figure 4-13, Figure 4-14, Figure 4-15 and Figure 4-16 show the results for Groups 1, 2, 3 and 4 respectively. It can be observed that the predictions using the proposed method correlate well with the strengths from the test simulations, and are significantly better than the predictions using the methods in AASHTO (2017), AISI (2016), and Eurocode (CEN 2006). The mean, median and coefficient of variation of the ratio of the resistance from test simulation to the strength predicted using the proposed method are equal to 1.06, 1.03 and 0.1 respectively.

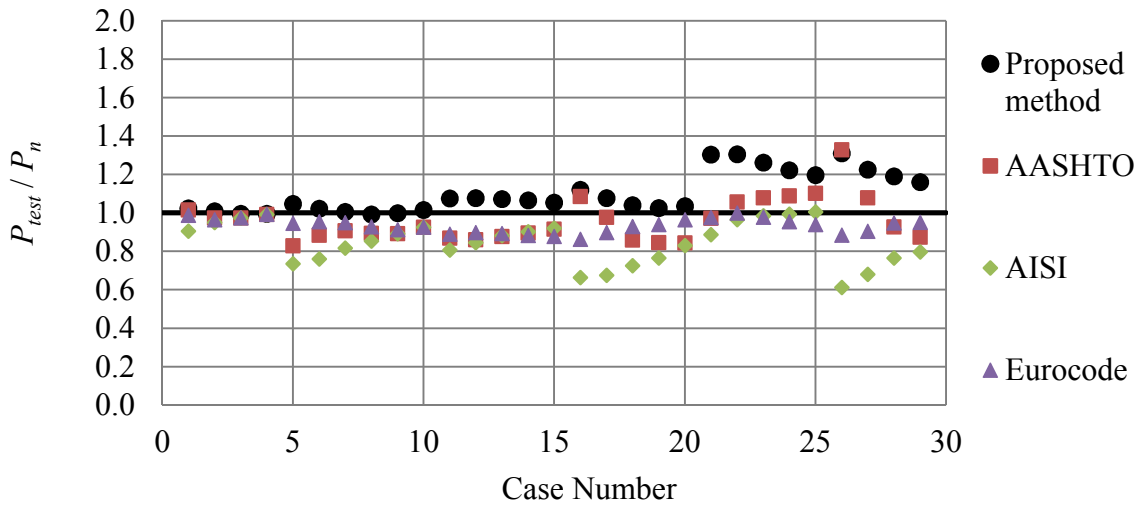

Figure 4-13 Comparison of the strength from test simulation with the strength predicted using the proposed method, the method in AASHTO (2017) Article 6.11.8.2, the method in Eurocode, and the method in AISI (2016), for Group 1 cases

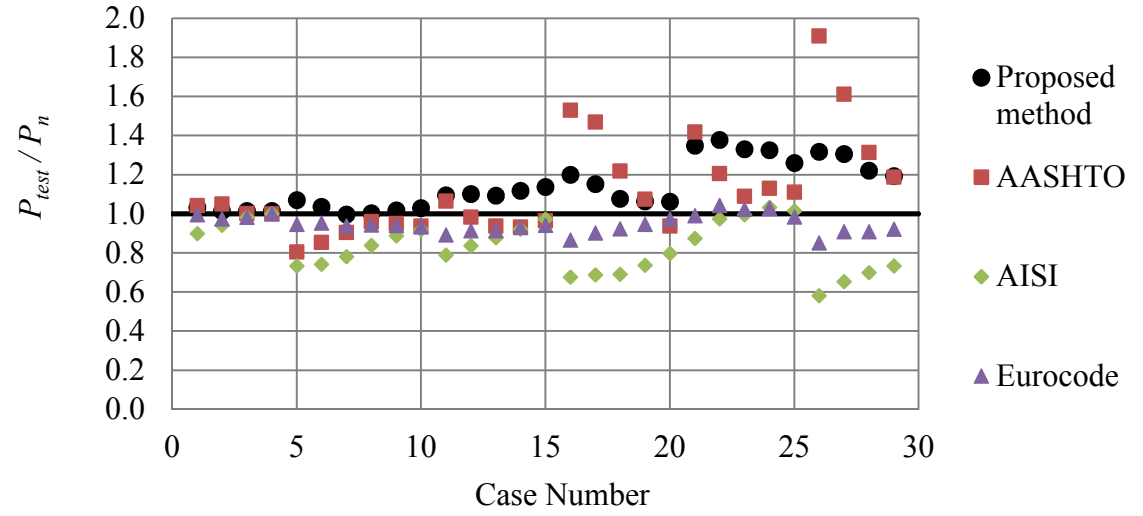

Figure 4-14 Comparison of the strength from test simulation with the strength predicted using the proposed method, the method in AASHTO (2017) Article 6.11.8.2, the method in Eurocode, and the method in AISI (2016), for Group 2 cases

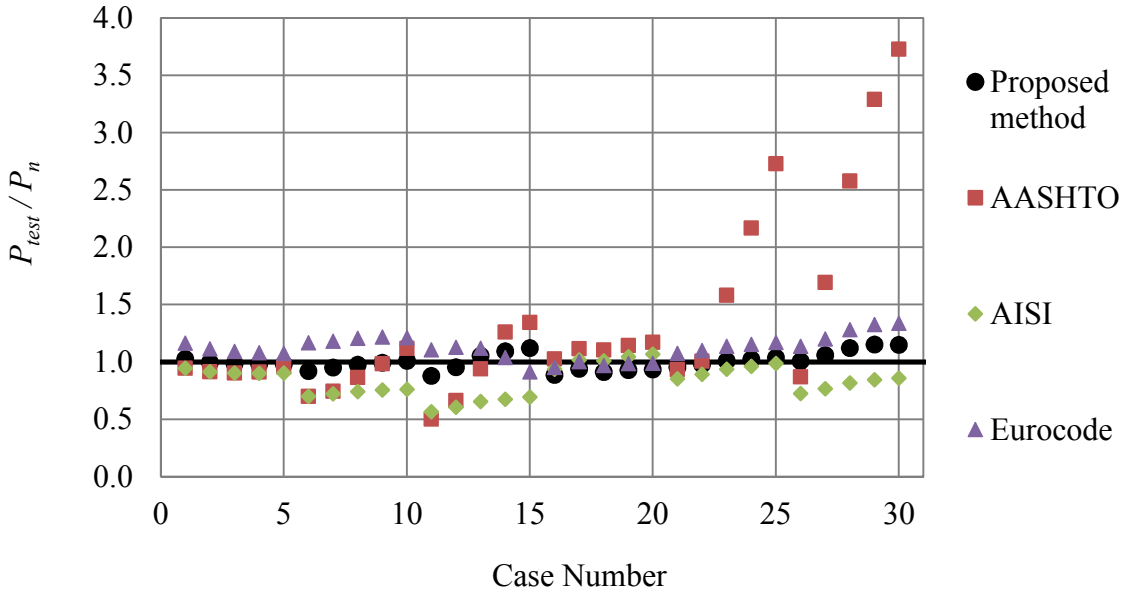

Figure 4-15 Comparison of the strength from test simulation with the strength predicted using the proposed method, the method in AASHTO (2017) Article 6.11.8.2, the method in Eurocode, and the method in AISI (2016), for Group 3 cases

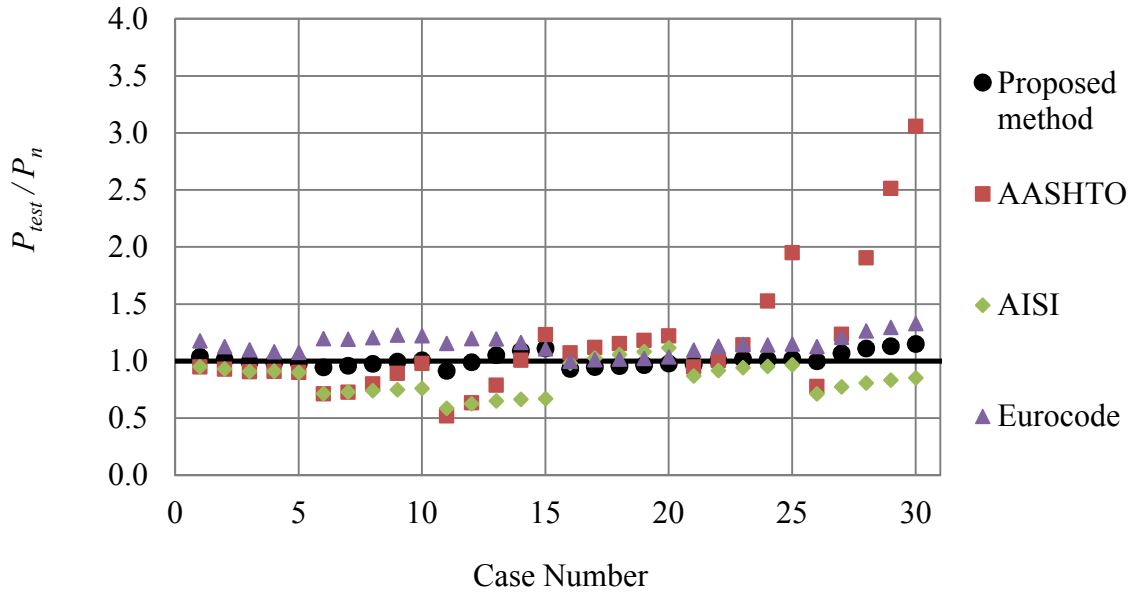

Figure 4-16 Comparison of the strength from test simulation with the strength predicted using the proposed method, the method in AASHTO (2017) Article 6.11.8.2, the method in Eurocode, and the method in AISI (2016), for Group 4 cases

Comparing the results of Group 1 and Group 2 cases (and also Group 3 and Group 4 cases) using the proposed method, it can be concluded that the compressive resistance of the plate is only mildly dependent on the stiffener type. Table 4-4 and Table 4-5 show a comparison of $\frac{I_s}{wI_p}$ values for Groups 1 and 2, and Groups 3 and 4 respectively. It can be observed from Table 4-4 and Table 4-5, and Figure 4-13 through Figure 4-16 that the parameter $\frac{I_s}{wI_p}$ has a very minor influence on the compressive resistance of longitudinally stiffened plates. Another reason for the minor difference between the results for Group 1 and Group 2 (and also Group 3 and Group 4 cases) using the proposed method, is that the proposed method uses the same AISC/AASHTO column curve for both Tee-section struts (Flat stiffeners) as well as I-section struts (Tee stiffeners).

Table 4-4 Comparison of $\frac{I_s}{wI_p}$ for Group 1 and 2 cases

Case number	Group 1 $\frac{I_s}{wI_p}$	Group 2 $\frac{I_s}{wI_p}$
1	4.0	3.3
2	11.4	8.7
3	36.9	27.0
4	122.0	86.4
5	6.5	5.1
6	11.4	8.7
7	25.2	18.6

8	54.3	39.3
9	122.0	86.4
10	242.7	168.7
11	41.3	30.0
12	68.8	49.5
13	141.0	99.8
14	233.4	163.4
15	469.3	323.0
16	41.3	30.0
17	68.8	49.5
18	141.0	99.8
19	233.4	163.4
20	469.3	323.0
21	100.1	71.3
22	206.7	145.4
23	343.4	239.2
24	506.6	349.8
25	693.6	475.3
26	100.1	71.3
27	231.8	162.7
28	472.0	326.5
29	693.6	475.3

Table 4-5 Comparison of $\frac{I_s}{wI_p}$ for Group 3 and 4 cases

Case number	Group 3 $\frac{I_s}{wI_p}$	Group 4 $\frac{I_s}{wI_p}$
1	11.4	8.7
2	36.9	27.0
3	74.4	53.4
4	122.0	86.4
5	178.4	125.1
6	11.4	8.7
7	36.9	27.0
8	74.4	53.4
9	122.0	86.4
10	178.4	125.1
11	11.4	8.7
12	36.9	27.0
13	74.4	53.4
14	122.0	86.4
15	178.4	125.1
16	100.1	71.3
17	206.7	145.4
18	343.4	239.2
19	506.6	349.8

20	693.6	475.3
21	100.1	71.3
22	206.7	145.4
23	343.4	239.2
24	506.6	349.8
25	693.6	475.3
26	100.1	71.3
27	206.7	145.4
28	343.4	239.2
29	506.6	349.8
30	693.6	475.3

It can be observed that the predictions become conservative for larger $\frac{w}{t_{sp}}$. In Groups 1 and 2 (Figure 4-13 and Figure 4-14), cases 1 to 10 have $\frac{w}{t_{sp}} = 20$, cases 11 to 20 have $\frac{w}{t_{sp}} = 40$, and cases 21 to 29 have $\frac{w}{t_{sp}} = 60$. The reason for this under-prediction of the plate resistance is that the larger available buckling and postbuckling resistance of the subpanels due to the additional restraint from the adjacent subpanels, is accounted for in an approximate manner by using the Winter's effective width equation instead of the modified Winter's effective width equation for plates with two or more longitudinal stiffeners. However, the aim of simplicity and ease of design justifies the use of this

approximate manner of accounting for the larger available buckling and postbuckling resistance of the subpanels.

Figure 4-2 shows a representative failure mode involving interaction between local and overall buckling in a longitudinally stiffened plate. The proposed method accounts for this interaction by using effective section properties (using effective widths of the subpanels between longitudinal stiffeners, taking into account their postbuckling resistance) while calculating the flexural buckling resistance of individual stiffener struts, P_{nsF} . The proposed method also considers the interaction between local and overall buckling of the longitudinally stiffened plate while calculating the compressive resistance provided by the half-width of the subpanels adjacent to the transversely-restrained longitudinal edge of the longitudinally stiffened plate, P_{nR} . A good correlation between the strength from test simulations and the strength predicted by the proposed method provides evidence that the approach used for accounting for the interaction between local buckling and overall buckling, works well.

The over-prediction of resistance using the AISI method can be attributed to:

- The lack of accounting for the interaction between local buckling of the plate panels between the stiffeners and overall buckling involving the transverse displacement of the stiffeners, in these provisions. This is because the buckling coefficient is calculated as the minimum of the coefficients for buckling of the plate between longitudinal stiffeners (as shown in Figure 4-7) and overall buckling of the plate along with the longitudinal stiffeners (as shown in Figure 4-6).

- The use of Winter's curve and counting on the postbuckling resistance for cases involving an interaction between local and global buckling.

The AISI method works better for cases where the failure modes are similar to those shown in Figure 4-6 and Figure 4-7, and for cases where there is little local-global buckling interaction and the plate resistance is close to the yield strength, i.e., Group 1 and 2 case numbers 1, 2, 3, 4, 21, 22, 23, 24, 25 and Group 3 and 4 case numbers 1, 2, 3, 4, 5, 16, 17, 18, 19, 20.

The longitudinal stiffeners in wide plates with more than two longitudinal stiffeners tend to behave as unconnected struts. The key property influencing the compressive resistance of these types of plates is the moment of inertia of their longitudinal stiffeners. However, as discussed earlier in Section 4.1.2.1, for these types of plates, the plate buckling coefficient in AASHTO, and hence the stiffened plate resistance, is expressed independently from this key property. This is the reason why the predictions using the AASHTO method do not show a good correlation with the results of the parametric study for Group 3 and Group 4 cases. Furthermore, in certain cases with $\frac{w}{t_{sp}} = 40$ and $\frac{w}{t_{sp}} = 60$ where the failure mode is similar to shown in Figure 4-6, e.g., Group 3 case 30, the solutions are conservative because the AASHTO method neglects the significant postbuckling resistance of the longitudinally stiffened plate subpanels.

In general, it can be observed that there is less scatter in the data for the predictions using the Eurocode method. As mentioned earlier, the Group 3 and 4 cases have short and wide plates with 3 or 5 longitudinal stiffeners, and 3 intermediate transverse stiffeners.

These plates have negligible transverse bending stiffness, and can be idealized as a series of disconnected stiffener struts. For these cases Eurocode predicts column-type behaviour (hardly any plate-type behaviour), and hence there is good correlation between the simulation strengths and predictions using Eurocode. However, for Group 1 and Group 2 cases Eurocode over-predicts the resistance because:

- It uses Winter's curve for calculating ρ (reduction factor corresponding to plate-type behaviour) and thus counts on the postbuckling resistance for cases involving the interaction between local and global buckling.
- It accounts for larger resistance of the half-width of the edge subpanels closest to the edge supports by considering that they reach the yield stress. However, the maximum resistance of the stiffened plate typically occurs before the half-width of the subpanel closest to the edge support reaches the yield stress.

4.3.2 Comparison with experimental tests from the literature

In addition to the parametric study, 28 experimental tests from Choi et al. (2009), Ghavami (1994), and Tanaka and Endo (1988) are used to evaluate the performance of the proposed method for characterizing the ultimate compressive resistance of longitudinally stiffened plates.

Table 4-6 shows a comparison of plate compressive resistance from experimental tests with the resistance predicted using the proposed method.

For the tests by Choi et al. (2009), the predictions using the proposed method correlate well with experimental test results for cases with 2 or more longitudinal stiffeners (Specimens R3, T1, T2), because for these cases the proposed method recognizes the larger restraint from the adjacent subpanels while calculating the postbuckling resistance of a subpanel between longitudinal stiffeners or between a longitudinal stiffener and an edge. This is done via the use of Winter's effective width equation instead of the modified Winter's effective equation, as explained in Section 4.2.

Except for Specimens D10, D11 and D12, the yield strength of the longitudinal stiffener and the plate are different for the specimens tested by Tanaka and Endo (1988) and Ghavami (1994). For the calculations using the proposed method, a single yield stress value was used which was calculated as the weighted average of the yield strength of the plate and the longitudinal stiffener. This ensures that the squash load is the same as that of the tested specimen. The use of this single yield stress value is a possible reason for the predictions using the proposed method not showing a good correlation with the results of some of the tests by Tanaka and Endo (1988) and Ghavami (1994).

For specimen D11, the slenderness of the longitudinal stiffener plate (flat longitudinal stiffener) is 2.1 times the limiting slenderness, $0.45\sqrt{E/F_y}$, required to prevent local buckling/tripping of the flat longitudinal stiffener. This explains the lower observed strength from experimental test for this specimen. For case D0A the yield strength of the longitudinal stiffener is significantly lower than the yield strength of the plate. For

such cases the early yielding of the longitudinal stiffeners nullifies the stiffening of the plate. For cases D1 and D2, the yield strength of the longitudinal stiffener is slightly lower than the yield strength of the plate. The mean, median and coefficient of variation of the ratio of P_{test}/P_n for all tests with equal yield strength plate and longitudinal stiffeners, are 1.24, 1.22 and 0.17 respectively.

Table 4-6 Comparison of plate compressive resistance from experimental tests with the resistance predicted using the proposed methods

Source	Specimen	P_{test}/P_n
Choi et al. (2009)	R1	1.28
Choi et al. (2009)	R2	1.15
Choi et al. (2009)	R3	1.09
Choi et al. (2009)	T1	1.03
Choi et al. (2009)	T2	1.02
Choi et al. (2009)	T3	1.18
Choi et al. (2009)	T4	1.67
Choi et al. (2009)	T5	1.51
Choi et al. (2009)	T6	1.38
Ghavami (1994)	P1R1T*	1.28
Ghavami (1994)	P1L1T*	1.17
Ghavami (1994)	P1T1T*	1.21
Ghavami (1994)	P2R1T*	0.98
Ghavami (1994)	P2L1T*	0.82
Ghavami (1994)	P2T1T*	0.89
Ghavami (1994)	P2R2T*	0.89
Ghavami (1994)	P2L2T*	0.94
Ghavami (1994)	P2T2T*	0.98
Tanaka and Endo (1988)	D0*	1.14
Tanaka and Endo (1988)	D0A*	1.06
Tanaka and Endo (1988)	D1*	1.24

Tanaka and Endo (1988)	D2*	1.19
Tanaka and Endo (1988)	D3*	1.33
Tanaka and Endo (1988)	D4*	1.26
Tanaka and Endo (1988)	D4A*	1.13
Tanaka and Endo (1988)	D10	1.26
Tanaka and Endo (1988)	D11	0.97
Tanaka and Endo (1988)	D12	1.41

* For these specimens the yield strength of the longitudinal stiffener and the plate are different

4.4 Salient features of the proposed method

The salient features of the proposed method are as follows:

1) It is derived using an orthotropic plate idealization and thus considers all three contributions to the buckling resistance-longitudinal bending stiffness, transverse bending stiffness, and torsional stiffness.

2) The buckling resistance obtained using the orthotropic plate idealization is expressed as an intuitive and easy-to-use column on elastic foundation model. The elastic torsional contribution from the plate is included directly in the ultimate strength calculation, with a calibrated reduction factor of 0.15. As pointed out by King (2017), the plate torsional stiffness provides much of the stability to plates with a buckling resistance close to the yield stress.

3) The explicit combination of the three contributions to the stiffened plate compressive resistance facilitates design optimization since the relative importance of each effect is clear.

4) The method is applicable to longitudinally stiffened plates with or without intermediate transverse stiffeners.

5) The characteristic buckling length is familiar to the engineer. This allows the engineer to make a good decision about whether transverse stiffening is needed, and at what spacing to place transverse stiffeners if they are used.

6) The method recognizes that the edge stress is larger than the ultimate stress of the stiffener strut, but it also takes into account the observation that the edge stress is typically less than the yield stress at the ultimate strength condition.

7) The method recognizes the postbuckling resistance of the plate panels between the longitudinal stiffeners, and/or between the longitudinal stiffeners and the transversely-restrained longitudinal edge of the stiffened plate.

8) The proposed method accounts for the interaction between local buckling of subpanels and overall buckling of the plate involving transverse displacement of the stiffeners.

9) Unlike Eurocode (CEN 2006), the method does not resort to an interpolation between column-type and plate-type behavior to determine the extent of the plate-like or column-like behavior.

10) The method does not recognize extensive postbuckling resistance of longitudinally stiffened plates with relatively weak longitudinal stiffener struts, which would fail at low values of the compression stress. These types of configurations are a quite inefficient use of the additional longitudinal stiffener material plus the fabrication cost in the context of welded box-section member construction. Therefore, this is not viewed as a limitation.

11) The plate elastic buckling stress predicted by the proposed method can be related to the non-dimensional parameters derived in Section 4.2.4. This facilitates the parametric study of longitudinally stiffened plate responses. It has also been shown that the compressive strength of longitudinally stiffened plates is largely independent of the type of longitudinal stiffener.

CHAPTER 5. AXIAL COMPRESSIVE RESISTANCE OF RECTANGULAR WELDED BOX-SECTION MEMBERS

A good prediction of the ultimate compressive resistance of non-longitudinally stiffened and longitudinally stiffened plates is crucial for obtaining a good quantification of the axial compressive resistance of welded box-section members. A detailed explanation of an improved characterization of the ultimate compressive resistance of these box-section component plates was provided in CHAPTER 2 and CHAPTER 4.

AASHTO (2017) does not have any guidance for calculating the axial compressive resistance of longitudinally stiffened box-section members. Thus, there is a need to develop a method for calculation of axial compressive resistance of longitudinally stiffened welded steel box-section members that is conceptually consistent with the method for non-longitudinally stiffened box-section members and incorporates an improved prediction of the ultimate compressive resistance of longitudinally stiffened plates.

At the present time (2018), there is no experimental or finite element simulation data in the literature quantifying the interaction between flexural and local buckling on the axial compressive resistance of longitudinally stiffened welded steel box-section members. As a part of this research effort, a parametric study has been performed using FE simulations to evaluate the performance of the proposed method. This has generated useful data quantifying the interaction between global buckling and local buckling in longitudinally stiffened welded steel box columns.

Particularly when studying the characteristics of longitudinally stiffened box-section members, experimental tests are quite expensive, if not prohibitive due to the size of the members. Therefore, studying the behavior and understanding the influence of different parameters on the behavior is not possible using physical experimental tests alone. Finite element test simulations provide an economical and effective way to advance the state of knowledge in these cases.

This chapter explains the development of the proposed method for an improved quantification of the axial compressive resistance of welded box-section members, and the evaluation of the performance of the proposed method via a parametric study performed using finite element test simulations.

5.1 Proposed method

A commonly used approach for calculating the compressive resistance of columns is the unified effective area approach (Pekoz 1986). As per this approach the axial compressive resistance, P_n, is given as follows:

$$P_n = F_{cr} A_{eff} \tag{108}$$

where:

- F_{cr} is the flexural buckling stress based on gross cross-section properties.
- The yield load used in the calculation of F_{cr}, is the gross cross-section yield load.
- A_{eff} is the effective area calculated at a stress level equal to F_{cr}.

Ideally, F_{cr} should be calculated based on member effective cross-section properties. However, this makes the calculations iterative as F_{cr} is based on the effective cross-section, and the effective cross-section is dependent on F_{cr}. Pekoz (1986) provides the following justification for calculating F_{cr} using gross-section properties- "*On the basis of tests and analytical studies, DeWolf, Pekoz and Winter (1973, 1974), and Kalyanaraman, Pekoz and Winter (1972, 1977) conclude that the overall buckling load can be calculated using the effective radius of gyration and the effective area, both calculated at the overall buckling stress. This results in an iterative procedure because the buckling stress depends on the effective section properties which in turn depend on the buckling stress. The reduction in the value of the radius of gyration resulting from local buckling is rather small. For small slenderness ratios where the column buckling stresses are high compared to the yield stress, the buckling stress is quite insensitive to the changes in the radius of gyration. However, the effective area is influenced directly and significantly by local buckling. For small stresses, namely large slenderness ratios, the local buckling is not significant. Therefore, for both cases the behavior is well represented by ignoring the reduction in the effective radius of gyration, but taking into account the reduction in the effective area in finding the ultimate load of the column.* "

The Eurocode (CEN 2005) uses a somewhat different approach for calculating the compressive resistance of columns. Per the Eurocode, the axial compressive resistance, P_n , is given as follows:

$$P_n = \chi F_y A_{eff} \tag{109}$$

where:

- The effective cross-section yield load (equal to the gross cross-section yield load for classes 1 to 3) is used in the calculation of the column strength factor χ. The Eurocode classification of cross-sections is explained in Section 3.1.1.2.
- A_{eff} is the effective area calculated at a stress level equal to F_y.

5.1.1 Proposed method for calculating the compressive resistance of box-section columns with non-longitudinally stiffened component plates

The proposed method for non-longitudinally stiffened box columns is based on the unified effective area approach. The axial compressive resistance, P_n, is given as follows:

$$P_n = F_{cr} A_{eff} \tag{110}$$

where:

- F_{cr} is the flexural buckling stress based on gross cross-section properties, calculated as follows:

  If $\frac{P_{os}}{P_e} \leq 2.25$, then

  $$F_{cr} = \left[0.658^{\frac{P_{os}}{P_e}}\right] F_y \tag{111}$$

  Otherwise,

  $$F_{cr} = \frac{0.877 P_e}{A_g} \tag{112}$$

- $P_{os} = \sum_{nlsp} F_y bt + \sum_{c} F_y A_c$ (113)

  = yield load

- $P_e = \dfrac{\pi^2 E}{\left(\dfrac{KL}{r_s}\right)^2} A_g$ (114)

  = member elastic buckling load;

- L is the unbraced length of the column corresponding to the axis of buckling;
- K is the effective length factor;
- r_s is the radius of gyration of the gross cross-section about the axis normal to the plane of buckling;
- A_g is the gross cross-sectional area of the member;
- $A_{eff} = \sum_{nlsp} b_e t + \sum_{c} A_c$ (115)
- b_e = effective width of the non-longitudinally stiffened element under consideration, determined using the modified Winter's effective width equation explained in Section 2.2 (for nonslender non-longitudinally stiffened plate elements, $b_e = b$) and calculated at a stress level equal to F_{cr};
- t = thickness of the element under consideration;
- A_c = gross cross-sectional area of the corner pieces of a box-section;
- $nlsp$ = Number of non-longitudinally stiffened plates;
- $c = 4$ is the number of corner pieces in a box-section.

5.1.2 Proposed method for calculating the compressive resistance of box-section columns with longitudinally stiffened component plates

The proposed method for calculating the compressive of longitudinally stiffened box columns is arrived at by modifying the method for calculating the strength of non-longitudinally stiffened box columns based on the following considerations:

1) If A_{eff} is calculated at a stress level equal to F_{cr}, then

$$A_{eff} = \sum_{lsp} \frac{P_{nsp}}{F_{cr}} \tag{116}$$

giving

$$P_n = F_{cr} A_{eff} = F_{cr} \frac{\sum_{lsp} P_{nsp}}{F_{cr}} = \sum_{lsp} P_{nsp} \tag{117}$$

where:

- P_{nsp} is the nominal compressive resistance of the longitudinally stiffened plate element under consideration, calculated using the proposed method explained in Section 4.2.
- lsp is the number of longitudinally stiffened plates.

Therefore, the strength of the column becomes independent of the flexural buckling stress of the column. This happens because the compressive resistance of the longitudinally stiffened component plates, P_{nsp}, calculated using the proposed method in Section 4.2, is

independent on the flexural buckling stress of the column, F_{cr}. This can be understood better by considering two square box-section columns with the following characteristics:

- All the longitudinally stiffened component plates have one longitudinal stiffener located at their mid-width, and have the same cross-section;
- There are no intermediate transverse stiffeners or diaphragms;
- The lengths of the two columns are ℓ_c and $2\ell_c$; where ℓ_c is the characteristic buckling length of the longitudinally stiffened component plates.

The proposed method in Section 4.2 predicts the same P_{nsp} for the component plates in both these columns, without taking into consideration the flexural buckling stress of the column, F_{cr}. One does not encounter this in the case of non-longitudinally stiffened box-columns because the calculation of the plate effective width using the modified Winter's effective width equation is dependent on the flexural buckling stress of the column, F_{cr}.

Therefore, in the proposed method for box-section columns with longitudinally stiffened plates the effective area, A_{eff}, is conservatively calculated at a stress level equal to F_y, i.e.,

$$A_{eff} = \sum_{lsp} \frac{P_{nsp}}{F_{ysp}} \tag{118}$$

This parallels the calculation of the effective area in the Eurocode provisions.

2) The results from parametric studies show that the predictions obtained using

$$P_n = F_{cr} A_{eff} = F_{cr} \sum_{lsp} \frac{P_{nsp}}{F_{ysp}} \tag{119}$$

significantly under-predict the column resistance, if the flexural buckling stress, F_{cr}, is calculated using the gross cross-section yield load. This over-conservatism is addressed by using an effective yield load in the calculation of F_{cr}, i.e.,

If $\frac{P_{os}}{P_e} \leq 2.25$, then

$$F_{cr} = \left[0.658^{\frac{P_{os}}{P_e}} \right] F_y \tag{120}$$

Otherwise,

$$F_{cr} = \frac{0.877 P_e}{A_g} \tag{121}$$

where:

- $P_{os} = F_y A_{eff}$ (122)
- $A_{eff} = \sum_{lsp} \frac{P_{nsp}}{F_{ysp}}$ (123)

This approach for calculating the compressive resistance of box-section columns with longitudinally stiffened component plates is similar to the Eurocode (CEN 2005) approach as it:

- Performs the effective area calculations at a stress level equal to F_y, and
- Uses an effective yield load in the calculation of the flexural buckling stress.

3) Local buckling-global buckling interaction: Using the above two modifications, it is observed that the predictions using the proposed method correlate well with the results from column flexural buckling parametric studies except for cases with large KL/r_s, and large w/t_{sp} for the longitudinally stiffened plate parallel to the axis of buckling. In these cases there is significant interaction between overall flexural buckling of the column and local buckling of the longitudinally stiffened plate parallel to the axis of buckling and subjected to uniform flexural compression corresponding to flexural buckling of the column, as shown in Figure 5-1.

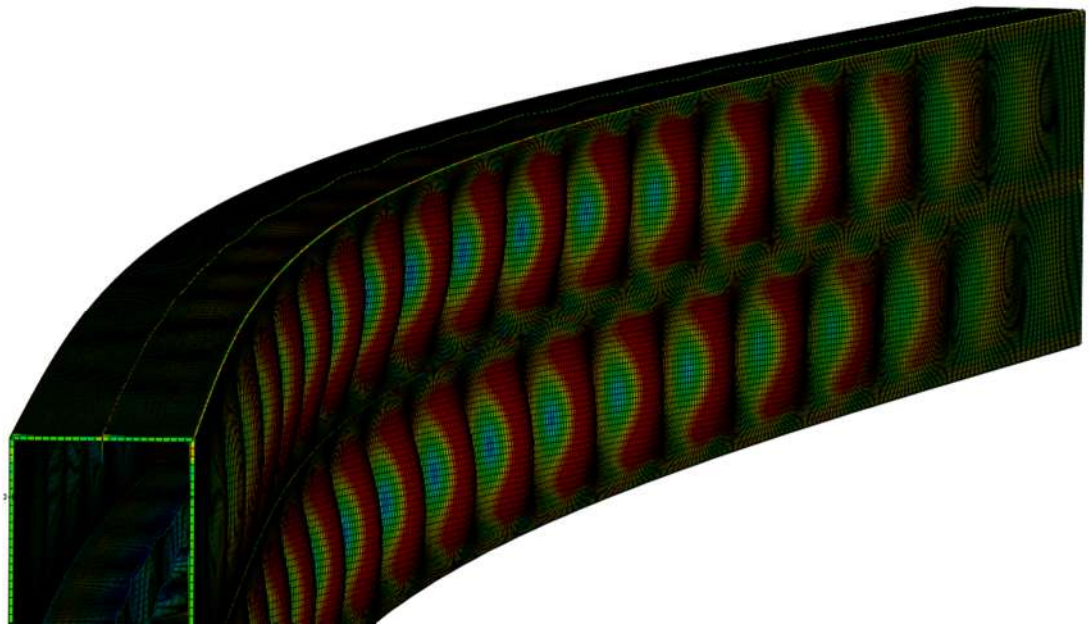

Figure 5-1 Global buckling-local buckling interaction for cases with large KL/r_s, and large w/t_{sp} for the longitudinally stiffened plate parallel to the axis of buckling

This happens because slender columns exhibit significant second-order bending as they approach their maximum compressive resistance, which results in additional compressive stress on one of the plates. This results in a significant reduction in the column strength.

This problem can be addressed by using a reduced flexural buckling stress in the prediction calculations by:

1) Using a reduced elastic buckling load, based on a reduced effective cross-section, in the calculation of P_n ,

2) Using a column strength curve that is a function of:

- KL/r_s , and
- The maximum w/t_{sp} of the plate parallel to the axis of buckling and subjected to uniform flexural compression corresponding to flexural buckling of the column, or

3) Multiplying by a global buckling-local buckling interaction reduction factor dependent on:

- KL/r_s , and
- The maximum w/t_{sp} of the plate parallel to the axis of buckling and subjected to uniform flexural compression corresponding to flexural buckling of the column.

With the aim of simplicity, ease of design, and consistency with the method for non-longitudinally stiffened box columns in mind, the third approach of using a global-local interaction reduction factor is adopted in this research.

5.1.3 *Proposed method for calculating the compressive resistance of box-section columns with non-longitudinally stiffened and longitudinally stiffened component plates*

The recommended calculation of the compressive resistance of steel box-section columns with non-longitudinally stiffened and longitudinally stiffened component plates is as follows:

$$P_n = \chi F_{cr} A_{eff} \tag{124}$$

where:

- $\chi = 1 - r_1 r_2$ (125)

  = Global buckling-local buckling interaction factor

  $\chi = 1$ if the flange plate is non-longitudinally stiffened. A flange plate is defined as the plate parallel to the axis of buckling and subjected to uniform flexural compression corresponding to flexural buckling of the column.

- $r_1 = 0.5 \dfrac{\left(\dfrac{KL}{r_s} - 50 \right)}{(140 - 50)}$ (126)

  such that $0 \le r_1 \le 0.5$. In AASHTO (2017), the maximum permissible slenderness of secondary compression members is $\dfrac{KL}{r_s} = 140$. Therefore, r_1 has a minimum value of 0.5 for column designs permitted by AASHTO.

- $r_2 = \dfrac{\lambda_{\max} - \lambda_r}{90 - \lambda_r}$ (127)

such that $0 \le r_2 \le 1$

- $\lambda_{\max}$ is the maximum w/t_{sp} for the flange plate. As a practical upper limit, $\lambda_{\max}$ shall not exceed 90.
- For a flange plate with one longitudinal stiffener,

$$\lambda_r = 1.09\sqrt{\frac{E}{F_y}} \tag{128}$$

- For a flange plate with two or more longitudinal stiffeners,

$$\lambda_r = 1.49\sqrt{\frac{E}{F_y}} \tag{129}$$

- If $\frac{P_{os}}{P_e} \le 2.25$, then

$$F_{cr} = \left[0.658^{\frac{P_{os}}{P_e}}\right] F_y \tag{130}$$

Otherwise,

$$F_{cr} = \frac{0.877 P_e}{\left(P_{os}/F_y\right)} \tag{131}$$

- $$P_{os} = F_y\left(\sum_{nlsp} bt + \sum_{c} A_c + \sum_{lsp}\left(A_{eff}\right)_{sp}\right) \tag{132}$$

= effective yield load;

- $$A_{eff} = \sum_{nlsp} b_e t + \sum_{c} A_c + \sum_{lsp}\left(A_{eff}\right)_{sp} \tag{133}$$
- $$\left(A_{eff}\right)_{sp} = \frac{P_{nsp}}{F_{ysp}} \tag{134}$$

- $P_e = \dfrac{\pi^2 E}{\left(\dfrac{KL}{r_s}\right)^2} A_g$ (135)

  = member elastic buckling load;

- b_e = effective width of the non-longitudinally stiffened element under consideration, determined using the modified Winter's effective width equation explained in Section 2.2 (for nonslender non-longitudinally stiffened plate elements, $b_e = b$) and calculated at a stress level equal to χF_{cr}.

The above method for calculating the axial compressive resistance of longitudinally stiffened box-section members is applicable for steels with yield strength up to 70 ksi.

5.2 Evaluation of the performance of the proposed method

The performance of the proposed method is evaluated below using the results of a parametric study performed using FE test simulations. Table 5-1 summarizes the parametric study design. The cross-section dimensions and lengths of the various cases listed in Table 5-1 are provided in Appendix E. Three non-dimensional parameters are investigated pertaining to each of the flange and web plates. All the box-section columns studied are doubly symmetric. Also, the overall slenderness L/r_s is varied for these longitudinally stiffened box-section members (all the cases studied have simply supported end conditions. Therefore, $K = 1$). A range of column slenderness values are considered to study the interaction between local buckling and global buckling (flexural buckling).

The dimensions of the 42 box-section members are obtained by setting the thickness of the flanges and webs as one inch. Flat plate longitudinal stiffeners are used, and it is ensured that the slenderness of the stiffener plate does not exceed $0.45\sqrt{E/F_{ysp}}$, to prevent local buckling/tripping of the longitudinal stiffener.

Table 5-1 Summary of parametric study variables for evaluating the performance of the proposed method for calculating the axial compressive resistance of longitudinally stiffened box-section members

Case Numbers	Web plates			Flange plates			Column L/r_s
	w/t_{sp}	n	A_{gs}/wt_{sp}	w/t_{sp}	n	A_{gs}/wt_{sp}	
1, 2, 3	20	1	1.1	20	2	1.1	50, 80, 110
4, 5, 6	20	1	1.1	20	2	1.4	50, 80, 110
7, 8, 9	20	1	1.1	60	1	1.1	50, 80, 110
10, 11, 12	20	1	1.1	60	1	1.4	50, 80, 110
13, 14, 15	20	1	1.1	60	2	1.1	50, 80, 110
16, 17, 18	20	1	1.1	60	2	1.4	50, 80, 110
19, 20, 21	20	2	1.1	60	1	1.1	50, 80, 110
22, 23, 24	20	2	1.1	60	1	1.4	50, 80, 110
25, 26, 27	20	2	1.1	60	2	1.1	50, 80, 110
28, 29, 30	20	2	1.1	60	2	1.4	50, 80, 110

31, 32, 33	60	1	1.1	60	2	1.1	50, 80, 110
34, 35, 36	60	1	1.1	60	2	1.4	50, 80, 110
37, 38, 39	60	1	1.4	60	2	1.1	50, 80, 110
40, 41, 42	60	1	1.4	60	2	1.4	50, 80, 110

The finite element modelling of these longitudinally stiffened box-section members is explained in Appendix A. Figure 5-2 shows a comparison of the member test simulation strength to the strengths predicted using the proposed method as well as using the corresponding procedures from AISI (2016) and Eurocode (CEN 2005).

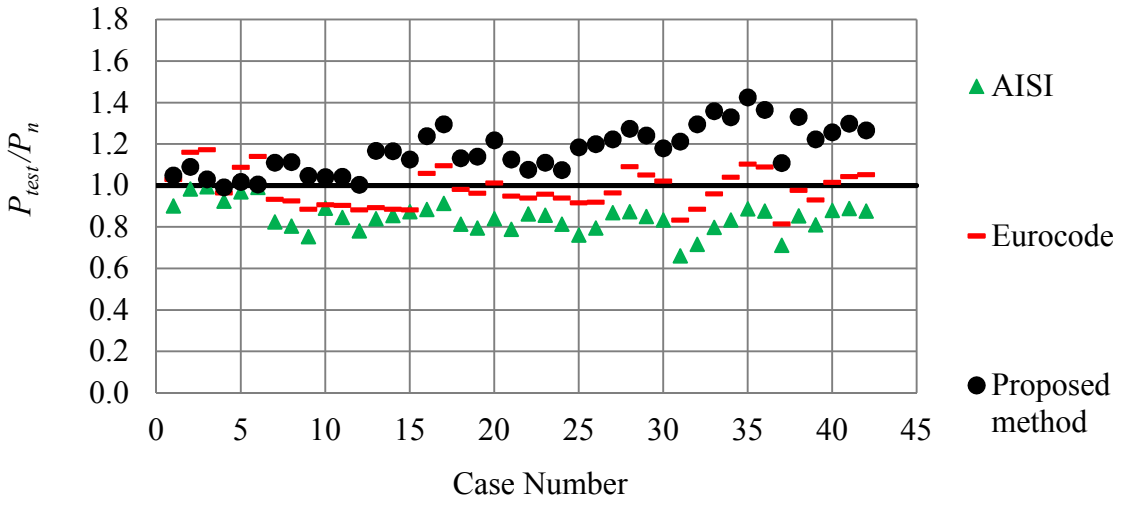

Figure 5-2 Comparison of the member strength from test simulation with the strength predicted using the proposed method and using the corresponding procedures from AISI (2016) and Eurocode (CEN 2005)

The unconservatism of the predictions using AISI (2016) and Eurocode (CEN 2006) methods can be attributed to their optimistic prediction of the ultimate compressive

resistance of longitudinally stiffened plates. This has been clearly demonstrated and discussed in Section 4.3. The drawbacks of the AISI (2016) and Eurocode (CEN 2006) methods for calculating the ultimate compressive resistance of longitudinally stiffened plates have been discussed in Section 4.1.

It has been found that the plate compressive resistance predictions using the proposed method explained in Section 4.2, become conservative with increase in w/t_{sp} . The reason for this under-prediction of the plate resistance is that the larger available buckling and postbuckling resistance of the subpanels between longitudinal stiffeners or between a longitudinal stiffener and an edge, due to the additional restraint from the adjacent subpanels, is accounted for in an approximate manner by using the Winter's effective width equation instead of the modified Winter's effective width equation for plates with two or more longitudinal stiffeners. This is why, in Figure 5-2, the predictions using the proposed method are conservative for cases with $w/t_{sp} = 60$. Another reason for conservatism of all the results is that the effective area of the longitudinally stiffened plates is conservatively calculated as $A_{eff} = \sum_{lsp} \frac{P_{nsp}}{F_{ysp}}$, as explained in Section 5.1.2.

Figure 5-3 shows a comparison of the member test simulation strengths to the strengths predicted using the proposed method, and using the proposed method with $\chi = 1$. This highlights the significant interaction between overall flexural buckling of the column and local buckling of the longitudinally stiffened flange plate for cases with large $\lambda_{\max}$ and L/r_s , and the performance of the global buckling-local buckling interaction reduction factor in capturing this effect. It can be observed that for cases 1 to 6 in which have

$\lambda_{max} = 20$ (theoretically no local buckling of the subpanels between the longitudinal stiffeners or between a longitudinal stiffener and a corner), the predictions using the proposed method without the global buckling-local buckling interaction reduction factor, correlate well with the test simulation strengths.

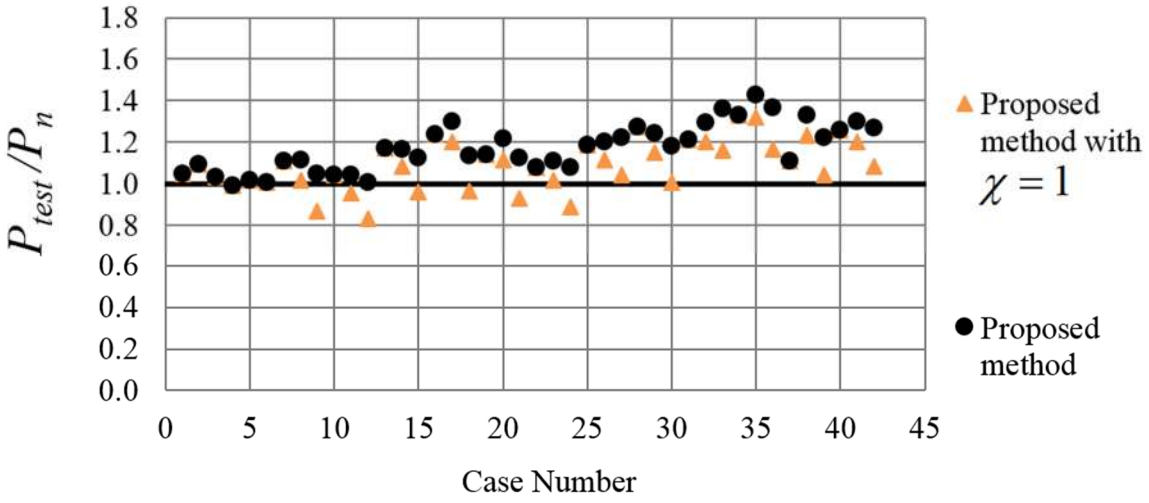

Figure 5-3 Comparison of the member strength from test simulation with the strength predicted using the proposed method, and using the proposed method with $\chi = 1$

Since the measure of local buckling in the calculation of χ is only based on λ_{max}, a potential question could be, what if the longitudinal stiffeners on the flange plate are such that $\lambda_{max} \le \lambda_r$, but the longitudinal stiffeners are relatively weak such that the flexural buckling of the column causes the flange plate to fail in an overall buckling mode with almost no buckling between the longitudinal stiffeners (see Figure 4-7)? Does the proposed method over-predict the resistance in such cases, since it would predict $\chi = 1$?

This is not a problem because, as mentioned in point #10 in Section 4.4, for such cases with weak longitudinal stiffeners the calculation of $\left(A_{eff}\right)_{sp}$ is conservative as it does

not take into account the postbuckling resistance corresponding to an overall buckling failure of the flange plate. Therefore, a possible over-prediction of F_{cr} is compensated by the under-prediction of $\left(A_{eff}\right)_{sp}$. Additionally, as pointed out in point #10 in Section 4.4, these types of configurations are a quite inefficient use of the additional longitudinal stiffener material plus the fabrication cost in the context of construction using welded box-section members.

A study is performed to investigate additional potential cases where local-global buckling interaction may cause the greatest unconservatism. These include cases with L/r_s up to 120, which is the maximum limit in the AASHTO LRFD Specifications for primary members, and with w/t_{sp} up to 90. Table 5-2 summarizes the study design, and Figure 5-4 shows a comparison of the member strength from test simulations with the strength predicted using the proposed method, and using the proposed with $\chi = 1$. The cross-section dimensions and lengths of the various listed in Table 5-2 are provided in Appendix E.

Table 5-2 Summary of parametric study variables for the additional cases

Case Numbers	Web plates			Flange plates			Column L/r_s
	w/t_{sp}	n	A_{gs}/wt_{sp}	w/t_{sp}	n	A_{gs}/wt_{sp}	
1, 2	20	1	1.2	20	1	1.2	50, 80
3, 4	40	1	1.2	40	1	1.2	50, 80
5	20	1	1.1	40	1	1.1	110
6	20	1	1.1	40	1	1.4	110
7	20	1	1.1	90	1	1.1	110
8	20	1	1.1	90	1	1.4	110
9	20	1	1.1	90	1	1.4	120

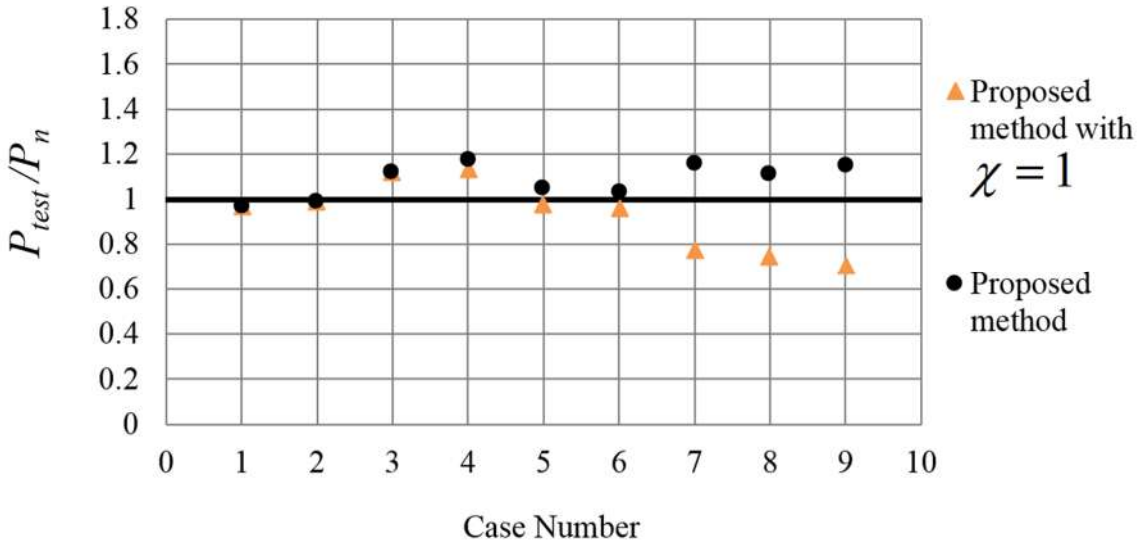

Figure 5-4 Comparison of the member strength from test simulation with the strength predicted using the proposed method, and using the proposed method with $\chi = 1$, for the additional cases

Figure 5-4 shows that the predictions using the proposed method show a good correlation (accurate to slightly conservative) with the test simulation strengths. It can be observed from Figure 5-4, that the predictions without the global buckling-local buckling interaction reduction factor, i.e., with $\chi = 1$ correlate well with the test simulation strengths for cases with $\lambda_{\max} = 20$ or 40. However, the predictions with $\chi = 1$ are too optimistic for cases with large $\lambda_{\max}$ and large L/r_s. The mean, median and coefficient of variation P_{test}/P_n for the 51 cases (42 cases from Figure 5-2 and 9 cases from Figure 5-4) are 1.16, 1.14 and 0.1 respectively.

It should be noted that for box-columns subjected to significant axial compression, the maximum w/t_{sp} will often be limited to values closer to 40, by AASHTO provisions that disallow theoretical plate buckling under construction, service and fatigue loading conditions. It should also be noted that generally large w/t_{sp} values will only be

encountered in longitudinally stiffened box-section beams. These members may have a small axial force and hence an engineer may need to calculate the axial compressive resistance of these members with large w/t_{sp} values. However, because P_u / P_n is small, the inaccuracy in the prediction of P_n will have a minor impact on the overall strength prediction for combined axial compression and bending for these members.

A good to conservative prediction of the resistance for cases 1, 4, 7, 10, 13, 16, 19, 22, 25, 28, 31, 34, 37, 40 in Figure 5-2, which have F_{cr} between $0.85F_y$ and $0.92F_y$, and have component plates with different ultimate stress capacity, shows that the proposed method works well even for cases involving significant force redistribution between relatively weak and relatively strong plate elements (One extreme example is Case 13 in Figure 5-2, in which the ultimate stress capacity of the web plate is 1/4th of the ultimate stress capacity of the flange plate).

The applicability of the proposed method for calculating the axial compressive resistance of welded box-section members made up of Grade 70 steel is evaluated by checking the $\frac{P_{test}}{P_n}$ values for critical box-section members- Cases 11 and 12 in Table 5-1 and Case 9 in Table 5-2. $\frac{P_{test}}{P_n}$ for Cases 11 and 12 in Table 5-1 are 0.98 and 0.92 respectively. $\frac{P_{test}}{P_n}$ for Case 9 in Table 5-2 is 1.06. Since these are extreme box-section members, it can be concluded that the proposed method can be used for practical box-section members made up of steels up to a yield strength of 70 ksi.

CHAPTER 6. FLEXURAL RESISTANCE OF RECTANGULAR WELDED LONGITUDINALLY STIFFENED BOX-SECTION MEMBERS

This chapter explains the proposed method for an improved quantification of the flexural resistance of longitudinally stiffened box-section members, and the evaluation of the performance of the proposed method using data collected from existing experimental tests, and parametric studies performed using finite element test simulations. Section 6.1 discusses the limitations of the various existing methods for calculation of the flexural resistance of longitudinally stiffened welded steel box-section members and highlights the motivation for the proposed method.

6.1 Limitations of existing methods and motivation

The AASHTO (2017) Specifications do not address non-composite box-section members with longitudinal stiffening. These Specifications address longitudinal stiffening in composite box girders; however they restrict the maximum flexural resistance of composite box girders to the yield moment of the compression or the tension flange. Similarly, the Eurocodes (CEN 2005; CEN 2006) limit the maximum flexural resistance of Class 4 sections to a maximum of the first yield moment of the effective cross-section in tension or compression. However, based on the observations for non-longitudinally stiffened box-section beams, there is significant reserve strength beyond the first yield of the tension flange. Section F2.4.1 of AISI (2016) allows the consideration of inelastic reserve strengths considering partial plastification, subject to certain restrictions including:

- The flexural resistance is not allowed to exceed 1.25 times the yield moment
- The ratio of the depth of the compressed portion of the webs to their thickness is not allowed to exceed $1.11\sqrt{E/F_y}$.

Based on the observations for non-longitudinally stiffened box-section beams, and also noting that $\frac{\lambda_{rw}}{2}$ for non-longitudinally stiffened webs (λ_{rw} defined in Section 3.2.1) is more than two times $1.11\sqrt{E/F_y}$, it appears that the AISI rules are too prohibitive and would result in a failure to consider larger available resistances.

In addition:

- AASHTO (2017) does not address the possibility of lateral torsional buckling.
- The Eurocode method requires an iterative or at least a two-step calculation for obtaining the effective cross-section for Class 4 sections.
- According to AISI (2016), the flexural resistance is calculated using effective section properties where the effective section is obtained using an effective width of the flanges and webs, using the provisions in Appendix 1 of AISI (2016). However, Appendix 1 does not specifically have provisions for longitudinally stiffened webs subjected to a stress gradient.

Therefore, a more general method is needed that provides a good prediction of the flexural resistance of practical longitudinally stiffened box beams and addresses the various issues discussed above. The data from the parametric studies performed using finite element test simulations and experimental tests discussed in Section 6.3 provides useful

information to answer the following questions, and arrive at a comprehensive yet simple, designer-friendly method:

1) How well does the effective cross-section model (effective flange and/or effective web, described in Section 6.2) work for capturing the buckling and postbuckling resistance of flange and web elements?

2) The R_b (web load-shedding factor) equation approved for the next release of the AASHTO LRFD specifications in 2020 neglects the contribution of the web longitudinal stiffeners when $\frac{d_s}{D_c} > 0.76$; where d_s is the distance from the centerline of the closest web longitudinal stiffener to the inner surface of the compression-flange element, and D_c is the depth of the web in compression. Can the web longitudinal stiffeners provide any measurable enhancement of the web postbuckling resistance when $\frac{d_s}{D_c} > 0.76$?

   It is not uncommon to have longitudinal stiffeners at the mid-depth of the web for some types of members, e.g., arch ribs.

3) A key attribute of narrow boxes is that a_{wc} (for box sections a_{wc} is the ratio of two times the web area in compression to half of the area of the compression flange) can be relatively large; outside the bounds of prior developments of the R_b equation for I-section members. How does web bend-buckling influence the flexural resistance of box-section members with large a_{wc} values?

4) In longitudinally stiffened box-section members where the neutral axis is closer to the compression flange than to the tension flange, first yielding in flexure occurs at the tension flange. Should the resistance of longitudinally stiffened box-section members be limited to the first yield of the tension flange? Is there significant available resistance beyond the first yield of the tension flange considering spread of yielding in the tension zone?

5) It is common knowledge that box sections are torsionally stiff. So, is lateral torsional buckling a concern for practical longitudinally stiffened box-section members?

6.2 Proposed methods

The proposed procedure for calculating the flexural resistance of longitudinally stiffened box-section members is slightly different depending on whether the compression flange is longitudinally stiffened, with or without longitudinal stiffening of the web, or the compression flange is non-longitudinally stiffened. Therefore, the calculations are presented below for these two separate cases. These calculations are conceptually consistent with each other and with the method for non-longitudinally stiffened box-section members, discussed in Section 3.2. In some design situations, longitudinal stiffening may be encountered on the tension flange. These cases are addressed as a subset of the above two cases and the non-longitudinally stiffened box-section member design procedure discussed in Section 3.2, simply by considering the additional contribution of the longitudinal stiffeners to the tension flange area, as well as the shift in the location of the

tension flange force through the depth due to the eccentricity of the tension flange stiffeners.

6.2.1 Procedure for box-section members with a longitudinally stiffened compression flange and with longitudinally or non-longitudinally stiffened webs

Unlike non-longitudinally stiffened plates, longitudinally stiffened plates are typically unable to sustain large inelastic axial compressive strains beyond their maximum resistance. Therefore, the flexural resistance of box sections with a longitudinally stiffened compression flange is limited to the first yield of the compression flange of the effective cross-section. A representative longitudinally stiffened box cross-section is shown in Figure 6-1. The corresponding effective cross-section is shown in Figure 6-2. The compression flange is represented by its effective area, located at the centroid of the effective flange, including the area of the longitudinal stiffeners. AISI (2016) uses a similar approach. In Figure 6-2,

- $A_{ecf} = \dfrac{P_{nsp}}{F_{yf}}$ (136)
- P_{nsp} = nominal compressive resistance of the longitudinally stiffened compression flange, calculated using the proposed method explained in Section 4.2
- c = the distance of the centroid of the gross area of the flange plate and its longitudinal stiffeners from the top of the web plates.

Variables corresponding to the effective cross-section, i.e., cross-section with the compression flange represented by its effective area given by Eq. 136 (shown in Figure 6-2), are denoted by the subscript e.

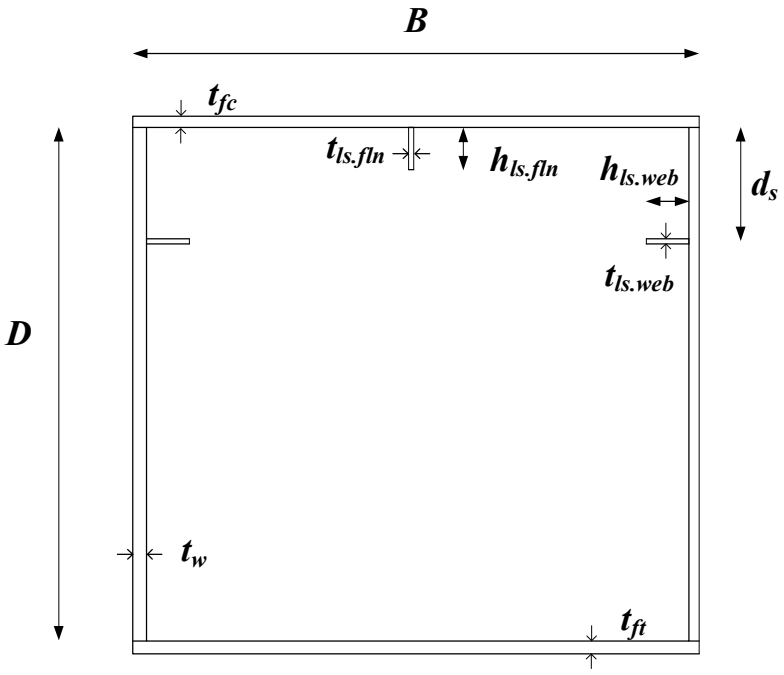

Figure 6-1 Representative longitudinally stiffened box cross-section

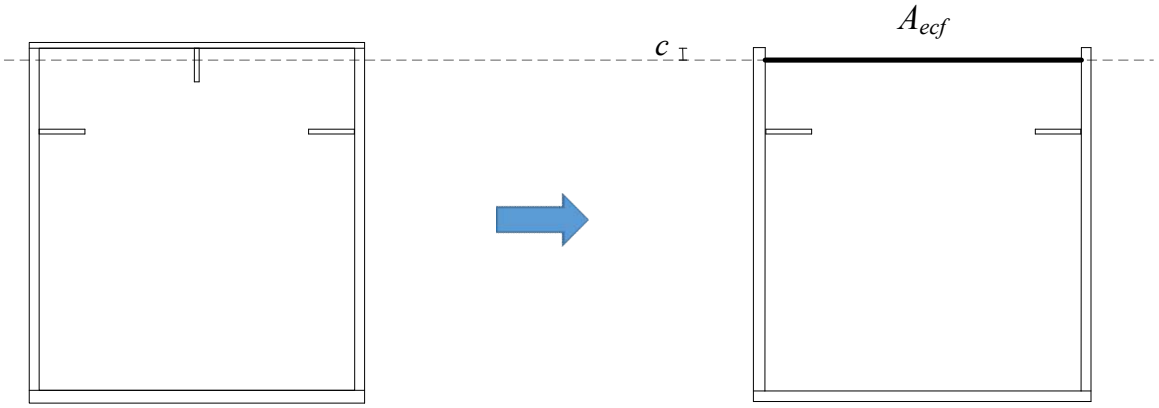

Figure 6-2 Effective box-section considering the resistance of the stiffened compression flange

The recommended calculation of the nominal flexural resistance, M_n, of a welded box-section member with a longitudinally stiffened compression flange is as follows:

If $L_b \le L_p$ then,

$$M_n = M_{cs} \tag{137}$$

If $L_p < L_b \le L_r$ then,

$$M_n = C_b\left[M_{cs} - \left(M_{cs} - F_{yr}S_{xce}\right)\left(\frac{L_b - L_p}{L_r - L_p}\right)\right] \le M_{cs} \tag{138}$$

where:

- M_{cs} is the cross-section resistance, calculated as follows.

  For homogeneous box-section members in which the compression flange of the effective cross-section yields first (i.e., $M_{yce} < M_{yte}$), and when:

  - $R_b = 1$, or
  - $a_{wce} \le 8$ and $d_s / D_{ce} < 0.76$

  $$M_{cs} = R_b F_{yc} S_{xce} \tag{139}$$

  For all other cases M_{cs} is to be calculated via a strain-compatibility analysis using the following effective cross-sections:

  - Figure 6-3 shows the effective cross-section and idealized stress distribution for a box section with noncompact or compact unstiffened webs ($\lambda_w \le \lambda_{rw}$).
  - Figure 6-4 shows the effective cross-section and idealized stress distribution for a box section with slender unstiffened webs ($\lambda_w > \lambda_{rw}$).

- Figure 6-5 shows the effective cross-section and idealized stress distribution for a box section with longitudinally stiffened webs having $\lambda_w \le \lambda_{rw}$, such that load shedding from the postbuckling response of the web in flexure may be neglected.
- Figure 6-6 shows the effective cross-section and idealized stress distribution for a box section with longitudinally stiffened webs $\lambda_w > \lambda_{rw}$, such that the postbuckling response of the web in flexure needs to be captured.

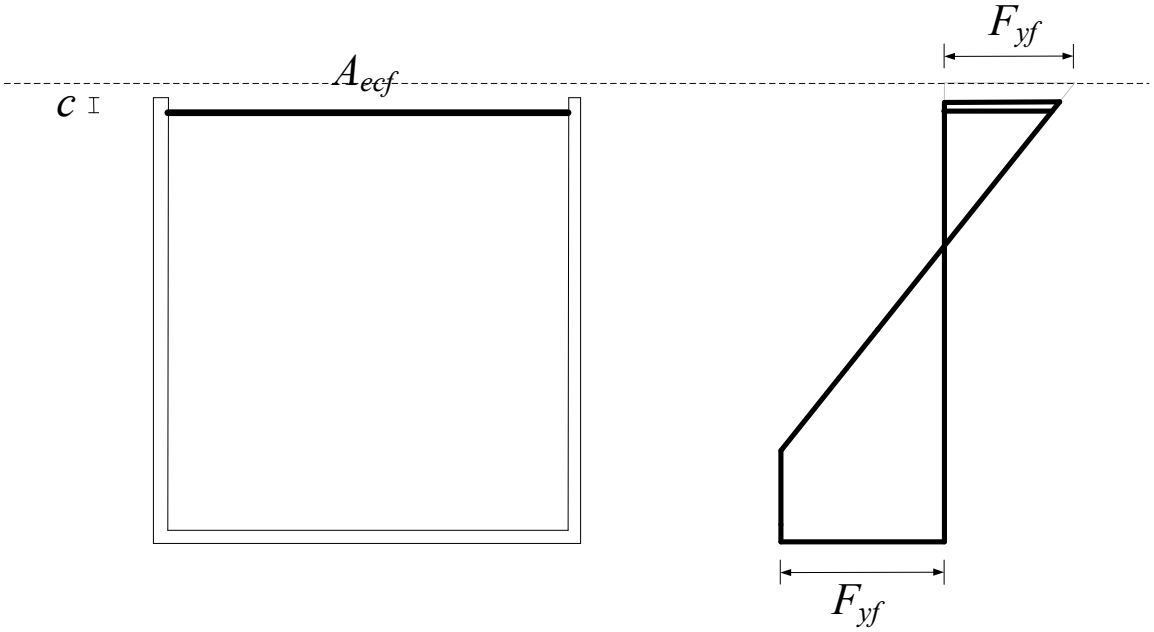

Figure 6-3 Effective cross-section and stress distribution for calculating M_{cs} using strain-compatibility analysis, for a box with unstiffened webs such that $\lambda_w \le \lambda_{rw}$

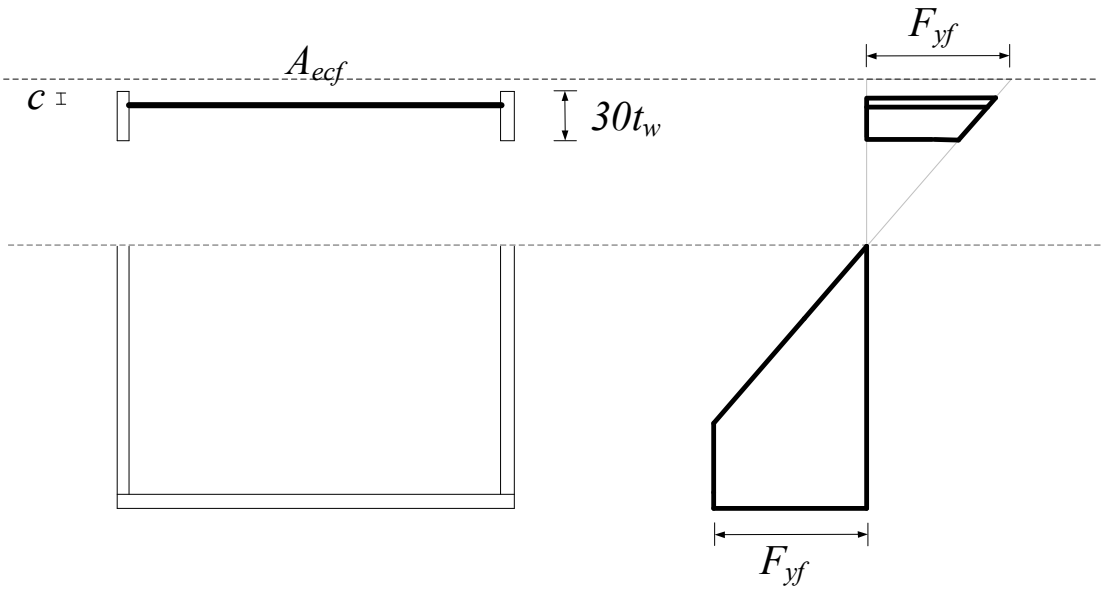

Figure 6-4 Effective cross-section and stress distribution for calculating M_{cs} using strain-compatibility analysis, for a box with unstiffened webs such that $\lambda_w > \lambda_{rw}$

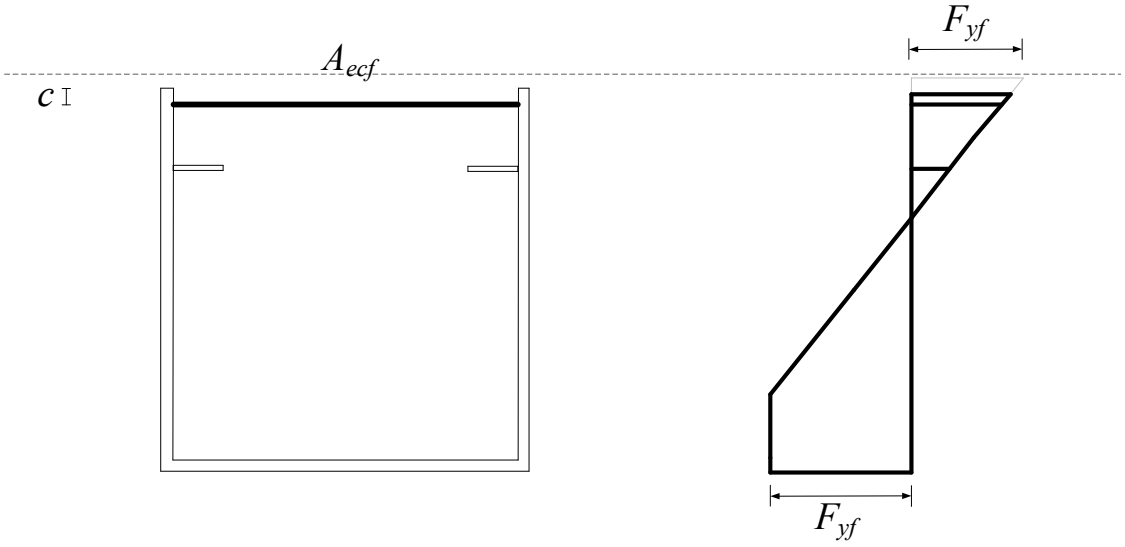

Figure 6-5 Effective cross-section and stress distribution for calculating M_{cs} using strain-compatibility analysis, for a box with longitudinally stiffened webs such that $\lambda_w \leq \lambda_{rw}$

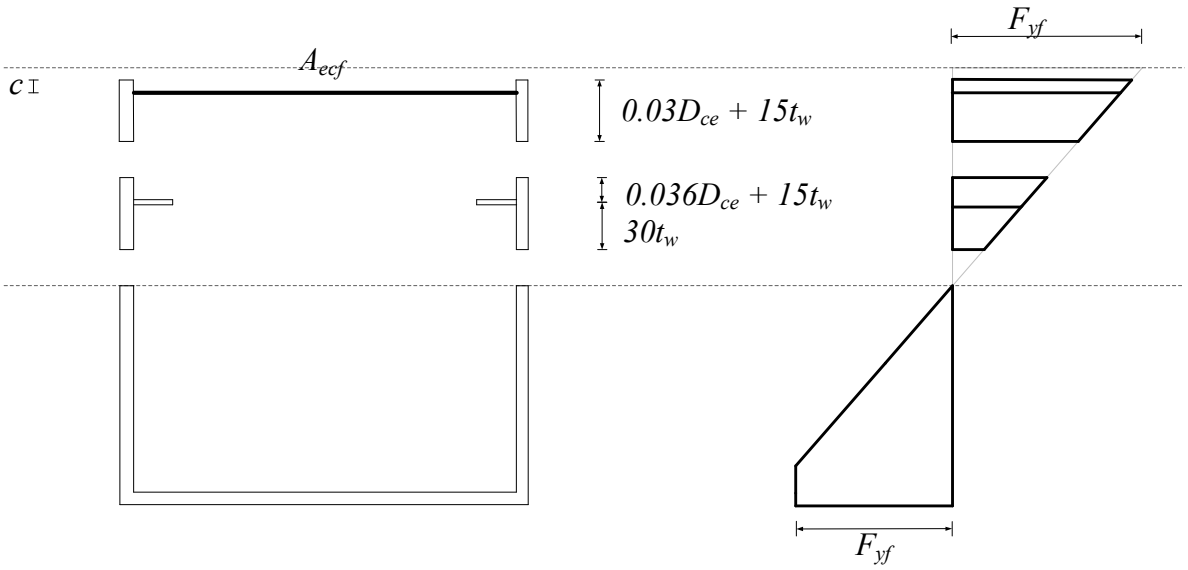

Figure 6-6 Effective cross-section and stress distribution for calculating M_{cs} using strain-compatibility analysis, for a box with longitudinally stiffened webs such that $\lambda_w > \lambda_{rw}$

For homogeneous box-section members the calculation of M_{cs} is based on the limit state of first yield of the compression flange of the effective cross-section. In Figure 6-3, Figure 6-4, Figure 6-5 and Figure 6-6, $F_{yf} = F_{yc} = F_{yt}$. Both flanges are assumed to have the same yield strength. The influence of web postbuckling in flexure, as well as early tension flange yielding in cases where $S_{xce} > S_{xte}$ is represented explicitly by the effective-cross sections and idealized stress distributions shown in Figure 6-3 through Figure 6-6.

For box sections with two or more web longitudinal stiffeners in compression per web, the above provisions may be applied by considering only the longitudinal stiffener closest to the compression flange within each web (neglecting all other web longitudinal stiffeners in compression). This conservatively neglects the

benefit from multiple web longitudinal stiffeners in compression; however, the predominant benefit of web longitudinal stiffening typically comes from the longitudinal stiffener closest to the compression flange.

For hybrid box-section members, the strain compatibility based calculations become more complex. Therefore, it is recommended that the cross-section resistance be conservatively calculated as

$$M_{cs} = R_b R_h F_{yc} S_{xce} \le R_h F_{yt} S_{xte} \tag{140}$$

i.e., taking the cross-section resistance as the minimum of, the resistance corresponding to the limit state of first yield of the compression flange, and the resistance corresponding to the limit state of first yield of the tension flange.

In lieu of performing a strain compatibility analysis corresponding to Figure 6-3 through Figure 6-6 for homogeneous box-section members, the cross-section resistance of all homogeneous box-section members ($S_{xce} \le S_{xte}$ as well as $S_{xce} > S_{xte}$) can be conservatively calculated as

$$M_{cs} = R_b F_{yc} S_{xce} \le F_{yt} S_{xte} \tag{141}$$

i.e., taking the cross-section resistance as the minimum of, the resistance corresponding to the limit state of first yield of the compression flange, and the resistance corresponding to the limit state of first yield of the tension flange.

- L_p, L_r and F_{yr} are defined using Eq. 41, 42 and 28 respectively, except the effective cross-section is as shown in Figure 6-2.

- $$J = \frac{4A_m^2}{\left(\frac{b_m}{t_{fc}} + \frac{b_m}{t_{ft}} + \frac{2h_m}{t_w}\right)} \quad (142)$$

  It is the St. Venant torsional constant neglecting the longitudinal stiffeners.

- $$b_m = B - t_w \quad (143)$$

- $$h_m = D + \frac{t_{fc}}{2} + \frac{t_{ft}}{2} \quad (144)$$

- $$A_m = b_m h_m \quad (145)$$

- $$a_{wce} = \frac{2D_{ce}t_w}{\left(\frac{A_{ecf}}{2}\right)} \quad (146)$$

- $$\lambda_w = \frac{2D_{ce}}{t_w} \quad (147)$$

- λ_{rw} is the limiting slenderness ratio for a noncompact web and is calculated as follows:

  - For non-longitudinally stiffened webs,

    $$\lambda_{rw} = 4.6\sqrt{\frac{E}{F_{yc}}} \quad (148)$$

  - For longitudinally stiffened webs in homogeneous box sections,

    $$\lambda_{rw} = \left(\frac{2D_{ce}}{D}\right)0.95\sqrt{\frac{Ek}{F_{yc}}} \quad (149)$$

    where k is calculated using the provisions in AASHTO (2017) Article 6.10.1.9.2.

  - For longitudinally stiffened webs in hybrid box sections,

$$\lambda_{rw} = 5.7\sqrt{\frac{E}{F_{yc}}} \tag{150}$$

- The web load-shedding factor, R_b, is calculated using the provisions recommended by Subramanian and White (2017) for longitudinally stiffened webs, using a_{wc} determined with $b_{fc}t_{fc}$ taken as $\frac{A_{ecf}}{2}$, and D_c taken as D_{ce}. These provisions have been balloted and approved for the next release of the AASHTO LRFD Specification in 2020.
- The hybrid factor, R_h, is calculated using AASHTO (2017) Eq. 6.10.1.10.1-1 with A_{fn} taken as one-half of the total effective compression flange area, $\frac{A_{ecf}}{2}$, if $D_n = D_{ce}$, and A_{fn} taken as $\frac{b_{ft}t_{ft}}{2}$ if $D_n = D - D_{ce}$.

In cases where compression flange longitudinal stiffeners are provided but are not required for strength, the longitudinal stiffeners may be neglected and the flange may be considered as non-longitudinally stiffened for purposes of calculating the member strength. In such cases, the member strength should be calculated using the method discussed in Section 3.2 if the webs are non-longitudinally stiffened, and using the procedure discussed in Section 6.2.2 if the webs are longitudinally stiffened.

6.2.2 *Procedure for box-section members with a non-longitudinally stiffened compression flange and longitudinally stiffened webs*

The proposed method for characterizing the flexural resistance of these member types is the same as that for non-longitudinally stiffened box-section members (discussed in Section 3.2) except,

- The web load-shedding factor, R_b, is calculated using the provisions recommended by Subramanian and White (2017) for longitudinally stiffened webs, using a_{wc} determined with $b_{fc}t_{fc}$ taken as $\frac{A_{eff}}{2}$, and D_c taken as D_{ce}, where A_{eff} is the effective area of the compression flange calculated using the modified Winter's effective equation discussed in Section 2.2.
- The hybrid factor, R_h, is calculated using AASHTO (2017) Eq. 6.10.1.10.1-1 with A_{fn} taken as one-half of the total effective compression flange area, $\frac{A_{eff}}{2}$, if $D_n = D_{ce}$, and A_{fn} taken as $\frac{b_{ft}t_{ft}}{2}$ if $D_n = D - D_{ce}$.
- For cases with $S_{xce} > S_{xte}$, the cross-section flexural resistance is calculated using the provisions in Table 3-3 but using the cross-section model and idealized stress distribution in Figure 6-7 and Figure 6-8, instead of Figure 3-1 and Figure 3-2 respectively.

Web longitudinal stiffeners, if present, should be included in the calculation of elastic gross and effective cross-section properties, and in the calculation of the moment corresponding to first yield of the compression flange of the effective cross-section. However, any web

longitudinal stiffeners subjected to compression should be neglected in the computation of M_{pe}. This is due to the limited ability of the web longitudinal stiffeners to develop larger inelastic strains necessary to develop yielding throughout the depth of the cross-section. Any enhancement of the resistance of compact or noncompact web sections due to the placement of web longitudinal stiffeners subjected to compression, other than the increase in the moment corresponding to first yield of the compression flange of the effective cross-section, is neglected.

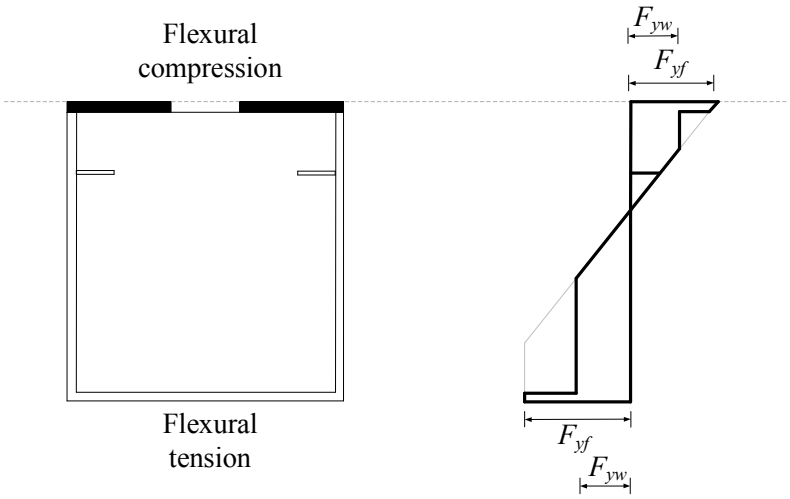

Figure 6-7 Cross-section model and stress distribution for calculation of M_{yct} for box-section members with longitudinally stiffened webs and an unstiffened compression flange, when $\lambda_w \leq \lambda_{rw}$

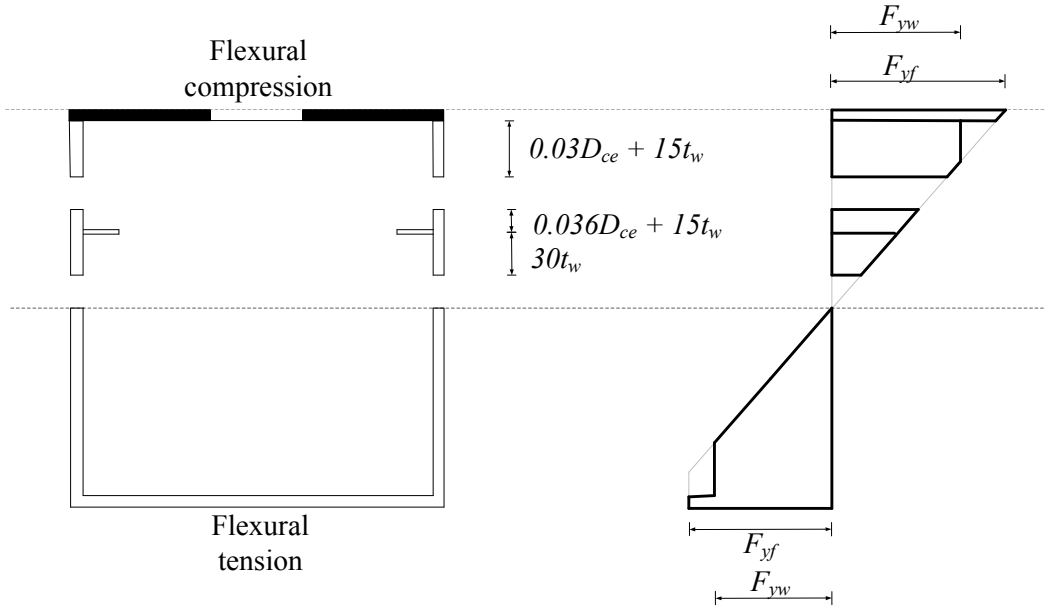

Figure 6-8 Cross-section model and stress distribution for calculation of M_{cs} for box-section members with longitudinally stiffened webs and an unstiffened compression flange, when $\lambda_w > \lambda_{rw}$

6.2.3 General box section proportion limits

The procedures discussed in Section 6.2.1 and 6.2.2 are applicable to box-section members satisfying the following limits:

1) $\frac{D}{t_w} \leq 150$ for webs without longitudinal stiffeners.

2) $\frac{D}{t_w} \leq 300$ for webs with longitudinal stiffeners.

3) $\frac{D}{b_{fc}}$ or $\frac{D}{B}$ shall not exceed 6.

4) For non-longitudinally stiffened compression and tension flanges, b_{fi}/t_{fc} or b_{fi}/t_{ft} shall not exceed 90.

5) For longitudinally stiffened compression or tension flanges, w/t_{sp} shall not exceed 90.

6) Web longitudinal stiffeners should satisfy the proportioning requirements in AASHTO (2017) Article 6.10.11.3.

6.3 Evaluation of the performance of the proposed method

The performance of the proposed methods is evaluated using the results of a parametric study performed using finite element test simulations (discussed in Section 6.3.1), and using data collected from experimental tests in the literature (discussed in Section 6.3.2).

6.3.1 Parametric study performed using finite element test simulations

This section explains the parametric study design, and discusses the results of the parametric study. The finite element modelling of these box-section members is explained in Appendix A.

6.3.1.1 Parametric study design

The parametric study is divided into 15 groups: Groups 1–8 are comprised of homogeneous box-section members, and Groups 9–15 are comprised of hybrid box-section members. Table 6-1 summarizes the parametric study design. The cross-section dimensions and lengths of the various cases listed in Table 6-1 are provided in Appendix

F. All the box-section members in the parametric study have a non-longitudinally stiffened tension flange. The box-section members used in the parametric study are designed to satisfy the general box section proportioning limits in Section 6.2.3, as well as the following practical limits:

1) $\frac{A_{wls}}{A_{cf}} \le 1.2$ where, A_{wls} is the total area of all the web longitudinal stiffeners in compression, and A_{cf} is the area of the compression flange including longitudinal stiffeners

2) $t_{ls.web} \le 2$ in.

3) $\frac{B}{h_{ls.web}} \ge 3$

4) $a_{wce} \le 20$

5) Thickness of all box-section component plates (including longitudinal stiffeners) ≤ 4 in.

In Table 6-1:

- n_{cfln} are the number of longitudinal stiffeners on the compression flange
- n_{web} are the number of longitudinal stiffeners on each of the webs
- L is the length of the box-section beam
- $L_{\max} = \max\left[30D, 200r_y\right]$ is the maximum practical length of the box-section beam
- w is the width of the subpanels in the compression flange, as shown in Figure 4-8.
- $A_g = wt_{fc} + h_{ls.fln}t_{ls.fln}$ (151)

Table 6-1 Summary of parametric study variables for evaluating the performance of the proposed method for characterizing the flexural resistance of longitudinally stiffened box-section members

Group #	Case #	S_{xce} and S_{xte}	Web			Compression flange			L
			n_{web}	$\frac{2D_{ce}}{t_w}$ and λ_{rw}	$\frac{d_s}{D_{ce}}$	n_{cfln}	$\frac{w}{t_{fc}}$	$\frac{A_g}{wt_{fc}}$	
1	1	$S_{xce} \le S_{xte}$	1	$\frac{2D_{ce}}{t_w} < \lambda_{rw}$	0.4	1	30	1.2	L_p
	2	$S_{xce} \le S_{xte}$	1	$\frac{2D_{ce}}{t_w} < \lambda_{rw}$	0.4	1	30	1.2	$\frac{L_p + L_{\max}}{2}$
	3	$S_{xce} \le S_{xte}$	1	$\frac{2D_{ce}}{t_w} < \lambda_{rw}$	0.4	1	30	1.2	$L_{\max}$
	4	$S_{xce} \le S_{xte}$	1	$\frac{2D_{ce}}{t_w} < \lambda_{rw}$	0.39	1	60	1.2	L_p
	5	$S_{xce} \le S_{xte}$	1	$\frac{2D_{ce}}{t_w} < \lambda_{rw}$	0.39	1	60	1.2	$\frac{L_p + L_{\max}}{2}$
	6	$S_{xce} \le S_{xte}$	1	$\frac{2D_{ce}}{t_w} < \lambda_{rw}$	0.39	1	60	1.2	$L_{\max}$
2	7	$S_{xce} \le S_{xte}$	1	$\frac{2D_{ce}}{t_w} > \lambda_{rw}$	< 0.76	1	30	1.2	L_p
	8	$S_{xce} \le S_{xte}$	1	$\frac{2D_{ce}}{t_w} > \lambda_{rw}$	< 0.76	1	30	1.2	$\frac{L_p + L_{\max}}{2}$
	9	$S_{xce} \le S_{xte}$	1	$\frac{2D_{ce}}{t_w} > \lambda_{rw}$	< 0.76	1	30	1.2	$L_{\max}$
	10	$S_{xce} \le S_{xte}$	1	$\frac{2D_{ce}}{t_w} > \lambda_{rw}$	< 0.76	1	60	1.2	L_p

	11	$S_{xce} \le S_{xte}$	1	$\frac{2D_{ce}}{t_w} > \lambda_{rw}$	< 0.76	1	60	1.2	$\frac{L_p + L_{\max}}{2}$
	12	$S_{xce} \le S_{xte}$	1	$\frac{2D_{ce}}{t_w} > \lambda_{rw}$	< 0.76	1	60	1.2	$L_{\max}$
3	13	$S_{xce} \le S_{xte}$	1	$\frac{2D_{ce}}{t_w} > \lambda_{rw}$	> 0.76	1	30	1.2	L_p
	14	$S_{xce} \le S_{xte}$	1	$\frac{2D_{ce}}{t_w} > \lambda_{rw}$	> 0.76	1	30	1.2	$\frac{L_p + L_{\max}}{2}$
	15	$S_{xce} \le S_{xte}$	1	$\frac{2D_{ce}}{t_w} > \lambda_{rw}$	> 0.76	1	30	1.2	$L_{\max}$
	16	$S_{xce} \le S_{xte}$	1	$\frac{2D_{ce}}{t_w} > \lambda_{rw}$	> 0.76	1	60	1.2	L_p
	17	$S_{xce} \le S_{xte}$	1	$\frac{2D_{ce}}{t_w} > \lambda_{rw}$	> 0.76	1	60	1.2	$\frac{L_p + L_{\max}}{2}$
	18	$S_{xce} \le S_{xte}$	1	$\frac{2D_{ce}}{t_w} > \lambda_{rw}$	> 0.76	1	60	1.2	$L_{\max}$
4	19	$S_{xce} > S_{xte}$	0	$\frac{2D_{ce}}{t_w} < \lambda_{rw}$	-	1	30	1.2	L_p
	20	$S_{xce} > S_{xte}$	0	$\frac{2D_{ce}}{t_w} < \lambda_{rw}$	-	1	30	1.2	$L_{\max}$
5	21	$S_{xce} > S_{xte}$	0	$\frac{2D_{ce}}{t_w} > \lambda_{rw}$	-	1	30	1.2	L_p
	22	$S_{xce} > S_{xte}$	0	$\frac{2D_{ce}}{t_w} > \lambda_{rw}$	-	1	30	1.2	$L_{\max}$
6	23	$S_{xce} > S_{xte}$	1	$\frac{2D_{ce}}{t_w} < \lambda_{rw}$	0.4	1	30	1.2	L_p

	24	$S_{xce} > S_{xte}$	1	$\frac{2D_{ce}}{t_w} < \lambda_{rw}$	0.4	1	30	1.2	$L_{\max}$
7	25	$S_{xce} > S_{xte}$	1	$\frac{2D_{ce}}{t_w} > \lambda_{rw}$	< 0.76	1	30	1.2	L_p
	26	$S_{xce} > S_{xte}$	1	$\frac{2D_{ce}}{t_w} > \lambda_{rw}$	< 0.76	1	30	1.2	$L_{\max}$
8	27	$S_{xce} > S_{xte}$	1	$\frac{2D_{ce}}{t_w} > \lambda_{rw}$	> 0.76	1	30	1.2	L_p
	28	$S_{xce} > S_{xte}$	1	$\frac{2D_{ce}}{t_w} > \lambda_{rw}$	> 0.76	1	30	1.2	$L_{\max}$
9	29	$S_{xce} \le S_{xte}$	0	$\frac{2D_{ce}}{t_w} < \lambda_{rw}$	-	1	30	1.2	L_p
	30	$S_{xce} \le S_{xte}$	0	$\frac{2D_{ce}}{t_w} < \lambda_{rw}$	-	1	30	1.2	$L_{\max}$
10	31	$S_{xce} \le S_{xte}$	1	$\frac{2D_{ce}}{t_w} > \lambda_{rw}$	< 0.76	1	30	1.2	L_p
	32	$S_{xce} \le S_{xte}$	1	$\frac{2D_{ce}}{t_w} > \lambda_{rw}$	< 0.76	1	30	1.2	$L_{\max}$
11	33	$S_{xce} \le S_{xte}$	1	$\frac{2D_{ce}}{t_w} > \lambda_{rw}$	> 0.76	1	30	1.2	L_p
	34	$S_{xce} \le S_{xte}$	1	$\frac{2D_{ce}}{t_w} > \lambda_{rw}$	> 0.76	1	30	1.2	$L_{\max}$
12	35	$S_{xce} > S_{xte}$	0	$\frac{2D_{ce}}{t_w} < \lambda_{rw}$	-	1	30	1.2	L_p
	36	$S_{xce} > S_{xte}$	0	$\frac{2D_{ce}}{t_w} < \lambda_{rw}$	-	1	30	1.2	$L_{\max}$

13	37	$S_{xce} > S_{xte}$	0	$\frac{2D_{ce}}{t_w} > \lambda_{rw}$	-	1	30	1.2	L_p
	38	$S_{xce} > S_{xte}$	0	$\frac{2D_{ce}}{t_w} > \lambda_{rw}$	-	1	30	1.2	$L_{\max}$
14	39	$S_{xce} > S_{xte}$	1	$\frac{2D_{ce}}{t_w} > \lambda_{rw}$	< 0.76	1	30	1.2	L_p
	40	$S_{xce} > S_{xte}$	1	$\frac{2D_{ce}}{t_w} > \lambda_{rw}$	< 0.76	1	30	1.2	$L_{\max}$
15	41	$S_{xce} > S_{xte}$	1	$\frac{2D_{ce}}{t_w} > \lambda_{rw}$	> 0.76	1	30	1.2	L_p
	42	$S_{xce} > S_{xte}$	1	$\frac{2D_{ce}}{t_w} > \lambda_{rw}$	> 0.76	1	30	1.2	$L_{\max}$

6.3.1.2 Results and discussion

Figure 6-9 and Figure 6-10 show the results for homogeneous (Groups 1-8) and hybrid (Groups 9-15) cases respectively. For the results shown in Figure 6-9 and Figure 6-10 the cross-section flexural resistance is calculated as follows:

- Proposed method
  - For homogeneous box-section members in which the compression flange of the effective cross-section yields first (i.e., $M_{yce} < M_{yte}$), and when:
    - $R_b = 1$, or
    - $a_{wce} \le 8$ and $d_s / D_{ce} < 0.76$

$$M_{cs} = R_b F_{yc} S_{xce}$$

- For all other homogeneous box-section members, M_{cs} is calculated using strain-compatibility analysis (Figure 6-3 through Figure 6-6).
- For hybrid box-section members, $M_{cs} = R_b R_h F_{yc} S_{xce} \le R_h F_{yt} S_{xte}$

- Simplified method
  - For homogeneous box-section members, $M_{cs} = R_b F_{yc} S_{xce} \le F_{yt} S_{xte}$
  - For hybrid box-section members, $M_{cs} = R_b R_h F_{yc} S_{xce} \le R_h F_{yt} S_{xte}$

The mean, median and coefficient of variation of M_{test}/M_n, using the proposed method for Groups 1-15, are 1.19, 1.14 and 0.15 respectively. The mean, median and coefficient of variation of M_{test}/M_n, using the simplified method for all groups except Group 3, are 1.22, 1.18 and 0.15 respectively. In general it can be observed that,

- For homogeneous cases, the predictions using the proposed method correlate well with the strengths from the test simulations (accurate to slightly conservative). Also, for the predictions using the proposed method the dispersion in results is much less as compared to the use of the simplified (more conservative) method which considers the limit state of tension flange yielding. This clearly shows the ability of the idealized stress distribution and/or effective cross-section model (effective flange and/or effective web) to capture the resistance corresponding to the spread of yielding in the tension zone, as well as the local buckling and postbuckling resistance of the compression flange and webs of the box-section member.

- For hybrid cases, the predictions are more conservative and there is more dispersion when using the proposed method, as compared to that for homogeneous cases. This is because for hybrid cases the proposed method is the same as the simplified (more conservative) method which considers the limit state of tension flange yielding. The reason for adopting this simpler approach is that the strain-compatibility analysis calculations using Figure 6-3 through Figure 6-8 become too complicated for normal design practice when applied to hybrid box-section members.

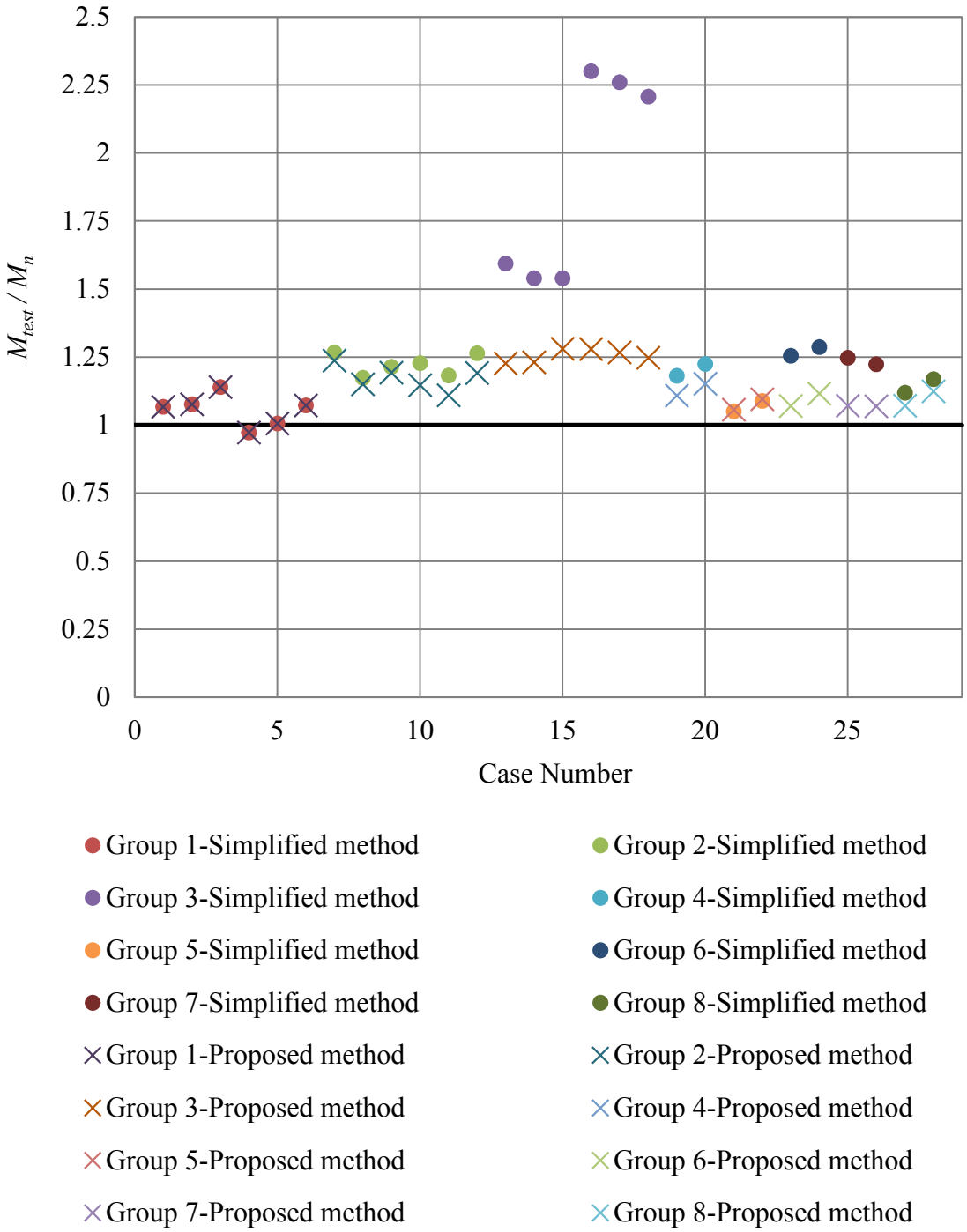

Figure 6-9 Comparison of the strength from test simulation with the strength predicted using the proposed method and using the method considering tension flange yielding, for homogeneous box-section members

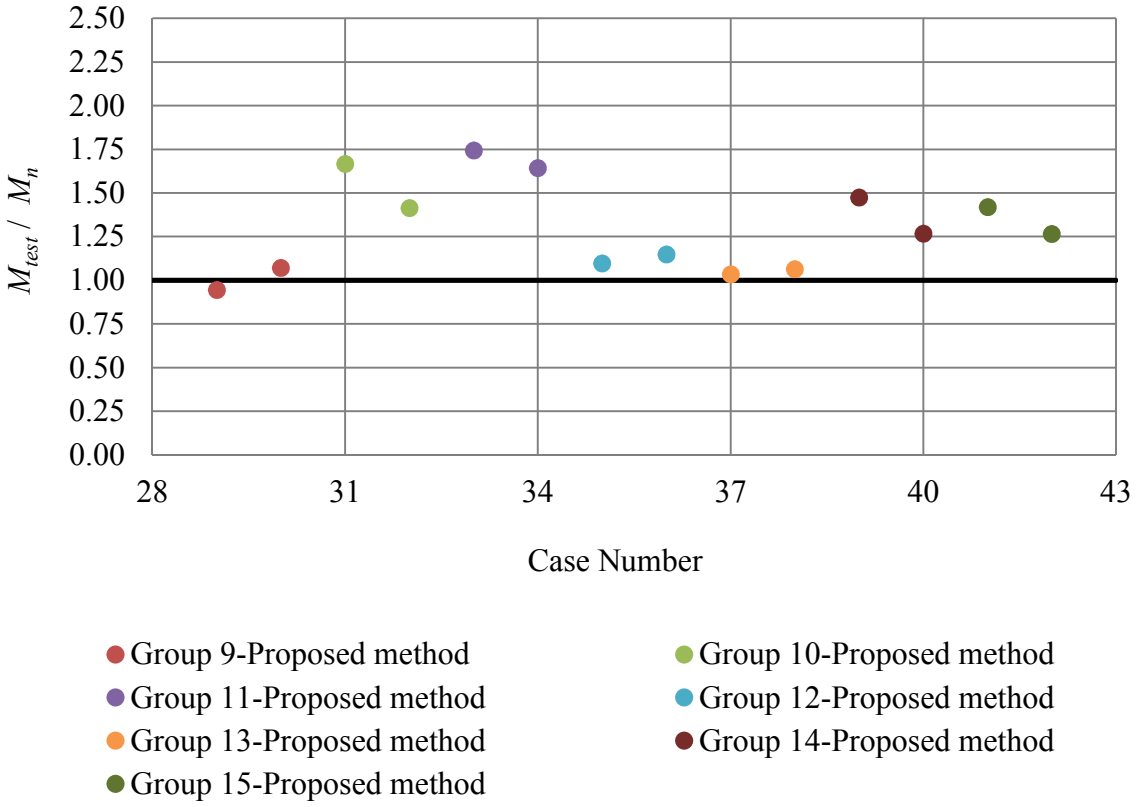

Figure 6-10 Comparison of the strength from test simulation with the strength predicted using the proposed method for hybrid box-section members

The good correlation of the strengths predicted using the proposed method and the strengths from the test simulations for Group 1 and Group 9 cases, clearly shows the inability of longitudinally stiffened compression flange plates to sustain large inelastic axial compressive strains beyond the peak load without a substantial reduction in their load carrying capacity, and therefore provides a justification for limiting the flexural resistance of box sections with a longitudinally stiffened compression flange to the first yield of the compression flange in the effective cross-section.

As discussed earlier in Section 6.1, for narrow box-section members a_{wce} can be very large; outside the bounds of prior developments of the R_b equation for I-section members. Group 2 cases belong to this category, where $a_{wce} = 10$ for cases 7, 8, 9, and $a_{wce} = 19$ for cases 10, 11, 12. It can be observed by comparing the predictions using the proposed method and using the simplified method that, for cases with large a_{wce} the predictions based on strain-compatibility analysis using the effective web cross-section model are better than those using the R_b equation.

As mentioned earlier in Section 6.1, the R_b equation approved for the next release of the AASHTO LRFD specifications in 2020 neglects the contribution of the web longitudinal stiffeners when $\frac{d_s}{D_{ce}} > 0.76$. It is not uncommon to have longitudinal stiffeners at the mid-depth of the web for some types of members, e.g., arch ribs. Group 3 cases belong to this category. It can be observed by comparing the predictions using the proposed method and using the simplified method that, using the R_b equation which neglects the contribution of the web longitudinal stiffeners significantly under-predicts the resistance of these cases, and that there is a much better correlation between the test simulation strengths and the predictions based on strain-compatibility analysis using the effective web cross-section model considering the contribution of the web longitudinal stiffeners.

A good correlation of resistance predicted using the proposed method and the test simulation strengths for cases belonging to Groups 4 through 8 (all these cases have $S_{xce} > S_{xte}$) clearly shows,

- The existence of larger available resistance beyond the first yield of the tension flange, and
- The ability of the proposed method using an effective cross-section model (effective compression flange and/or effective web) and strain-compatibility analysis, to predict the flexural resistance of these cases.

It can be observed from Figure 6-9 and Figure 6-10, that the inelastic LTB resistance calculated by considering a linear interpolation gives good correlation with the test simulation strengths. For the beams included in the parametric study, it is found that for the longest practical box-section beam the inelastic lateral torsional buckling resistance is as low as 80.1% of the cross-section resistance.

Figure 6-11 shows the variation of the flexural resistance with change in length of a box-section member having the same cross-section as that for Cases 7, 8 and 9. For this member, the reduction in flexural resistance at L_{max} is 19.7% compared to the resistance at $0.5L_p$. It can be seen that the inelastic lateral torsional buckling resistance calculated by considering a linear interpolation gives reasonably good predictions.

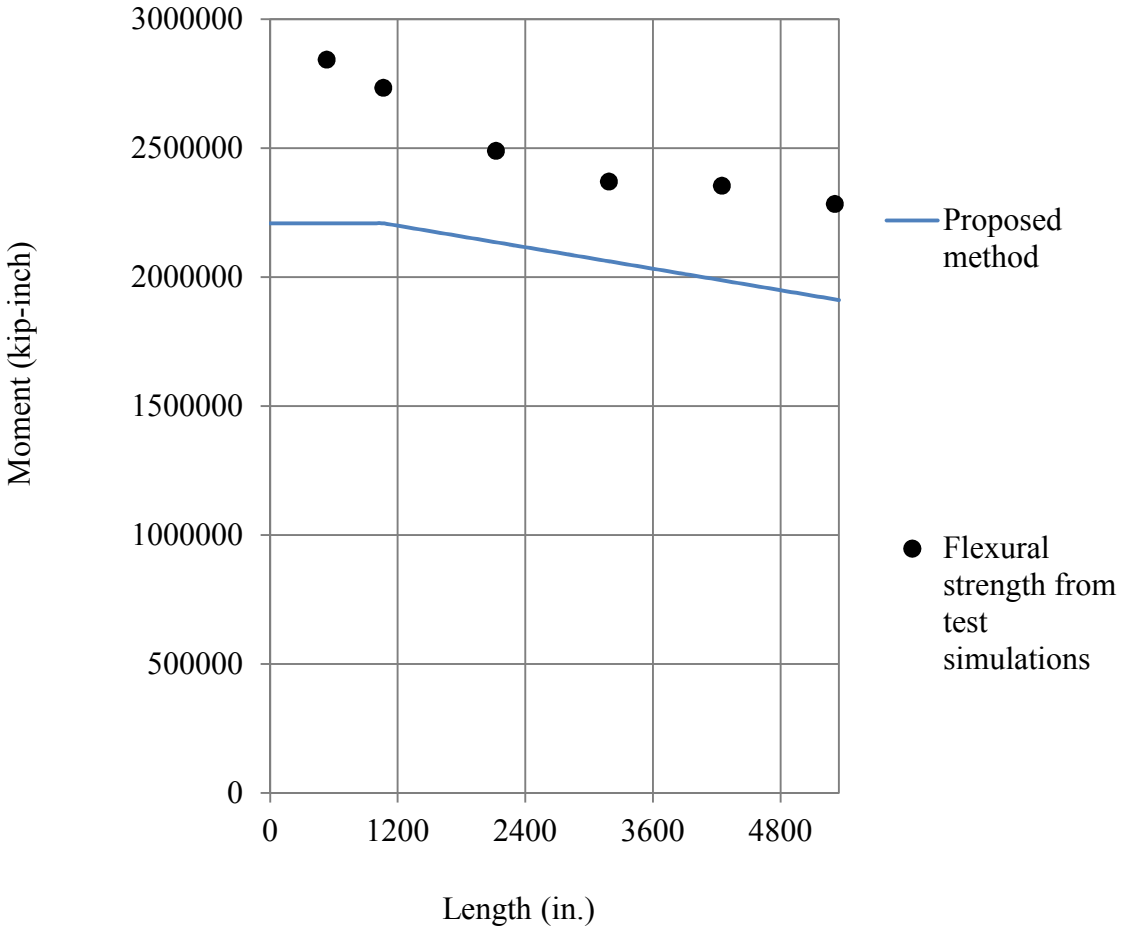

Figure 6-11 Variation of flexural resistance with change in length of a box-section member

6.3.2 Comparison with experimental tests from the literature

In addition to the parametric study, experimental data from Saad-Eldeen et al. (2010), Gordo and Soares (2015a), Gordo and Soares (2015b), Gordo and Soares (2015c), Gordo and Soares (2004), Gordo and Soares (2008), Gordo and Soares (2009) is used to evaluate the performance of the proposed method for characterizing the flexural resistance of longitudinally stiffened box-section members. All the box-section members in these

tests are short enough that their flexural resistance is their cross-section resistance (i.e., no influence of inelastic lateral torsional buckling).

Table 6-2 shows a comparison of flexural resistance from experimental tests with the resistance predicted using the proposed method. It can be observed that the proposed method gives an accurate to conservative estimate of the flexural resistance of these box-section members. The experimental tests listed in Table 6-2 included initial loading cycles allowing for residual stress relief. This explains the larger resistances observed in the experimental tests than those predicted using the proposed method. The box-section member tested by Saad-Eldeen et al. (2010) has webs with unequal thickness (3.95 mm and 3.85 mm). In the calculations using the proposed method, both webs are assumed to have the same thickness, equal to 3.85 mm. This explains the slightly conservative prediction of the flexural resistance of the box-section member tested by Saad-Eldeen et al. (2010). The box-section members tested by Gordo and Soares (2015b), Gordo and Soares (2015c) and Gordo and Soares (2004), all have stiffeners with a different yield stress than that of the plate (yield stress of stiffener is greater than the yield stress of the plate). In the calculations using the proposed method, both the stiffener and plate are assumed to have the same yield strength, equal to the lower plate yield strength value. In addition to this, the box-section members tested by Gordo and Soares (2015c) and Gordo and Soares (2004), have $\frac{d_s}{D_{ce}}$ equal to 0.82 and 0.895 respectively, and $S_{xce} < S_{xte}$. Thus both these cases belong to Group 3 as defined in Table 6-1. It is known from the results of the parametric study (see Figure 6-9), that the predictions using the effective web cross-section model of the proposed method is slightly conservative for Group 3 cases. This explains the

conservatism of the flexural resistance predictions using the proposed method for box-section members tested by Gordo and Soares (2015b), Gordo and Soares (2015c) and Gordo and Soares (2004). The mean, median and coefficient of variation of M_{test}/M_n using the proposed method, for all tests with equal yield strength plate and longitudinal stiffeners, are 1.12, 1.12 and 0.12 respectively.

Table 6-2 Comparison of flexural resistance from experimental tests with the resistance predicted using the proposed methods

Test #	Source	Ultimate bending moment from experimental test, M_{test} (kN-m)	Ultimate bending moment predicted by the proposed method, M_n (kN-m)	$\frac{M_{test}}{M_n}$
1	Saad-Eldeen et al. (2010)	568.9	541.2	1.05
2	Gordo and Soares (2008)	643.0	638.7	1.01
3	Gordo and Soares (2009)	1526.0	1209.3	1.26
4	Gordo and Soares (2009)	1269.0	1035.1	1.23
5	Gordo and Soares (2009)	1026.0	861.2	1.19
6	Gordo and Soares (2015a)	328.0	345.2	0.95
7	Gordo and Soares (2015b)	452.0	416.5	1.09
8	Gordo and Soares (2015c)	172.8	103.1	1.68
9	Gordo and Soares (2004)	349.1	247.7	1.41

6.4 Salient features of the proposed method

The proposed method encapsulate a significant advancement in the understanding of the behavior of rectangular longitudinally stiffened welded box-section members

subjected to flexure, and provides a conceptually unified characterization of their resistance which correlates well with the results of a parametric study performed using finite element simulations, and with results from experimental tests. The salient features of the method are as follows:

1) The proposed method better handles the following:

- It accounts for:
    - The different failure modes of a longitudinally stiffened compression flange plate. The method does this via an improved quantification of the flange ultimate compressive resistance (discussed in CHAPTER 4), which is then used to determine an effective cross-section. .
    - Web bend-buckling and the corresponding postbuckling resistance via the web-bend buckling factor or an effective web section. This avoids the need to perform iterative or two-step calculations when obtaining an effective cross-section.
    - Lateral torsional buckling: The method recognizes that for the longest practical longitudinally stiffened box-section beams the reduction in the flexural resistance relative to the cross-section resistance can be significant. In the parametric studies discussed in Section 6.3.1, it is found that for the longest practical box-section beams the inelastic lateral torsional buckling resistance can be as small as 80.1% of the cross-section resistance.

- The proposed method addresses the interaction between local postbuckling (i.e. flange local buckling or web bend buckling) and global buckling (lateral torsional buckling). This interaction is considered via the use of effective section properties and/or web bend buckling factor, in the inelastic lateral torsional buckling equation.

➢ The method addresses all practical ranges of component plate slenderness.

➢ It is possible for steel box-section members subjected to flexure to have webs with lower yield strength than that of the flanges. The proposed method addresses hybrid as well as homogenous box-section members.

Thus the proposed method better characterizes the flexural resistance of all practical longitudinally stiffened welded steel box-section members.

2) Except for hybrid box-section members with a longitudinally stiffened compression flange, the proposed method eliminates the need to consider a separate tension flange yielding (TFY) limit state for box-section members. The member response is addressed rigorously via the direct calculation of the yield moment to the compression flange, considering early yielding of the section on the tension side of the neutral axis, and considering web bend-buckling and flange buckling effects as applicable. Thus, the proposed method recognizes the inelastic reserve strength corresponding to the spread of yielding in the tension zone.

3) It recognizes the inability of longitudinally stiffened flange plates to sustain large inelastic axial compressive strains beyond the peak load without a substantial reduction in their load carrying capacity, and therefore limits the flexural resistance of box-section

members with a longitudinally stiffened compression flange to the first yield of the compression flange in the effective cross-section.

4) The proposed method for longitudinally stiffened box beams is conceptually consistent with the method for determining the flexural resistance of non-longitudinally stiffened box-section members, discussed in Section 3.2.

CHAPTER 7. SUMMARY OF KEY CONTRIBUTIONS, IMPACT OF THIS RESEARCH ON THE STATE-OF-THE-ART FOR DESIGN OF WELDED BOX-SECTION MEMBERS, AND RECOMMENDATIONS FOR FUTURE WORK

The key contributions from this research to the body of knowledge are discussed in Section 7.1. The impact of this research on the state-of-the-art for design of welded box-section members, and recommendations for future work are discussed in Sections 7.2 and 7.3 respectively.

7.1 Summary of key contributions from this research to the body of knowledge

In summary, the objectives of this research were:

(1) The conceptual and theoretical development and improvement of methods for characterization of the flexural and axial compressive resistance of non-composite welded steel box-section members, and

(2) The evaluation of the performance of these methods using data compiled from existing experimental tests and generated from parametric studies performed using finite element test simulations.

The contributions to the body of knowledge from this research are as follows:

Primary contributions:

(1) Development of new methods and improvement of existing methods for a conceptually unified characterization of the flexural and axial compressive resistance of non-longitudinally stiffened welded box-section members, and ensuring a good correlation with results from experimental tests and finite element test simulations.

(2) Development of new methods and improvement of existing methods for a conceptually unified characterization of the flexural and axial compressive resistance of longitudinally stiffened welded box-section members, and ensuring a good correlation with results from experimental tests and finite element test simulations.

Supporting contributions:

(1) Improved quantification of the postbuckling resistance of non-longitudinally stiffened plates subjected to uniform axial compression in welded box-section members.

(2) Improved characterization of the ultimate compressive resistance of longitudinally stiffened plates.

Additionally, a particularly new development is the development of finite element test simulation data considering the interaction between global (flexural) and local buckling in longitudinally stiffened welded box columns.

7.2 Research impact

This research effort has led to a significant advancement in the understanding of the behavior of non-longitudinally stiffened as well as longitudinally stiffened welded steel box-section members, further leading to an improved characterization of the resistance of these members. It is hoped that the results of this research will lead to updates to the following Articles/Sections of the AASHTO (American Association of State Highway and Transportation Officials) and AISC 360 (American Institute of Steel Construction-Specification for Structural Steel Buildings) provisions:

- AASHTO Article 6.12.2.2.2: Flexural resistance of non-composite box-section members.
- AASHTO Article 6.9.4: Axial compressive resistance of non-composite box-section members.
- AASHTO Article 6.11.8.2.2: Compressive resistance of longitudinally stiffened flange plates.
- AISC Section F7: Flexural resistance of box-section members.

Thus, this research has led to a significant advancement of the state-of-the-art for design of welded steel box-section members.

7.3 Recommendations for future work

The following are the recommendations for future work:

1) The focus of this research was on calculation of the flexural and axial compressive resistance of box-section members. The most general loading on a box-section member

involves axial load, plus biaxial bending, plus shear due bending and torsion. White et al. (2018) provide interaction equations to predict the resistance of box-section members subjected to combined loading. It is believed that these equations provide an accurate to conservative estimate of the resistance of box-section members. It would be useful to perform a parametric study to further evaluate the performance of these interaction equations.

2) The flexural resistance equations in CHAPTER 3 and CHAPTER 6 count on the larger available resistance corresponding to the spread of yielding in the tension zone. Additional studies should be performed to evaluate the impact of the spread of yielding when considering bending-shear interaction, when the shear strength is calculated by accounting for the tension field action. Prior studies for I-section members considered by White et al. (2008) suggest that these combined strengths are adequately predicted without the need for consideration of moment-shear interaction.

3) White et al. (2018) provide valuable guidance for the design of transverse stiffeners in longitudinally stiffened plates. It would be useful to perform a parametric study to further demonstrate the performance of these recommendations.

4) Extension of this work to improve the composite box-girder design provisions in AASHTO (2017) would be useful.

5) In many applications, box-section section members are non-prismatic. White (2015) provides valuable guidance for design of non-prismatic members. It would be useful to perform additional studies to demonstrate the performance of these recommendations for non-prismatic box-section members.

6) At the present time (2018), in the literature there is no experimental data for non-longitudinally stiffened welded box-section members subjected to pure bending. In addition to this, in the literature there is no experimental data for studying the interaction between flexural buckling and local buckling of longitudinally stiffened box-columns. It would be useful to have experimental data for these member types for further validation of the proposed methods.

APPENDIX A. FINITE ELEMENT MODELLING OF NON-LONGITUDINALLY STIFFENED BOX-SECTION MEMBERS, LONGITUDINALLY STIFFENED PLATES, AND LONGITUDINALLY STIFFENED BOX-SECTION MEMBERS

This section discusses the finite element modelling of non-longitudinally stiffened box-section members, longitudinally stiffened plates, and longitudinally stiffened box-section members.

A.1 General

The commercial software ABAQUS version 6.13 (Simulia 2013) is used in this research for finite element analysis of box-section members and plates. The four node shell element S4R is used to model the box-section flange plates, web plates and longitudinal stiffeners. S4R is a large strain quadrilateral shell element which uses a reduced (single point) numerical integration with an algorithm for stabilization of the corresponding spurious zero-energy modes. It is a general purpose shell element that allows transverse shear deformation; using thick shell theory for thicker shells, and using the Kirchoff thin shell theory for thinner shells. A five point Simpson's rule is applied for integration of the stresses through the thickness of the shell element.

Web transverse stiffeners in longitudinally stiffened box beams are modelled using the B31 beam element in ABAQUS. B31 is a two-node linear Timoshenko beam element (allows transverse shear deformation). The Modified Riks method in ABAQUS is used to perform geometric and material nonlinear analysis of the box-section members and plates.

Figure A-0-1 shows a non-longitudinally stiffened box-section member subjected to uniform bending, Figure A-0-2 shows a longitudinally stiffened plate subjected to uniform axial compression, and Figure A-0-3 shows a longitudinally stiffened box-section member subjected to uniform bending.

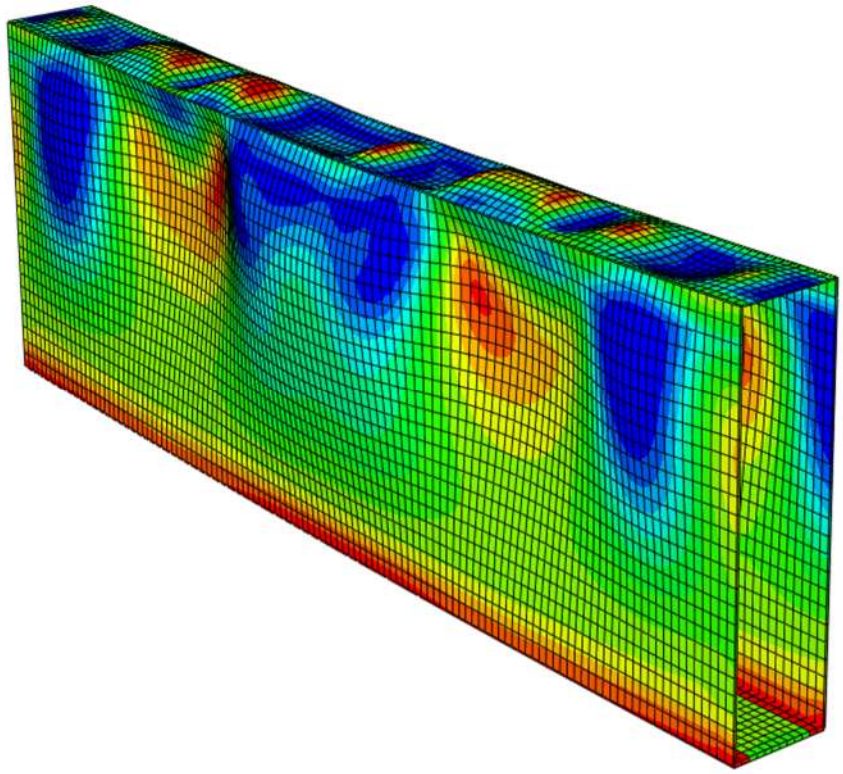

Figure A-0-1 Non-longitudinally stiffened box-section member subjected to uniform bending

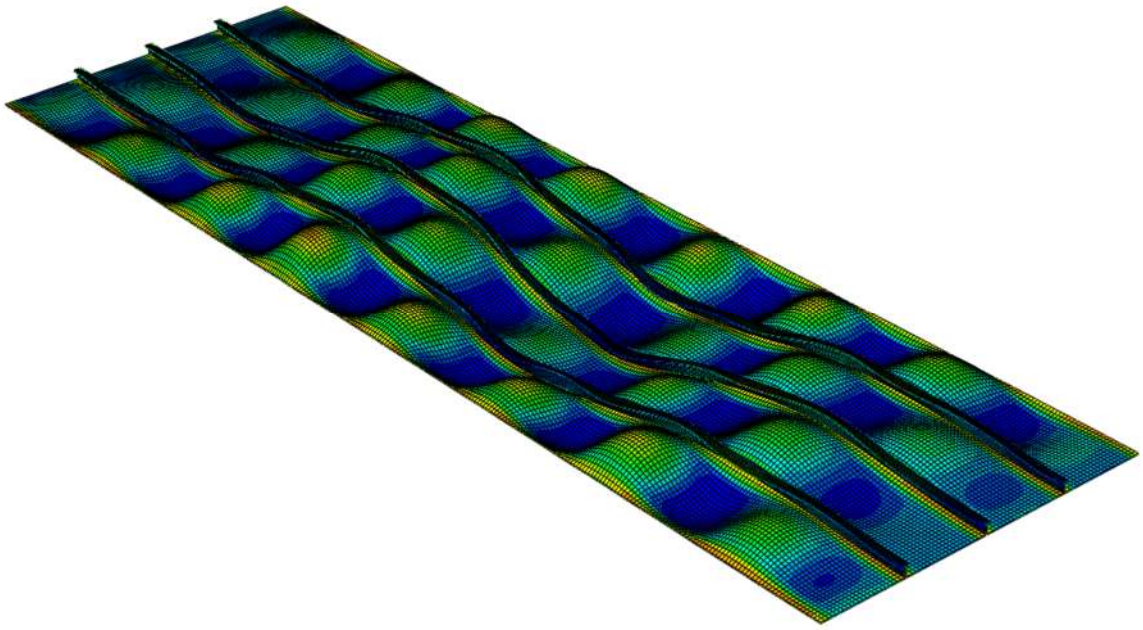

Figure A-0-2 Longitudinally stiffened plate subjected to uniform axial compression

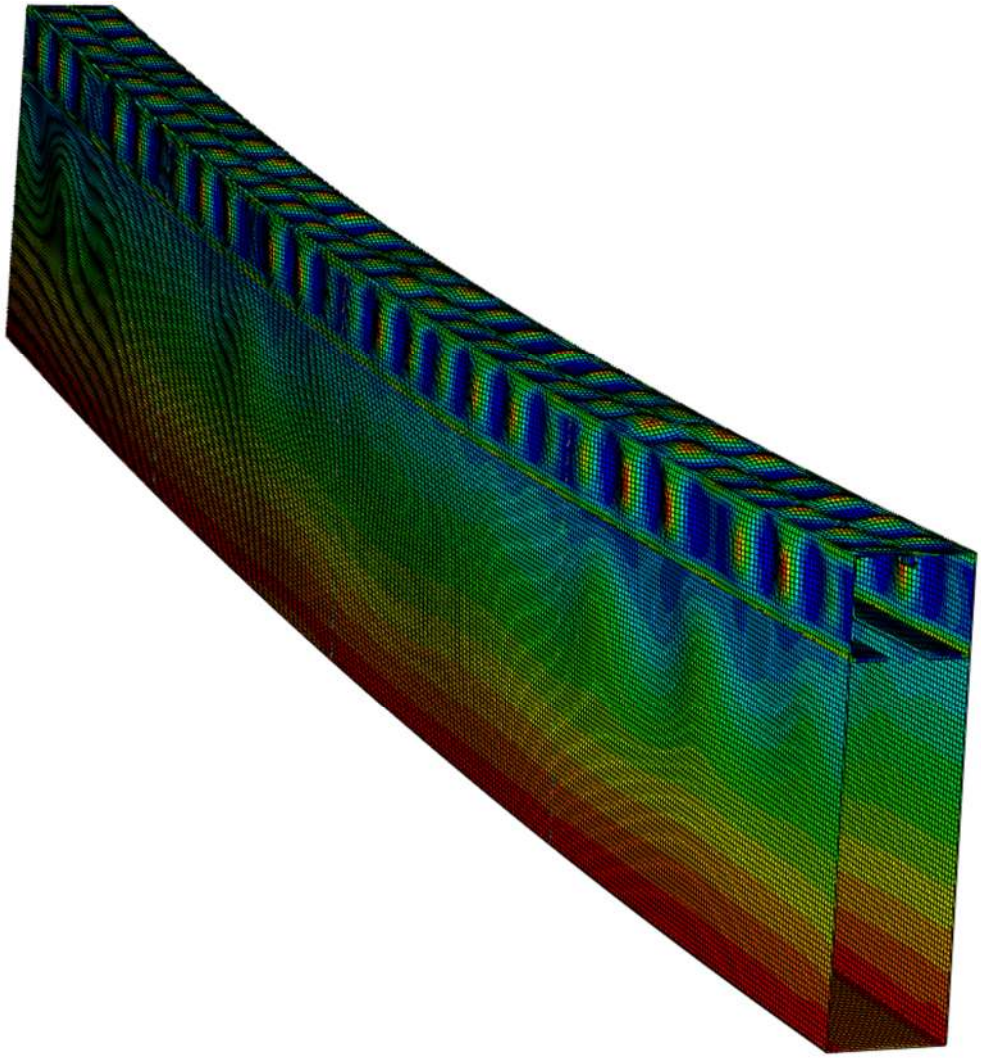

Figure A-0-3 Longitudinally stiffened box-section member subjected to uniform bending

The material properties of steel are modeled in all the test simulation studies of this research using the stress-strain curve shown in Figure A-0-4. The slope of the stress-strain curve is,

- E in the elastic region (shown as Slope 1 in Figure A-0-4)
- $\frac{E}{1000}$ in the yield plateau region (shown as Slope 2 in Figure A-0-4)

- $\frac{E}{50}$ in the strain-hardening region (shown as Slope 3 in Figure A-0-4)

The modulus of elasticity, *E* is taken as 29000 ksi. For homogenous box-section members all the box-section component plates are modeled as Grade 50 steel. For hybrid box-section members the flange plates are modeled as Grade 70 steel, and the web plates are modeled as Grade 50 steel. Grade 50 steel has a yield stress, $F_y = 50$ ksi, and ultimate stress, $F_u = 65$ ksi. Grade 70 steel has a yield stress, $F_y = 70$ ksi, and ultimate stress, $F_u = 90$ ksi. In Figure A-0-4 the yield strain, $\varepsilon_y = \frac{F_y}{E}$.

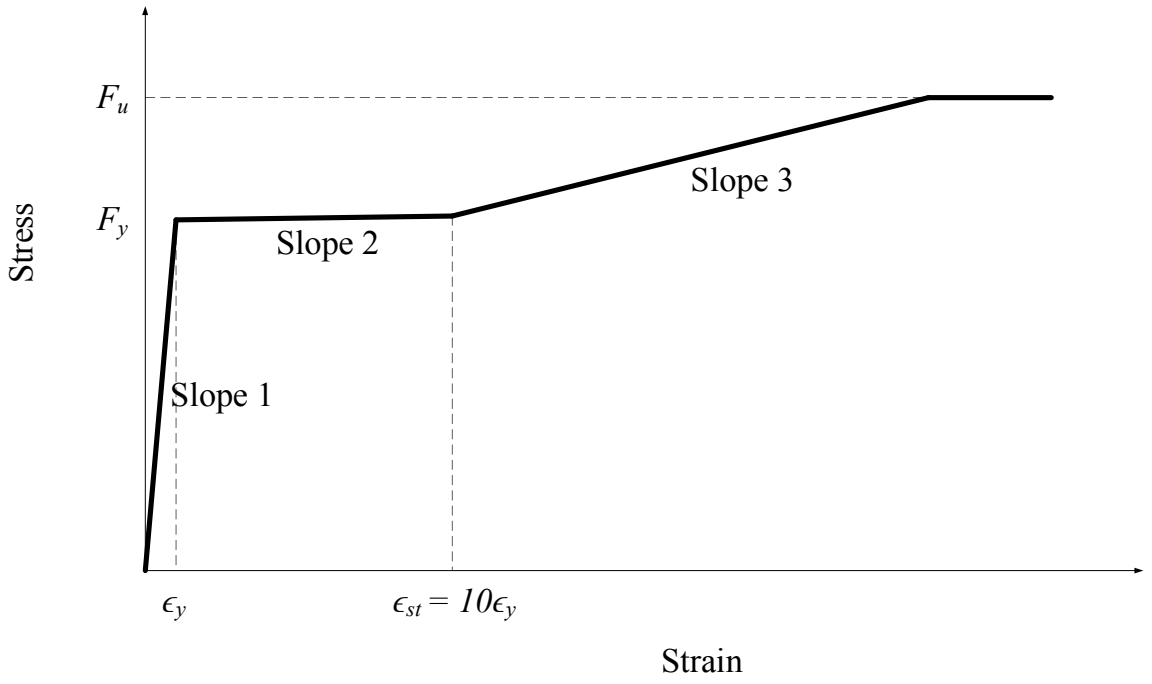

Figure A-0-4 Steel stress-strain curve assumed in the finite element analysis

A.2 Non-longitudinally stiffened box-section members

This section discusses the geometric imperfections, residual stresses, loading and boundary conditions used in the FE modelling of non-longitudinally stiffened box-section beams.

A.2.1 Geometric imperfection

Both global and local imperfections are modeled as shown in Figure A-0-5 and Figure A-0-6. For global imperfection, the lateral displacement of the bottom flange is restrained and the top flange is given a sweep. The maximum magnitude of the global imperfection is taken as 1/1000 of the beam length. For local imperfections, the displacement of the corner nodes is constrained within the plane of the cross-section and an eigenvalue buckling analysis is performed with the member subjected to axial load. The maximum magnitude of local imperfection of each plate is taken as 1/200 of the plate width.

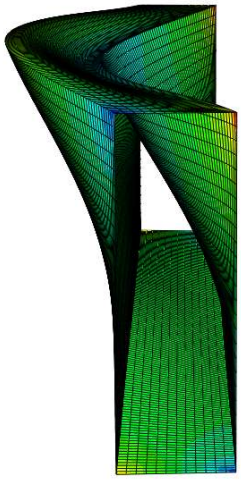

Figure A-0-5 Global imperfection for non-longitudinally stiffened beams

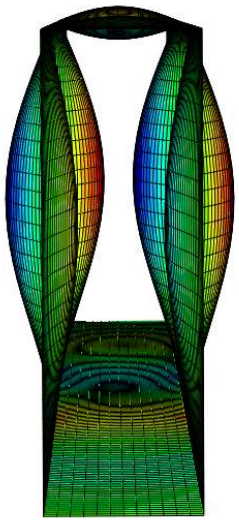

Figure A-0-6 Local imperfection for non-longitudinally stiffened beams

A.2.2 Residual stress

Previous researchers who have performed finite element simulations of welded steel box-section members, e.g., Kim and Yoo (2008), Tao et al. (2009), used a constant compressive residual stress value equal to $0.2F_y$. However in reality, the magnitude of compressive residual stresses vary based on a number of factors, and in many situations the compressive residual stresses in welded steel box sections are much higher than $0.2F_y$, as can be seen from Figure A-0-7. Thus, there is a need to develop a residual stress model for FE simulations of welded steel box-section members.

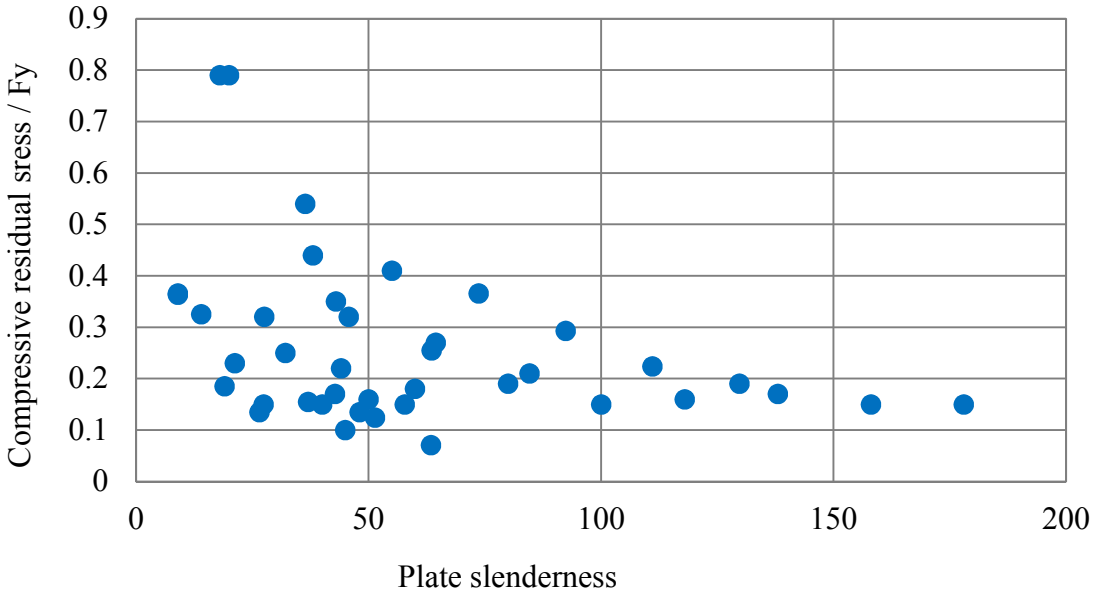

Figure A-0-7 Synthesis of measured residual stresses in welded steel box sections from the literature

Figure A-0-8 shows the residual stress pattern for a non-longitudinally stiffened box-section. In Figure A-0-8, $\sigma_{c.lw}$, $\sigma_{c.tf}$, $\sigma_{c.rw}$ and $\sigma_{c.bf}$ denote the compressive residual stresses in the left web, top flange, right web and bottom flange respectively.

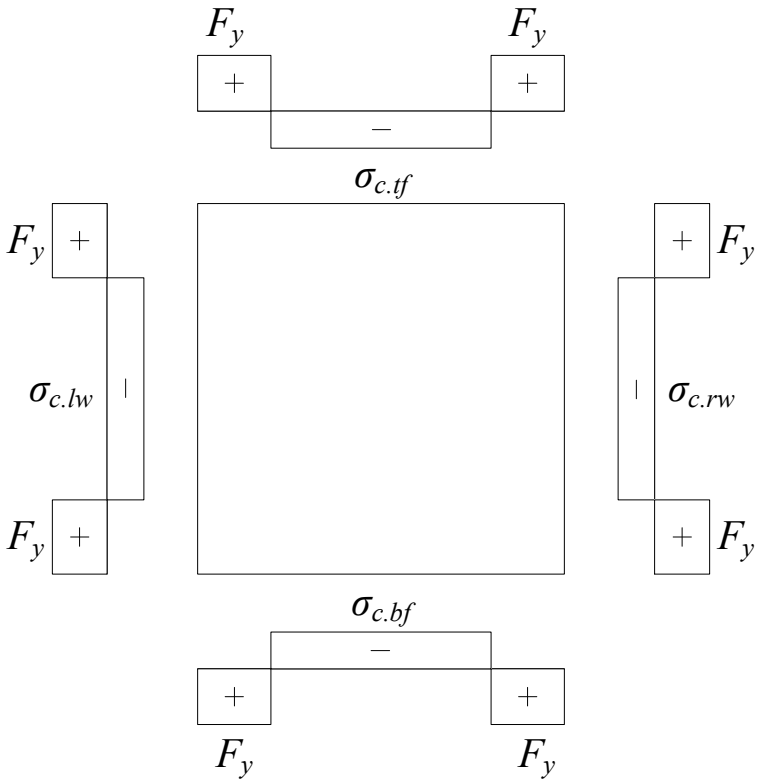

Figure A-0-8 Residual stress pattern for a non-longitudinally stiffened box-section

In this research, a residual stress model has been developed which is a reasoned modification, extension of the rules from ECCS (1976). ECCS (1976) has valuable guidance for estimating the residual stresses in welded steel members considering the influence of plate rolling, flame cutting and welding of component plates. ECCS (1976) also provides the residual stress pattern for four cases:

1) Plate width to thickness = 20, and heavy weld

2) Plate width to thickness = 20, and light weld

3) Plate width to thickness = 40, and heavy weld

4) Plate width to thickness = 40, and light weld.

However, it does not provide a residual stress pattern for other values of plate slenderness and welding level. While performing a parametric study, different levels of plate slenderness are encountered. Additionally, the weld level is unknown. Since the weld size is unknown, using the ECCS (1976) equations for calculating the width of the tensile residual stress block may give too large or too small values for the size of the tensile residual stress block, thus giving unrealistic compressive residual stress values. Thus, there is a need to limit the width of the tensile residual stress block based on:

- Generally observed size of tensile residual stress block. For example, Dwight and Moxham (1969) state that- "*The area carrying this locked-in tension typically extends two to four times thicknesses out from the weld on each side*".
- Ensuring the compressive residual stresses are realistic. For example:
    - Ensuring that the compressive residual stress is limited such that it is less than the local buckling stress of the box-section component plates.
    - By setting upper and lower limits on the magnitude of compressive residual stresses.

For a parametric study, since the weld size, welding process and number of passes during welding are unknown, there should be a reasoned way for using certain values for

calculation of the width of the tensile stress block. For example, in the proposed model the weld size is taken as an average of the minimum and maximum weld size from AWS (2002); along with a limit that the weld size cannot exceed the thickness of the two plates being welded.

The major features of this model are listed below:

- Tensile residual stress is present at the weld locations and is equal to F_y. Compressive residual stresses are present in the remaining portion of the plate, as shown in Figure A-0-8, such that equilibrium is satisfied.
- Residual stresses due to flame cutting and welding are considered, whereas residual stresses due to plate rolling are neglected since there is an uncertainty about the location from which the box-section component plate will be flame cut from a large rolled plate. According to ECCS (1976), the plate rolling stresses have a parabolic shape and are opposite in nature to the residual stresses due to welding or flame cutting, i.e., tensile residual stress in the middle portion of the plate and compressive residual stress at the corners. Therefore, neglecting the plate rolling stresses is conservative. Another important point is that when a rolled plate is cut, the residual stresses due to plate rolling are released. Thus there is a justification to neglect the residual stresses due to plate rolling.

  The contribution of flame cutting to the residual stress is generally much smaller than that from welding. Additionally, if the plate is instead cut using plasma cutting or water jet cutting the residual stresses due to plate cutting are even smaller.
- One of the unknowns while estimating the residual stresses in welded box sections used in a parametric study, is the weld size. In this model, the weld size used in the

calculation of the width of the tensile residual stress block is taken as an average of the minimum and maximum weld size from AWS (2002); along with a limit that the weld size cannot exceed the thickness of the two plates being welded.

- The width of the tensile residual stress block is limited to four times the thickness of the plate plus size of the weld. This is a thumb rule based on the observation by Dwight and Moxham (1969).
- The compressive residual stress is limited such that it is less than the local buckling stress of the box-section component plates.
- It is ensured that the compressive residual stresses are greater than or equal to $0.2F_y$ or $0.1F_y$, depending on whether the critical buckling stress of the plate is greater than or less than $0.2F_y$. This sets a lower limit on the compressive residual stress. Similarly as an upper limit, the compressive residual stresses are limited to $0.55F_y$.
- The weld is assumed to be a continuous single pass weld. Since the weld size is unknown there is a further uncertainty about the number of passes during welding. A continuous single pass weld gives the largest value of residual stress for a given weld size, using the ECCS equations for the width of the tensile residual stress block.
- Assuming that the welding process is submerged arc welding. Submerged arc welding is assumed conservatively since it has the largest process efficiency factor resulting in larger residual stresses for a given weld size as compared to other welding processes. The assumed weld type is fillet weld.
- The model captures important trends such as a decrease in the compressive residual stress with an increase in slenderness of the plate. This has been confirmed by

comparing the residual stress predictions from the model with residual stresses measured by other researchers.

- The model neglects a distribution of residual stresses in the plane of the plate, shown in Figure A-0-9. These residual stresses are compressive below the surface and tensile in the center of the plate thickness. King (2018) points out that for a member made of very thick plate, welded with relatively small fillet welds, the residual stresses from weld shrinkage are very small, but the through thickness plate residual stresses remain large. For certain practical box-section members, King (2018) performed non-linear finite element (FE) analyses modelling the through-thickness residual stress pattern shown in Figure A-0-9. He found that the buckling resistance obtained from the FE analyses was very close to that obtained using column strength curves generated using the residual stress pattern shown in Figure A-0-8. Therefore as a simplification, for practical box-section members, neglecting the through-thickness variation of residual stresses is justified.

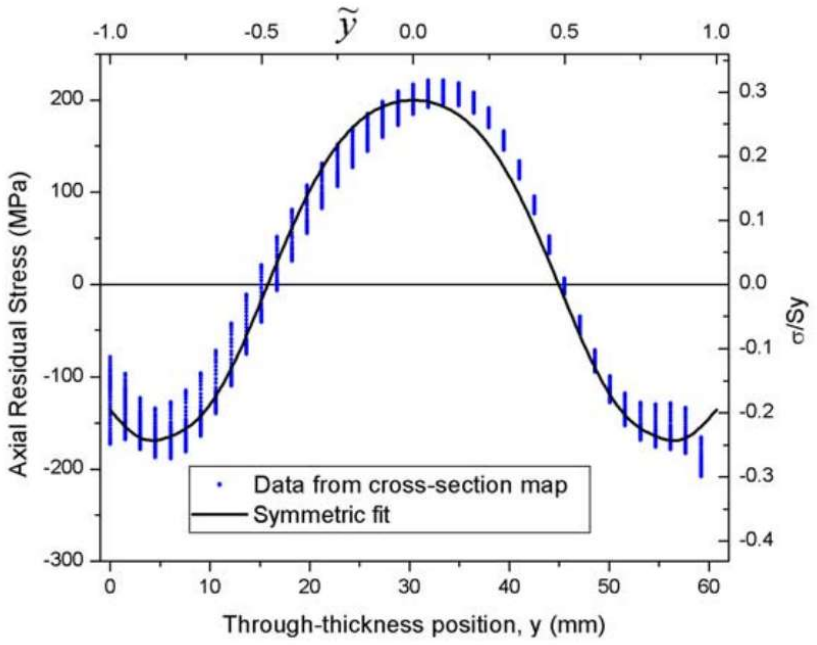

Figure A-0-9 Through-thickness variation of residual stresses in quenched HSLA-100 plate (Credit: Prime 2005)

The algorithm for computing residual stresses in a general welded box-section with equal or unequal size of component plates is explained below. Figure A-0-10 explains the nomenclature used in the algorithm for computing residual stresses. In Figure A-0-10,

- b_1, b_2, b_3, b_4 and t_1, t_2, t_3, t_4 are the widths and thicknesses of the four box-section component plates respectively.
- $WS_{corner1}$, $WS_{corner2}$, $WS_{corner3}$, $WS_{corner4}$ denote the weld size at the four corners of the welded box-section.
- $Aw_{corner1}$, $Aw_{corner2}$, $Aw_{corner3}$, $Aw_{corner4}$ denote the area of the weld at the four corners of the welded box-section.
- c_f denotes the width of the tensile residual stress block due to flame cutting.

- $\sigma_{c1.final}$, $\sigma_{c2.final}$, $\sigma_{c3.final}$ and $\sigma_{c4.final}$ denote the final compressive residual stress values in plates one through four respectively.
- $c_{1.final}$, $c_{2.final}$, $c_{3.final}$ and $c_{4.final}$ denote the widths of the tensile residual stress block in plates one through four respectively considering both welding and flame cutting.

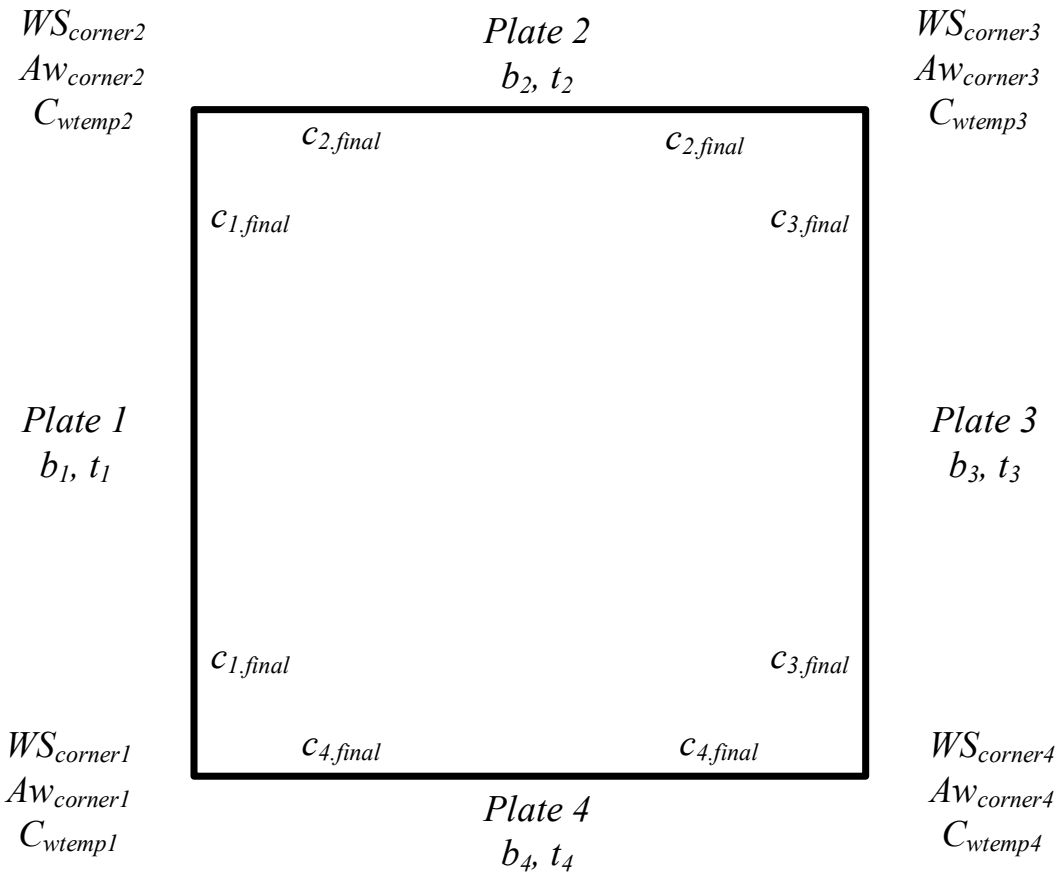

Figure A-0-10 Nomenclature used in the algorithm for computing residual stresses

Weld area algorithm

The weld area for the four corners is calculated as explained below:

- **Corner 1 (intersection of plates 4 and 1)**

$$WS_{corner1} = \min\left[\max\left\{A_4 + 0.5\left(B_4 - A_4\right), A_1 + 0.5\left(B_1 - A_1\right)\right\}, t_4, t_1\right]$$

$$Aw_{corner1} = 0.6\left(WS_{corner1}\right)^2$$

- **Corner 2 (intersection of plates 1 and 2)**

$$WS_{corner2} = \min\left[\max\left\{A_1 + 0.5\left(B_1 - A_1\right), A_2 + 0.5\left(B_2 - A_2\right)\right\}, t_1, t_2\right]$$

$$Aw_{corner2} = 0.6\left(WS_{corner2}\right)^2$$

- **Corner 3 (intersection of plates 2 and 3)**

$$WS_{corner3} = \min\left[\max\left\{A_2 + 0.5\left(B_2 - A_2\right), A_3 + 0.5\left(B_3 - A_3\right)\right\}, t_2, t_3\right]$$

$$Aw_{corner3} = 0.6\left(WS_{corner3}\right)^2$$

- **Corner 4 (intersection of plates 3 and 4)**

$$WS_{corner4} = \min\left[\max\left\{A_3 + 0.5\left(B_3 - A_3\right), A_4 + 0.5\left(B_4 - A_4\right)\right\}, t_3, t_4\right]$$

$$Aw_{corner4} = 0.6\left(WS_{corner4}\right)^2$$

where:

- A_1 is the minimum weld size per AWS $= If\left[t_1 < 20mm, 6, 8\right]$
- B_1 is the maximum weld size per AWS $= If\left[t_1 < 6mm, t_1, t_1 - 2\right]$
- A_2 is the minimum weld size per AWS $= If\left[t_2 < 20mm, 6, 8\right]$
- B_2 is the maximum weld size per AWS $= If\left[t_2 < 6mm, t_2, t_2 - 2\right]$
- A_3 is the minimum weld size per AWS $= If\left[t_3 < 20mm, 6, 8\right]$
- B_3 is the maximum weld size per AWS $= If\left[t_3 < 6mm, t_3, t_3 - 2\right]$
- A_4 is the minimum weld size per AWS $= If\left[t_4 < 20mm, 6, 8\right]$
- B_4 is the maximum weld size per AWS $= If\left[t_4 < 6mm, t_4, t_4 - 2\right]$

The residual stress calculations for left web plate are explained below.

Step 1: The width of the tensile residual stress block corresponding to flame cutting is

$$c_f = \frac{1100\sqrt{t_1}}{F_y} \tag{152}$$

Step 2: The widths of the tensile residual stress blocks corresponding to welding at the two edges of the plate are calculated as follows,

$$c_{w,temp1} = \frac{12000\, pAw_{corner1}}{F_y(t_4 + t_1)} \tag{153}$$

$$c_{w,temp2} = \frac{12000\, pAw_{corner2}}{F_y(t_1 + t_2)} \tag{154}$$

where $p = 0.9$ is the process efficiency factor for submerged arc welding.

$$c_{w.a} = If\left[b > 2c_{wtemp1}, \min\left\{c_{wtemp1}, \left(4\max(t_4, t_1) + WS_{corner1}\right)\right\}, 4\max(t_4, t_1) + WS_{corner1}\right] \quad (155)$$

$$c_{w.b} = If\left[b > 2c_{wtemp2}, \min\left\{c_{wtemp2}, \left(4\max(t_1, t_2) + WS_{corner2}\right)\right\}, 4\max(t_1, t_2) + WS_{corner2}\right] \quad (156)$$

Step 3: Combining the residual stress due to flame cutting and welding at the two edges of the plate,

$$c_{a.\text{int}} = \left(c_f{}^4 + c_{w.a}{}^4\right)^{\frac{1}{4}} \quad (157)$$

$$c_{b.\text{int}} = \left(c_f{}^4 + c_{w.b}{}^4\right)^{\frac{1}{4}} \quad (158)$$

Step 4: Calculating the compressive residual stress,

$$\sigma_{c1.\text{int}} = \frac{F_y(c_{a.\text{int}} + c_{b.\text{int}})}{b_1 - (c_{a.\text{int}} + c_{b.\text{int}})} \quad (159)$$

$\sigma_{c1.final}$ is calculated as follows:

- If $\sigma_{cr} \geq 0.2F_y$,

$$\sigma_{c1.final} = \min\left[0.55F_y, \max\left[0.2F_y, \min\left(\sigma_{cr}, \sigma_{c1.\text{int}}\right)\right]\right] \quad (160)$$

- If $\sigma_{cr} < 0.2F_y$,

$$\sigma_{c1.final} = \max\left[\min\left\{\sigma_{cr}, \sigma_{c1.\text{int}}\right\}, 0.1F_y\right] \quad (161)$$

where,

$$\sigma_{cr} = \frac{4\pi^2 E}{12\left(1-\nu^2\right)\left(\frac{b_1 - \frac{c_{a.\text{int}} + c_{b.\text{int}}}{2}}{t_1}\right)^2} \tag{162}$$

Step 5: Calculating the width of the tensile residual stress block,

$$c_{1.final} = \frac{\sigma_{c1.final} b_1}{2\left(\sigma_{c1.final} + F_y\right)} \tag{163}$$

The calculations for the other three component plates (top flange, right web and bottom flange) are similar to the calculations explained above.

The predictions of the proposed residual stress model relative to measurements made by other researchers is shown below in Figure A-0-11. It can be observed that the model captures important trends such as a decrease in the compressive residual stress with an increase in slenderness of the plate.

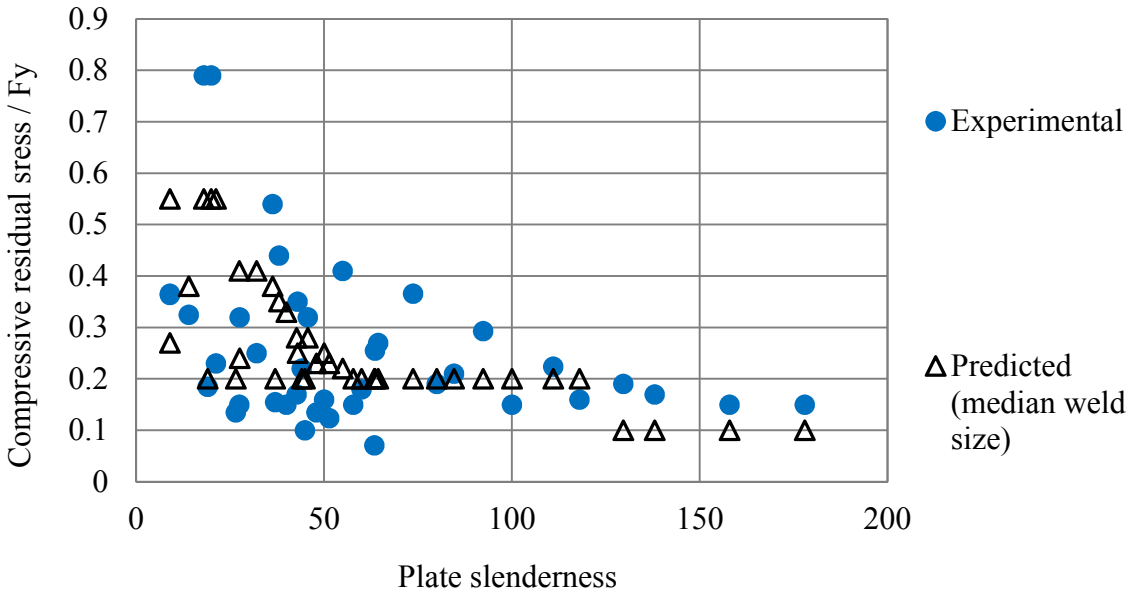

Figure A-0-11 Predictions of the suggested residual stress model relative to the measurements made by other researchers

A.2.3 Boundary conditions and loading

Non-longitudinally stiffened box beams are flexurally and torsionally simply supported at the ends, and are subjected to uniform bending. The beam multipoint constraint in ABAQUS is used to apply the end boundary conditions and loading.

A.3 Longitudinally stiffened plates

This section discusses the geometric imperfections, residual stresses, loading and boundary conditions used in the FE modelling of longitudinally stiffened plates.

A.3.1 Geometric imperfection

Both global and local imperfections are modeled as shown in Figure A-0-12 and Figure A-0-13.

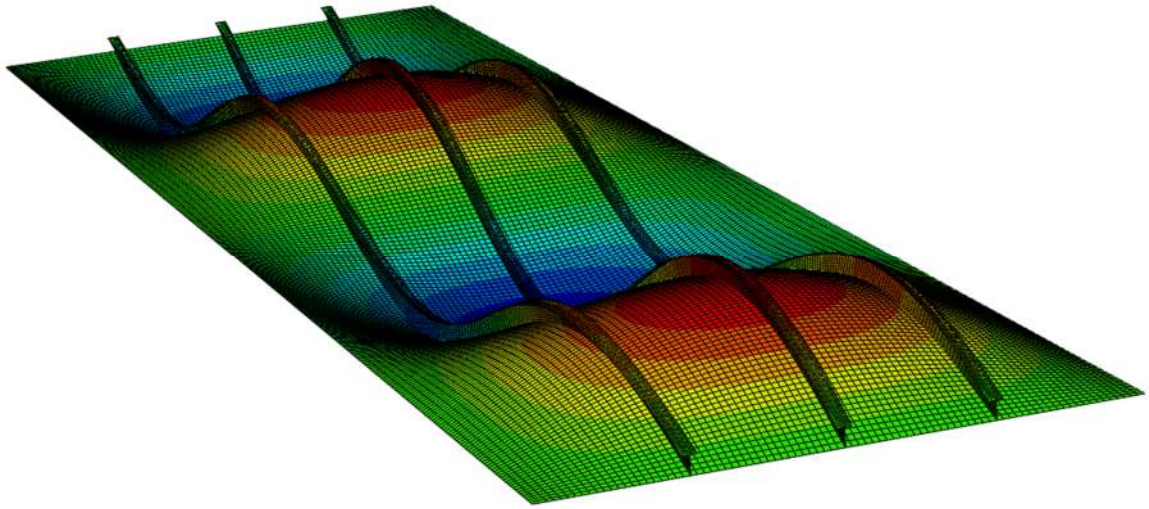

Figure A-0-12 Global imperfection for longitudinally stiffened plates

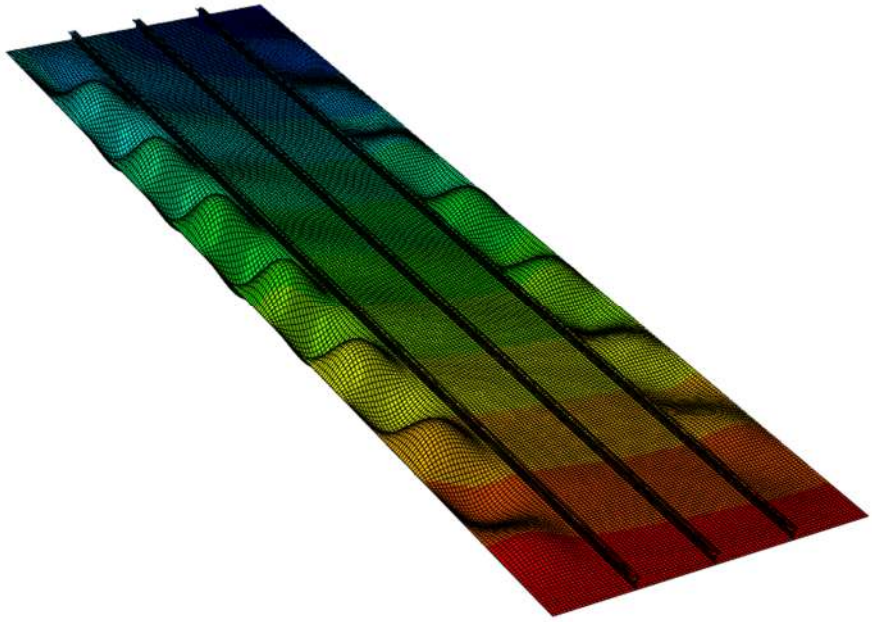

Figure A-0-13 Local imperfection for longitudinally stiffened plates

Considering X as the longitudinal direction, Y as the transverse direction, Z as the lateral direction of the longitudinally stiffened plate, and the origin at the corner of the stiffened plate; the transverse displacement, δ for the global imperfection is calculated using the following equation:

$$\delta = \delta_o \sin\left(\frac{\pi x}{L}\right)\sin\left(\frac{\pi z}{B}\right) \tag{164}$$

where,

- B is the width of the longitudinally stiffened plate
- $L = \min\left(l_c, a\right)$ (165)
- l_c is the characteristic buckling length explained in Section 4.2
- a is the transverse stiffener spacing
- $\delta_o = 0.8\left(\frac{L}{480}\right)$ (166)

  where,

  - The fabrication tolerance equal to $\frac{L}{480}$ is from Section 11.4.13.3 of the AASHTO LRFD Bridge Construction Specifications (2010)
  - 80% of the geometric fabrication tolerance is used based on the recommendation in Annex C.5 of the Eurocode (CEN 2006).

For local imperfections, the lateral and transverse displacement of the longitudinal edges and the longitudinal stiffener nodes are constrained, and an eigenvalue buckling

analysis is performed with the plate subjected to axial load. The maximum magnitude of local imperfection is taken as $0.8\left(\frac{w}{144\sqrt{t_{sp}}}\right)$ where,

- The fabrication tolerance equal to $\frac{w}{144\sqrt{t_{sp}}}$ is from Section 11.4.13.2 of the AASHTO LRFD Bridge Construction Specifications (2010)
- w and t_{sp} are as shown in Figure 4-8.
- 80% of the geometric fabrication tolerance is used based on the recommendation in Annex C.5 of the Eurocode (CEN 2006).

A.3.2 Residual stress

The self-equilibrating residual stress pattern shown in Figure A-0-15 and Figure A-0-14 is used. A compressive residual stress value of $0.25F_y$ has been used previously by Chou et al. (2006). The residual stress pattern for flat longitudinal stiffeners is from Subramanian (2015). In Figure A-0-14 and Figure A-0-15, a positive sign represents tensile residual stress, and a negative sign represents compressive residual stress.

A.3.3 Boundary conditions and loading

Intermediate transverse stiffeners are modeled by restraining the lateral and transverse displacements of the nodes at the transverse stiffener locations. The boundary conditions are modelled as follows:

- Transverse displacements of nodes along both the longitudinal edges are restrained.

- Beam multipoint constraint in ABAQUS is used to apply the end boundary conditions and loading. All degrees of freedom of both end reference nodes, except longitudinal displacement of one end reference node, are restrained; and axial compressive load is applied via the reference nodes. These boundary condition are believed to be representative of the boundary conditions in a physical experimental test. The end boundary conditions have a minor influence on the ultimate compressive resistance of longitudinally stiffened plates because the failure is farther away from the ends.
- Lateral displacements of nodes at the mid-width of the stiffened plate along its entire length are restrained.

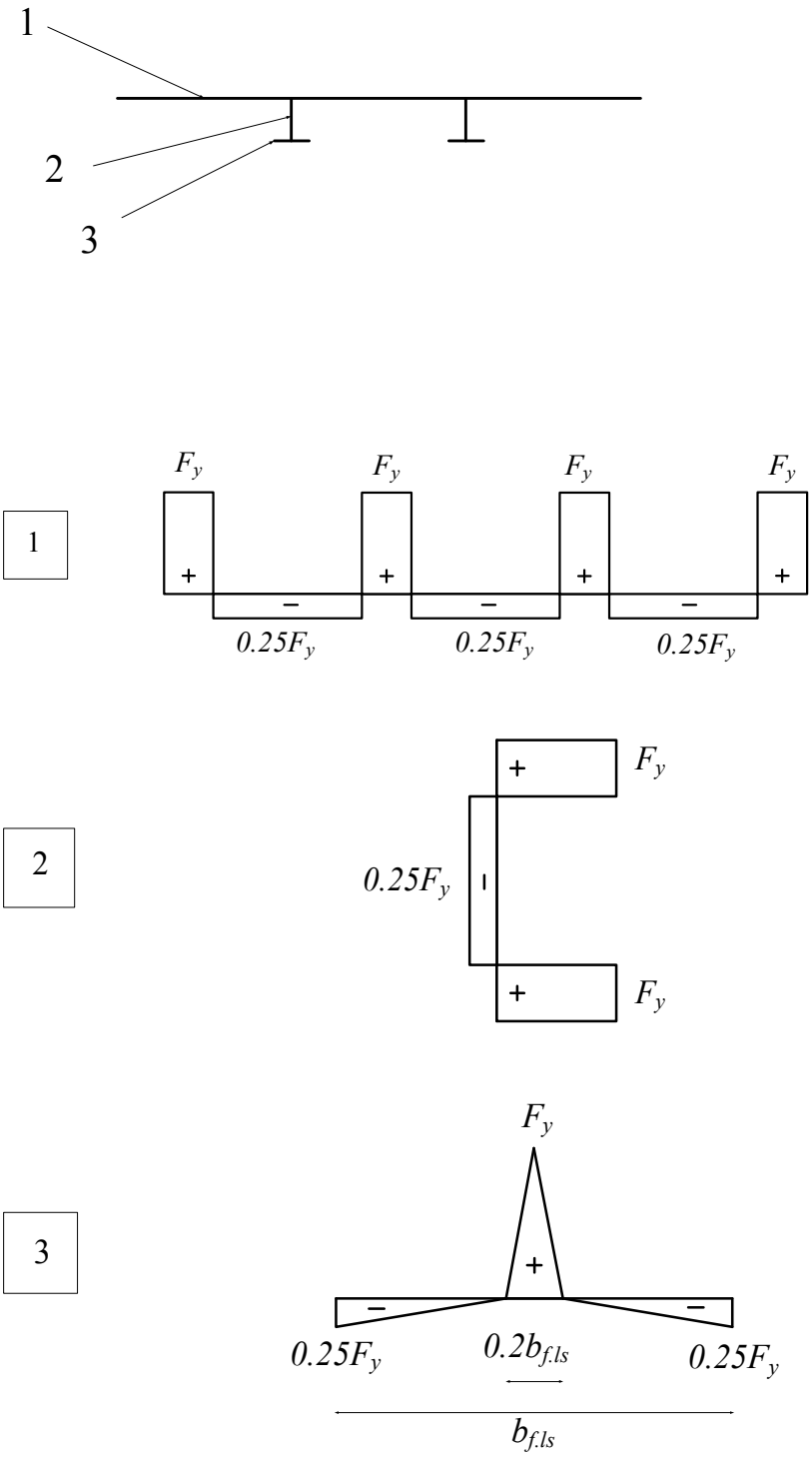

Figure A-0-14 Residual stress pattern for longitudinally stiffened plates with Tee longitudinal stiffeners

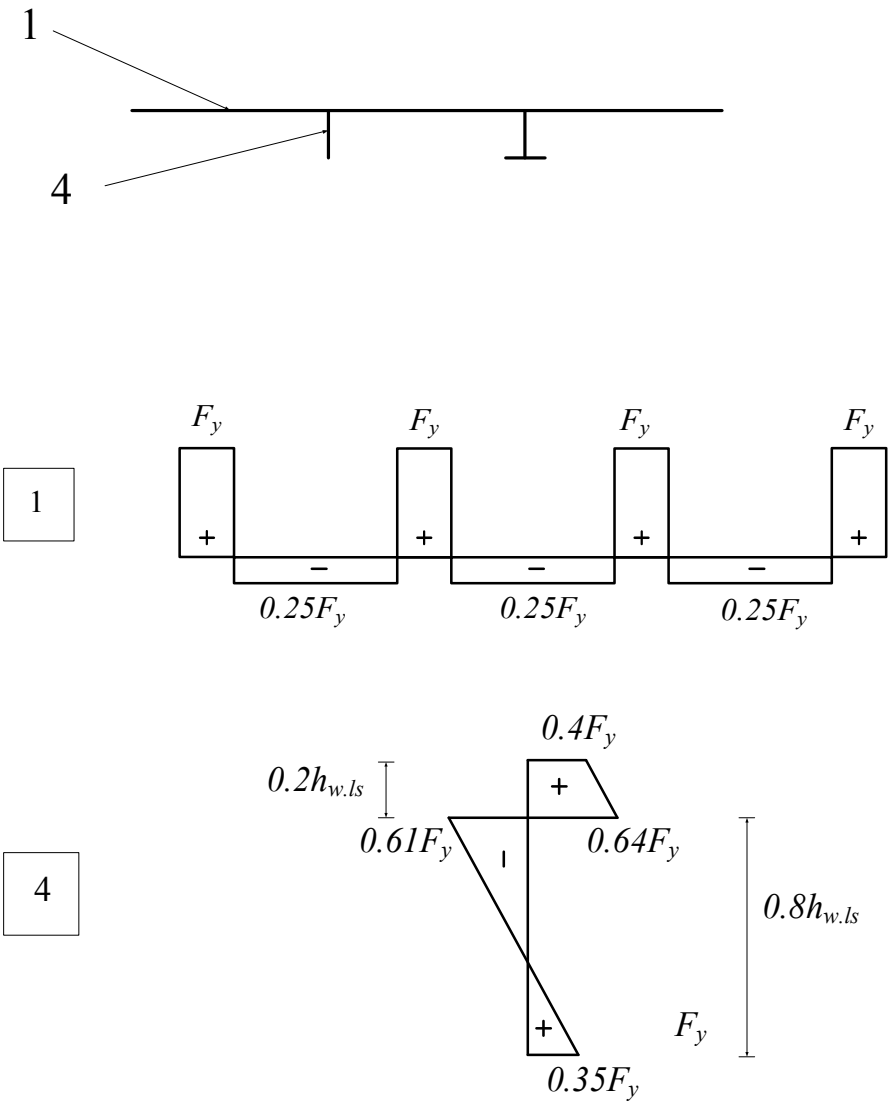

Figure A-0-15 Residual stress pattern for longitudinally stiffened plates with flat longitudinal stiffeners

A.4 Longitudinally stiffened box-section members

This section discusses the geometric imperfections, residual stresses, loading and boundary conditions used in the FE modelling of longitudinally stiffened box-section members.

A.4.1 Geometric imperfection

Geometric imperfections for each of the four component plates of the box-section member are modelled as shown in Figure A-0-12 and Figure A-0-13. In addition to that:

- For longitudinally stiffened box columns, an overall sweep corresponding to a flexural buckling failure mode is given with a maximum magnitude of global imperfection taken equal to $0.8\left(\frac{L}{1000}\right)$ as shown in Figure A-0-16, where L is the length of the box column. 80% of the geometric fabrication tolerance is used based on the recommendation in Annex C.5 of the Eurocode (CEN 2006).
- For longitudinally stiffened box beams, the lateral displacement of the bottom flange is restrained and the top flange is given a sweep with a maximum magnitude of global imperfection taken equal to $0.8\left(\frac{L}{1000}\right)$ as shown in Figure A-0-17, where L is the length of the box beam. 80% of the geometric fabrication tolerance is used based on the recommendation in Annex C.5 of the Eurocode (CEN 2006).

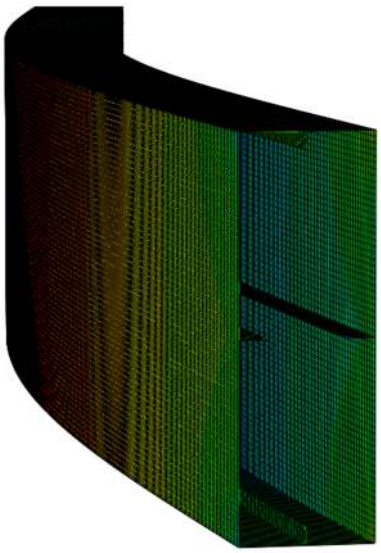

Figure A-0-16 Global imperfection for longitudinally stiffened box columns

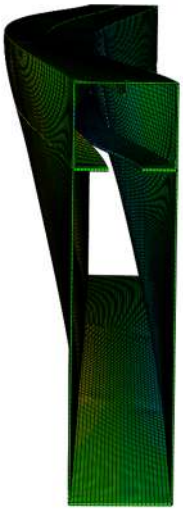

Figure A-0-17 Global imperfection for longitudinally stiffened box beams

A.4.2 Residual stress

The residual stress pattern for each of the longitudinally stiffened component plates is the same as that in Figure A-0-14 and Figure A-0-15. The residual stress pattern for non-

longitudinally stiffened component plates in longitudinally stiffened box-section members is as shown in Figure A-0-18.

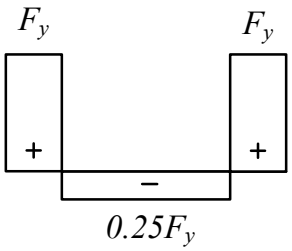

Figure A-0-18 Residual stress pattern for non-longitudinally stiffened component plates in longitudinally stiffened box-section members

A.4.3 Boundary conditions and loading

Longitudinally stiffened box columns are flexurally and torsionally simply supported at the ends, and are subjected to uniform axial compression. Similarly, the longitudinally stiffened box beams are flexurally and torsionally simply supported at the ends, and are subjected to uniform bending. The beam multipoint constraint in ABAQUS is used to apply the end boundary conditions and loading.

A.5 Comparison of results of experimental tests with the results from FE simulations of the experimental tests

The performance of the FE models is evaluated by comparing the results of experimental tests with the results from FE simulations of those experimental tests. The experimental tests from Pavlovcic et al. (2012) are used to evaluate the performance of the FE models of box-section members. A summary of the comparison is shown in Table A-0-1. The tests from Pavlovcic et al. (2012) are selected for this purpose for the following reasons:

- Box-section members in these tests are susceptible to combined global buckling and local buckling.
- Pavlovcic et al. (2012) provide detailed measurements of initial imperfections, accidental load eccentricities, and residual stresses.

Similarly, the performance of the FE models of longitudinally stiffened plates is evaluated by using experimental tests from Ghavami (1994) and Chou et al. (2006), and are shown in Table A-0-2 and Table A-0-3. For tests by Ghavami (1994) without intermediate transverse stiffeners, the plates were not continuously simply supported but were closely discretized simply supported. Because of the uncertainty and hence the difficulty in modelling these supports, only the tests by Ghavami (1994) with intermediate transverse stiffeners are modelled as these had continuously simply supported boundary conditions.

It can be observed from Table A-0-1, Table A-0-2 and Table A-0-3, that in general the results from FE simulations of experimental tests show a good correlation with the experimental test results. The poor performance of the FE simulations for specimens P2R1T and P2T1T in Table A-0-2 can be attributed to the unavailability of enough information about the actual geometric imperfection pattern and residual stresses, that they could be properly modelled. Following the approach adopted by Ghavami and Khedmati (2006), the complex pattern of residual stresses and initial deflection was considered by only considering geometric imperfections with the magnitude of maximum deflection of the plate taken equal to that measured by Ghavami and reported in Column 7 of Table 2 in Ghavami (1994).

Table A-0-1 Performance of the FE modelling of box-section members, using experimental tests from Pavlovcic et al. (2012)

Specimen	Description	Length (m)	$P_{\max.experiment}$ (kN)	$P_{\max.simulation}$ (kN)	$\frac{P_{\max.simulation}}{P_{\max.experiment}}$
W-S	Column	3.65	706.5	699.4	0.99
W-L	Column	4.85	564	592.2	1.05
W-E2	Beam-column	3.65	566.5	572.2	1.01
W-E6	Beam-column	3.65	384.5	392.2	1.02
W-E20	Beam-column	3.65	206.5	201.5	0.98

Table A-0-2 Performance of the FE modelling of longitudinally stiffened plates, using experimental tests from Ghavami (1994)

Specimen	Number of longitudinal stiffeners	Number of intermediate transverse stiffeners	$P_{\max.experiment}$ (N)	$P_{\max.simulation}$ (N)	$\frac{P_{\max.simulation}}{P_{\max.experiment}}$
P1R1T	1	1	119.2	109.1	0.92
P1T1T	1	1	119.1	115.7	0.97
P2R1T	2	1	149.4	120.9	0.81
P2T1T	2	1	179.2	207.8	1.16
P2R2T	2	2	149.2	150.7	1.01
P2T2T	2	2	204.3	195.7	0.96

Table A-0-3 Performance of the FE modelling of longitudinally stiffened plates, using experimental test from Chou et al. (2006)

Specimen number	$\sigma_{\max.experiment}$ (ksi)	$\sigma_{\max.simulation}$ (ksi)	$\frac{\sigma_{\max.simulation}}{\sigma_{\max.experiment}}$
2	60	60.44	1.01

A.6 Verification of FE test simulation

A basic verification of the finite element models is performed to ascertain the correctness of the FE models. The verification is done by considering three cases for which analytical solutions are available, and comparing the predictions from finite element analysis of these cases with the available closed form analytical solutions. This approach is similar to that used by Subramanian (2015). The cases considered are as follows:

Case 1- Elastic lateral torsional buckling of a long simply supported box-section beam subjected to uniform bending.

Case 2- A box-section beam with $L_b < L_p$ and subjected to uniform bending. The slenderness of the box-section component plates are chosen such that they are not susceptible to local buckling.

Case 3- Elastic buckling of a simply supported unstiffened plate subjected to uniform axial compression in the longitudinal direction.

For Case 1, an elastic eigenvalue buckling analysis of a simply supported box-section beam subjected to uniform bending is performed. The dimensions of the box-

section beam are as follows: $b_{fc} = 10\,\text{in.}$, $t_{fc} = 0.5\,\text{in.}$, $b_{ft} = 10\,\text{in.}$, $t_{ft} = 0.5\,\text{in.}$, $D = 60\,\text{in.}$, $t_w = 1.5\,\text{in.}$, $L_b = 583.33\,\text{ft}$; where b_{fc}, t_{fc}, b_{ft}, t_{ft}, D, t_w are as shown in Figure 2-4, and L_b is the unbraced length of the box-section beam. The elastic LTB moment from the FE analysis is 45138.22 kip-in, which is just 1.0027 times the theoretical elastic lateral torsional buckling resistance, $M_{cr} = \frac{\pi}{L_b}\sqrt{EI_yGJ} = 45016.677$ kip-inch.

For Case 2, the theoretical resistance is the plastic moment capacity of the gross cross-section. It can be observed from the results for cases 1, 4, 7, 37 in Figure 3-4 that the test simulation strength is equal to the plastic moment capacity of the gross cross-section.

For Case 3, an elastic eigenvalue buckling analysis of a simply supported unstiffened plate subjected to uniform axial compression in the longitudinal direction, is performed. The dimensions of the plate are as follows: $width = 60\,\text{in.}$, $thickness = 1\,\text{in.}$ and $length = 480\,\text{in.}$ The elastic buckling load from the FE analysis is 1761.34 kips, which is just 1.008 times the theoretical buckling load, $P_{cr} = \frac{4\pi^2 E}{12\left(1-\nu^2\right)\left(\frac{width}{thickness}\right)^2}\left(width\right)\left(thickness\right) = 1747.37$ kips.

APPENDIX B. DETAILS OF THE PARAMETRIC STUDY DESIGN FOR EVALUATING THE PERFORMANCE OF THE PROPOSED METHOD FOR CALCULATING THE FLEXURAL RESISTANCE OF NON-LONGITUDINALLY STIFFENED BOX SECTION MEMBERS

Table B-0-1 gives the cross-section dimensions and lengths of the various cases listed in Table 3-4.

Table B-0-1 Dimensions of members considered in the parametric study used for evaluating the performance of the proposed method for calculating the flexural resistance of non-longitudinally stiffened box-section members

Cross-section #	b_{fc} (in.)	t_{fc} (in.)	b_{ft} (in.)	t_{ft} (in.)	D (in.)	t_w (in.)	Length = $0.5L_p$ (in.)	Length = $\frac{0.5L_p + L_{\max}}{2}$ (in.)	Length = $L_{\max}$ (in.)
1	10.00	0.50	10.00	0.50	36.00	0.83	113.40	495.41	877.42
2	10.00	0.50	10.00	0.50	52.60	0.57	88.95	494.67	900.40
3	12.50	0.75	12.50	0.75	75.00	0.50	94.85	607.97	1121.09
4	18.00	1.00	18.00	0.50	69.80	1.16	206.75	907.86	1608.97
5	18.00	1.00	18.00	0.50	90.00	0.90	175.05	903.46	1631.86
6	17.00	1.00	17.00	0.50	102.00	0.68	142.00	845.72	1549.43
7	53.00	3.00	53.00	0.50	132.50	1.50	735.90	-	3975.00
8	53.00	3.00	53.00	0.50	180.00	1.50	640.25	2672.82	4705.39
9	53.00	3.00	53.00	0.50	225.00	1.50	572.35	2675.18	4778.01

10	18.00	0.50	18.00	1.00	54.00	1.00	222.80	906.80	1590.81
11	18.00	0.50	18.00	1.00	70.00	0.77	188.80	899.38	1609.97
12	17.00	0.50	17.00	1.00	87.46	0.58	144.30	838.58	1532.86
13	18.00	0.50	18.00	0.50	56.88	0.95	235.75	931.64	1627.53
14	17.00	0.50	17.00	0.50	70.00	0.73	188.55	870.24	1551.93
15	16.00	0.50	16.00	0.50	84.86	0.57	147.30	809.29	1471.28
16	53.00	1.65	53.00	0.50	106.00	1.50	888.75	-	3180.00
17	53.00	1.65	53.00	0.50	174.90	1.50	705.95	2775.12	4844.28
18	53.00	1.65	53.00	0.50	225.00	1.50	615.00	-	4904.14
19	33.00	0.50	33.00	1.50	70.74	1.40	498.20	-	-
20	33.00	0.50	33.00	1.50	96.00	1.03	421.95	1650.98	2880.00
21	32.40	0.50	32.40	1.50	120.75	0.81	349.80	1620.87	2891.94
22	33.00	0.50	33.00	1.00	73.79	1.34	524.20	-	2213.70
23	33.00	0.50	33.00	1.00	99.00	1.00	447.80	-	-
24	32.40	0.50	32.40	1.00	120.74	0.81	380.25	1663.85	2947.45
25	33.00	0.50	33.00	0.50	76.72	1.29	549.95	-	2301.60
26	33.00	0.50	33.00	0.50	100.00	0.99	483.85	1741.93	3000.00
27	32.40	0.50	32.40	0.50	120.75	0.80	418.25	-	-
28	53.00	0.50	53.00	2.30	53.00	1.50	1117.50	-	1590.00
29	53.00	0.50	53.00	2.50	113.37	1.40	756.75	-	3401.10
30	52.00	0.50	52.00	3.00	153.00	1.02	585.50	2514.17	4442.85
31	53.00	0.50	53.00	1.65	53.00	1.50	1173.70	-	1590.00
32	53.00	0.50	53.00	1.65	118.46	1.34	814.55	-	3553.80
33	52.00	0.50	52.00	1.65	153.00	1.02	679.15	2634.58	4590.00

34	53.00	0.50	53.00	0.50	79.50	1.50	1147.10	-	2385.00
35	53.00	0.50	53.00	0.50	125.40	1.27	926.90	-	3762.00
36	52.00	0.50	52.00	0.50	153.00	1.02	813.75	-	-
37	78.00	4.00	78.00	0.50	156.00	1.50	1153.70	-	4680.00
38	10.00	0.50	10.00	0.50	35.88	0.84	103.15	-	877.21
39	10.00	0.50	10.00	0.50	49.20	0.61	84.75	-	896.92
40	12.50	0.75	12.50	0.75	75.00	0.50	83.60	-	1121.09
41	16.00	0.50	16.00	0.50	48.00	1.00	193.25	-	1432.95
42	15.50	0.50	15.50	0.50	61.00	0.76	159.65	-	1406.36
43	14.00	0.50	14.00	0.50	79.38	0.53	110.25	-	1284.35
44	53.00	0.50	53.00	0.50	53.00	1.50	1230.45	-	1590.00
45	52.70	0.50	52.70	0.50	116.13	1.36	891.65	-	3483.90
46	52.40	0.50	52.40	0.50	153.54	1.02	772.90	-	-

APPENDIX C. JUSTIFICATION FOR THE USE OF ORTHOTROPIC PLATE IDEALIZATION FOR PLATES WITH ONE OR TWO LONGITUDINAL STIFFENERS

This appendix shows that for plates with one or two longitudinal stiffeners the buckling load calculated by considering a column on elastic foundation model (where the column represents the stiffener strut and elastic foundation stiffness represents the transverse bending stiffness of the plate) along with the consideration of torsional stiffness of the plate, gives a buckling load approximately equal to that obtained using the orthotropic plate idealization. This justifies the use of the orthotropic plate approach by the proposed method for any number of longitudinal stiffeners.

Plates with one longitudinal stiffener:

For a column on elastic foundation model of the stiffener strut (where the column represents the stiffener strut and elastic foundation stiffness represents the transverse bending stiffness of the plate) along with the consideration of torsional stiffness of the plate, the governing differential equation of equilibrium is

$$EI_s\delta^{iv} - P\delta'' + \frac{2GJ_{trib}}{w^2}\delta'' + k_p\delta = 0 \tag{167}$$

where:

- $I_s = I_x + \frac{wt_{sp}^{\ 3}}{12} + wt_{sp}c_1^2$ (168)

- k_p is the foundation stiffness and is calculated by modeling the plate in the transverse direction as a "wide beam" loaded by a concentrated force, W at the mid width of the plate (i.e., at the longitudinal stiffener location). Therefore

$$k_p = \frac{W}{\left(\frac{W b_{sp}^{\ 3}}{48 E I_p}\right)} = \frac{48 E I_p}{b_{sp}^{\ 3}} \tag{169}$$

- The term $\frac{2GJ_{trib}}{w^2}\delta''$ corresponds to the contribution from the resistance to twisting of the plate associated with the transverse displacement of the longitudinal stiffener. This resistance can be approximated as

$$2\frac{(dT/dx)}{w} = 2\frac{\frac{d}{dx}\left(GJ_{trib}\frac{d\theta}{dx}\right)}{w} = 2\frac{\frac{d}{dx}\left(GJ_{trib}\frac{1}{w}\frac{d\delta}{dx}\right)}{w} = \frac{2GJ_{trib}}{w^2}\delta'' \tag{170}$$

where:

$$J_{trib} = \frac{w t_{sp}^{\ 3}}{3} \tag{171}$$

This is approximate because a simplifying assumption is made that the strip considered above is pinned along the edge of the plate as well as along the longitudinal stiffener. This neglects the continuity across the longitudinal stiffener (King 2017a).

The buckled shape is given by

$$\delta = \delta_{\max} \sin\frac{\pi x}{\ell} \tag{172}$$

where ℓ is the buckling length, taken as the smaller of the transverse stiffener spacing, *a*, and the characteristic buckling length, ℓ_c.

Substituting the displacement solution $\delta = \delta_{\max} \sin\frac{\pi x}{\ell}$, which satisfies the boundary conditions, in the above governing differential equation we obtain

$$EI_s\delta_{\max}\left(\frac{\pi}{\ell}\right)^4 \sin\frac{\pi x}{\ell} - P\delta_{\max}\left(\frac{\pi}{\ell}\right)^2 \sin\frac{\pi x}{\ell} + \frac{2GJ_{trib}}{w^2}\delta_{\max}\left(\frac{\pi}{\ell}\right)^2 \sin\frac{\pi x}{\ell} + k_p\delta_{\max}\sin\frac{\pi x}{\ell} = 0 \tag{173}$$

Simplifying,

$$P = \left[EI_s\frac{\pi^2}{\ell^2} + 96w\frac{EI_p}{b_{sp}{}^4}\frac{\ell^2}{\pi^2}\right] + \frac{8}{b_{sp}{}^2}\frac{Gwt_{sp}{}^3}{3} \tag{174}$$

This is very close to the buckling load obtained using the orthotropic plate idealization

$$\begin{aligned} P &= \left[EI_s\frac{\pi^2}{\ell^2} + \pi^4 w\frac{EI_p}{b_{sp}^4}\frac{\ell^2}{\pi^2}\right] + \frac{\pi^2}{(1-\nu)b_{sp}^2}\frac{Gwt_{sp}^3}{3} \\ &= \left[EI_s\frac{\pi^2}{\ell^2} + 97.2w\frac{EI_p}{b_{sp}^4}\frac{\ell^2}{\pi^2}\right] + \frac{14.08}{b_{sp}^2}\frac{Gwt_{sp}^3}{3} \end{aligned} \tag{175}$$

The slight differences are because of the approximate calculation of the transverse bending stiffness and torsion stiffness contribution.

Plates with two longitudinal stiffeners:

For a column on elastic foundation model of the stiffener strut (where the column represents the stiffener strut and elastic foundation stiffness represents the transverse bending stiffness of the plate) along with the consideration of torsional stiffness of the plate, the governing differential equation of equilibrium is

$$EI_s\delta^{iv} - P\delta'' + \frac{GJ_{trib}}{w^2}\delta'' + k_p\delta = 0 \tag{176}$$

where:

- $I_s = I_x + \frac{wt_{sp}^{\ 3}}{12} + wt_{sp}c_1^2$ (177)
- k_p is the foundation stiffness and is calculated by modeling the plate in the transverse direction as a "wide beam" loaded by a concentrated force, W at the mid width of the plate (i.e., at the longitudinal stiffener location). Therefore

$$k_p = \frac{W}{\left(\frac{5Wb_{sp}^{\ 3}}{162EI_p}\right)} = \frac{162EI_p}{5b_{sp}^{\ 3}} \tag{178}$$

- The term $\frac{GJ_{trib}}{w^2}\delta''$ corresponds to the contribution from the resistance to twisting of the plate caused by the transverse displacement of the longitudinal stiffener. This resistance can be approximated as

$$\frac{(dT/dx)}{w} = \frac{\frac{d}{dx}\left(GJ_{trib}\frac{d\theta}{dx}\right)}{w} = \frac{\frac{d}{dx}\left(GJ_{trib}\frac{1}{w}\frac{d\delta}{dx}\right)}{w} = \frac{GJ_{trib}}{w^2}\delta'' \tag{179}$$

where

$$J_{trib} = \frac{w t_{sp}^{\ 3}}{3} \tag{180}$$

This is approximate because a simplifying assumption is made that the strip considered above is pinned along the edge of the plate as well as along the longitudinal stiffener. This neglects the continuity across the longitudinal stiffener (King 2017a).

The buckled shape is given by

$$\delta = \delta_{\max} \sin \frac{\pi x}{\ell} \tag{181}$$

where ℓ is the buckling length, taken as the smaller of the transverse stiffener spacing, *a*, and the characteristic buckling length, ℓ_c.

Substituting the displacement solution $\delta = \delta_{\max} \sin \frac{\pi x}{\ell}$, which satisfies the boundary conditions, in the above governing differential equation we obtain

$$EI_s \delta_{\max} \left(\frac{\pi}{\ell}\right)^4 \sin \frac{\pi x}{\ell} - P \delta_{\max} \left(\frac{\pi}{\ell}\right)^2 \sin \frac{\pi x}{\ell} + \frac{GJ_{trib}}{w^2} \delta_{\max} \left(\frac{\pi}{\ell}\right)^2 \sin \frac{\pi x}{\ell} + k_p \delta_{\max} \sin \frac{\pi x}{\ell} = 0 \tag{182}$$

Simplifying,

$$P = \left[EI_s \frac{\pi^2}{\ell^2} + 97.2 w \frac{EI_p}{b_{sp}^{\ 4}} \frac{\ell^2}{\pi^2} \right] + \frac{9}{b_{sp}^{\ 2}} \frac{G w t_{sp}^{\ 3}}{3} \tag{183}$$

This is very close to the buckling load obtained using the orthotropic plate idealization

$$P = \left[EI_s \frac{\pi^2}{\ell^2} + \pi^4 w \frac{EI_p}{b_{sp}^4} \frac{\ell^2}{\pi^2} \right] + \frac{\pi^2}{(1-\nu) b_{sp}^2} \frac{Gwt_{sp}^3}{3}$$
$$= \left[EI_s \frac{\pi^2}{\ell^2} + 97.2 w \frac{EI_p}{b_{sp}^4} \frac{\ell^2}{\pi^2} \right] + \frac{14.08}{b_{sp}^2} \frac{Gwt_{sp}^3}{3} \quad (184)$$

The slight difference is because of the approximate calculation of the torsion stiffness contribution.

Thus it can be seen that for plates with one or two longitudinal stiffeners the buckling load calculated by considering a column on elastic foundation model (where the column represents the stiffener strut and elastic foundation stiffness represents the transverse bending stiffness of the plate) along with the consideration of torsional stiffness of the plate, gives a buckling load approximately equal to that obtained using the orthotropic plate idealization. This justifies the use of the orthotropic plate approach by the proposed method for any number of longitudinal stiffeners.

APPENDIX D. DETAILS OF THE PARAMETRIC STUDY DESIGN FOR EVALUATING THE PERFORMANCE OF THE PROPOSED METHOD FOR CALCULATING THE ULTIMATE COMPRESSIVE RESISTANCE OF LONGITUDINALLY STIFFENED PLATES

The cross-section dimensions and lengths of the various cases in Groups 1 through 4 are provided in Table D-0-1 through Table D-0-4 respectively. In Table D-0-1 through Table D-0-4:

- $h_{w.ls}$ is the depth of a flat longitudinal stiffener or the depth of the web of a Tee longitudinal stiffener;
- $t_{w.ls}$ is the thickness of a flat longitudinal stiffener or the thickness of the web of a Tee longitudinal stiffener;
- $b_{f.ls}$ is the width of the flange of a Tee longitudinal stiffener;
- $t_{f.ls}$ is the thickness of the flange of a Tee longitudinal stiffener;
- L is the total length of the longitudinally stiffened plate;
- $n_{transstiff}$ is the number of intermediate transverse stiffeners.

Table D-0-1 Cross-section dimensions and lengths of Group 1 cases

Case #	b_{sp} (in.)	t_{sp} (in.)	n	$h_{w.ls}$ (in.)	$t_{w.ls}$ (in.)	$b_{f.ls}$ (in.)	$t_{f.ls}$ (in.)	L (in.)
1	60.00	1.50	1	5.087	0.442	-	-	425.840
2	60.00	1.50	1	7.194	0.626	-	-	553.876
3	60.00	1.50	1	10.173	0.885	-	-	745.178
4	60.00	1.50	1	14.387	1.251	-	-	1009.209
5	90.00	1.50	2	6.019	0.523	-	-	719.755
6	90.00	1.50	2	7.194	0.626	-	-	828.883
7	90.00	1.50	2	9.099	0.791	-	-	1010.562
8	90.00	1.50	2	11.374	0.989	-	-	1226.159
9	90.00	1.50	2	14.387	1.251	-	-	1502.902
10	90.00	1.50	2	17.621	1.532	-	-	1786.418
11	120.00	1.50	1	12.460	1.083	-	-	1529.807
12	120.00	1.50	1	14.387	1.251	-	-	1741.036
13	120.00	1.50	1	17.621	1.532	-	-	2088.674
14	120.00	1.50	1	20.347	1.769	-	-	2373.616
15	120.00	1.50	1	24.920	2.167	-	-	2833.642
16	180.00	1.50	2	12.460	1.083	-	-	2286.851
17	180.00	1.50	2	14.387	1.251	-	-	2600.188
18	180.00	1.50	2	17.621	1.532	-	-	3114.522
19	180.00	1.50	2	20.347	1.769	-	-	3535.054
20	180.00	1.50	2	24.920	2.167	-	-	4212.829
21	180.00	1.50	1	17.621	1.532	-	-	2867.898

22	180.00	1.50	1	21.581	1.877	-	-	3446.848
23	180.00	1.50	1	24.920	2.167	-	-	3920.955
24	180.00	1.50	1	27.861	2.423	-	-	4327.491
25	180.00	1.50	1	30.520	2.654	-	-	4686.078
26	270.00	1.50	2	17.621	1.532	-	-	4283.202
27	270.00	1.50	2	22.289	1.938	-	-	5290.041
28	270.00	1.50	2	27.298	2.374	-	-	6325.563
29	270.00	1.50	2	30.520	2.654	-	-	6967.243

Table D-0-2 Cross-section dimensions and lengths of Group 2 cases

Case #	b_{sp} (in.)	t_{sp} (in.)	n	$h_{w.ls}$ (in.)	$t_{w.ls}$ (in.)	$b_{f.ls}$ (in.)	$t_{f.ls}$ (in.)	L (in.)
1	60.00	1.50	1	2.912	0.416	2.496	0.416	405.243
2	60.00	1.50	1	4.119	0.588	3.530	0.588	518.044
3	60.00	1.50	1	5.824	0.832	4.992	0.832	689.694
4	60.00	1.50	1	8.237	1.177	7.060	1.177	927.130
5	90.00	1.50	2	3.446	0.492	2.954	0.492	678.513
6	90.00	1.50	2	4.119	0.588	3.530	0.588	775.170
7	90.00	1.50	2	5.209	0.744	4.465	0.744	937.749
8	90.00	1.50	2	6.512	0.930	5.582	0.930	1131.475
9	90.00	1.50	2	8.237	1.177	7.060	1.177	1379.627
10	90.00	1.50	2	10.088	1.441	8.647	1.441	1632.230
11	120.00	1.50	1	7.133	1.019	6.114	1.019	1413.557
12	120.00	1.50	1	8.237	1.177	7.060	1.177	1604.251

13	120.00	1.50	1	10.088	1.441	8.647	1.441	1917.824
14	120.00	1.50	1	11.649	1.664	9.985	1.664	2174.136
15	120.00	1.50	1	14.267	2.038	12.229	2.038	2585.704
16	180.00	1.50	2	7.133	1.019	6.114	1.019	2112.477
17	180.00	1.50	2	8.237	1.177	7.060	1.177	2394.956
18	180.00	1.50	2	10.088	1.441	8.647	1.441	2858.043
19	180.00	1.50	2	11.649	1.664	9.985	1.664	3235.427
20	180.00	1.50	2	14.267	2.038	12.229	2.038	3839.996
21	180.00	1.50	1	10.088	1.441	8.647	1.441	2637.280
22	180.00	1.50	1	12.355	1.765	10.590	1.765	3160.061
23	180.00	1.50	1	14.267	2.038	12.229	2.038	3586.705
24	180.00	1.50	1	15.951	2.279	13.672	2.279	3951.157
25	180.00	1.50	1	17.473	2.496	14.977	2.496	4271.515
26	270.00	1.50	2	10.088	1.441	8.647	1.441	3937.159
27	270.00	1.50	2	12.761	1.823	10.938	1.823	4844.425
28	270.00	1.50	2	15.629	2.233	13.396	2.233	5772.316
29	270.00	1.50	2	17.473	2.496	14.977	2.496	6343.849

Table D-0-3 Cross-section dimensions and lengths of Group 3 cases

Case #	b_{sp} (in.)	t_{sp} (in.)	n	$n_{transstiff}$	$h_{w.ls}$ (in.)	$t_{w.ls}$ (in.)	$b_{f.ls}$ (in.)	$t_{f.ls}$ (in.)	L (in.)
1	120.00	1.00	5	3	4.80	0.42	-	-	150.10
2	120.00	1.00	5	3	6.78	0.59	-	-	260.52
3	120.00	1.00	5	3	8.31	0.72	-	-	352.78

4	120.00	1.00	5	3	9.59	0.83	-	-	431.19
5	120.00	1.00	5	3	10.72	0.93	-	-	491.78
6	120.00	1.00	5	3	4.80	0.42	-	-	264.89
7	120.00	1.00	5	3	6.78	0.59	-	-	455.90
8	120.00	1.00	5	3	8.31	0.72	-	-	620.89
9	120.00	1.00	5	3	9.59	0.83	-	-	766.57
10	120.00	1.00	5	3	10.72	0.93	-	-	913.31
11	120.00	1.00	5	3	4.80	0.42	-	-	379.67
12	120.00	1.00	5	3	6.78	0.59	-	-	663.13
13	120.00	1.00	5	3	8.31	0.72	-	-	959.56
14	120.00	1.00	5	3	9.59	0.83	-	-	1245.67
15	120.00	1.00	5	3	10.72	0.93	-	-	1615.86
16	240.00	1.00	3	3	11.75	1.02	-	-	380.18
17	240.00	1.00	3	3	14.39	1.25	-	-	510.74
18	240.00	1.00	3	3	16.61	1.44	-	-	621.51
19	240.00	1.00	3	3	18.57	1.62	-	-	730.79
20	240.00	1.00	3	3	20.35	1.77	-	-	815.31
21	240.00	1.00	3	3	11.75	1.02	-	-	714.74
22	240.00	1.00	3	3	14.39	1.25	-	-	984.99
23	240.00	1.00	3	3	16.61	1.44	-	-	1222.31
24	240.00	1.00	3	3	18.57	1.62	-	-	1438.75
25	240.00	1.00	3	3	20.35	1.77	-	-	1630.61
26	240.00	1.00	3	3	11.75	1.02	-	-	1018.89
27	240.00	1.00	3	3	14.39	1.25	-	-	1422.77

28	240.00	1.00	3	3	16.61	1.44	-	-	1781.67
29	240.00	1.00	3	3	18.57	1.62	-	-	2101.03
30	240.00	1.00	3	3	20.35	1.77	-	-	2371.80

Table D-0-4 Cross-section dimensions and lengths of Group 4 cases

Case #	b_{sp} (in.)	t_{sp} (in.)	n	$n_{transstiff}$	$h_{w.ls}$ (in.)	$t_{w.ls}$ (in.)	$b_{f.ls}$ (in.)	$t_{f.ls}$ (in.)	L (in.)
1	120.00	1.00	5	3	2.746	0.392	2.353	0.392	132.103
2	120.00	1.00	5	3	3.883	0.555	3.328	0.555	219.080
3	120.00	1.00	5	3	4.755	0.679	4.076	0.679	298.773
4	120.00	1.00	5	3	5.491	0.785	4.707	0.785	351.702
5	120.00	1.00	5	3	6.139	0.877	5.262	0.877	417.947
6	120.00	1.00	5	3	2.746	0.392	2.354	0.392	231.188
7	120.00	1.00	5	3	3.883	0.555	3.328	0.555	388.868
8	120.00	1.00	5	3	4.755	0.679	4.076	0.679	526.101
9	120.00	1.00	5	3	5.491	0.785	4.707	0.785	652.113
10	120.00	1.00	5	3	6.139	0.877	5.262	0.877	755.520
11	120.00	1.00	5	3	2.746	0.392	2.354	0.392	330.269
12	120.00	1.00	5	3	3.883	0.555	3.328	0.555	558.655
13	120.00	1.00	5	3	4.755	0.679	4.076	0.679	779.409
14	120.00	1.00	5	3	5.491	0.785	4.707	0.785	981.834
15	120.00	1.00	5	3	6.139	0.877	5.262	0.877	1173.467
16	240.00	1.00	3	3	6.725	0.961	5.765	0.961	321.459

17	240.00	1.00	3	3	8.237	1.177	7.060	1.177	434.442
18	240.00	1.00	3	3	9.511	1.359	8.153	1.359	530.073
19	240.00	1.00	3	3	10.634	1.519	9.115	1.519	624.753
20	240.00	1.00	3	3	11.649	1.664	9.985	1.664	697.123
21	240.00	1.00	3	3	6.725	0.961	5.765	0.961	600.989
22	240.00	1.00	3	3	8.237	1.177	7.060	1.177	818.755
23	240.00	1.00	3	3	9.511	1.359	8.153	1.359	1022.283
24	240.00	1.00	3	3	10.634	1.519	9.115	1.519	1187.031
25	240.00	1.00	3	3	11.649	1.664	9.985	1.664	1349.270
26	240.00	1.00	3	3	6.725	0.961	5.765	0.961	866.543
27	240.00	1.00	3	3	8.237	1.177	7.060	1.177	1186.360
28	240.00	1.00	3	3	9.511	1.359	8.153	1.359	1476.631
29	240.00	1.00	3	3	10.634	1.519	9.115	1.519	1728.484
30	240.00	1.00	3	3	11.649	1.664	9.985	1.664	1956.441

APPENDIX E. DETAILS OF THE PARAMETRIC STUDY DESIGN FOR EVALUATING THE PERFORMANCE OF THE PROPOSED METHOD FOR CALCULATING THE COMPRESSIVE RESISTANCE OF LONGITUDINALLY STIFFENED BOX-SECTION MEMBERS

Table E-0-1 and Table E-0-2 give the cross-section dimensions and lengths of the various cases listed in Table 5-1 and Table 5-2 respectively. Figure E-0-1 illustrates the variables used in Table E-0-1 and Table E-0-2. The cross-sections for all cases are doubly symmetric. In Table E-0-1 and Table E-0-2, n_{fln} and n_{web} are the number of longitudinal stiffeners on each flange and web respectively, and L is the length of the box column.

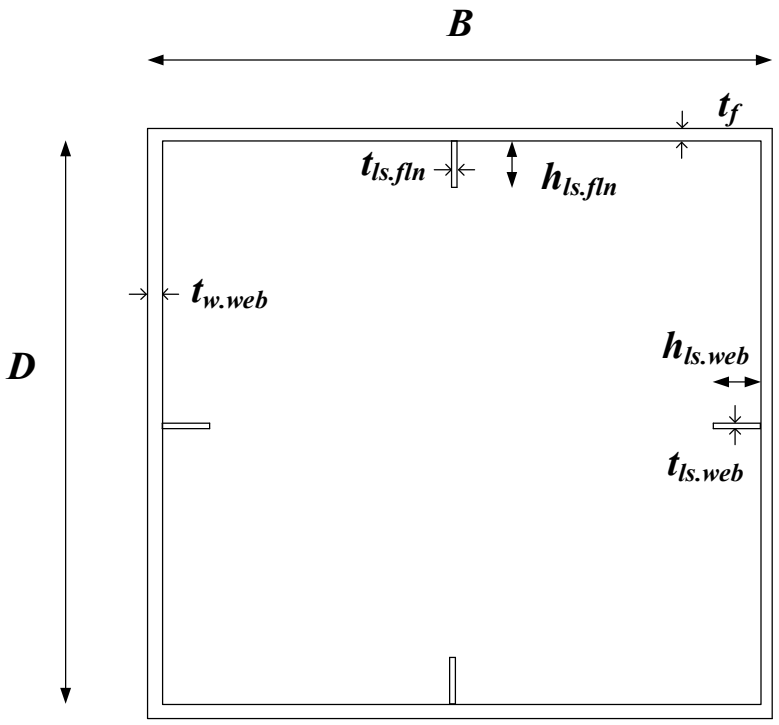

Figure E-0-1 Illustration of variables used in Table E-0-1 and Table E-0-2

Table E-0-1 Dimensions of members listed in Table 5-1

Case #	B (in.)	t_f (in.)	$n_{.fl\,n}$	$h_{ls.f\,ln}$ (in.)	$t_{ls.fl\,n}$ (in.)	D (in.)	t_{web} (in.)	n_{web}	$h_{ls.web}$ (in.)	$t_{ls.web}$ (in.)	L (ft.)
1	41	1	1	4.796	0.417	59	1	2	4.796	0.417	70.71
2	41	1	1	4.796	0.417	59	1	2	4.796	0.417	113.13
3	41	1	1	4.796	0.417	59	1	2	4.796	0.417	155.56
4	41	1	1	4.796	0.417	59	1	2	9.592	0.834	69.61
5	41	1	1	4.796	0.417	59	1	2	9.592	0.834	111.37
6	41	1	1	4.796	0.417	59	1	2	9.592	0.834	153.13
7	41	1	1	4.796	0.417	119	1	1	8.307	0.722	75.25
8	41	1	1	4.796	0.417	119	1	1	8.307	0.722	120.41
9	41	1	1	4.796	0.417	119	1	1	8.307	0.722	165.56
10	41	1	1	4.796	0.417	119	1	1	16.613	1.445	72.88
11	41	1	1	4.796	0.417	119	1	1	16.613	1.445	116.62
12	41	1	1	4.796	0.417	119	1	1	16.613	1.445	160.35
13	41	1	1	4.796	0.417	179	1	2	8.307	0.722	77.16
14	41	1	1	4.796	0.417	179	1	2	8.307	0.722	123.46
15	41	1	1	4.796	0.417	179	1	2	8.307	0.722	169.76
16	41	1	1	4.796	0.417	179	1	2	16.613	1.445	73.70
17	41	1	1	4.796	0.417	179	1	2	16.613	1.445	117.92
18	41	1	1	4.796	0.417	179	1	2	16.613	1.445	162.14
19	61	1	2	4.796	0.417	119	1	1	8.307	0.722	109.12
20	61	1	2	4.796	0.417	119	1	1	8.307	0.722	174.59
21	61	1	2	4.796	0.417	119	1	1	8.307	0.722	240.07

22	61	1	2	4.796	0.417	119	1	1	16.613	1.445	107.23
23	61	1	2	4.796	0.417	119	1	1	16.613	1.445	171.57
24	61	1	2	4.796	0.417	119	1	1	16.613	1.445	235.90
25	61	1	2	4.796	0.417	179	1	2	8.307	0.722	112.98
26	61	1	2	4.796	0.417	179	1	2	8.307	0.722	180.76
27	61	1	2	4.796	0.417	179	1	2	8.307	0.722	248.55
28	61	1	2	4.796	0.417	179	1	2	16.613	1.445	109.89
29	61	1	2	4.796	0.417	179	1	2	16.613	1.445	175.82
30	61	1	2	4.796	0.417	179	1	2	16.613	1.445	241.75
31	121	1	1	8.307	0.722	179	1	2	8.307	0.722	212.73
32	121	1	1	8.307	0.722	179	1	2	8.307	0.722	340.36
33	121	1	1	8.307	0.722	179	1	2	8.307	0.722	468.00
34	121	1	1	8.307	0.722	179	1	2	16.613	1.445	212.29
35	121	1	1	8.307	0.722	179	1	2	16.613	1.445	339.67
36	121	1	1	8.307	0.722	179	1	2	16.613	1.445	467.04
37	121	1	1	16.613	1.445	179	1	2	8.307	0.722	206.95
38	121	1	1	16.613	1.445	179	1	2	8.307	0.722	331.12
39	121	1	1	16.613	1.445	179	1	2	8.307	0.722	455.29
40	121	1	1	16.613	1.445	179	1	2	16.613	1.445	207.09
41	121	1	1	16.613	1.445	179	1	2	16.613	1.445	331.35
42	121	1	1	16.613	1.445	179	1	2	16.613	1.445	455.60

Table E-0-2 Dimensions of members listed in Table 5-2

Case #	B (in.)	t_f (in.)	$n_{.fl\,n}$	$h_{ls.f\,ln}$ (in.)	$t_{ls.fl\,n}$ (in.)	D (in.)	t_{web} (in.)	n_{web}	$h_{ls.web}$ (in.)	$t_{ls.web}$ (in.)	L (ft.)
1	42	1	1	6.584	0.608	40	1	1	6.584	0.608	68.21
2	42	1	1	6.584	0.608	40	1	1	6.584	0.608	109.13
3	82	1	1	9.311	0.859	80	1	1	9.311	0.859	135.13
4	82	1	1	9.311	0.859	80	1	1	9.311	0.859	216.21
5	42	1	1	4.656	0.430	80	1	1	6.584	0.608	163.92
6	42	1	1	4.656	0.430	80	1	1	13.168	1.215	160.48
7	42	1	1	4.656	0.430	180	1	1	9.876	0.911	174.00
8	42	1	1	4.656	0.430	180	1	1	19.752	1.823	167.38
9	42	1	1	4.656	0.430	180	1	1	19.752	1.823	182.60

APPENDIX F. DETAILS OF THE PARAMETRIC STUDY DESIGN FOR EVALUATING THE PERFORMANCE OF THE PROPOSED METHOD FOR CALCULATING THE FLEXURAL RESISTANCE OF LONGITUDINALLY STIFFENED BOX SECTION MEMBERS

Table F-0-1 and Table F-0-2 give the cross-section dimensions and lengths of the various cases listed in Table 6-1. Figure 6-1 illustrates the variables used in Table F-0-1 and Table F-0-2. In Table F-0-2, n_{trans} is the number of equally spaced web transverse stiffeners, b_{trans} is the width of the transverse stiffener, and t_{trans} is the thickness of the transverse stiffener.

Table F-0-1 Dimensions of the tension and compression flange of the box-section beam cases listed in Table 6-1

Case #	B (in.)	t_{ft} (in.)	t_{fc} (in.)	$h_{ls.fl\,n}$ (in.)	$t_{ls.fl\,n}$ (in.)
1	62.00	1.90	1	8.064	0.744
2	62.00	1.90	1	8.064	0.744
3	62.00	1.90	1	8.064	0.744
4	123.10	2.50	1	11.404	1.052
5	123.10	2.50	1	11.404	1.052
6	123.10	2.50	1	11.404	1.052
7	61.90	3.00	1	8.064	0.744
8	61.90	3.00	1	8.064	0.744

9	61.90	3.00	1	8.064	0.744
10	122.40	4.00	1	11.404	1.052
11	122.40	4.00	1	11.404	1.052
12	122.40	4.00	1	11.404	1.052
13	61.90	3.00	1	8.064	0.744
14	61.90	3.00	1	8.064	0.744
15	61.90	3.00	1	8.064	0.744
16	122.30	4.00	1	11.404	1.052
17	122.30	4.00	1	11.404	1.052
18	122.30	4.00	1	11.404	1.052
19	62.60	0.70	1	8.064	0.744
20	62.60	0.70	1	8.064	0.744
21	61.68	0.69	1	8.064	0.744
22	61.68	0.69	1	8.064	0.744
23	60.96	0.68	1	8.064	0.744
24	60.96	0.68	1	8.064	0.744
25	60.80	0.68	1	8.064	0.744
26	60.80	0.68	1	8.064	0.744
27	60.82	0.68	1	8.064	0.744
28	60.82	0.68	1	8.064	0.744
29	64.74	3.20	1	7.413	0.809
30	64.74	3.20	1	7.413	0.809
31	61.74	3.10	1	7.413	0.809
32	61.74	3.10	1	7.413	0.809

33	61.94	3.10	1	7.413	0.809
34	61.94	3.10	1	7.413	0.809
35	62.74	0.70	1	7.413	0.809
36	62.74	0.70	1	7.413	0.809
37	61.66	0.69	1	7.413	0.809
38	61.66	0.69	1	7.413	0.809
39	61.68	0.70	1	7.413	0.809
40	61.68	0.70	1	7.413	0.809
41	62.00	0.70	1	7.413	0.809
42	62.00	0.70	1	7.413	0.809

Table F-0-2 Dimensions of the web, and length of the box-section beam cases listed in Table 6-1

Case #	D (in.)	t_w (in.)	d_s (in.)	$h_{ls.web}$ (in.)	$t_{ls.web}$ (in.)	n_{trans}	b_{trans} (in.)	t_{trans} (in.)	L (in.)
1	250	1.00	50.95	20.049	1.850	2	10.40	0.65	1178.55
2	250	1.00	50.95	20.049	1.850	6	10.40	0.65	3291.27
3	250	1.00	50.95	20.049	1.850	10	10.40	0.65	5404.00
4	345	1.55	76.25	21.675	2.000	8	13.60	0.85	3764.47
5	345	1.55	76.25	21.675	2.000	16	13.60	0.85	7057.24
6	345	1.55	76.25	21.675	2.000	24	13.60	0.85	10350.00
7	285	0.95	72.75	20.591	1.900	1	11.52	0.72	1061.97
8	285	0.95	72.75	20.591	1.900	5	11.52	0.72	3184.96
9	285	0.95	72.75	20.591	1.900	9	11.52	0.72	5307.95

10	359	1.20	107.00	21.675	2.000	6	14.08	0.88	3470.42
11	359	1.20	107.00	21.675	2.000	11	14.08	0.88	6867.33
12	359	1.20	107.00	21.675	2.000	17	14.08	0.88	10264.24
13	285	0.95	126.50	20.591	1.900	2	11.52	0.72	1161.22
14	285	0.95	126.50	20.591	1.900	5	11.52	0.72	3234.59
15	285	0.95	126.50	20.591	1.900	9	11.52	0.72	5307.95
16	344	1.15	173.00	21.675	2.000	6	13.60	0.85	3779.47
17	344	1.15	173.00	21.675	2.000	11	13.60	0.85	6972.25
18	344	1.15	173.00	21.675	2.000	17	13.60	0.85	10165.02
19	126	1.30	-	-	-	-	-	-	2066.19
20	126	1.30	-	-	-	-	-	-	3780.00
21	126	0.84	-	-	-	-	-	-	1798.80
22	126	0.84	-	-	-	-	-	-	3780.00
23	124	0.48	21.84	9.645	0.890	5	6.24	0.39	1316.12
24	124	0.48	21.84	9.645	0.890	15	6.24	0.39	3720.00
25	120	0.40	15.84	8.562	0.790	4	6.08	0.38	1198.29
26	120	0.40	15.84	8.562	0.790	15	6.08	0.38	3600.00
27	123	0.41	42.84	8.887	0.820	5	6.24	0.39	1291.09
28	123	0.41	42.84	8.887	0.820	15	6.24	0.39	3690.00
29	194	2.37	-	-	-	-	-	-	1344.49
30	194	2.37	-	-	-	-	-	-	5749.69
31	260	0.87	74.55	20.591	1.900	1	10.72	0.67	810.28
32	260	0.87	74.55	20.591	1.900	9	10.72	0.67	5193.88
33	290	0.97	127.55	20.591	1.900	1	11.68	0.73	852.00

34	290	0.97	127.55	20.591	1.900	9	11.68	0.73	5319.40
35	126	1.37	-	-	-	-	-	-	1581.18
36	126	1.37	-	-	-	-	-	-	3780.00
37	124	0.83	-	-	-	-	-	-	1383.10
38	124	0.83	-	-	-	-	-	-	3720.00
39	252	0.84	57.35	20.591	1.900	1	10.40	0.65	896.23
40	252	0.84	57.35	20.591	1.900	10	10.40	0.65	5470.27
41	300	1.00	110.35	20.916	1.930	1	12.00	0.75	935.09
42	300	1.00	110.35	20.916	1.930	9	12.00	0.75	5621.17

APPENDIX G. SAMPLE CALCULATIONS

This Appendix provides sample calculations for calculating the following:

1) Ultimate compressive resistance of longitudinally stiffened plates

2) Flexural resistance of non-longitudinally stiffened welded box-section members

3) Axial compressive resistance of welded box-section members

4) Flexural resistance of longitudinally stiffened welded box-section members

Compressive resistance of longitudinally stiffened plates

Group 1 Case # 6 (See Table D-0-1)

Proposed method

$b := 90in$ $t := 1.5in$ $n_{long} := 2$ $n_{trans} := 0$ $L_{total} := 828.883in$

$E := 29000ksi$ $F_y := 50ksi$ $h_{w\_T} := 7.194in$ $t_{w\_T} := 0.626in$

Pns

$$w := \frac{b}{n_{long} + 1} = 30\,in$$

$$c_1 := \frac{\left[h_{w\_T} \cdot t_{w\_T} \cdot \left(\frac{t}{2} + \frac{h_{w\_T}}{2}\right)\right]}{(w \cdot t) + \left(h_{w\_T} \cdot t_{w\_T}\right)} = 0.4\,in$$

$$c_2 := \left(\frac{t}{2} + \frac{h_{w\_T}}{2}\right) - c_1 = 3.95\,in$$

$$A_s := h_{w\_T} \cdot t_{w\_T} = 4.5\,in^2$$

$$I_x := \left(\frac{t_{w\_T} \cdot h_{w\_T}^{\,3}}{12}\right) + \left[t_{w\_T} \cdot h_{w\_T} \cdot (c_2)^2\right] = 89.742\,in^4$$

$$I_p := \frac{t^3}{12 \cdot \left(1 - 0.3^2\right)} = 0.31 \cdot in^3$$

$$I_s := (w \cdot I_p) + \left[w \cdot t \cdot (c_1)^2\right] + I_x = 106.052\,in^4$$

$$k_p := \pi^4 \cdot w \cdot \frac{E \cdot I_p}{b^4} = 0.4\,ksi$$

$$L_c := \left(\frac{E \cdot I_s \cdot \pi^4}{k_p}\right)^{0.25} = 165.51\,in \qquad a := \frac{L_{total}}{n_{trans}+1} = 828.88\,in$$

$$L := \min\left(L_c, a\right) = 165.51\,in$$

$$P_{esF} := \frac{\pi^2 \cdot E \cdot I_s}{L^2} + k_p \cdot \frac{L^2}{\pi^2} = 2216.09191\,kip$$

$$\lambda := \frac{w}{t} = 20 \qquad \lambda_r := 1.49 \cdot \sqrt{\frac{E}{F_y}} = 35.88$$

$$F_{el} := \left(1.31 \cdot \frac{\lambda_r}{\lambda}\right)^2 \cdot F_y = 276.22\,ksi$$

$$w_e := if\left[\lambda \le \lambda_r \cdot \sqrt{\frac{F_y}{F_y}}, w, w \cdot \left[\left(1 - 0.18 \cdot \sqrt{\frac{F_{el}}{F_y}}\right) \cdot \sqrt{\frac{F_{el}}{F_y}}\right]\right] = 30\,in$$

$$A_{es} := A_s + w_e \cdot t = 49.5\,in^2 \qquad A_{gs} := A_s + w \cdot t = 49.5\,in^2$$

$$P_{yes} := F_y \cdot A_{es} = 2475.1722\,kip \quad P_{ys} := F_y \cdot A_{gs} = 2475.1722\,kip$$

$$P_{nsF} := if\left[\frac{P_{ys}}{P_{esF}} \le 2.25, \left[0.658^{\left(\frac{P_{ys}}{P_{esF}}\right)}\right] \cdot P_{yes}, 0.877 \cdot \frac{P_{esF}}{A_{gs}} \cdot A_{es}\right] = 1550.8877\,kip$$

$$G := \frac{E}{2 \cdot (1 + 0.3)} = 11153.85\,ksi$$

$$P_{esT} := \frac{\pi^2}{(1 - 0.3) \cdot b^2} \cdot \frac{G \cdot w \cdot t^3}{3} = 655.2622\,kip$$

$$P_{ns} := \min\left(P_{nsF} + 0.15 \cdot P_{esT}, P_{yes}\right) = 1649.177\,kip$$

PnR

$$A_{gR} := \frac{w}{2}\cdot t = 22.5\,in^2 \qquad P_{yeR} := F_y\cdot\frac{w_e}{2}\cdot t = 1125\,kip$$

$$P_{nR} := \min\left[\left(1-\frac{P_{ns}}{P_{yes}}\right)\cdot\left[\left(F_y+\frac{P_{ns}}{A_{es}}\right)\cdot 0.45\cdot A_{gR}\right]+\left(\frac{P_{ns}}{P_{yes}}\right)\cdot P_{yeR}\,,P_{yeR}\right] = 1031\,kip$$

$$\boxed{P_{n.plate} := n_{long}\cdot P_{ns}+2P_{nR} = 5360.5129\,kip}$$

AISI

$b := 90in$ $t := 1.5in$ $n_{long} := 2$ $n_{trans} := 0$ $L_{total} := 828.8829in$

$E := 29000ksi$ $F_y := 50ksi$ $h_{w\_T} := 7.193747in$ $t_{w\_T} := 0.625543in$

$$b_p := \frac{b}{n_{long} + 1} = 30\,in$$

$$k_{loc} := 4 \cdot \left(\frac{b}{b_p}\right)^2 = 36$$

$$I_{sp} := \left[\left(\frac{t_{w\_T} \cdot h_{w\_T}^{\ 3}}{12}\right) + \left[t_{w\_T} \cdot h_{w\_T} \cdot \left(\frac{t}{2} + \frac{h_{w\_T}}{2}\right)^2\right]\right] = 104.435\,in^4$$

$$\gamma := \frac{10.92 \cdot I_{sp}}{b \cdot t^3} = 3.755$$

$$\beta_{temp} := \left[1 + \gamma \cdot \left(n_{long} + 1\right)\right]^{\frac{1}{4}} = 1.871$$

$$L_{br} := \frac{L_{total}}{n_{trans} + 1} = 828.883\,in$$

$$\beta := if\left(L_{br} < \beta_{temp} \cdot b, \frac{L_{br}}{b}, \beta_{temp}\right) = 1.871$$

$$A_s := t_{w\_T} \cdot h_{w\_T} = 4.5\,in^2$$

$$\delta := \frac{A_s}{b \cdot t} = 0.033$$

$$k_d := \frac{\left(1+\beta^2\right)^2 + \gamma\cdot\left(1+n_{long}\right)}{\beta^2\cdot\left[1+\delta\cdot\left(1+n_{long}\right)\right]} = 8.185$$

Assuming $R := 2$

$$k := \min\left(R\cdot k_d, k_{loc}\right) = 16.371$$

$$F_{crL} := k\cdot\frac{\pi^2\cdot E}{12\cdot\left(1-0.3^2\right)}\cdot\left(\frac{t}{b}\right)^2 = 119.19\,ksi$$

$$\lambda := \sqrt{\frac{F_y}{F_{crL}}} = 0.648 \qquad \text{Assuming f=Fy}$$

$$\rho := if\left[\lambda \le 0.673, 1, \frac{\left(1-\frac{0.22}{\lambda}\right)}{\lambda}\right] = 1$$

$$A_g := \left(b\cdot t\right) + n_{long}\cdot\left(h_{w\_T}\cdot t_{w\_T}\right) = 144\,in^2$$

$$b_e := \rho\cdot\left(\frac{A_g}{t}\right) = 96\,in$$

$$\boxed{P_n := b_e\cdot t\cdot F_y = 7199.9998\,kip}$$

Eurocode

$b := 90in$ $t := 1.5in$ $n_{long} := 2$ $n_{trans} := 0$ $L_{total} := 828.8829in$

$E := 29000ksi$ $F_y := 50ksi$

Flat stiffener or T longitudinal stiffener

$h_{w\_T} := 7.193747in$

$t_{w\_T} := 0.625543in$

$b_{f\_T} := 0in$

$t_{f\_T} := 0in$

Type of stiffener $Type := 1$ 1 if Flat and 2 if T-Stiffener

A) Ultimate compressive strength of a stiffened plate

Effective area of a stiffener (Asl_eff)

$\psi := 1$

For flat stiffeners

Longitudinal stiffener web

$k_{\sigma\_flat\_web} := 0.43$ $\lambda_{p\_flat\_web} := \dfrac{\frac{h_{w\_T}}{t_{w\_T}}}{28.4 \cdot \sqrt{\frac{235MPa}{F_y}} \cdot \sqrt{k_{\sigma\_flat\_web}}} = 0.75$

$\rho_{flat\_web} := \text{if}\left(\lambda_{p\_flat\_web} \le 0.748, 1, \min\left(\dfrac{\lambda_{p\_flat\_web} - 0.188}{\lambda_{p\_flat\_web}^{2}}, 1\right)\right) = 1$

$A_{sl\_eff\_flat} := n_{long} \cdot \rho_{flat\_web} \cdot h_{w\_T} \cdot t_{w\_T} = 9\,in^2$

$A_{sl\_eff} := A_{sl\_eff\_flat} = 9\,in^2$

Effective width of subpanel (bc_loc, ρ_loc)

$$b_{c\_loc} := \frac{b}{n_{long} + 1} = 30\,in$$

$$k_{\sigma\_bc\_loc} := 4 \qquad \lambda_{p\_bc\_loc} := \frac{\frac{b_{c\_loc}}{t}}{28.4 \cdot \sqrt{\frac{235MPa}{F_y}} \cdot \sqrt{k_{\sigma\_bc\_loc}}} = 0.43$$

$$\rho_{loc} := if\left[\lambda_{p\_bc\_loc} \le 0.5 + \sqrt{0.085 - 0.055 \cdot \psi}, 1, \min\left[\frac{\lambda_{p\_bc\_loc} - 0.055 \cdot (3 + \psi)}{\lambda_{p\_bc\_loc}^{2}}, 1\right]\right] = 1$$

Reduction for overall buckling (ρ_c)

a) Plate type behavior (σ_crp, ρ)

$$L_{trans} := \frac{L_{total}}{n_{trans} + 1} = 828.88\,in$$

Column on elastic foundation

For one longitudinal stiffener

$$b_{1\_onestiff} := \frac{b}{n_{long} + 1} = 30\,in \qquad b_{2\_onestiff} := \frac{b}{n_{long} + 1} = 30\,in$$

Flange of the column $fl_{col} := \frac{b}{n_{long} + 1} = 30\,in$

Centroid of the column relative to the top of the plate

$$c_{col} := \frac{\left(fl_{col} \cdot t \cdot \frac{t}{2}\right) + \left[h_{w\_T} \cdot t_{w\_T} \cdot \left(t + \frac{h_{w\_T}}{2}\right)\right] + \left[b_{f\_T} \cdot t_{f\_T} \cdot \left(t + h_{w\_T} + \frac{t_{f\_T}}{2}\right)\right]}{\left(fl_{col} \cdot t\right) + \left(h_{w\_T} \cdot t_{w\_T}\right) + \left(b_{f\_T} \cdot t_{f\_T}\right)} = 1.15\,in$$

$$I_{sl1\_onestiff} := \left[\frac{fl_{col}\cdot t^3}{12} + fl_{col}\cdot t\cdot\left(\frac{t}{2} - c_{col}\right)^2\right] \ldots + \left[\frac{t_{w\_T}\cdot h_{w\_T}^3}{12} + t_{w\_T}\cdot h_{w\_T}\cdot\left(t + \frac{h_{w\_T}}{2} - c_{col}\right)^2\right] \ldots + \left[\frac{b_{f\_T}\cdot t_{f\_T}^3}{12} + b_{f\_T}\cdot t_{f\_T}\cdot\left(t + h_{w\_T} + \frac{t_{f\_T}}{2} - c_{col}\right)^2\right] = 105.14\,in^4$$

$$A_{sl1\_onestiff} := \left(fl_{col}\cdot t\right) + \left(t_{w\_T}\cdot h_{w\_T}\right) + \left(t_{f\_T}\cdot b_{f\_T}\right) = 49.5\,in^2$$

$$B_{star\_onestiff} := b = 90\,in$$

$$a_{c\_onestiff} := 4.33\cdot\sqrt[4]{\frac{I_{sl1\_onestiff}\cdot b_{1\_onestiff}^2\cdot b_{2\_onestiff}^2}{t^3\cdot B_{star\_onestiff}}} = 99.64\,in$$

$$temp\_var\_1 := \frac{1.05\cdot E\cdot\sqrt{I_{sl1\_onestiff}\cdot t^3\cdot B_{star\_onestiff}}}{A_{sl1\_onestiff}\cdot b_{1\_onestiff}\cdot b_{2\_onestiff}} = 122.15\,ksi$$

$$temp\_var\_2 := \frac{\pi^2\cdot E\cdot I_{sl1\_onestiff}}{A_{sl1\_onestiff}\cdot L_{trans}^2} \ldots + \frac{E\cdot t^3\cdot B_{star\_onestiff}\cdot L_{trans}^2}{4\cdot\pi^2\cdot\left(1 - 0.3^2\right)\cdot A_{sl1\_onestiff}\cdot b_{1\_onestiff}^2\cdot b_{2\_onestiff}^2} = 4202.43\,ksi$$

$$\sigma_{cr\_sl\_onestiff} := if\left(L_{trans} \geq a_{c\_onestiff}, temp\_var\_1, temp\_var\_2\right) = 122.15\,ksi$$

For two longitudinal stiffeners

Case 1

$$b_{1\_twostiff\_case1} := \frac{b}{n_{long} + 1} = 30\,in \qquad b_{2\_twostiff\_case1} := \frac{b}{n_{long} + 1} = 30\,in$$

$$I_{sl1\_twostiff\_case1} := I_{sl1\_onestiff} = 105.14\,in^4$$

$$A_{sl1\_twostiff\_case1} := A_{sl1\_onestiff} = 49.5\,in^2$$

$$B_{star\_twostiff\_case1} := \frac{2 \cdot b}{3} = 60\,in$$

$$a_{c\_twostiff\_case1} := 4.33 \cdot \sqrt[4]{\frac{I_{sl1\_twostiff\_case1} \cdot b_{1\_twostiff\_case1}^{\,2} \cdot b_{2\_twostiff\_case1}^{\,2}}{t^3 \cdot B_{star\_twostiff\_case1}}} = 110\,in$$

$$temp\_var\_3 := \frac{1.05 \cdot E \cdot \sqrt{I_{sl1\_twostiff\_case1} \cdot t^3 \cdot B_{star\_twostiff\_case1}}}{A_{sl1\_twostiff\_case1} \cdot b_{1\_twostiff\_case1} \cdot b_{2\_twostiff\_case1}} = 99.73\,ksi$$

$$temp\_var\_4 := \frac{\pi^2 \cdot E \cdot I_{sl1\_twostiff\_case1}}{A_{sl1\_twostiff\_case1} \cdot L_{trans}^{\,2}} \ldots + \frac{E \cdot t^3 \cdot B_{star\_twostiff\_case1} \cdot L_{trans}^{\,2}}{4 \cdot \pi^2 \cdot \left(1 - 0.3^2\right) \cdot A_{sl1\_twostiff\_case1} \cdot b_{1\_twostiff\_case1}^{\,2} \cdot b_{2\_twostiff\_case1}^{\,2}}$$

$$\sigma_{cr\_sl\_twostiff\_case1} := if\left(L_{trans} \geq a_{c\_twostiff\_case1}, temp\_var\_3, temp\_var\_4\right) = 99.73\,ksi$$

Case 2

For uniformly spaced stiffeners case 1 and case 2 are the same

$$\sigma_{cr\_sl\_twostiff\_case2} := \sigma_{cr\_sl\_twostiff\_case1} = 99.73\,ksi$$

Case 3

$$b_{1\_twostiff\_case3} := \frac{b}{2} = 45\,in \qquad b_{2\_twostiff\_case3} := \frac{b}{2} = 45\,in$$

$$I_{sl1\_twostiff\_case3} := 2 \cdot I_{sl1\_twostiff\_case1} = 210.29\,in^4$$

$$A_{sl1\_twostiff\_case3} := 2 \cdot A_{sl1\_twostiff\_case1} = 99\,in^2$$

$$B_{star\_twostiff\_case3} := b = 90\,in$$

$$a_{c\_twostiff\_case3} := 4.33 \cdot \sqrt[4]{\frac{I_{sl1\_twostiff\_case3} \cdot b_{1\_twostiff\_case3}^{2} \cdot b_{2\_twostiff\_case3}^{2}}{t^{3} \cdot B_{star\_twostiff\_case3}}} = 178\,in$$

$$temp\_var\_5 := \frac{1.05 \cdot E \cdot \sqrt{I_{sl1\_twostiff\_case3} \cdot t^{3} \cdot B_{star\_twostiff\_case3}}}{A_{sl1\_twostiff\_case3} \cdot b_{1\_twostiff\_case3} \cdot b_{2\_twostiff\_case3}} = 38.39\,ksi$$

$$temp\_var\_6 := \frac{\pi^{2} \cdot E \cdot I_{sl1\_twostiff\_case3}}{A_{sl1\_twostiff\_case3} \cdot L_{trans}^{2}} \ldots + \frac{E \cdot t^{3} \cdot B_{star\_twostiff\_case3} \cdot L_{trans}^{2}}{4 \cdot \pi^{2} \cdot \left(1 - 0.3^{2}\right) \cdot A_{sl1\_twostiff\_case3} \cdot b_{1\_twostiff\_case3}^{2} \cdot b_{2\_twostiff\_case3}^{2}}$$

$$\sigma_{cr\_sl\_twostiff\_case3} := if\left(L_{trans} \geq a_{c\_twostiff\_case3}, temp\_var\_5, temp\_var\_6\right) = 38.39\,ksi$$

$$\sigma_{cr\_sl\_twostiff} := \min\left(\sigma_{cr\_sl\_twostiff\_case1}, \sigma_{cr\_sl\_twostiff\_case2}, \sigma_{cr\_sl\_twostiff\_case3}\right) = 38\,ksi$$

$$\sigma_{cr\_p} := if\left(n_{long} = 1, \sigma_{cr\_sl\_onestiff}, \sigma_{cr\_sl\_twostiff}\right) = 38.39\,ksi$$

$$A_c := \left(n_{long} \cdot b_{c\_loc} \cdot t\right) + \left[n_{long} \cdot \left[\left(h_{w\_T} \cdot t_{w\_T}\right) + \left(b_{f\_T} \cdot t_{f\_T}\right)\right]\right] = 99\,in^{2}$$

$$A_{c\_eff\_loc} := \left(n_{long} \cdot \rho_{loc} \cdot b_{c\_loc} \cdot t\right) + \left(A_{sl\_eff}\right) = 99\,in^{2}$$

$$\beta_{Ac\_platelike} := \frac{A_{c\_eff\_loc}}{A_c} = 1$$

$$\lambda_p := \sqrt{\frac{\beta_{Ac\_platelike} \cdot F_y}{\sigma_{cr\_p}}} = 1.14$$

$$\rho := if\left[\lambda_p \leq 0.5 + \sqrt{0.085 - 0.055 \cdot \psi}, 1, \min\left[\frac{\lambda_p - 0.055 \cdot (3 + \psi)}{\lambda_p^{2}}, 1\right]\right] = 0.71$$

b) Column type behavior (σ_crc, χc)

$I_{sl1} := I_{sl1\_onestiff} = 105.14\,in^4$ $\qquad A_{sl1} := A_{sl1\_onestiff} = 49.5\,in^2$

$$\sigma_{cr\_c} := \frac{\pi^2 \cdot E \cdot I_{sl1}}{A_{sl1} \cdot L_{trans}^{\,2}} = 0.88\,ksi$$

$$A_{sl1\_eff} := \left(\rho_{loc} \cdot fl_{col} \cdot t\right) + \frac{A_{sl\_eff}}{n_{long}} = 49.5\,in^2$$

$$\beta_{Ac\_columnlike} := \frac{A_{sl1\_eff}}{A_{sl1}} = 1$$

$$\lambda_c := \sqrt{\frac{\beta_{Ac\_columnlike} \cdot F_y}{\sigma_{cr\_c}}} = 7.52$$

$$e_1 := \left| \frac{\left(\rho_{loc} \cdot fl_{col} \cdot t \cdot \frac{t}{2}\right) + \left[h_{w\_T} \cdot t_{w\_T} \cdot \left(t + \frac{h_{w\_T}}{2}\right)\right]}{\left(\rho_{loc} \cdot fl_{col} \cdot t\right) + \left(h_{w\_T} \cdot t_{w\_T}\right)} - \frac{t}{2} \right| = 0.4\,in$$

$$e_2 := \left| \left(t + \frac{h_{w\_T}}{2}\right) \ldots + - \frac{\left(\rho_{loc} \cdot fl_{col} \cdot t \cdot \frac{t}{2}\right) + \left[h_{w\_T} \cdot t_{w\_T} \cdot \left(t + \frac{h_{w\_T}}{2}\right)\right]}{\left(\rho_{loc} \cdot fl_{col} \cdot t\right) + \left(h_{w\_T} \cdot t_{w\_T}\right)} \right| = 3.95\,in$$

$$\alpha_e := 0.49 + \frac{0.09}{\frac{\sqrt{\frac{I_{sl1}}{A_{sl1}}}}{\max\left(e_1, e_2\right)}} = 0.73 \qquad \phi := 0.5\left[1 + \alpha_e \cdot \left(\lambda_c - 0.2\right) + \lambda_c^{\,2}\right] = 31.44$$

$$\chi_c := \min\left(1, \frac{1}{\phi + \sqrt{\phi^2 - \lambda_c^{\,2}}}\right) = 0.02$$

c) Interpolation (σ_crc, χc)

$$\xi := \max\left(0, \min\left(\frac{\sigma_{cr\_p}}{\sigma_{cr\_c}} - 1, 1\right)\right) = 1$$

$$\rho_c := \left(\rho - \chi_c\right)\cdot\xi\cdot(2 - \xi) + \chi_c = 0.71$$

Final

$$A_{c\_eff\_loc} := A_{sl\_eff} + \left(n_{long}\cdot\rho_{loc}\cdot b_{c\_loc}\cdot t\right) = 99\,in^2$$

$$A_{c\_eff} := \left(\rho_c\cdot A_{c\_eff\_loc}\right) + \left(\rho_{loc}\cdot b_{c\_loc}\cdot t\right) = 115.02\,in^2$$

$$\boxed{P_{n.plate} := A_{c\_eff}\cdot F_y = 5751.18\,kip}$$

AASHTO

$b := 90in$ $t := 1.5in$ $n_{long} := 2$ $n_{trans} := 0$ $L_{total} := 828.8829in$

$E := 29000ksi$ $F_y := 50ksi$

Flat stiffener or T longitudinal stiffener

$h_{w\_T} := 7.193747in$

$t_{w\_T} := 0.625543in$

Ultimate compressive strength of a stiffened plate

$$I_s := \frac{t_{w\_T}\cdot\left(h_{w\_T}^{3}\right)}{12} + t_{w\_T}\cdot h_{w\_T}\cdot\left(\frac{h_{w\_T}}{2}\right)^{2} = 77.62\,in^4$$

$$w := \frac{b}{n_{long}+1} = 30\,in$$

$$k_{eqn} := if\left[n_{long} = 1, \left(\frac{8\cdot I_s}{w\cdot t^3}\right)^{\frac{1}{3}}, \left(\frac{0.894\cdot I_s}{w\cdot t^3}\right)^{\frac{1}{3}}\right] = 0.88$$

$$k := \max\left(1, \min\left(k_{eqn}, 4\right)\right) = 1 \qquad F_{yr} := (1-0.3)\cdot F_y = 35\,ksi$$

$$\lambda_f := \frac{w}{t} = 20$$

$$\lambda_p := 0.57\sqrt{\frac{E\cdot k}{F_y}} = 13.73 \qquad \lambda_r := 0.95\sqrt{\frac{E\cdot k}{F_{yr}}} = 27.35$$

$$F_{cb\_1} := F_y$$

$$F_{cb\_2} := F_y \cdot \left[1 - \left(1 - \frac{1 - 0.3}{1} \right) \cdot \left(\frac{\lambda_f - \lambda_p}{\lambda_r - \lambda_p} \right) \right]$$

$$F_{cb\_3} := \frac{0.9 \cdot E \cdot k}{\lambda_f^{\,2}}$$

$$F_{cb} := \text{if}\left(\lambda_f \le \lambda_p, F_{cb\_1}, \text{if}\left(\lambda_f \le \lambda_r, F_{cb\_2}, F_{cb\_3}\right)\right)$$

$$F_{nc} := F_{cb} = 43.09\,\text{ksi}$$

$$\boxed{P_n := F_{nc} \cdot \left[(b \cdot t) + \left[n_{long} \cdot \left(h_{w\_T} \cdot t_{w\_T} \right) \right] \right] = 6205.1\,\text{kip}}$$

Flexural resistance of non-longitudinally stiffened box-section members

Cross-section # 34 and length= Lmax (See Table B-0-1)

Proposed method

$F_{yf} := 50$ $F_{yw} := 50$ $b_{fc} := 53$ $t_{fc} := 0.5$ $b_{ft} := b_{fc}$ $t_{ft} := 0.5$ $D := 79.5$

$t_w := 1.5$ $L_b := 2385$

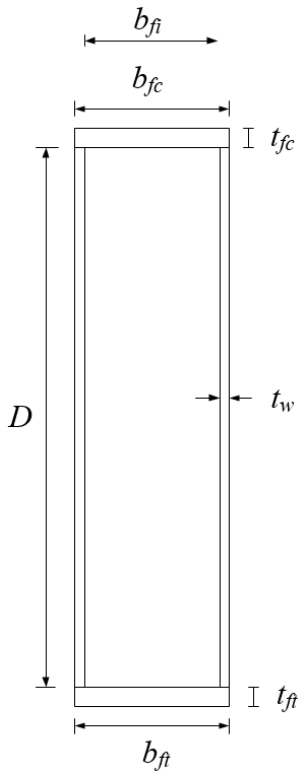

Flange effective width and Rf

$$\lambda_{pf} := 1.09\sqrt{\frac{29000}{F_{yf}}} = 26.251 \qquad \lambda_{rf} := 1.7\sqrt{\frac{29000}{F_{yf}}} = 40.941$$

$$b_{fi} := b_{fc} - 2 \cdot t_w = 50 \qquad \lambda_f := \frac{b_{fi}}{t_{fc}} = 100$$

$$R_f := \text{if}\left[\lambda_f \le \lambda_{pf}, 1, \text{if}\left[\lambda_f \le \lambda_{rf}, \min\left[1, 1 - 0.15 \cdot \left(\frac{\lambda_f - \lambda_{pf}}{\lambda_{rf} - \lambda_{pf}}\right)\right], 0.85\right]\right] = 0.85$$

$$\lambda_r := 1.09\sqrt{\frac{29000}{F_{yf}}} = 26.251 \qquad F_{el} := \left(1.74 \cdot \frac{\lambda_r}{\lambda_f}\right)^2 \cdot F_{yf} = 10.432$$

$$b_{fi\_eff} := \text{if}\left[\lambda_f \le \lambda_r \cdot \sqrt{\frac{F_{yf}}{F_{yf}}}, b_{fi}, b_{fi} \cdot \left[\left[\left(1 - 0.22 \cdot \sqrt{\frac{F_{el}}{F_{yf}}}\right) \cdot \sqrt{\frac{F_{el}}{F_{yf}}}\right] - 0.075\right]\right] = 16.793$$

Effective section properties

$$D_{ce} := \left[\frac{\left(b_{fi\_eff} \cdot t_{fc} \cdot \frac{t_{fc}}{2}\right) + \left(2 \cdot t_w \cdot t_{fc} \cdot \frac{t_{fc}}{2}\right) \ldots + \left[\left[2 \cdot D \cdot t_w \cdot \left(t_{fc} + \frac{D}{2}\right)\right] + \left[b_{ft} \cdot t_{ft} \cdot \left(t_{fc} + D + \frac{t_{ft}}{2}\right)\right]\right]}{\left(b_{fi\_eff} \cdot t_{fc}\right) + \left(2 \cdot t_w \cdot t_{fc}\right) + \left(2 \cdot D \cdot t_w\right) + \left(b_{ft} \cdot t_{ft}\right)}\right] - t_{fc} = 42.166$$

$$D_{cpe} := \frac{\left(2 \cdot D \cdot t_w \cdot F_{yw}\right) + \left(b_{ft} \cdot t_{ft} \cdot F_{yf}\right) - \left(b_{fi\_eff} \cdot t_{fc} \cdot F_{yf}\right) - \left(2 \cdot t_w \cdot t_{fc} \cdot F_{yf}\right)}{4 \cdot t_w \cdot F_{yw}} = 42.517$$

$$I_{xe} := \left[\frac{b_{fi\_eff} \cdot {t_{fc}}^3}{12} + b_{fi\_eff} \cdot t_{fc} \cdot \left(D_{ce} + \frac{t_{fc}}{2}\right)^2\right] \ldots + \left[2 \cdot \left[\frac{t_w \cdot {t_{fc}}^3}{12} + t_w \cdot t_{fc} \cdot \left(D_{ce} + \frac{t_{fc}}{2}\right)^2\right] \ldots + \left[2 \cdot \left[\frac{t_w \cdot D^3}{12} + D \cdot t_w \cdot \left(D_{ce} - \frac{D}{2}\right)^2\right] \ldots + \left[\frac{b_{ft} \cdot {t_{ft}}^3}{12} + b_{ft} \cdot t_{ft} \cdot \left(D - D_{ce} + \frac{t_{ft}}{2}\right)^2\right]\right]\right] = 182245.718$$

$$S_{xce} := \frac{I_{xe}}{\left(D_{ce} + t_{fc}\right)} = 4271.455$$

$$M_{yce} := F_{yf} \cdot S_{xce} = 213572.775$$

$$M_{pe} := \left[b_{fi\_eff} \cdot t_{fc} \cdot F_{yf} \cdot \left(D_{cpe} + \frac{t_{fc}}{2} \right) \right] + 2 \cdot \left[t_w \cdot t_{fc} \cdot F_{yf} \cdot \left(D_{cpe} + \frac{t_{fc}}{2} \right) \right] \dots = 308653.878$$
$$+ \left[2 \cdot \left(D_{cpe} \cdot t_w \cdot F_{yw} \cdot \frac{D_{cpe}}{2} \right) \dots \right.$$
$$+ \left[2 \cdot \left[\left(D - D_{cpe} \right) \cdot t_w \cdot F_{yw} \cdot \left(\frac{D - D_{cpe}}{2} \right) \right] \dots \right.$$
$$\left. \left. + \left[b_{ft} \cdot t_{ft} \cdot F_{yf} \cdot \left(D - D_{cpe} + \frac{t_{ft}}{2} \right) \right] \right] \right]$$

Gross section properties

$$D_c := \left[\frac{\left(b_{fi} \cdot t_{fc} \cdot \frac{t_{fc}}{2} \right) + \left(2 \cdot t_w \cdot t_{fc} \cdot \frac{t_{fc}}{2} \right) \dots}{+ \left[\left[2 \cdot D \cdot t_w \cdot \left(t_{fc} + \frac{D}{2} \right) \right] + \left[b_{ft} \cdot t_{ft} \cdot \left(t_{fc} + D + \frac{t_{ft}}{2} \right) \right] \right]} {\left(b_{fi} \cdot t_{fc} \right) + \left(2 \cdot t_w \cdot t_{fc} \right) + \left(2 \cdot D \cdot t_w \right) + \left(b_{ft} \cdot t_{ft} \right)} \right] - t_{fc} = 39.75$$

$$D_{cp} := \frac{\left(2 \cdot D \cdot t_w \cdot F_{yw} \right) + \left(b_{ft} \cdot t_{ft} \cdot F_{yf} \right) - \left(b_{fi} \cdot t_{fc} \cdot F_{yf} \right) - \left(2 \cdot t_w \cdot t_{fc} \cdot F_{yf} \right)}{4 \cdot t_w \cdot F_{yw}} = 39.75$$

$$I_x := \left[\frac{b_{fi} \cdot t_{fc}^{\,3}}{12} + b_{fi} \cdot t_{fc} \cdot \left(D_c + \frac{t_{fc}}{2} \right)^2 \right] \dots = 210416.073$$
$$+ \left[2 \cdot \left[\frac{t_w \cdot t_{fc}^{\,3}}{12} + t_w \cdot t_{fc} \cdot \left(D_c + \frac{t_{fc}}{2} \right)^2 \right] \dots \right.$$
$$+ \left[2 \cdot \left[\frac{t_w \cdot D^3}{12} + D \cdot t_w \cdot \left(D_c - \frac{D}{2} \right)^2 \right] \dots \right.$$
$$\left. \left. + \left[\frac{b_{ft} \cdot t_{ft}^{\,3}}{12} + b_{ft} \cdot t_{ft} \cdot \left(D - D_c + \frac{t_{ft}}{2} \right)^2 \right] \right] \right]$$

$$S_{xc} := \frac{I_x}{\left(D_c + t_{fc} \right)} = 5227.729$$

$$M_{yc} := F_{yf} \cdot S_{xc} = 261386.426$$

$$M_p := \left[b_{fi} \cdot t_{fc} \cdot F_{yf} \cdot \left(D_{cp} + \frac{t_{fc}}{2} \right) \right] + 2 \cdot \left[t_w \cdot t_{fc} \cdot F_{yf} \cdot \left(D_{cp} + \frac{t_{fc}}{2} \right) \right] \ldots = 343009.375$$
$$+ \left[2 \cdot \left(D_{cp} \cdot t_w \cdot F_{yw} \cdot \frac{D_{cp}}{2} \right) \ldots \right.$$
$$+ \left[2 \cdot \left[\left(D - D_{cp} \right) \cdot t_w \cdot F_{yw} \cdot \left(\frac{D - D_{cp}}{2} \right) \right] \ldots \right.$$
$$\left. \left. + \left[b_{ft} \cdot t_{ft} \cdot F_{yf} \cdot \left(D - D_{cp} + \frac{t_{ft}}{2} \right) \right] \right] \right]$$

$$I_y := 2 \cdot \left[\frac{D \cdot {t_w}^3}{12} + D \cdot t_w \cdot \left(\frac{b_{fc} - t_w}{2} \right)^2 \right] + \left(\frac{t_{fc} \cdot {b_{fc}}^3}{12} \right) + \left(\frac{t_{ft} \cdot {b_{ft}}^3}{12} \right) = 170591.542$$

$$A := \left(b_{fc} \cdot t_{fc} \right) + 2 \cdot \left(D \cdot t_w \right) + \left(b_{ft} \cdot t_{ft} \right) = 291.5$$

$$r_y := \sqrt{\frac{I_y}{A}} = 24.191$$

Rh

$R_h := 1$ Since this is a homogeneous section

Rb

$$\lambda_w := \frac{2 \cdot D_{ce}}{t_w} = 56.221$$

$$\lambda_{pw} := 3.1 \cdot \left(\frac{D_{ce}}{D_{cpe}} \right) \cdot \sqrt{\frac{29000}{F_{yf}}} = 74.041 \qquad \lambda_{rw} := 4.6 \cdot \sqrt{\frac{29000}{F_{yf}}} = 110.783$$

$$a_{wce} := \frac{2 \cdot D_{ce} \cdot t_w}{\frac{\left(b_{fi\_eff} \cdot t_{fc} + 2 \cdot t_{fc} \cdot t_w\right)}{2}} = 25.564$$

$$R_b := \text{if}\left[\lambda_w \le \lambda_{rw}, 1, \min\left[1, 1 - \left(\frac{a_{wce}}{1200 + 300 \cdot a_{wce}}\right) \cdot \left(\frac{2D_{ce}}{t_w} - \lambda_{rw}\right)\right]\right] = 1$$

Rpc

$$R_{pc} := \text{if}\left[\lambda_w \le \lambda_{pw}, \frac{M_{pe}}{M_{yce}}, \text{if}\left[\lambda_w > \lambda_{rw}, R_h, \min\left[\frac{M_{pe}}{M_{yce}}, \frac{M_{pe}}{M_{yce}} \cdot \left[1 - \left(1 - \frac{R_h \cdot M_{yce}}{M_{pe}}\right) \cdot \left(\frac{\lambda_w - \lambda_{pw}}{\lambda_{rw} - \lambda_{pw}}\right)\right]\right]\right]\right] = 1.445$$

Inelastic lateral torsional buckling

$$b_m := b_{fc} - t_w = 51.5 \qquad h_m := D + 0.5 \cdot t_{fc} + 0.5 \cdot t_{ft} = 80 \qquad A_m := b_m \cdot h_m = 4120$$

$$h_{mc} := D_c + \frac{t_{fc}}{2} = 40 \qquad h_{mt} := D - D_c + \frac{t_{ft}}{2} = 40$$

$$I_{ym} := \frac{b_m^{\,3} \cdot \left(t_{fc} + t_{ft}\right)}{12} + \frac{t_w \cdot h_m \cdot b_m^{\,2}}{2} = 170517.573$$

$$J := \frac{4 \cdot A_m^{\,2}}{\left(\frac{b_m}{t_{fc}}\right) + \left(\frac{b_m}{t_{ft}}\right) + \left(\frac{h_m}{t_w}\right) + \left(\frac{h_m}{t_w}\right)} = 217156.503$$

$$G := 0.385 \cdot 29000 = 11165 \qquad F_{yr} := 0.5 \cdot F_{yf} = 25$$

$$L_p := \frac{0.1 \cdot 29000 \cdot r_y \cdot \sqrt{J \cdot A}}{M_{yce}} = 2613.469$$

$$L_r := \frac{0.6 \cdot 29000 \cdot r_y \cdot \sqrt{J \cdot A}}{F_{yr} \cdot S_{xce}} = 31361.622$$

$$S_{xce} := \frac{I_{xe}}{\left(D_{ce} + t_{fc}\right)} = 4271.455 \qquad S_{xte} := \frac{I_{xe}}{\left(D - D_{ce} + t_{ft}\right)} = 4816.977$$

Since Sxce < Sxte, compression flange of the effective cross-section yields first

$$M_{CS} := R_f \cdot R_b \cdot R_{pc} \cdot M_{yce} = 262355.796$$

$$M_n := \text{if}\left[L_b \le L_p, M_{CS}, \left[M_{CS} - \left(M_{CS} - F_{yr} \cdot S_{xce}\right) \cdot \left(\frac{L_b - L_p}{L_r - L_p}\right)\right]\right] = 262355.796$$

AASHTO

$F_{yf} := 50 \quad F_{yw} := 50 \quad b_{fc} := 53 \quad t_{fc} := 0.5 \quad b_{ft} := b_{fc} \quad t_{ft} := 0.5 \quad D := 79.5$

$t_w := 1.5 \quad L_b := 2385$

AASHTO equation is only applicable to homogeneous doubly symmetric box-section members

$b_{fi} := b_{fc} - 2 \cdot t_w = 50$

$$D_c := \left[\frac{\left(b_{fi} \cdot t_{fc} \cdot \frac{t_{fc}}{2} \right) + \left(2 \cdot t_w \cdot t_{fc} \cdot \frac{t_{fc}}{2} \right) \ldots + \left[\left[2 \cdot D \cdot t_w \cdot \left(t_{fc} + \frac{D}{2} \right) \right] + \left[b_{ft} \cdot t_{ft} \cdot \left(t_{fc} + D + \frac{t_{ft}}{2} \right) \right] \right]}{\left(b_{fi} \cdot t_{fc} \right) + \left(2 \cdot t_w \cdot t_{fc} \right) + \left(2 \cdot D \cdot t_w \right) + \left(b_{ft} \cdot t_{ft} \right)} \right] - t_{fc} = 39.75$$

$$I_x := \left[\frac{b_{fi} \cdot t_{fc}^{\,3}}{12} + b_{fi} \cdot t_{fc} \cdot \left(D_c + \frac{t_{fc}}{2} \right)^2 \right] \ldots + \left[2 \cdot \left[\frac{t_w \cdot t_{fc}^{\,3}}{12} + t_w \cdot t_{fc} \cdot \left(D_c + \frac{t_{fc}}{2} \right)^2 \right] \ldots + \left[2 \cdot \left[\frac{t_w \cdot D^3}{12} + D \cdot t_w \cdot \left(D_c - \frac{D}{2} \right)^2 \right] \ldots + \left[\frac{b_{ft} \cdot t_{ft}^{\,3}}{12} + b_{ft} \cdot t_{ft} \cdot \left(D - D_c + \frac{t_{ft}}{2} \right)^2 \right] \right] \right] = 210416.073$$

$$S := \frac{I_x}{\left(D_c + t_{fc} \right)} = 5227.729 \qquad \text{or} \qquad S := \frac{I_x}{\left(D - D_c + t_{ft} \right)} = 5227.729$$

$$I_y := 2 \cdot \left[\frac{D \cdot t_w^{\,3}}{12} + D \cdot t_w \cdot \left(\frac{b_{fc} - t_w}{2} \right)^2 \right] + \left(\frac{t_{fc} \cdot b_{fc}^{\,3}}{12} \right) + \left(\frac{t_{ft} \cdot b_{ft}^{\,3}}{12} \right) = 170591.542$$

$b_m := b_{fc} - t_w = 51.5$

$$h_m := D + 0.5 \cdot t_{fc} + 0.5 \cdot t_{ft} = 80$$

$$A := b_m \cdot h_m = 4120$$

$$M_n := F_{yf} \cdot S \cdot \left(1 - \frac{0.064 \cdot F_{yf} \cdot S \cdot L_b}{A \cdot 29000} \cdot \sqrt{\frac{\frac{b_{fc}}{t_{fc}} + 2 \cdot \frac{D}{t_w} + \frac{b_{ft}}{t_{ft}}}{I_y}} \right) = 257617.878$$

Axial compressive resistance of longitudinally stiffened box-section members

Main study Case # 9 (See Table E-0-1)

Proposed method

$B := 41in$ $t_f := 1in$ $n_{fln} := 1$ $h_{ls\_fln} := 4.796in$

$t_{ls\_fln} := 0.417in$ $D := 119in$ $t_{web} := 1in$ $n_{web} := 1$

$h_{ls\_web} := 8.307in$ $t_{ls\_web} := 0.722in$ $L := (165.56 \cdot 12)in$

$K := 1$ $E := 29000ksi$

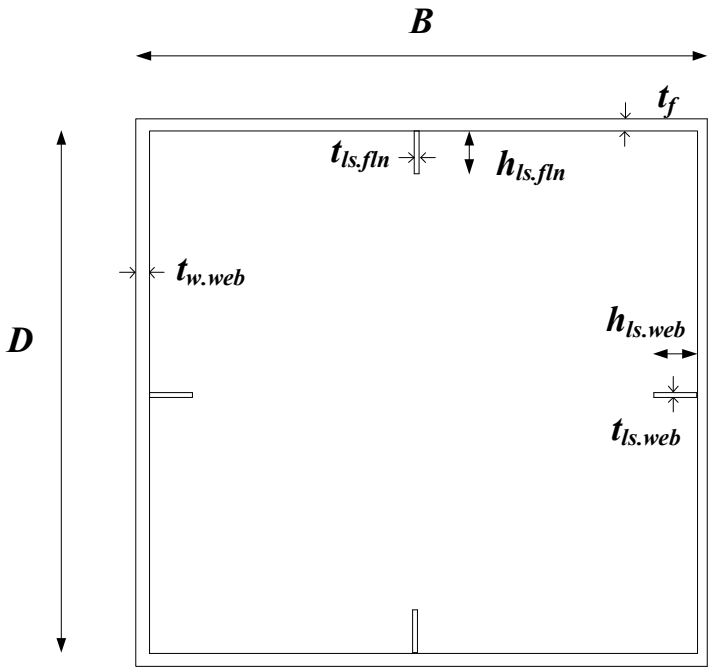

$P_{n\_flange} := 1948.24kip$

$P_{n\_web} := 2335.231kip$

Obtained using the proposed method for calculating the ultimate compressive resistance of longitudinally stiffened plates

$$A_{eff} := \left(4 \cdot t_{web} \cdot t_f\right) + \left(2 \cdot \frac{P_{n\_flange}}{50ksi}\right) + \left(2 \cdot \frac{P_{n\_web}}{50ksi}\right) = 175.34\,in^2$$

$$Temp\_var1 := 2\left[\left(\frac{t_f \cdot B^3}{12}\right) + n_{fln} \cdot \left(\frac{h_{ls\_fln} \cdot t_{ls\_fln}^3}{12}\right)\right]$$

$$Temp\_var2 := \left(\frac{D \cdot t_{web}^3}{12}\right) + \left[D \cdot t_{web} \cdot \left(\frac{B}{2} - \frac{t_{web}}{2}\right)^2\right]$$

$$Temp\_var3 := n_{web} \cdot \left[\left(\frac{t_{ls\_web} \cdot h_{ls\_web}^3}{12}\right) \ldots + \left[h_{ls\_web} \cdot t_{ls\_web} \cdot \left(\frac{B}{2} - t_{web} - \frac{h_{ls\_web}}{2}\right)^2\right]\right]$$

$$I_y := Temp\_var1 + \left[2 \cdot \left(Temp\_var2 + Temp\_var3\right)\right] = 109600.78\,in^4$$

$$A_g := 2 \cdot \left[\left(B \cdot t_f\right) + \left(n_{fln} \cdot h_{ls\_fln} \cdot t_{ls\_fln}\right) + \left(D \cdot t_{web}\right) \ldots + \left(n_{web} \cdot h_{ls\_web} \cdot t_{ls\_web}\right)\right] = 336\,in^2$$

$$r_s := \sqrt{\frac{I_y}{A_g}} = 18.06\,in$$

$$P_{os} := 50ksi \cdot \left[\left(4 \cdot t_{web} \cdot t_f\right) + \left(2 \cdot \frac{P_{n\_flange}}{50ksi}\right) + \left(2 \cdot \frac{P_{n\_web}}{50ksi}\right)\right] = 8766.94\,kip$$

$$P_e := \frac{\pi^2 \cdot E}{\left(\frac{K \cdot L}{r_s}\right)^2} \cdot A_g = 7947.64\,\text{kip}$$

$$F_{cr} := \text{if}\left[\frac{P_{os}}{P_e} \le 2.25, \left[0.658^{\left(\frac{P_{os}}{P_e}\right)}\right] \cdot 50, \frac{0.877 \cdot P_e}{\left(\frac{P_{os}}{50}\right)}\right] = 31.51$$

$$\lambda_r := 1.09 \cdot \sqrt{\frac{E}{50\text{ksi}}} = 26.25$$

$$r_1 := \max\left[0, \min\left[0.5 \cdot \frac{\left(\frac{K \cdot L}{r_s}\right) - 50}{90}, 0.5\right]\right] = 0.33$$

$$r_2 := \max\left[0, \min\left[\frac{\left(\frac{D}{n_{web} + 1}\right)}{t_{web}} - \lambda_r}{90 - \lambda_r}, 1\right]\right] = 0.52$$

$$\chi := 1 - r_1 \cdot r_2 = 0.83$$

$$\boxed{P_n := \chi \cdot F_{cr} \cdot A_{eff} = 4564.47\,\text{in}^2}$$

Flexural resistance of longitudinally stiffened box-section members

Case # 19 (See Table F-0-1 and F-0-2)

Proposed method

Top flange

$P_{n\_flange} := 2778.26kip$ Ultimate compressive strength of the stiffened flange plate calculated using the proposed method.

$c := 0in$ *c* is the distance of the centroid of the gross area of the flange plate and its longitudinal stiffeners from the top of the web plates.. It is very small... approximately equal to zero

$t_{f\_TF} := 1in$

Web dimensions $D := 126in$ $t_w := 1.3in$

Bottom flange dimensions $B := 62.6in$ $t_{f\_BF} := 0.7in$

Yield strength $F_{yf} := 50ksi$

As mentioned in Table 6-1, unbraced length = Lp. Therefore, Mn = Cross-section flexural resistance

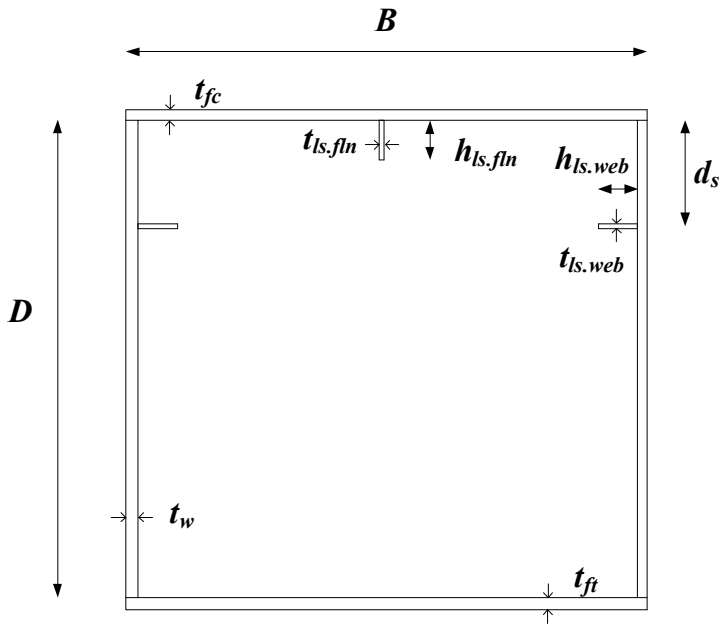

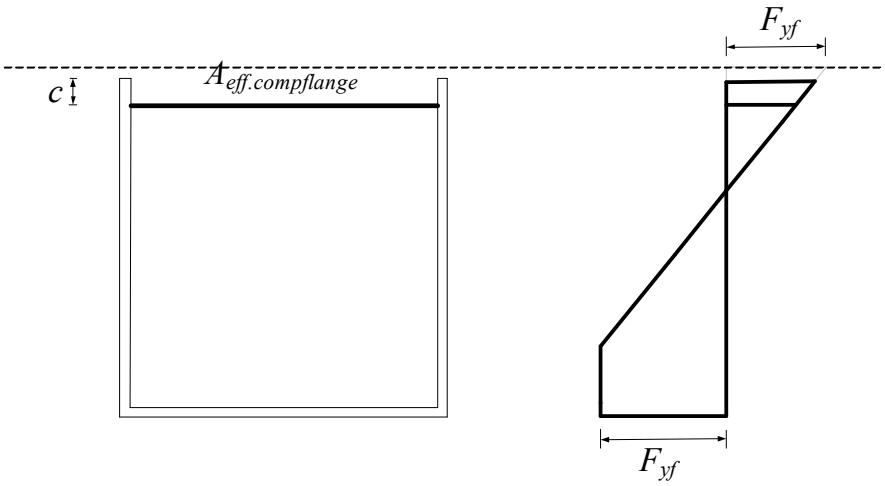

$$A_{eff\_compflange} := \frac{P_{n\_flange}}{F_{yf}} + 2 \cdot t_w \cdot t_{f\_TF} = 58.17 \cdot in^2$$

$$s_1 := F_{yf}$$

$$F_1 := (s_1) \cdot (A_{eff\_compflange})$$

$$F_2 := 2\left[\frac{1}{2} \cdot (F_{yf}) \cdot (D_{ce} \cdot t_w)\right]$$

$$F_3 := 2\left[\frac{1}{2} \cdot (F_{yf}) \cdot (D_{ce} \cdot t_w)\right]$$

$$F_4 := 2 \cdot \left[(F_{yf}) \cdot \left[(D - 2 \cdot D_{ce}) \cdot t_w\right]\right]$$

$$F_5 := (F_{yf}) \cdot (B \cdot t_{f\_BF})$$

$$F_1 + F_2 - F_3 - F_4 - F_5 = 0 \text{ solve}, D_{ce} \rightarrow 60.241 \cdot in$$

$$D_{ce} := 60.241in$$

$$\text{if}(D > 2 \cdot D_{ce}, \text{"OK"}, \text{"NOT OK"}) = \text{"OK"}$$

$s_1 := F_{yf} = 50\,ksi$

$F_1 := (s_1)\cdot(A_{eff\_compflange}) = 2908.26\,kip$

$F_2 := 2\left[\frac{1}{2}\cdot(F_{yf})\cdot(D_{ce}\cdot t_w)\right] = 3915.66\,kip$

$F_3 := 2\left[\frac{1}{2}\cdot(F_{yf})\cdot(D_{ce}\cdot t_w)\right] = 3915.66\,kip$

$F_4 := 2\cdot\left[(F_{yf})\cdot\left[(D - 2\cdot D_{ce})\cdot t_w\right]\right] = 717.34\,kip$

$F_5 := (F_{yf})\cdot(B\cdot t_{f\_BF}) = 2191\,kip$

$$M_n := (F_1\cdot D_{ce}) + \left[F_2\cdot\left(\frac{2}{3}\cdot D_{ce}\right)\right] \ldots + \left[\left[F_3\cdot\left(\frac{2}{3}\cdot D_{ce}\right)\right] \ldots + \left[\left[F_4\cdot\left(D_{ce} + \frac{D - 2\cdot D_{ce}}{2}\right)\right] \ldots + \left[F_5\cdot\left(D - D_{ce} + \frac{t_{f\_BF}}{2}\right)\right]\right]\right] = 679745.2\,in\cdot kip$$

APPENDIX H. GLOSSARY

- c_1, c_2, c_3 are effective width imperfection adjustment factors
- λ_r is the element width-to-thickness or slenderness ratio limit for a plate subjected to uniform axial compression
- F_{el} is the elastic local buckling stress
- b_e is the effective width of a non-longitudinally stiffened plate with gross width b
- F_{yc} yield strength of the compression flange
- F_{yt} yield strength of the tension flange
- λ_w is the web slenderness
- λ_{pw} is the compact web slenderness limit
- λ_{rw} is the noncompact web slenderness limit
- D_{ce} is the distance of the elastic neutral axis from the inside surface of the compression flange in the effective cross-section
- D_{cpe} is the distance of the plastic neutral axis from the inside surface of the compression flange in the effective cross-section
- R_{pc} is the web plastification factor
- R_b is the web load-shedding factor
- R_h is the hybrid factor
- S_{xce} is the elastic section modulus of the effective cross-section about the axis of bending to the compression flange

- S_{xte} is the elastic section modulus of the effective cross-section about the axis of bending to the tension flange
- M_{pe} is the plastic moment capacity of the effective cross-section
- λ_f is the compression flange slenderness
- λ_{pf} is the compact flange slenderness limit
- λ_{rf} is the noncompact flange slenderness limit
- R_f is the compression flange slenderness factor
- M_{cs} is the cross-section flexural resistance
- L_b is the unbraced length for lateral torsional buckling
- L_{max} is the maximum practical unbraced length for lateral torsional buckling
- L_p is the limiting unbraced length to achieve the cross-section flexural resistance under uniform moment
- L_r is the limiting unbraced length for calculation of the lateral torsional buckling resistance
- F_{yr} is the compression flange stress at the onset of nominal yielding within the cross-section
- C_b is the moment gradient modifier
- J is the St. Venant torsional constant
- β_x is the mono-symmetry parameter of the gross cross-section
- y_o is the distance between the shear center and the centroid of the gross cross-section
- E is the modulus of elasticity for steel

- G is the shear modulus of elasticity for steel
- I_x is the moment of inertia about the major principal axis of the gross cross-section
- r_y is the radius of gyration about the minor axis
- δ is the transverse displacement of the plate
- D_x flexural stiffness of the longitudinally stiffened plate for bending about the y axis
- D_y flexural stiffness of the longitudinally stiffened plate for bending about the x axis
- H torsional stiffness of the longitudinally stiffened plate
- I_x is taken as the moment of inertia of an individual longitudinal stiffener about an axis parallel to the face of the longitudinally stiffened plate element and passing through the centroid of the stiffener strut
- c_1 is the distance between the centroid of the longitudinally stiffened plate element and the centroid of the stiffener strut
- P_x is the buckling load of the longitudinally stiffened plate
- ℓ is the buckling length, taken as the smaller of the transverse stiffener spacing, and the characteristic buckling length
- a is the transverse stiffener spacing
- ℓ_c is the characteristic buckling length
- P_{es} is the buckling load of a stiffener strut
- P_{esF} is the elastic flexural buckling resistance of an individual stiffener strut

- P_{esT} is the plate torsional stiffness contribution to the elastic buckling resistance of an individual stiffener strut
- k_p is the plate transverse stiffness coefficient
- P_{nsp} is the nominal compressive resistance of a longitudinally stiffened plate subjected to uniform axial compression
- P_{ns} is the nominal compressive resistance of an individual stiffener strut composed of the stiffener plus the tributary width of the longitudinally stiffened plate
- P_{nsF} is the nominal flexural buckling resistance of an individual stiffener strut
- P_{yes} is the effective yield load of an individual stiffener strut
- P_{nR} is the compressive resistance provided by the half-width of a subpanel adjacent to a transversely-restrained longitudinal edge of the longitudinally stiffened plate
- P_{yeR} is the effective yield load of the half-width of a subpanel adjacent to a transversely-restrained longitudinal edge of the longitudinally stiffened plate
- P_{ys} is the yield load of an individual stiffener strut
- A_{es} is the effective area of an individual stiffener strut
- A_{gs} is the gross area of an individual stiffener strut
- A_s is the gross area of an individual longitudinal stiffener, excluding the tributary width of the longitudinally stiffened plate
- F_{ysp} is the specified minimum specified yield strength of the longitudinally stiffened plate

- w_e is the effective width of the plate between the longitudinal stiffeners or between a longitudinal stiffener and the transversely-restrained longitudinal edge of the longitudinally stiffened plate, as applicable
- J_s is the St. Venant torsional constant of the longitudinal stiffener alone, not including the contribution from the stiffened plate
- I_{ps} is the polar moment of inertia of the longitudinal stiffener alone about the attached edge
- $F_{cr.tor}$ is the elastic torsional buckling stress of the stiffener for buckling about the edge attached to the plate
- K is the effective length factor
- r_s is the radius of gyration about the axis normal to the plane of buckling
- A_c is the gross cross-sectional area of the corner pieces of a box-section
- $nlsp$ is the number of non-longitudinally stiffened plates
- lsp is the number of longitudinally stiffened plates
- χ is the global buckling-local buckling interaction reduction factor
- $\lambda_{\max}$ is the maximum slenderness of a subpanel (between longitudinal stiffeners or between a longitudinal stiffener and a corner) on the flange plate
- P_{os} is the yield load of a box-section
- P_e is the member elastic buckling load
- d_s is the distance from the centerline of the closest web longitudinal stiffener to the inner surface of the compression-flange element
- M_n is the nominal flexural resistance of a box-section member

- n_{cfln} is the number of longitudinal stiffeners on the compression flange
- n_{web} are the number of longitudinal stiffeners on each of the webs

REFERENCES

AASHTO (2010). "AASHTO LRFD Bridge Construction Specifications." Third Edition, American Association of State Highway and Transportation Officials, Washington DC.

AASHTO (2017). "AASHTO LRFD Bridge Design Specifications." Eighth Edition, American Association of State Highway and Transportation Officials, Washington DC.

AISC (2016). "Specification for Structural Steel Buildings." American Institute of Steel Construction, Chicago, IL.

AISI (2016). "North American Specification for the Design of Cold-Formed Steel Structural Members." American Iron and Steel Institute, Washington, DC.

Allen H. and Bulson P. (1980) "Background to Buckling." McGraw-Hill, London.

AWS (2002). "Bridge Welding Code." AASHTO/AWS D1.5M/D1.5, An American National Standard, American Association of Highway and Transportation Officials, Washington, DC.

Barbre, R. (1939). "Stability of rectangular plates with longitudinal or transverse stiffeners under uniform compression." NACA – National Advisory Committee for Aeronautics – Technical Memorandum No. 904, Washington, USA.

Bleich, F. (1952). "Buckling Strength of Metal Structures." New York: McGraw-Hill.

Brush, D.O. & Almroth, B.O. (1975). "Buckling of Bars, Plates, and Shells." McGraw-Hill, New York.

BSI (2000). "Steel, Concrete and Composite Bridges, British Standard BS 5400: Part 3, Code of Practice for Design of Steel Bridges." British Standards Institution, London.

CEN (2005). *Design of Steel Structures, Part 1-1: General Rules and rules for buildings, EN 1993-1-1:2005:E, Incorporating Corrigendum February 2006*, European Committee for Standardization, Brussels, Belgium.

CEN (2006). *Eurocode 3: Design of Steel Structures, Part 1-5: General Rules - Plated Structural Elements, EN 1993-1-5:2006: E, Incorporating Corrigendum April 2009*, European Committee for Standardization, Brussels, Belgium.

Chou CC, Uang CM, Seible F. (2006). "Experimental evaluation of compressive behavior of orthotropic steel plates for the new San Francisco — Oakland Bay bridge." J Bridge Eng, ASCE 2006;11(2):140–50

Chou, C. (2011). "Akashi Kaikyo Bridge." Retrieved from https://www.flickr.com/photos/chitaka/10109544695/.

Chwalla, E. (1936a): Stahlbau 9, S. 161.

Chwalla, E. (1936b): Die Bemessung der Waagerecht ausgesteiften Stegbleche vollwandiger Trager. Vorbericht zum 2. Kongress der Intern. Vereinig. fur Bruckenbau und Hochbau, 1936, S. 957.

Clarin, M. (2007). "Plate Buckling Resistance. Patch Loading of Longitudinally Stiffened Webs and Local Buckling." Doctoral thesis: 31, Lulea ˚ University of Technology, 2007, ISRNLTU-DT-07Ú31–SE.

CSA (2001). "S16-01 Limit States Design of Steel Structures." Canadian Standards Association, Toronto, Canada.

CRC. In: Johnston BG, editor (1960). "Guide to design criteria for metal compression members." 2nd ed. New York (NY): Column Research Council: Wily; 1960.

DeWolf, J.T., Pekoz, T. and Winter. G. (1973). "Local and Overall Buckling of Cold Formed Compression Members." Department of Structural Engineering, Report, Cornell University.

DeWolf, J.T., Pekoz, T. and Winter. G. (1974). "Local and Overall Buckling of Cold Formed Steel Members." Journal of the Structural Division, ASCE, October, 1974.

Dwight, J. B. and Moxham, K. E. (1969). “Welded steel plates in compression.” The Structural Engineer, 47 (1969) 49- 66.

ECCS. (1976). “Manual on stability of steel structures.” 2nd ed. European Convention for Constructional Steelwork.

EN 1090. “Execution of steel structures and aluminium structures (3 parts).”

Galambos T.V. and Surovek A.E., Structural Stability of Steel: Concepts and Applications for Structural Engineers, John Wiley & Sons, New Jersey, 2008.

Ghavami K. (1994). “Experimental study of stiffened plates in compression up to collapse.” Journal of Constructional Steel Research 1994;28(2):197–222.

Ghavami K, Khedmati M.R. (2006). “Numerical and experimental investigations on the compression behaviour of stiffened plates.” Journal of Constructional Steel Research 2006;62:1087–100.

Goldberg, J.E. and Leve, H.L. (1957). “Theory of Prismatic Folded Plate Structures.” *IABSE*, Vol. 16, International Association for Bridge and Structural Engineers, Zurich, Switzerland, 59-86.

Gordo J.M., Guedes Soares C. (2004). “Experimental evaluation of the ultimate bending moment of a box girder.” Marine Systems & Ocean Technology 2004;1:33–46.

Gordo J.M., Guedes Soares C. (2008). “Experimental evaluation of the behaviour of a mild steel box girder under bending moment.” Ships and Offshore Structures, 3:4, 347-358, DOI: 10.1080/17445300802370479.

Gordo J.M., Guedes Soares C. (2009). “Tests on ultimate strength of hull box girders made of high-tensile steel.” Marine Structures 2009;22:770–90.

Gordo, J.M. & Guedes Soares, C. (2015a). “Experimental analysis of a box girder with double span subject to pure bending moment.” in C.S.T.A. Guedes Soares, (ed.), Maritime Technology and Engineering. London: Taylor & Francis Group, 399 405.

Gordo, J.M. & Guedes Soares, C. (2015b). "Ultimate bending moment of a double span box girder with narrow stiffener spacing." Towards Green Marine Technology and Transport – Guedes Soares, Dejhalla & Pavleti (Eds), Taylor & Francis Group, London, ISBN 978-1-138-02887-6.

Gordo, J.M. & Guedes Soares, C. (2015c). "Experimental Evaluation of the Ultimate Bending Moment of a Slender Thin-Walled Box Girder." Journal of Offshore Mechanics and Arctic Engineering, 137(2), 021604.

GSG (2013). "Lupu Bridge." Retrieved from https://www.globalsalesgrowth.com.

Herman, R.S. (2001). "Behavior of Stiffened Compression Flanges of Trapezoidal Box Girder Bridges." Ph.D. dissertation, The University of Texas at Austin.

Horne, M. R., and Narayanan, R. (1977), "Design of Axially Loaded Stiffened Plates," *ASCE J. Struct. Div.*, Vol. 103, No. ST11, pp. 2243–2257.

Johansson, B., Maquoi, R., Sedlacek, G., Muller, C., and Beg, D. (2007). "Commentary and Worked Examples to EN 1993-1-5, Plated Structural Elements." 1st Edition, ECCS - JRC Report No. EUR 22898 EN.

Johansson, B. and Veljkovic, M. (2009). "Review of Plate Buckling Rules in EN 1993-1 5." Steel Construction, 2(4), 228-234.

Kalyanaraman, V., Pekoz, T. and Winter, G. (1972). "Performance of Unstiffened Compression Elements." Department of Structural Engineering Report, Cornell University.

Kim, K., Yoo, C.H. (2008). "Ultimate strengths of steel rectangular box beams subjected to combined action of bending and torsion." Eng. Struct. 30, 1677–1687.

King C.M. (2016). "Private communication with Dr. Charles King."

King C.M. (2017a). "A New Design Method for Longitudinally Stiffened Plates." Proceedings of the Annual Stability Conference, Structural Stability Research Council, San Antonio, TX, March.

King C.M. (2017b). "Private communication with Dr. Charles King."

King C.M. (2018). “Private communication with Dr. Charles King.”

Lindner, J., Scheer, J., Schmidt, H. “DIN 18800 Teil 1 bis 4 - Stahlbauten: Beuth Kommentare (German: commentary on DIN 18800 - Design of Steel Structures)”, Beuth Berlin, 1994.

Little, G.H. (1976). “Stiffened Steel Compression Panels: Theoretical Failure Analysis.” Struct. Eng., Vol. 54, No. 12, pp. 489–500.

Lokhande, A. and White, D.W. (2017). “Behavior and Design of Noncomposite Nonlongitudinally Stiffened Welded Steel Box-Section Members.” Proceedings of the Annual Stability Conference, Structural Stability Research Council, San Antonio, TX, March.

Murray, N. W. (1973). “Buckling of Stiffened Panel Loaded Axially and in Bending.” Struct. Eng., Vol. 51, No. 8, pp. 285–301.

Nakai H, Murayama Y, Kitada T, Takada Y. (1990). “An experimental study on ultimate strength of thin-walled box beams subjected to bending and torsion”. Journal of Structural Engineering, JSCE; 36A:63–70.

Pavlovcic L, Froschmeier B, Kuhlmann U, Beg D. (2012). “Finite element simulation of slender thin-walled box columns by implementing real initial conditions.” Advances in Engineering Software, 44:63–74.

Peköz, T. (1969). "Torsional flexural buckling of thin-walled sections under eccentric load." *Cornell Engineering Research Bulletin*, September 1969.

Pekoz, T.B (1986). “Development of a Unified Approach to the Design of Cold-Formed Steel Members.” Report SG-86-4, American Iron and Steel Institute, 1986.

Prime, B. (2005). “Residual stresses measured in quenched HSLA-100 steel plate.” Proceedings of the 2005 SEM Annual Conference and Exposition on Experimental and Applied Mechanics June 7-9, 2005 Portland, OR, USA.

Saad-Eldeen, S., Garbatov, Y., and Guedes Soares, C. (2010). “Experimental assessment of the ultimate strength of a box girder subjected to four-point bending moment.” Proceedings, 11th International Symposium on Practical Design of Ships and other Floating Structures (PRADS2010), Rio de Janeiro, Brazil, 1134–1143.

Schafer, B.W. (1997). "Cold-formed steel behavior and design: analytical and numerical modeling of elements and members with longitudinal stiffeners." Doctoral Dissertation, Cornell University.

Schillo, N., Taras, A., and Feldman, M. (2015). "Assessment of Safety Factor for Local Buckling." presentation to Eurocode TC8 Bochum, Nov. 6.

Schillo, N., (2017a). "Local and global buckling of box columns made of high strength steel." Ph.D. dissertation, RWTH Aachen University.

Schillo, N., (2017b). "Private communication between Dr. Nicole Schillo and Prof. Donald White."

Schillo, N. and Taras, A. (2018). "A reappraisal of the reliability of local buckling rules based on the Winter curve." Proceedings of the Annual Stability Conference, Structural Stability Research Council, Baltimore, Maryland, April.

Sheikh IA, Grondin GY, Elwi AE. (2002). "Stiffened steel plates under uniaxial compression." J Constr Steel Res 2002;58 (5–8):1061–80.

Simulia. (2013). "ABAQUS, Software and Analysis User's Manual." Version 6.13.

Subramanian, L.P. (2015). "Flexural resistance of longitudinally stiffened plate girders," Ph.D. dissertation, Georgia Institute of Technology.

Subramanian, L.P., and D.W. White. (2017). "Improved Strength Reduction Factors for Steel Girders with Longitudinally Stiffened Webs." Research Report, School of Civil and Environmental Engineering, Georgia Institute of Technology, Atlanta, GA, January.

Tanaka Y, Endo H. (1988). "Ultimate strength of stiffened plates with their stiffeners locally buckled in compression." Journal of the Society of Naval Architects of Japan 1988;164 [in Japanese]

Tao Z, Uy B, Han LH, Wang ZB. (2009). "Analysis and design of concrete-filled stiffened thin-walled steel tubular columns under axial compression." Thin-Walled Structures 2009; 47: 1544–1556.

Taras et al. (2013). "Coupled Instability Behavior of Members with Thin-Walled Welded Box Sections Loaded in Bending and Compression." SEMC 2013, University of Capetown, September.

Taras (2016). "Private communication between Prof. Andreas Taras and Prof. Donald White."

Timoshenko, S. (1921): Eisenbau 12 (1921), S. 147.

Vincent, G.S. (1969). "Tentative Criteria for Load Factor Design of Steel Highway Bridges," *AISI Bulletin No. 15*, American Iron and Steel Institute, Washington, D.C., 65 pp.

Wittrick, W. H. (1968). "A Unified Approach to the Initial Buckling of Stiffened Panels in Compression." *Aeronaut. Q.*, Vol. 19, p. 265.

White D.W. (2012). "Steel Bridge Design Handbook: Structural Behavior of Steel." Publication No. FHWA-IF-12-052 - Vol. 4.

White, D.W., Barker, M. and Azizinamini, A. (2008). "Shear Strength and Moment-Shear Interaction in Transversely-Stiffened Steel I-girders," *Journal of Structural Engineering*, ASCE, 134(9), 1437-1449.

White, D.W. and A.M. Lokhande. (2017). "A Review of Winter's Equation and Various Plate Postbuckling Resistance Approximations." Structural Engineering Mechanics and Materials Report No. 17-04, School of Civil and Environmental Engineering, Georgia Institute of Technology, Atlanta, GA.

White D.W., A.M. Lokhande, C.M. King, M.A. Grubb, F. Russo, and A. Ream. (2018). "Resistance of General Noncomposite Steel Box Section Members," Report to Federal Highway Administration, FHWA ID/IQ DTFH610- 14-D-00049, August.

Winter, G. (1970). Light Gage Cold-Formed Steel Design Manual: Commentary of the 1968 Edition, American Iron and Steel Institute, Washington, DC.

Wolchuk, R., and Mayrbourl, R. M. (1980). "Proposed Design Specification for Steel Box Girder Bridges." Rep. No. FHWA-TS 80205, U.S. Department of Transportation, Federal Highway Administration, Washington, DC.

Yoo CH, Choi BH, Ford EM. (2001). “Stiffness requirements for longitudinally stiffened box-girder flanges.” J Struct Eng, ASCE 2001;127(6):705–11.

Young, W.C. (2002). “Roark’s Formulas for Stress & Strain.” 6th Edition, Mc-Graw-Hill Professional Publishing, New York, NY.

Ziemian, R.D. (2010). “Guide to Stability Design Criteria for Metal Structures.” 6th Edition. New York: John Wiley & Sons, Inc.

AJINKYA LOKHANDE'S VITA

Ajinkya Mahadeo Lokhande was born on 28th October, 1990 and spent his childhood in Navi Mumbai, India. He completed his schooling and junior college from Fr. Agnel Multipurpose School and Junior College. He received his Bachelor of Technology in Civil Engineering degree in 2012 from Visvesvaraya National Institute of Technology, Nagpur. He worked as a Structural Engineering at FLUOR Corporation, before joining Georgia Institute of Technology in Fall 2013. He received his Masters degree in Civil Engineering (Specialization: Structural Engineering) in December 2014. His M.S. thesis research was on the stability bracing behavior of beams and beam-columns. He entered the Ph.D. program at Georgia Institute of Technology in January 2015.

Email: ajinkyalokhande2890@gmail.com